BioMed Research International

Advances and Challenges at the Waste-to-Bioenergy/Biorefinery Nexus

Lead Guest Editor: Shijian Ge
Guest Editors: Joseph Usack and Bin Ma

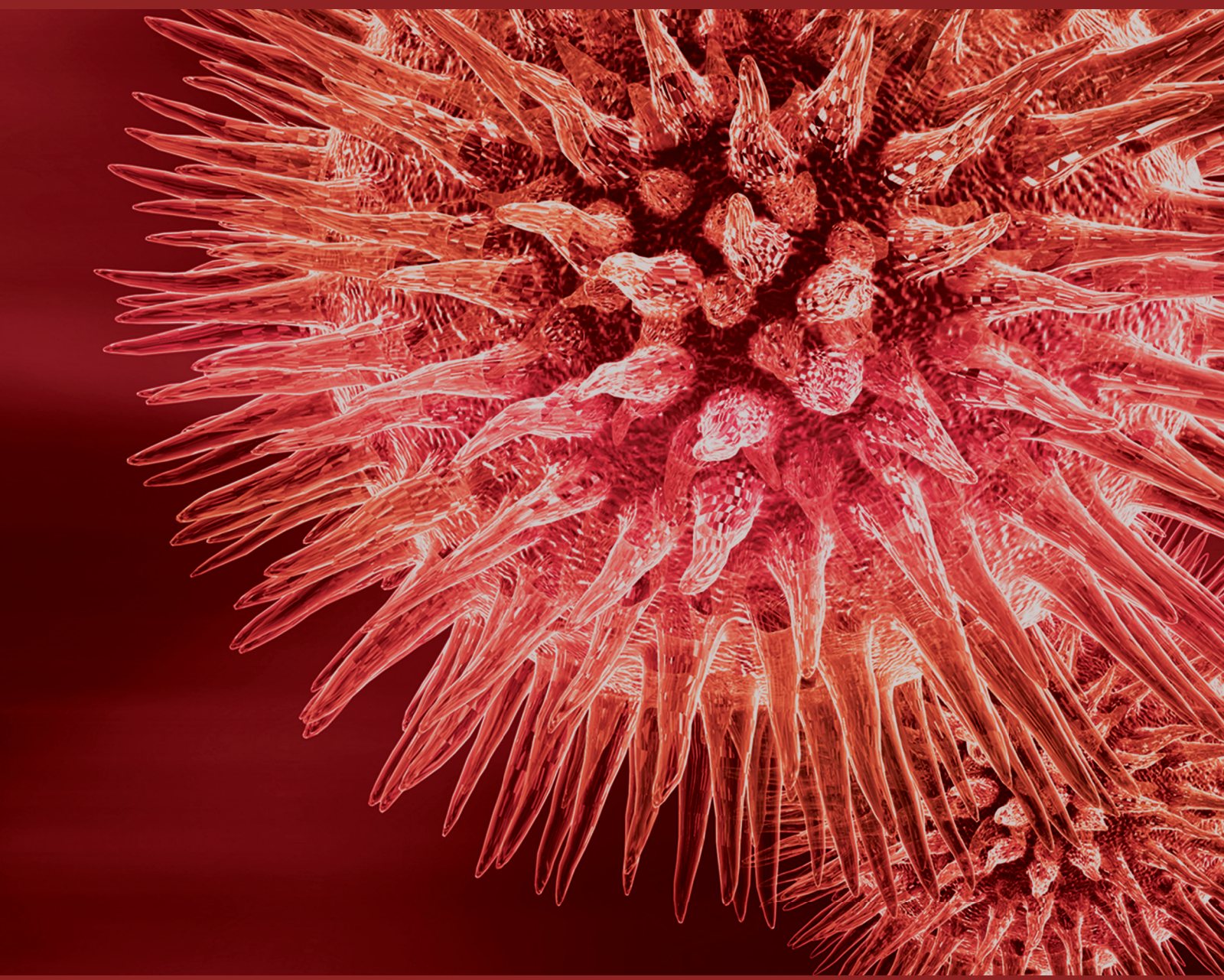

Advances and Challenges at the Waste-to-Bioenergy/Biorefinery Nexus

BioMed Research International

Advances and Challenges at the Waste-to-Bioenergy/Biorefinery Nexus

Lead Guest Editor: Shijian Ge
Guest Editors: Joseph Usack and Bin Ma

Contents

Hindawi
BioMed Research International
Volume 2018, Article ID 3642363, 2 pages
https://doi.org/10.1155/2018/3642363

Editorial

Advances and Challenges at the Waste-to-Bioenergy/Biorefinery Nexus

Shijian Ge[1], **Joseph Usack**[2] **and Bin Ma**[3]

[1]*Jiangsu Key Laboratory of Chemical Pollution Control and Resources Reuse, School of Environmental and Biological Engineering, Nanjing University of Science and Technology, Xiao Ling Wei 200, Nanjing, Jiangsu 210094, China*
[2]*University of Tübingen, Center for Applied Geoscience. Hölderlinstr. 12, Tübingen 72074, Germany*
[3]*Department of Environmental Sciences and Engineering, Hainan University, Renmin Avenue 58, Haikou, Hainan 570228, China*

Correspondence should be addressed to Shijian Ge; geshijian1221@njust.edu.cn

Received 24 May 2018; Accepted 25 May 2018; Published 14 June 2018

Population growth and industrialization across the globe are leading to the production of larger waste volumes. This will occur even though the current rate of waste production is already exceeding the capacity of existing waste management infrastructure in many parts of the world. The environmental consequences of inadequate waste management are already being realized on both the small and global scale through, for example, the pollution of local air/water bodies and climate change. While these increases in waste production pose many challenges, they also present many opportunities to develop novel technologies to not only better stabilize or utilize these wastes, but also recover valuable resources, such as energy, green chemicals, and nutrients. Thus, in response to this emerging scientific field, this special issue was organized to serve as a platform for novel research that addresses these challenges and specific applications of the removal, utilization, and bioconversion of biowaste. A total of 9 quality papers were published covering various topics as presented below.

The paper authored by Z. Chen et al. presents a review on determination of microalgal lipid content and fatty acid for biofuel production by summarizing and comparing different approaches of extraction and quantification of microalgal lipids including the pretreatment of microalgal cells, as well as describing the principles and procedures for the production and quantification of fatty acids in detail. Apart from the traditional extraction methods using conventional organic solvents, this review also introduces newly-developed lipid-extraction techniques, such as CO_2-based solvents, ionic liquids, and switchable solvents. The authors make specific suggestions about the determination methods of microalgal lipids (*i.e.*, gravimetric method, Nile red lipid visualization method, sulfo-phospho-vanillin method, and thin-layer chromatography method) as well.

The paper titled "Effect of Free Nitrous Acid on Nitrous Oxide Production and Denitrifying Phosphorus Removal by Polyphosphorus-Accumulating Organisms in Wastewater Treatment" by Z. Miao et al. studied the relationship between free nitrite acid (FNA) and nitrous oxide (N_2O) in denitrifying phosphorus removal process. The results showed that FNA, rather than nitrite and pH, was likely the true inhibitor of N_2O production. Moreover, the nitrite reduction rate, phosphorus uptake rate, N_2O reduction rate, and PHA degradation rate also decreased as the concentration of FNA increased. The highest proportion of N_2O to TN was 78.42% because FNA prevented the step from NO_2-to-N_2O and N_2O-to-N_2. Meanwhile, this part of dissolved N_2O, as a significant greenhouse gas (~300 times greater warming potential than CO_2), could be diffused into air.

The paper written by Q. Chang et al. proposed an alternative low- and high-ammonium influent regime to maintain a completely autotrophic nitrogen removal over nitrite (CANON) treatment for low ammonium wastewater. Their findings showed that excessive proliferation of nitrite oxidizing bacteria (NOB) in a low-ammonium environment was still a challenge for stable CANON operation. However, with 28 days of high-ammonium treatment combined with a controlled sludge retention time, the overproliferation of

NOB in the low ammonium operational period could be avoided. They suggested that when the nitrite oxidation rate reached 8 g $N/m^3/h$, the CANON system should enter the high-ammonium influent operating mode. The proposed strategy can be realized if wastewater treatment plants have a sludge digestion unit, from which the higher-ammonium influent can be supplied.

The paper written by F. Yang et al. employed the Malmquist-Luenberger productivity index to evaluate the productivity change of environmentally friendly production technologies that simultaneously reduce wastewater discharges and generate economic outputs for 30 administrative provinces in China during 2003-2015. During this period, they observed a downward trend and growing spatial disparities for China's water preferable productivity index in many of these provinces. The major cause of these developments can be attributed to environmentally friendly technology changes, while only a minor effect can be attributed to the improvement of the technical efficiency.

The paper authored by S. Xu et al. entitled "Analysis of Bacterial Community Structure of Activated Sludge from Wastewater Treatment Plants in Winter" investigated the microbial-community structure of activated sludge in wastewater treatment plants and identified the bacteria that caused bulking of activated sludge in winter. This result will help optimize wastewater treatment and water reclamation practices.

The paper titled "Efficient Utilization of Waste Carbon Source for Advanced Nitrogen Removal of Landfill Leachate" by K. Wang et al. assessed the nitrogen removal adaptability of a modified single sequencing batch reactor (SBR). The operation mode of the SBR was filling, stirring, aeration, stirring, and settling which could enhance the nitrogen removal rate of leachate. The chemical oxygen demand (COD) and ammonia of the SBR effluent were less than 500 mg/L and 40 mg/L under the condition without a carbon source. Furthermore, the removal rates of COD and total nitrogen were greater than 85% and 95%, respectively. The maximum specific nitrogen removal rate reached 1.48 mg N/h/g VSS. Polyhydroxyalkanoates were the primary carbon source in the sludge for nitrogen removal. In whole experiment period (*i.e.,* 160 days), the sludge concentration remained nearly unchanged because most of the organic matter in the raw wastewater was used for denitrification.

In the paper titled "Study of Nitrogen Removal Performance When Treating Low Carbon Sewage Using External Solid Carbon Sources in SBBR Systems," L. Zhang et al. used the waste from corncob processing as the external solid carbon source for biological nitrogen removal. The results showed that a low-nitrogen effluent could be obtained using this wastewater treatment system.

The paper titled "Analysis of the Metabolites of Indole Degraded by an Isolated *Acinetobacter pittii* L1" by Z. Yang et al. isolated an efficient indole degrading *Acinetobacter pittii* L1 from a coking wastewater. *A. pittii* L1 was demonstrated as a promising candidate for the degradation of nitrogen heterocyclic compounds, the production of indigoids, soil remediation, and the treatment of indole containing wastewaters.

In the paper titled "Start-Up and Aeration Strategies for a Completely Autotrophic Nitrogen Removal Process in an SBR," X. Zhang et al. demonstrated that Planctomycete-like anammox bacteria and *Nitrosomonas*-like aerobic ammonium oxidization bacteria could be cultivated in an SBR using intermittent aeration, so as to achieve autotrophic nitrogen removal for reducing energy consumption of wastewater treatment and water reclamation.

Acknowledgments

The editors would like to acknowledge the authors who submitted their research articles and all reviewers for their contributions to this special issue. Contributions of Professor Shijian Ge and Professor Bin Ma are supported by the National Natural Science Foundation of China (51708294 and 51508008), the Fundamental Research Funds for the Central Universities (30918011306), and the General Program of Science and Technology Development Project of Beijing Municipal Education Commission of China (KM201710005001).

Shijian Ge
Joseph Usack
Bin Ma

Hindawi
BioMed Research International
Volume 2018, Article ID 1503126, 17 pages
https://doi.org/10.1155/2018/1503126

Review Article

Determination of Microalgal Lipid Content and Fatty Acid for Biofuel Production

Zhipeng Chen, Lingfeng Wang, Shuang Qiu, and Shijian Ge

Jiangsu Key Laboratory of Chemical Pollution Control and Resources Reuse, School of Environmental and Biological Engineering, Nanjing University of Science and Technology, Xiao Ling Wei 200, Nanjing, Jiangsu 210094, China

Correspondence should be addressed to Shuang Qiu; qiushuang89@njust.edu.cn and Shijian Ge; geshijian1221@njust.edu.cn

Received 29 December 2017; Revised 12 March 2018; Accepted 4 April 2018; Published 21 May 2018

Academic Editor: Xiaoling Miao

Biofuels produced from microalgal biomass have received growing worldwide recognition as promising alternatives to conventional petroleum-derived fuels. Among the processes involved, the downstream refinement process for the extraction of lipids from biomass greatly influences the sustainability and efficiency of the entire biofuel system. This review summarizes and compares the current techniques for the extraction and measurement of microalgal lipids, including the gravimetric methods using organic solvents, CO_2-based solvents, ionic liquids and switchable solvents, Nile red lipid visualization method, sulfo-phospho-vanillin method, and the thin-layer chromatography method. Each method has its own competitive advantages and disadvantages. For example, the organic solvents-based gravimetric method is mostly used and frequently employed as a reference standard to validate other methods, but it requires large amounts of samples and is time-consuming and expensive to recover solvents also with low selectivity towards desired products. The pretreatment approaches which aimed to disrupt cells and support subsequent lipid extraction through bead beating, microwave, ultrasonication, chemical methods, and enzymatic disruption are also introduced. Moreover, the principles and procedures for the production and quantification of fatty acids are finally described in detail, involving the preparation of fatty acid methyl esters and their quantification and composition analysis by gas chromatography.

1. Introduction

Nowadays, limited stock of petroleum-derived fuel resources combined with perpetually increasing demands for energy due to the rapid industrialization and population growth has troubled many governments and organizations across the world [1]. Moreover, the combustion of fossil-derived fuels has led to increasing emission of greenhouse gases such as carbon dioxide (CO_2), leading to global climate change and posing threats to the biosphere [2]. In order to achieve sustainable development, the critical issues noted above and the gradually rising fossil-derived fuel prices have called for the needs to search for alternative sustainable and renewable energy sources [3].

Biofuels, produced from biomass, are promising alternatives to fossil-derived fuels due to several distinct advantages including carbon neutrality, reduced emissions of gaseous pollutants (e.g., carbon monoxide, CO_2, and sulfur oxides), continuous availability of biomass feedstocks, and their safety of production by farming [4]. According to their physical characteristics, biofuels are divided into solid (i.e., biochar), liquid (i.e., bioethanol, vegetable oil, and biodiesel), and gaseous (i.e., biogas, biosyngas, and biohydrogen) fuels. Based on the types of used feedstocks, biofuels are categorized into three generations. The first generation feedstocks mainly include food crops such as corn, soybean, rapeseed, sunflower, and palm oil. The second-generation biofuels are derived from nonedible feedstocks like *Jatropha*, *Miscanthus*, Switch grass, and other organic wastes. Nevertheless, the expanding demand for edible feedstocks as food sources and their need for large areas of arable land for production have limited the development of both the first- and second-generation biofuels. The use of microalgae as a third-generation biofuel feedstock avoids these issues and presents several distinct advantages of not requiring agricultural or arable lands for production, high photosynthetic efficiencies and biomass productivities (biomass doubled in less than one day), and 100 times more lipids per acre of land [5, 6].

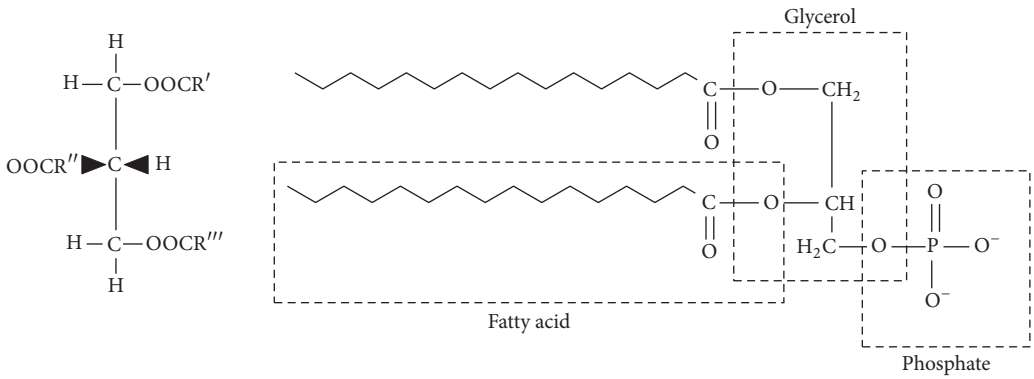

Figure 1: Lipid molecules. Triacylglycerol (NL) on the left. Phospholipid (polar lipid) on the right. R′, R″, and R‴ in the triacylglycerol molecule represent fatty acid chains. Phospholipid molecule is negatively charged [15].

Moreover, the main storage lipids in microalgae are neutral lipids (NLs) or triacylglycerols that can be esterified to FAMEs with the primary profiles of C16 and C18, proven to be the most suitable for biofuel production [7]. Microalgae exhibit great adaption to various environmental conditions, making them easy to cultivate. For instance, they can grow on marginal land in both the open pond and closed systems using waste streams like wastewater, waste or CO_2-enriched gas (biogas, flue gas), waste organics (i.e., crude glycerol), and waste heat to provide nutrients and carbon and temperature maintenance (in a cold climate), achieving economically feasible and environmentally sustainable biofuel production and waste bioremediation [8]. Moreover, various routes of microalgal metabolisms can be adopted for enhanced growth and lipid production. Traditionally, phototrophic algae are grown autotrophically with CO_2 as the unique carbon source and light providing all the energy needed. Moreover, some microalgae species can grow heterotrophically using only organic compounds, while others can grow mixotrophically using both organic compounds and CO_2 to support growth [9].

Currently, the high costs of the important microalgal harvesting and lipid extraction processes are the primary obstacles impeding on the commercial application of microalgae-derived biofuel production [10–12]. For example, lipid extraction is a high-power-consumption process because lipids are stored in microalgal cells and the cell wall is a thick and rigid layer composed of complex carbohydrates and glycoproteins with high mechanical strength and chemical resistance, posing difficulties for lipid extraction [13]. Therefore, certain cell disruption techniques are generally considered prior to lipid extraction to improve the extraction efficiencies. Nevertheless, the efficiencies of cell disruption and lipid extraction vary with methods selected with different operating conditions (e.g., temperature, atmospheric pressure, and humidity), microalgae species, and biomass amount.

This review summarizes and compares the methodologies employed for the extraction and quantification of microalgal lipids. The pretreatment methods supporting cell disruption and subsequent lipid extraction are also included. Finally, the principles and procedures for the production and quantification of fatty acids in microalgae are discussed in detail.

2. Microalgal Lipids

Microalgal lipids can be divided into two groups according to their structures: nonpolar NLs (acylglycerols, sterols, free fatty acids, wax, and steryl esters) and polar lipids (phosphoglycerides, glycosylglycerides, and sphingolipids). Figure 1 shows the structural formula of the polar lipid and NLs [14, 15]. These lipids play different but important roles in microalgal metabolism and growth period. Some lipids such as phosphoglycerides, glycosylglycerides, and sterols are imperative structural components of biological membranes, while lipids like inositol lipids, sphingolipids, and oxidative products of polyunsaturated fatty acids may act as key intermediates in the cell signaling pathways and play a role in sensing changes in the environment [16]. The quantities of these microalgal lipids vary with the type of species, growth conditions, and ambient environments. It was reported that the lipid contents ranged at 20–50% of dry biomass including *Chlorella*, *Crypthecodinium*, *Cylindrotheca*, *Dunaliella*, *Isochrysis*, *Nannochloris*, *Nannochloropsis*, *Neochloris*, *Nitzschia*, *Phaeodactylum*, *Porphyridium*, *Schizochytrium*, and *Tetraselmis* [17].

3. Microalgal Cell Disruption Methods

Specific microalgal cell pretreatment procedures must be considered prior to the subsequent lipid extraction due to the microalgal cell wall structure. When the extraction is conducted from the wet biomass, the pretreatment step is mandatory to disrupt the microalgal cell walls and allow the lipids to be released into the extracting mixture. The commonly used pretreatment methods are summarized below.

3.1. Bead Beating. Bead beating, also known as bead mill or ball mill, disrupts cells by the impact of high-speed spinning of fine beads on the biomass slurry. The whole disruption process could be done within minutes, and it could be applied to any kinds of microalgae without preparation [18, 19]. Two common types of bead mills are shaking vessels and agitated beads [20]. Shaking vessels usually consist of multiple containers or well-plates on a vibrating platform, and the cell disruption is done by shaking the entire vessel

on a vibrating platform. The shaking vessels are usually employed in laboratory, as they are only suitable for multiple samples requiring similar disruption treatment conditions. Comparatively, the agitated beads type that is made up of a rotating agitator in a fixed vessel filled with beads and cell culture could achieve better disruption efficiencies. However, the cooling jackets must be equipped to protect the heat-sensitive biomolecules as the rotating agitator generates heat during disruption process [18, 19]. The combination of agitation, collision, and grinding of the beads could produce a higher disruption efficiency [20]. To sum up, the simplicity of the equipment and the rapidness of the treatment process are the two main advantages of bead beating methods, while the requirement of an extensive cooling system to protect the target products has limited it to scale up [18].

3.2. Microwave. Microwave is an electromagnetic wave with the frequency ranging between 300 MHz and 300 GHz, which is lower than that of infrared and higher than that of radio waves. Microwave-assisted extraction technology has been studied for extracting target compounds in a few fields, including microalgal lipid extraction [50]. When microalgal cells are exposed to the microwave with the specific frequency (approximately 2450 MHz), cell molecules generate a rapid oscillation within the rapidly oscillating electric field, resulting in the heat generation due to the frictional forces from the inter- and intramolecular movements [51]. The intracellular heating causes the water to vapor, which disrupts the cells and subsequently opens up the cell membrane. This method exhibits strong advantages of short reaction time, low-operating costs, and efficient extraction with all of the species, but the requirement of a vast cooling system to protect target products limits its large-scale application [18, 19].

3.3. Ultrasonication. Ultrasonication has been a well-known method for the microbial cell disruption due to its short reaction time with high productivity [52]. When the ultrasound is applied to the liquid cultures, small "vacant regions" called microbubbles are momentarily formed as the liquid molecules are moved by the acoustic waves. Meanwhile, the production of microbubbles causes cavitation, which in turn creates pressure on the cells to break up [53]. During the treatment, the rapid compression/decompression cycles of the sonic waves generate transient and stable cavitation. The transient cavitation occurs when oscillations that cavitation undergoes are unsteady and implode ultimately. This type of implosion could produce extremely localized shock waves and high temperature, the conditions of which impart mechanical stress on the cells and crack the cell wall and membrane [54]. On the other hand, the cavitation that oscillates for many cycles is referred to as stable cavitation, which can produce microscale eddies, inducing stress or physiological changes in microorganisms [55]. Ultrasonic horn and bath are the two basic types of sonicators, and they are commonly employed in batch operations but can also be adapted for continuous operations [56]. Horns use piezoelectric generators, which are made of lead zirconate titanate crystals and vibrate with amplitude of 10–15 mm. As the energy generated at the horn tip dissipates rapidly with distance, the cavitation must be created with sufficient disruptive force. Transducers placed at the bottom of the sonicator are used in sonicator baths to generate ultrasonic waves. In sonicator baths, the number and arrangement of transducers vary according to the capacity and shape of the sonicator [20]. The working conditions of ultrasonication treatment are easy to set up and the whole process could be done in a very short time while with high reproducibility [19]. However, it is difficult to scale up as cavitation, the strong effect of which is able to achieve cell disruption only occurs in small regions near ultrasonic probes.

3.4. Chemical Method. The rupture of cells occurs when chemicals are used to increase the permeability of cell up to a particular value [57]. It was reported that, through chemical treatments with acids (i.e., HCl and H_2SO_4), alkalis (i.e., NaOH), and surfactants, chemical linkages on the microalgal cell envelope were degraded followed by the lysis of cell wall [58]. Comparatively, chemical treatment consumes less energy because it does not require a large amount of heat or electricity while showing higher efficiency of cell disruption. However, the continuous consumption of chemicals challenges the economic sustainability of this method. Moreover, acids and alkalis have a high risk of corroding the reactor and attacking microalgal lipids, thus ruining the whole process [18].

3.5. Enzymatic Disruption. In addition to the autolysis, the use of foreign lytic enzymes is extensively investigated because enzymes are the commercially available and easily controlled biological materials [59]. Specific enzyme is able to degrade certain structural cell components, thus improving the release of desired intracellular compounds [60]. In some cases, a mixture of different enzymes is reported to have a better economic and technical feasibility, and the lipid yields could be improved when enzymatic hydrolysis is combined with acid/alkaline pretreatment. Compared to the chemical method that possibly destroys every particle existing in the solution and even induces side-reactions of the target products (i.e., lipids), the reaction condition of enzymatic method is mild, and its selectivity is high with specific chemical linkages. Moreover, enzymatic disruption combined with other methods is usually considered for economic process and improved disruption performance [18]. However, more researches need to be conducted to reduce the high cost and relatively long treatment time, which have limited the large-scale application of this method.

3.6. Other Methods. Apart from the methods noted above, there are some other microalgal cell disruption approaches that have been investigated as well. For example, when the mixture of microalgae and other solvents is sprayed through a narrow tube under high pressure, hydraulic shear force is generated and high pressure homogenization (HPH), also known as French press, makes use of this force to extract internal substances of microalgae. By measuring the increase in the soluble chemical oxygen demand (SCOD) during the cell disruption, lots of researchers have evaluated the cell disruption efficiency and found that HPH exhibited high cell

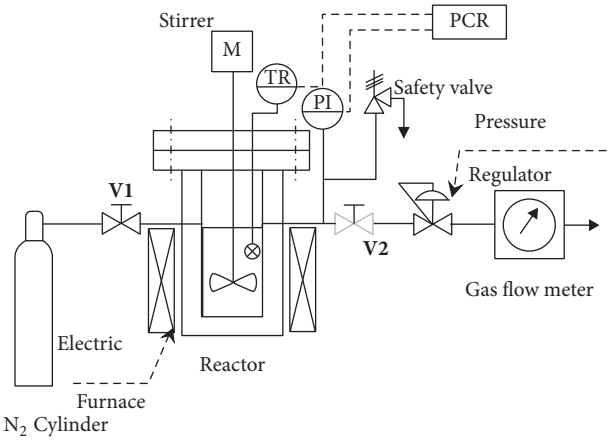

Figure 2: Schematic diagram of thermal pretreatment apparatus [61].

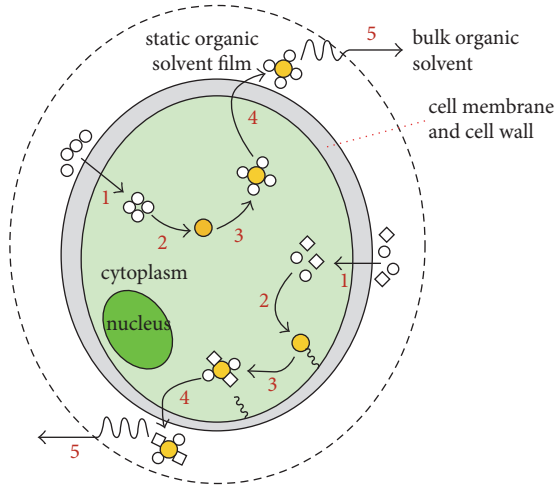

Figure 3: Schematic diagram of the organic solvent-based microalgal lipid extraction mechanisms. The pathway shown at the top of the cell is for nonpolar organic solvent while the pathway shown at the bottom of the cell is for nonpolar/polar organic solvent mixture. Orange circle: lipids, white circle: nonpolar organic solvent, and white diamond: polar organic solvent [15].

disruption efficiency. It is worth mentioning that HPH has lots of advantages such as producing less heat during the extraction process, thus requiring less cooling cost and it is easy to scale up. However, the pretreatment process relying on HPH requires a relatively long time and consumes quite a few amount of power. Electroporation can achieve permanent cell disruption by applying a much stronger electromagnetic field (EF) to the biomass that can damage the cell envelopes beyond their healing abilities since the application of an EF of suitable intensity will lead to the formation of pores on the cell envelopes of the cells, and the pores are closed by a healing process when the EF is removed. Electroporation is a promising cell disruption method as it requires simple equipment and operation procedures with high energy efficiency [18, 20]. Thermal treatment could achieve effective recovery of hydrocarbons as well and a typical process of thermal pretreatment is shown in Figure 2. Firstly, place the samples in vessel and replace the air in the vessel by nitrogen gas. Then, heat vessel to the set temperature, and afterwards, cool the vessel to the ambient temperature after maintaining the samples at the set temperature. Then, stir the samples mechanically. Finally, open the autoclave and carefully remove the samples for further analysis [61]. Recently, plenty of work have been done to compare the efficiency of different cell disruption methods; however, due to the different species of microalgae used in experiments so as the different operating temperatures, atmospheric pressures, and other influence factors, the efficiency of different cell disruption methods is short of comparability.

4. Microalgal Lipid Extraction and Quantification Approach

The microalgal lipid extraction refers to the process of separating the valuable NLs and fatty acids from the cellular matrix and water. As far, multiple methods have been reported for the quantification of microalgal lipids, mainly including the conventional gravimetric method using extraction solvents, Nile red lipid visualization method, SPV, and TLC [62–64].

4.1. Gravimetric Method. The gravimetric method is most widely used to determine microalgal lipid content. It is also frequently used as a reference standard to validate other methods. The gravimetric method consists of the lipid extraction using solvents and lipid quantification achieved by recording the weight of extracted lipids after evaporating the extracting solvents. The extraction solvents used include the conventional organic solvents, CO_2-based solvents, ionic liquids (ILs), and switchable solvent.

4.1.1. Organic Solvent Extraction. The chemistry concept of "like dissolving like" is the basic principle underlying the organic solvent-based extraction of microalgal lipids. Figure 3 illustrates the principle of the 5-step-microalgae lipid extraction mechanism. Typically, the organic solvents penetrate through the cell membrane into the cytoplasm (step 1) and interact with the lipid complex (step 2). During this process, the nonpolar organic solvent interacts with NLs through van der Waals associations, while the polar organic solvent interacts with the polar lipids by generating hydrogen bonds that are strong enough to replace the lipid-protein associations that prevent nonpolar organic solvent from accessing the lipids. Subsequently, an organic solvent-lipids complex is produced (step 3), followed by the organic solvent-lipids complex diffusing across the cell membrane (step 4) and the static organic solvent film (step 5) into the bulk organic solvent driven by a concentration gradient.

The commonly used organic solvent extraction procedures are summarized in Table 1. The nonpolar organic solvents, such as hexane, benzene, toluene, diethyl ether, ethyl acetate, and chloroform, are usually combined with the polar organic solvents to maximize the extraction efficiency of NLs. As such, when lipid extraction is achieved with the use of a nonpolar/polar organic solvent mixture, the

Table 1: Determination of microalgal lipid content using conventional organic solvents.

Lipid extraction		Determination of lipid content		Ref.
Reagent(s)	Extraction process	Treatment for final determination	Expression of lipid content	
Chloroform : isopropanol (1 : 1, v/v) andhexane.	Add solvent mixture to frozen pellets; centrifuge and transfer supernatants; reextract pellets with hexane and centrifuge to collect supernatants.	Dry the combined supernatant in a speed vacuum and record the weight.	A percentage of total fresh weight (% w/w)	[21]
Ethyl ether.	Ground dry samples to powder and use the Soxhlet extractor.	Distill the solvent, dry the residue, and record the weight.	A percentage of dry cell weight (% w/w)	[22]
Methanol : chloroform : 1% NaCl (2 : 2 : 1, v/v/v).	Extract the biomass with the solvent mixture.	Evaporate the chloroform layer; dry the sample and record the weight.	The weight ratio of extracted lipid to lyophilized pellets (% w/w)	[23]
Deionized (DI) water : methanol : chloroform (1 : 2 : 1, v/v/v); chloroform.	Add solvent mixture to harvested biomass and react for 24 h; mix and then add solvent to achieve a final DI water : methanol : chloroform ratio of 0.9 : 1 : 1; centrifuge, remove, and filter the lipid-chloroform layer; repeat the above steps for second extraction.	Evaporate the chloroform layer; cool the tube and record the weight.	A percentage of total biomass weight (%, w/w)	[24]
Chloroform : methanol (2 : 1, v/v).	Mix dry algal powder with the solvent mixture; put under water bath with the aid of ultrasound; centrifuge and repeat the above steps three times.	Evaporate the organic solvent and weight.	A percentage of total biomass weight (%, w/w)	[25]
Chloroform : methanol (2 : 1, v/v).	Extract lipid from dry biomass with the solvent mixture.	Evaporate the solvent and weight.	Weight difference between the blank flask and the flask containing the extracted oil	[26]

Table 2: Comparisons between conventional organic solvents extraction and CO_2-based solvents extraction approaches.

Items	Organic solvent	$scCO_2$	lCO_2
Heavy metal contamination	Unavoidable	Free of heavy metals	Free of heavy metals
Inorganic salt content	Difficult to avoid	Free of inorganic salts	Free of inorganic salts
Selectivity	Poor selectivity	Highly selective	Highly selective
Extracted compounds	Polar and nonpolar compounds	Nonpolar compounds	Nonpolar compounds
Safety	Flammable and/or toxic	Nontoxic and nonflammable	Nontoxic and nonflammable
Operation condition	Regular temperature and pressure	High temperature and pressure	Lower temperature and pressure than $scCO_2$
Recycling	Solvent recovery is expensive	CO_2 could be recycled and reused	CO_2 could be recycled and reused
Operation cost	High power consumption (in solvent recovery)	High power consumption	Lower than $scCO_2$
Extraction time	Time-consuming	Shorter than solvent extraction	Shorter than solvent extraction

polar organic solvent is intended to disrupt the neutral-polar lipid complexes while the nonpolar organic solvent aims to solubilize the intracellular NLs [65]. Moreover, the lipid yields vary with the type of used organic solvents and the ratios of polar solvents to nonpolar solvents. Therefore, the final lipid extraction efficiencies using different organic solvents extraction methods cannot be impartially compared. In addition, the different experiment steps, equipment, and experimental conditions involved in the extraction process also contribute to various extraction results.

The organic solvent-based extraction methods usually require a relatively large quantity of biomass and have few environmental impacts. In addition, organic solvents are not highly selective towards the desired neutral (mono-, di-, and triacylglycerols) lipids and free fatty acid components; some of them are not easily removable, posing difficulties to the subsequent process. An ideal solvent for the lipid extraction should be free of toxicity, easy to remove, and more selective towards target products. These characteristics have been found in CO_2-based solvents, ionic liquids, and switchable solvents, which will be introduced hereinafter.

4.1.2. CO_2-Based Solvent Extraction. The supercritical ($scCO_2$) and liquid (lCO_2) CO_2 are able to solubilize many organic molecules and can be easily recycled at the end of the process while leaving no residual solvents, making them promising alternatives to traditional organic solvents.

(1) $scCO_2$ Extraction. The supercritical fluid extraction (SFE) is a promising green technology that can potentially displace the use of traditional lipid extraction procedure, due to its high selectivity, short extraction time, and their absent use of toxic organic solvents [66]. As can be seen from Table 2, $scCO_2$ has been regarded with interest in the field of SFEs, because it offers advantages of negligible environmental impact, high diffusivity, no toxicity, no oxidation or thermal degradation of extracts, and easy separation of desired bio-products [67]. Moreover, $scCO_2$ has high selectivity towards microalgal NLs (mono-, di-, and triacylglycerols) and has been used in the lipid extraction of microalgae such as *Cylindrotheca closterium, Arthrospira maxima, Nannochloropsis oculate, Chlorella vulgaris,* and *Spirulina platensis* [68–71]. For example, Halim et al. [72] employed $scCO_2$ into a wet *Chlorococum* sp. paste to obtain a yield of 7.1 wt% at a temperature of 333 K and a pressure of 30 MPa over an 80 min extraction time. Moreover, coupling the nonpolar $scCO_2$ with the polar cosolvents (i.e., methanol, ethanol, and toluene) could enhance the affinity towards NLs that form complexes with polar lipids, resulting in a greater biofuel production [73]. The general procedure of $scCO_2$ extraction is described as follows: CO_2 is first condensed to lCO_2 and then to the $scCO_2$. Subsequently, the fluid is pumped into the extraction vessel under the desired and controlled conditions of pressure and temperature. After the extraction, the extracted lipids are precipitated and collected into a glass trap, cooled in an ice bath with the amount assessed by gravimetry. It should be noted that the effects of operating conditions (i.e., extraction vessel size and type, pressure, and extraction time) involved in the $scCO_2$ extraction process noted above on the lipid yield and selectivity should be investigated on a case-by-case basis. Moreover, the high temperature (i.e., 100°C) and pressure (i.e., 41 MPa) requirement are the main concerns that have limited this approach from industrial-scale application [74].

(2) lCO_2 Extraction. Comparatively, lCO_2 shares many of the same benefits as $scCO_2$ while it requires lower temperature and pressure than $scCO_2$ extraction (Table 2) and therefore has emerged as a possible substitute. Paudel et al. [75] recovered about 26 wt% of the extractable lipids using lCO_2 directly from the wet biomass of *Chlorella vulgaris* under different pressures (6.8–17 MPa) and a constant temperature of 25°C. An extraction example using lCO_2 is described as follows. Firstly, lCO_2 is pressurized to a certain pressure (i.e., 6.8 MPa) using the high pressure pump and during this process, a coolant (i.e., 75% ethyleneglycol in distilled water) must be used to keep the pump at −5°C to prevent it from being heated. Secondly, the pressurized lCO_2 is delivered through the tube coil to tube vessel, aiming to make CO_2 coming from the cold pump warm up to the temperature of the water bath. Thirdly, the vessel containing dry algae is heated in water bath at 25°C for 2 h, during which the required pressure in the system is maintained by backpressure regulator (BPR). After the extraction, the remaining CO_2 is vented into the flask, and the remaining extract exiting the

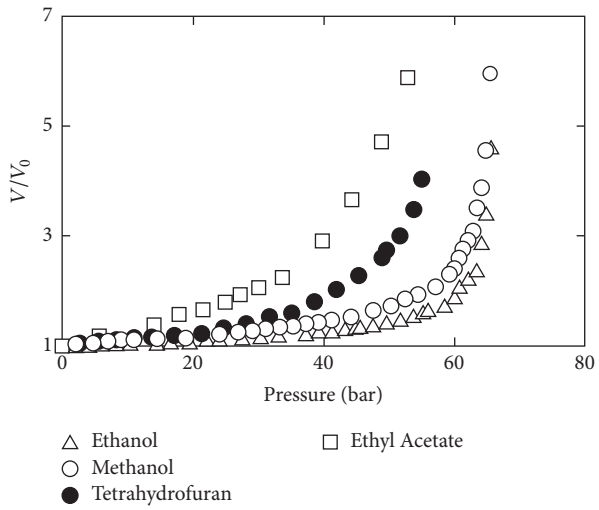

Figure 4: Isothermal volumetric expansion of benign solvents by CO_2 at 40°C [77].

BPR is captured, separated, and dried. The extract is then preserved in the ice-cold isopropanol.

(3) Gas Expanded Liquids Extraction. Gas expanded liquids (GXLs) are liquids expanded in volume by the application of modest pressures with a compressible gas, among which CO_2 is one of the most commonly used gases [76]. The GXLs are made up of a mixture of compressed gases and conventional solvents. Jessop and Subramaniam [77] reported that GXL solvents have the combined beneficial properties of a compressed gas and organic solvent, so the properties of solvent can be adjusted through variations in the pressure. As can be seen from Figure 4, the gaseous CO_2 has a considerable solubility in many benign organic solvents at adequate pressures (<8 MPa) such as ethanol, methanol that show a 2- to 3-fold volumetric expansion at relatively mild pressures and moderate temperatures [77]. As such, various principles and applications of CO_2-expanded liquids (CXLs) including lipid extraction have been proposed [78, 79]. Due to the fact that CXLs can be operated at mild temperatures and pressures, a reduction in process costs and energy consumption could be realized. The mass transfer rates can also be improved via CXLs by reducing interfacial tension and viscosity as well as increasing diffusivity [80]. Wang et al. [78] used the CO_2-expanded ethanol to successfully extract lipids from *Schizochytrium* sp. with a 35.7 wt% lipid content of dry biomass. The CO_2-expanded methanol increased up to 82% of the selectivity of methanol towards the extraction of biodiesel-desirable NLs and free fatty acids [75].

4.1.3. ILs Extraction. ILs are organic salts with the melting point below 100°C, and they typically consist of large asymmetric organic cations coupled with smaller anions [81]. Advantages such as thermal stability, synthetic flexibility, nonvolatility, nonflammability, recyclability, and unique solvent properties have made ILs promising replacements of traditional organic solvents in lipid extraction as they can dissolve highly recalcitrant biopolymers [82]. For instance, ILs are capable of disrupting cell structure in wet microalgae biomass under mild conditions. This allows either autopartitioning of the lipids or presumably improving access of cosolvents to the intracellular lipids, thus facilitating the extraction of lipids from microalgae and making it faster than organic solvent extraction processes. Most solvent-based extraction processes, however, are incompatible with wet biomass, which add significant costs to the overall process since dewatering and drying processes are thought to be responsible for up to 70% of the biofuel production cost [83].

A typical lipid extraction procedure with the aid of ILs is described as follows [84]. Firstly, mix microalgae paste with 1 : 10 mass ratio of dry equivalent microalgae to [C_2mim][$EtSO_4$] and incubate the mixture. Secondly, add water to the mixture to improve separation after the addition of hexane and remove the top layer to a new container. The procedures noted above are repeated three times to achieve a high extraction efficiency. After the extraction, wash the extracts with NaCl and transfer the target part to a preweighed vessel. The mass of extractable lipids is measured after evaporating the solvent. For ILs recycling, add methanol/water to the mixture to precipitate the residual solids and pool hexane with the previous extraction. Subsequently, filter the solvent and wash with methanol/methanol to collect ILs, and then ILs are recovered by evaporation.

4.1.4. Switchable Solvents Extraction. Switchable solvents, known as "reversible" or "smart" solvents, can reversibly change their properties upon addition or removal of a "trigger." The switchable solvents (subclass of ILs) are divided into two categories, switchable polarity solvents (SPSs) and switchable hydrophilicity solvents (SHSs) [85, 86]. Specifically, the polarity of SPSs exhibits variation with the solution CO_2 concentration. The polarity of the solvents can be reversed by removing the CO_2 from the system by heating or sparging the solution with nonacidic gases. SPSs are divided into two classes, which are either single-component or two-component species. In the two-component SPSs, a base with an alcohol or with an amine is usually included while single-component SPSs require a primary or secondary amine [85]. Unlike SPSs, SHSs can change from a hydrophobic solvent into a hydrophilic one, and their potential applications have extended to the extraction of microalgal lipids [87]. In the SHSs system, the hydrophobic form creates a biphasic mixture with water, and the hydrophilic form is the corresponding bicarbonate salt; thus SHSs could also be reversibly converted between the above two forms by the addition or removal of CO_2 [88, 89]. A proposed lipid extraction procedure using SHSs is illustrated in Figure 5. Briefly, SHSs are employed to dissolve or extract lipids in their hydrophobic state; the carbonated water is introduced to revert SHSs's hydrophilic form and form a two-phase of the lipid and SHSs/water; finally, the SHSs/water mixture would be separated into two components and then be reused by flushing air through [88].

4.2. Nile Red Lipid Visualization Method. Compared with the mostly used gravimetric methods noted above, Nile

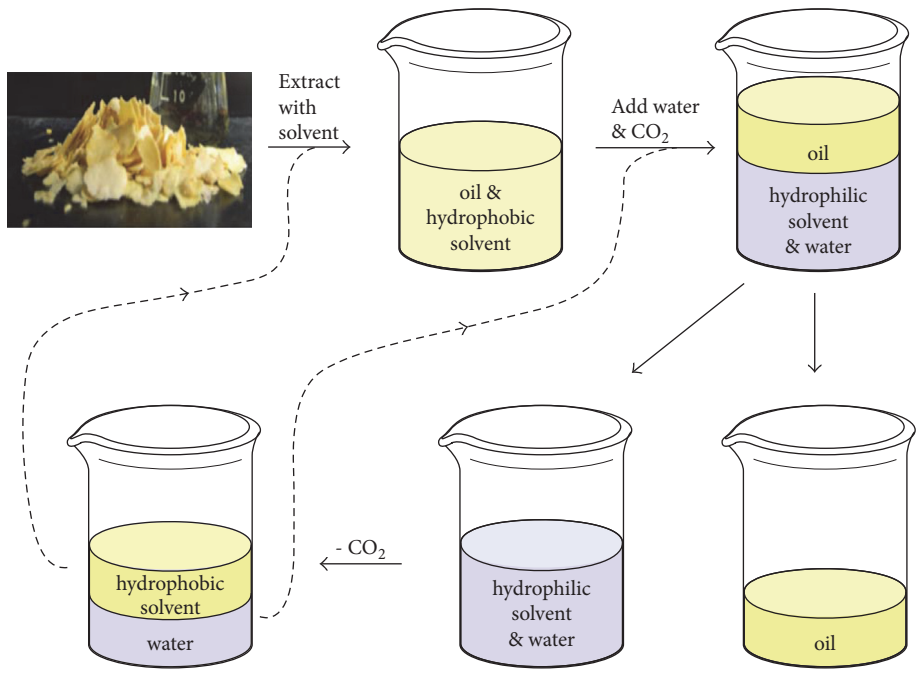

Figure 5: The process of SHSs used for soybean oil extraction from soybean flakes without a distillation step. The dashed lines indicate the recycling of the solvent and the aqueous phase [88].

red lipid visualization method is more convenient as the number of samples and preparation time are greatly reduced. The Nile red (9-diethylamino-5H-benzo[α]phenoxazine-5-one) is a lipid-soluble probe that fluoresces at the defined wavelengths depending upon the polarity of the surrounding medium. However, due to the composition and structure of the thick and rigid cell walls in some microalgae species, Nile red is prevented from penetrating the cell wall and cytoplasmic membrane, and therefore, lipids cannot provide the desired fluorescence. Thus, the dimethyl sulfoxide (DMSO) is introduced to microalgal samples as the stain carrier at an elevated temperature [63]. When microalgal lipids are measured by Nile red visualization method, a standard curve preparation is included in most cases. Table 3 summarizes some specific Nile red lipid procedures for the determination of microalgal lipids. Different solvents are combined with Nile red solution to stain microalgal culture samples, and the samples are diluted if necessary. The lipid content determination is achieved by comparing the resulting fluorescence values to a certain standard curve, in which the wavelength of excitation and emission may be different. Nevertheless, the lipid contents measured by this method are usually interfered by the environmental factors and other components in the cell cytoplasm, and the fluorescence intensity varies between samples. Thus, the optimal spectra and reaction conditions should be determined for each type of sample prior to the fluorescent measurement [90].

4.3. SPV Method. The colorimetric SPV method is a rapid alternative for lipid measurement because of its fast response and relative ease in sample handling [91]. The SPV reacts with lipids to produce a distinct pink color, and the intensity is quantified using spectrophotometric methods; therefore, it is employed for direct quantitative measurement of lipids within liquid microalgal cultures [40]. However, the results of SPV assay can be affected by lots of factors such as the degree of oil saturation, incubation time, heating, and cooling; thus the SPV assay may give misleading results [27].

The general procedure of SPV method includes the sample addition, solvent evaporation, sulfuric acid addition, samples incubation, color developing by adding phosphovanillin reagent, absorbance reading, and measurement of the lipid content based on the standard curve [62]. Phosphovanillin reagent is prepared by dissolving vanillin in absolute ethanol and DI water, followed by the addition of concentrated H_3PO_4. To prepare standard lipid stocks, canola oil is firstly added to chloroform, and then different amount of standard lipid stocks is added to the tubes. After that, these tubes are treated to evaporate the solvent followed by the addition of water. Subsequently, these samples are prepared by following SPV reaction methods: (1) suspend tested samples in water and place in a glass tube; (2) add concentrated sulfuric acid followed by heat treatment and ice bath; (3) add freshly prepared phosphovanillin reagent and incubate in incubator shaker; (4) read absorbance at 530 nm and determine the lipid content by comparing to the standard curve.

4.4. TLC Method. TLC is also a promising alternative to conventional lipids measurement approaches as it requires minimal equipment which is available in most laboratories, and it can also provide additional information about lipid classes, which is important for biofuel production [92]. Among different solvent systems, the multi-one-dimensional TLC (MOD-TLC) separates the lipid classes rapidly and

Table 3: Nile red assay procedures for the determination of microalgal lipids.

Reagent(s)	Nile red lipid assay procedure	Fluorescence determination	Ref.
Isopropyl alcohol (IPA); Nile red solution; bleach solution; methanol; corn oil (dissolved in 2 : 1 methanol/chloroform).	Suspend lipid extracts in chloroform; dilute extracts with methanol; add diluted samples and corn oil to the microplate to achieve a range; incubate the plate and evaporate the solvents; add IPA and cool the plate; add Nile red solution; add bleach solution to each well; incubate the plate.	Determine fluorescence using a plate reader with excitation set to 530 nm and emission set to 575 nm with a 570 nm cut-off; read the plate; use the first reading after the fluorescence peak for quantitation.	[27]
DMSO; Nile red solution; triolein.	Place microalgal cells in microcentrifuge tubes and put under microwave treatment; mix with DMSO; put under second microwave treatment using the previous conditions; add Nile red solution and incubate the tubes in the dark; pipet the samples into 96 well microplates.	Measure fluorescence using Fluorescence Analyzer with excitation at 535 nm and emission at 580 nm; measure untreated suspension and medium containing Nile red alone as autofluorescence; convert fluorescence to dry weight of lipids.	[28]
DMSO; Nile red solution; virgin olive oil.	Stain diluted microalgal culture samples with Nile red using DMSO as carrier; top up the volume and incubate with agitation.	Read the fluorescence using Microplate Reader with excitation set to 520 nm and emission captured at 570 nm; compare the fluorescence to a virgin olive oil standard curve.	[29, 30]
Pure triolein; chloroform; isopropanol; Nile red stock (in 100% spectral grade acetone).	*Standardized sample fluorescence*: add triolein to chloroform and dilute with isopropanol; prepare working standards by bringing intermediate stocks with DI water. *Nile red assay*: add Nile red to cell suspension or to a lipid standard.	Measure fluorescence using spectrophotofluorometer with excitation set to 475 nm and emission set to 580 nm; express cellular neutral lipid as triolein equivalents.	[31]

reproducibly. The MOD-TLC method can achieve the quantification for the majority of microalgal lipids through modifications in solvent mixtures and lengths of separation times, and the mass of each resolved lipid band is determined by comparing band intensities of unknown samples (visualized by the lipophilic dye primulin followed by an automated laser-fluorescence detector scanning) to dilution curves of authentic standards. Compared to two-dimensional thin-layer chromatography, MOD-TLC directly analyzes multiple samples on a single TLC plate, while still providing good resolution for the quantification of most major classes of lipid species [32]. Some TLC running procedures are introduced in detail (Table 4). Usually, TLC plates must be activated before TLC running, and NLs are separated by certain solvents such as a mixture of chloroform : methanol : acetic acid : water (85 : 12.5 : 12.5 : 3, v/v/v/v). The determination of microalgal lipid content is finally achieved by comparing the resulting fluorescence values with a standard curve.

5. Quantification for Microalgal Fatty Acids

The theoretical biofuel potentials of microalgal biomass are ultimately determined by the acyl chains of the lipids, and therefore the lipid contents are quantified as the sum of their fatty acid constituents. The fatty acids constituents vary with their structural features such as chain length, degree of saturation, branching of carbon chain, positional isomers, configuration of double bonds, or other chemical groups (i.e., hydroxy, epoxy, cyclo, and keto) [93]. It was reported that C16 and C18 are the most abundant microalgal fatty acids including palmitic acid (hexadecanoic, C16:0), stearic acid (octadecanoic, C18:0), oleic acid (octadecenoic, C18:1), linoleic acid (octadecadienoic, C18:2), and linolenic acid (octadecatrienoic, C18:3). The other fatty acids such as C14, C20, and C26–C32 are relatively in low concentrations [94].

Table 5 summarizes and compares different methods of the measurement and quantification of microalgal fatty acids. These methods consisted of two steps: (1) the preparation of FAMEs; (2) quantification and composition analysis of FAMEs by gas chromatography (GC). In the first step via the transesterification or in situ transesterification process, the triglycerides contained in algal lipids are reacted with methanol to produce FAMEs and glycerol. Catalysts (acid catalyst, base catalyst, or the mixture) and heat (water or oil bath) are usually required during the transesterification process to speed up the reaction. The common catalysts for this transesterification include NaOH [95], HCl [35], H_2SO_4 [37], acetyl chloride/methanol (1 : 10, v/v) [42], and a mixture of methanol, H_2SO_4, and chloroform (1.7 : 0.3 : 2.0, v/v/v) [47]. In the second step, the separation of FAMEs from the mixture and their quantification are performed using GC. The procedure noted above is based on the amount of fatty acids after the lipid extraction in algal biomass. Comparatively, the in situ transesterification is a relatively simpler process and achieves the transesterification to get FAMEs directly from the whole biomass with no requirement of lipid extraction. Therefore, it is able to obtain all fatty acids in the biomass and accurately represent the reflection of biofuels potential [49, 96]. In addition, various procedures for transesterification are followed in terms of microalgal species, lipid contents, and targeted FAMEs fraction. The specific transesterification procedures performed in literature are listed in Table 5. In brief, the lipid extracts or the algal biomass are mixed with the catalysts and methanol and are reacted at the conditions of high temperature. The produced FAMEs are then recovered in solvents like hexane for further purification and quantification. Subsequently, the purified FAMEs are separated and analyzed by GC equipped with the flame ionization detector (FID) and specific columns running at various temperatures. The identification and quantification standards are required such as the commercial 37-component standards, pentadecanoic acid, and heptadecanoic acid [40, 41, 47, 48, 97]. Specific FAMEs are quantified by comparing their peak areas with those of the standards. It should be noted that there is still not a routine method for the quantification of fatty acids specific to algal biomass issued by Association of Analytical Communities (AOAC) International. All the methods noted above vary significantly including the procedures, types of used chemicals and their doses, and analytical apparatus. This might result in a lack of comparability between FAMEs concentrations obtained from different methods.

6. Conclusion

Microalgae have proven to be one of the most promising feedstocks for the production of third-generation biofuels that are both economically feasible and environmentally sustainable. Rapid, accurate, sustainable, and cost-effective methods for the lipid extraction and quantification are essential for the rational application of microalgae-based biofuel production. Gravimetric method is most widely used but requires quite a few amount of samples; Nile red lipid visualization method is rapid as the number of samples and preparation time are greatly reduced while a correlation between fluorescence and lipid levels must be previously established as the cell staining varies among different microalgae species; the results of SPV assay can be affected by lots of factors such as the degree of oil saturation, incubation time, heating, and cooling; thus the SPV assay may give misleading results; in addition to the quantitative measurement of microalgal lipids, TLC can also provide additional information about lipid classes which is important for biofuel production. Various lipid quantification methods could be considered on a case-by-case basis, but more effective and greener techniques (e.g., CO_2-based methods) for microalgal cell disruption and extraction are still required to maximize lipid yields while avoiding the issues of toxicity, flammability, and time consumption for extraction. In addition, the identification and quantification of fatty acids in extracted lipids are also important to evaluate the quality of microalgae-derived biofuel, during which transesterification and in situ transesterification are involved in the preparation of FAMEs for the further the quantification and composition analysis of FAMEs by GC. It is worth mentioning that *in situ* transesterification is relatively simpler and more convenient as it does not require lipid extraction, thus achieving the transesterification to get FAMEs directly from the whole biomass.

Table 4: Processes of TLC running for the measurement of microalgal lipid content.

Preparation for TLC analysis	TLC analysis	Ref.
Prepare the solvent by shaking and degassing; add solvents to the TLC tank and equilibrate TLC tank.	Add samples to plates; dry the samples and run the plates in hexane : diethyl ether : acetone (60 : 40 : 5, v/v/v); dry plates and run in chloroform : methanol : ammonium hydroxide : water (60 : 35 : 4 : 1, v/v/v/v) to 18 cm; score plates and break apart with hand pressure; determine the line on a different plate or spray only the outside lane of the plate to be cut; rotate the lower portion by 180° and run in chloroform : methanol : acetic acid : water (85 : 12.5 : 12.5 : 3, v/v/v/v) in the original orientation; dry the plates and spray with a solution of primulin dye; visualize lipid spots and scan the plates by laser-excited fluorescent detection; quantify spots and compare to standard curves.	[32]
Elute silica gel with chloroform; elute lipids with chloroform to yield NLs; dry NLs and re-suspend in chloroform; activate plates in an oven.	Subject the NL fraction to TLC for lipid class separation and identification; use hexane/diethyl ether/acetic acid (70 : 30 : 1, v/v) for lipid separation; co-chromatography with pure standards; stain bands of lipid classes with 2, 7-dichlorofluorescein; visualize under UV light.	[33]
Elute silica gel with chloroform; elute lipids with chloroform to yield NLs; dry NLs and resuspend in chloroform; activate plates in an oven.	Use 80 : 20 : 1 hexane/diethyl ether/acetic acid for lipid separation; spray the plate with a solution of primulin dye; illuminate the plate with UV light.	[27, 32, 33]

Table 5: Methods employed for determining fatty acids after lipid extraction, including the transesterification and in situ transesterification. Both methods consist of the preparation of FAMEs and the quantification and composition analysis of FAMEs by GC.

Method	Preparation of FAMEs	GC operation	Standards used	Ref.
Transesterification	Redissolve total lipid extracts and elute neutral lipids and polar lipids with different solvents; after drying under nitrogen gas, derivatize to FAMEs and recover the FAMEs.	GC equipped with FID and Agilent CP-Wax 52 CB column.	(1) Internal standard: tripentadecanoin, C15:0 triacylglycerol, Sigma-Aldrich. (2) Identification and quantification standard: Supelco® 37-component standards.	[34]
	Add HCl and methanol to lipid extracts and heat mixture with hexane and methyl-tert-butyl ether; wash the upper organic phase with sodium hydroxide; aspirate two-thirds of the organic extracts and transfer to a sample vial.	GC equipped with FID and a special performance capillary column (Hewlett Packard model #HP-5 MS).	(1) Internal standard: hexadecane (Sigma-Aldrich #H6703) standard. (2) Calibration standard: olive oil.	[35, 36]
	Add H_2SO_4 to lipid extracts and heat; cool the sample to room temperature and mix with DI water to separate lipid extracts; move the lower part liquid into a vial.	GC equipped with FID and a Supelco NucolTM column (355 33-03A, film thickness) using Helium as the carrier gas (flow 20 mL·min^{-1}).	(1) Internal standard: pentadecanoic acid (C15:0). (2) Identification standard: authentic standards (Sigma-Aldrich, MO, USA).	[37, 38]
	Add methanolic HCl to lipid extracts and flush headspace with nitrogen and seal tightly and heat; cool vials and add aqueous K_2CO_3; centrifuge and remove the upper phase and dry.	GC equipped with FID and a SGE Sol Gel-WaxTM capillary column using helium as the carrier gas.	(1) Identification standard: standard fatty acids (Nu-Chek Prep Inc., Elysian, MN). (2) Quantification standard: heptadecanoic acid (C17:0).	[39]
	Add chloroform containing heptadecanoic acid (C17:0), methanol, and sulfuric acid to each tube and heat; cool down, add DI, centrifuge, and separate the lower chloroform phase and filter for test.	GC equipped with FID and HP19091N-213 HP-INNOWax polyethylene glycol column.	(1) Internal standard: heptadecanoic acid (C17:0). (2) Identification and quantification standard: 37 component FAME standard mix (Supelco, Bellefonte, USA).	[40]
	Add BHT (butulated hydroxy toluene, 1% in methanol) to prevent oxidation prior to methylation.	GC equipped with FID and the capillary column DB-23 (Agilent Technologies) using helium as the carrier gas (1 mL·min^{-1}, splitless).	(1) Quantification standard: C19:0 (nonadecanoic Acid 72332-1 G-F/analytical standard, Sigma-Aldrich). (2) Identification standard: Supelco TM 37 Component FAME Mix, Sigma.	[41]
	Add freshly prepared acetyl chloride/methanol (1 : 10), methanol into lipid extracts, and seal vials and heat; cool down and add K_2CO_3, hexane; centrifuge the samples and recover the hexane supernatant.	GC equipped with FID and a BPX70 capillary column (120 m × 0.25 mm internal diameter, 0.25 μm film thickness, SGE Analytical Science, Ringwood, VIC, Australia) using helium as carrier gas (1.5 mL·min^{-1}).	(1) Internal standard: C23:0. (2) Identification standard: a series of mixed and individual standards from Sigma-Aldrich.	[42, 43]
	Mix H_2SO_4, methanol, THF, and lipid extracts; reflux the reaction mixture at 90°C with continuous stirring for 3 h; neutralize the mixture with $NaHCO_3$ and extract it with hexane.	GC equipped with FID and HP-INNOWax column (30 m × 320 μm × 0.25 μm film of polyethylene glycol) using helium as carrier gas.	(1) The standard FAMES: C14:0, C16:0, C16:3, C18:0, C18:1, C18:2, C18:3, and C20:0. (2) Supelco TM 37 Component FAME Mix, Sigma-Aldrich.	
	Treat extracted lipids with methanolic sulfuric acid and heat; recover FAMEs in hexane; centrifuge the suspension and aspirate hexane, containing FAMEs, into new glass tube.	GC equipped with DB-5 capillary column (30 mm : 0.25 mm : 1 μm) and FID using helium as carrier gas (1 mL·min^{-1}).	NISTIL.S database.	[44–46]

Table 5: Continued.

Method	Preparation of FAMEs	GC operation	Standards used	Ref.
In situ transesterification	Add a mixture of methanol, sulfuric acid, and chloroform into dried cell biomass and heptadecanoic acid (C17:0) as an internal standard and heat; cool down, add DI water, mix, and settle; transfer the lower phase containing FAMEs to a clean vial and dry with anhydrous Na_2SO_4.	GC equipped with FID and SGE Sol Gel-WaxTM capillary column (30 m × 0.25 mm × 0.25 μm) using helium as the carrier gas.	(1) Identification standard: standard fatty acids (Sigma, MO). (2) Quantification standard: internal standard (C17:0).	[47, 48]
	There are many different ways to add a catalyst, such as methanolic hydrogen chloride, NaOMe and BF_3, NaOMe, and tetramethyl guanidine and methanol; tridecanoic acid methyl ester (C13-FAME) as an internal standard and heat.	GC equipped with FID (Agilent 6890N, HP 5-MS column (Agilent, USA), 30 m 0.25 mm ID and 0.25 μm FT) using helium as the carrier gas (1.5 mL·min^{-1}).	(1) C8–C24, SIGMA cat #18918 C13–C21, SIGMA cat #1896.	[49]

Note. (1) All samples prepared for FAMEs contain the corresponding internal standards that have been listed in the table above. (2) FID: flame ionization detector.

Conflicts of Interest

The authors declare that they have no conflicts of interest.

Acknowledgments

The authors would like to graciously acknowledge the National Natural Science Foundation of China (51708294), the Fundamental Research Funds for the Central Universities (30918011306 and 30918011308), and Research Start-Up Grant of NJUST for the funding and support provided for this research.

References

[1] S. Shafiee and E. Topal, "When will fossil fuel reserves be diminished?" *Energy Policy*, vol. 37, no. 1, pp. 181–189, 2009.

[2] Y. Chisti, "Biodiesel from microalgae," *Biotechnology Advances*, vol. 25, no. 3, pp. 294–306, 2007.

[3] A. Demirbas and M. F. Demirbas, "Importance of algae oil as a source of biodiesel," *Energy Conversion and Management*, vol. 52, no. 1, pp. 163–170, 2011.

[4] Y. Li, S. Lian, D. Tong et al., "One-step production of biodiesel from Nannochloropsis sp. on solid base Mg-Zr catalyst," *Applied Energy*, vol. 88, no. 10, pp. 3313–3317, 2011.

[5] I. Hariskos and C. Posten, "Biorefinery of microalgae - opportunities and constraints for different production scenarios," *Biotechnology Journal*, vol. 9, no. 6, pp. 739–752, 2014.

[6] M. R. Tredici, "Photobiology of microalgae mass cultures: Understanding the tools for the next green revolution," *Biofuels*, vol. 1, no. 1, pp. 143–162, 2010.

[7] S. Ge, P. Champagne, W. C. Plaxton, G. B. Leite, and F. Marazzi, "Microalgal cultivation with waste streams and metabolic constraints to triacylglycerides accumulation for biofuel production," *Biofuels, Bioproducts and Biorefining*, vol. 11, no. 2, pp. 325–343, 2017.

[8] S. Ge and P. Champagne, "Nutrient removal, microalgal biomass growth, harvesting and lipid yield in response to centrate wastewater loadings," *Water Research*, vol. 88, pp. 604–612, 2016.

[9] E. Sforza, R. Cipriani, T. Morosinotto, A. Bertucco, and G. M. Giacometti, "Excess CO 2 supply inhibits mixotrophic growth of Chlorella protothecoides and Nannochloropsis salina," *Bioresource Technology*, vol. 104, pp. 523–529, 2012.

[10] S. Ge, M. Agbakpe, Z. Wu, L. Kuang, W. Zhang, and X. Wang, "Influences of surface coating, UV irradiation and magnetic field on the algae removal using magnetite nanoparticles," *Environmental Science & Technology*, vol. 49, no. 2, pp. 1190–1196, 2015.

[11] S. Ge, M. Agbakpe, W. Zhang, and L. Kuang, "Heteroaggregation between PEI-coated magnetic nanoparticles and algae: Effect of particle size on algal harvesting efficiency," *ACS Applied Materials & Interfaces*, vol. 7, no. 11, pp. 6102–6108, 2015.

[12] S. Ge, P. Champagne, H. Wang, P. G. Jessop, and M. F. Cunningham, "Microalgae Recovery from Water for Biofuel Production Using CO2-Switchable Crystalline Nanocellulose," *Environmental Science & Technology*, vol. 50, no. 14, pp. 7896–7903, 2016.

[13] A. Steriti, R. Rossi, A. Concas, and G. Cao, "A novel cell disruption technique to enhance lipid extraction from microalgae," *Bioresource Technology*, vol. 164, pp. 70–77, 2014.

[14] I. A. Guschina and J. L. Harwood, "Complex lipid biosynthesis and its manipulation in plants," *Improvement of Crop Plants for Industrial End Uses*, pp. 253–279, 2007.

[15] R. Halim, M. K. Danquah, and P. A. Webley, "Extraction of oil from microalgae for biodiesel production: a review," *Biotechnology Advances*, vol. 30, no. 3, pp. 709–732, 2012.

[16] M. A. Borowitzka and N. R. Moheimani, "Algae for biofuels and energy," *Algae for Biofuels and Energy*, pp. 1–288, 2013.

[17] T. M. Mata, A. A. Martins, and N. S. Caetano, "Microalgae for biodiesel production and other applications: a review," *Renewable & Sustainable Energy Reviews*, vol. 14, no. 1, pp. 217–232, 2010.

[18] J. Kim, G. Yoo, H. Lee et al., "Methods of downstream processing for the production of biodiesel from microalgae," *Biotechnology Advances*, vol. 31, no. 6, pp. 862–876, 2013.

[19] R. Ranjith Kumar, P. Hanumantha Rao, and M. Arumugam, "Lipid Extraction Methods from Microalgae: A Comprehensive Review," *Frontiers in Energy Research*, vol. 2, 2015.

[20] A. K. Lee, D. M. Lewis, and P. J. Ashman, "Disruption of microalgal cells for the extraction of lipids for biofuels: Processes and specific energy requirements," *Biomass & Bioenergy*, vol. 46, pp. 89–101, 2012.

[21] S. O. Kotchoni, E. W. Gachomo, K. Slobodenko, and D. H. Shain, "AMP deaminase suppression increases biomass, cold tolerance and oil content in green algae," *Algal Research*, vol. 16, pp. 473–480, 2016.

[22] Y. Li, M. Horsman, B. Wang, N. Wu, and C. Q. Lan, "Effects of nitrogen sources on cell growth and lipid accumulation of green alga *Neochloris oleoabundans*," *Applied Microbiology and Biotechnology*, vol. 81, no. 4, pp. 629–636, 2008.

[23] W. Zhang, Y. Zhao, B. Cui, H. Wang, and T. Liu, "Evaluation of filamentous green algae as feedstocks for biofuel production," *Bioresource Technology*, vol. 220, pp. 407–413, 2016.

[24] A. Mehrabadi, M. M. Farid, and R. Craggs, "Effect of CO2 addition on biomass energy yield in wastewater treatment high rate algal mesocosms," *Algal Research*, vol. 22, pp. 93–103, 2017.

[25] Q. Lu, W. Zhou, M. Min et al., "Mitigating ammonia nitrogen deficiency in dairy wastewaters for algae cultivation," *Bioresource Technology*, vol. 201, pp. 33–40, 2016.

[26] A. Silkina, M.-P. Zacharof, G. Hery, T. Nouvel, and R. W. Lovitt, "Formulation and utilisation of spent anaerobic digestate fluids for the growth and product formation of single cell algal cultures in heterotrophic and autotrophic conditions," *Bioresource Technology*, vol. 244, pp. 1445–1455, 2017.

[27] B. T. Higgins, A. Thornton-Dunwoody, J. M. Labavitch, and J. S. Vandergheynst, "Microplate assay for quantitation of neutral lipids in extracts from microalgae," *Analytical Biochemistry*, vol. 465, pp. 81–89, 2014.

[28] A. E. M. Abdelaziz, G. B. Leite, M. A. Belhaj, and P. C. Hallenbeck, "Screening microalgae native to Quebec for wastewater treatment and biodiesel production," *Bioresource Technology*, vol. 157, pp. 140–148, 2014.

[29] Y.-Z. Wang, P. C. Hallenbeck, G. B. Leite, K. Paranjape, and D.-Q. Huo, "Growth and lipid accumulation of indigenous algal strains under photoautotrophic and mixotrophic modes at low temperature," *Algal Research*, vol. 16, pp. 195–200, 2016.

[30] G. B. Leite, K. Paranjape, A. E. M. Abdelaziz, and P. C. Hallenbeck, "Utilization of biodiesel-derived glycerol or xylose for increased growth and lipid production by indigenous microalgae," *Bioresource Technology*, vol. 184, pp. 123–130, 2015.

[31] J. C. Priscu, L. R. Priscu, A. C. Palmisano, and C. W. Sullivan, "Estimation of neutral lipid levels in antarctic sea ice microalgae by nile red fluorescence," *Antarctic Science*, vol. 2, no. 2, pp. 149–155, 1986.

[32] T. White, S. Bursten, D. Federighi, R. A. Lewis, and E. Nudelman, "High-resolution separation and quantification of neutral lipid and phospholipid species in mammalian cells and sera by multi-one-dimensional thin-layer chromatography," *Analytical Biochemistry*, vol. 258, no. 1, pp. 109–117, 1998.

[33] J. Liu, J. Huang, Z. Sun, Y. Zhong, Y. Jiang, and F. Chen, "Differential lipid and fatty acid profiles of photoautotrophic and heterotrophic Chlorella zofingiensis: Assessment of algal oils for biodiesel production," *Bioresource Technology*, vol. 102, no. 1, pp. 106–110, 2011.

[34] C. J. Hulatt, O. Berecz, E. S. Egeland, R. H. Wijffels, and V. Kiron, "Polar snow algae as a valuable source of lipids?" *Bioresource Technology*, vol. 235, pp. 338–347, 2017.

[35] S. N. Genin, J. Stewart Aitchison, and D. Grant Allen, "Design of algal film photobioreactors: Material surface energy effects on algal film productivity, colonization and lipid content," *Bioresource Technology*, vol. 155, pp. 136–143, 2014.

[36] I. Smid and M. Salfinger, "Mycobacterial identification by computer-aided gas-liquid chromatography," *Diagnostic Microbiology And Infectious Disease*, vol. 19, no. 2, pp. 81–88, 1994.

[37] H.-M. Pham, H. S. Kwak, M.-E. Hong, J. Lee, W. S. Chang, and S. J. Sim, "Development of an X-Shape airlift photobioreactor for increasing algal biomass and biodiesel production," *Bioresource Technology*, vol. 239, pp. 211–218, 2017.

[38] A. M. Santos, M. Janssen, P. P. Lamers, W. A. C. Evers, and R. H. Wijffels, "Growth of oil accumulating microalga Neochloris oleoabundans under alkaline-saline conditions," *Bioresource Technology*, vol. 104, pp. 593–599, 2012.

[39] D. J. Pyle, R. A. Garcia, and Z. Wen, "Producing docosahexaenoic acid (DHA)-rich algae from biodiesel-derived crude glycerol: Effects of impurities on DHA production and algal biomass composition," *Journal of Agricultural and Food Chemistry*, vol. 56, no. 11, pp. 3933–3939, 2008.

[40] S. K. Mishra, W. I. Suh, W. Farooq et al., "Rapid quantification of microalgal lipids in aqueous medium by a simple colorimetric method," *Bioresource Technology*, vol. 155, pp. 330–333, 2014.

[41] M. Tossavainen, A. Nykänen, K. Valkonen, A. Ojala, S. Kostia, and M. Romantschuk, "Culturing of Selenastrum on diluted composting fluids; conversion of waste to valuable algal biomass in presence of bacteria," *Bioresource Technology*, vol. 238, pp. 205–213, 2017.

[42] N. D. Q. Duy, D. S. Francis, and P. C. Southgate, "The nutritional value of live and concentrated micro-algae for early juveniles of sandfish, Holothuria scabra," *Aquaculture*, vol. 473, pp. 97–104, 2017.

[43] J. A. Conlan, P. L. Jones, G. M. Turchini, M. R. Hall, and D. S. Francis, "Changes in the nutritional composition of captive early-mid stage Panulirus ornatus phyllosoma over ecdysis and larval development," *Aquaculture*, vol. 434, pp. 159–170, 2014.

[44] N. Arora, A. Patel, P. A. Pruthi, and V. Pruthi, "Recycled de-Oiled algal biomass extract as a feedstock for boosting biodiesel production from chlorella minutissima," *Applied Biochemistry and Biotechnology*, vol. 180, no. 8, pp. 1534–1541, 2016.

[45] N. Arora, A. Patel, P. A. Pruthi, and V. Pruthi, "Synergistic dynamics of nitrogen and phosphorous influences lipid productivity in Chlorella minutissima for biodiesel production," *Bioresource Technology*, vol. 213, pp. 79–87, 2015.

[46] P. Jain, N. Arora, J. Mehtani, V. Pruthi, and C. B. Majumder, "Pretreated algal bloom as a substantial nutrient source for microalgae cultivation for biodiesel production," *Bioresource Technology*, vol. 242, pp. 152–160, 2017.

[47] Z. Chi, D. Pyle, Z. Wen, C. Frear, and S. Chen, "A laboratory study of producing docosahexaenoic acid from biodiesel-waste glycerol by microalgal fermentation," *Process Biochemistry*, vol. 42, no. 11, pp. 1537–1545, 2007.

[48] E. Indarti, M. I. A. Majid, R. Hashim, and A. Chong, "Direct FAME synthesis for rapid total lipid analysis from fish oil and cod liver oil," *Journal of Food Composition and Analysis*, vol. 18, no. 2-3, pp. 161–170, 2005.

[49] L. M. L. Laurens, M. Quinn, S. Van Wychen, D. W. Templeton, and E. J. Wolfrum, "Accurate and reliable quantification of total microalgal fuel potential as fatty acid methyl esters by in situ transesterification," *Analytical and Bioanalytical Chemistry*, vol. 403, no. 1, pp. 167–178, 2012.

[50] S. Balasubramanian, J. D. Allen, A. Kanitkar, and D. Boldor, "Oil extraction from Scenedesmus obliquus using a continuous microwave system - design, optimization, and quality characterization," *Bioresource Technology*, vol. 102, no. 3, pp. 3396–3403, 2011.

[51] F. Amarni and H. Kadi, "Kinetics study of microwave-assisted solvent extraction of oil from olive cake using hexane. Comparison with the conventional extraction," *Innovative Food Science and Emerging Technologies*, vol. 11, no. 2, pp. 322–327, 2010.

[52] A. F. Ferreira, A. P. S. Dias, C. M. Silva, and M. Costa, "Effect of low frequency ultrasound on microalgae solvent extraction: Analysis of products, energy consumption and emissions," *Algal Research*, vol. 14, pp. 9–16, 2016.

[53] K. S. Suslick and D. J. Flannigan, "Inside a collapsing bubble: Sonoluminescence and the conditions during cavitation," *Annual Review of Physical Chemistry*, vol. 59, pp. 659–683, 2008.

[54] F. Adam, M. Abert-Vian, G. Peltier, and F. Chemat, "'Solvent-free' ultrasound-assisted extraction of lipids from fresh microalgae cells: a green, clean and scalable process," *Bioresource Technology*, vol. 114, pp. 457–465, 2012.

[55] M. S. Doulah, "Mechanism of disintegration of biological cells in ultrasonic cavitation," *Biotechnology and Bioengineering*, vol. 19, no. 5, pp. 649–660, 1977.

[56] R. Halim, A. Hosikian, S. Lim, and M. K. Danquah, "Chlorophyll extraction from microalgae: A review on the process engineering aspects," *International Journal of Chemical Engineering*, Article ID 391632, 2010.

[57] M. Vaara, "Agents that increase the permeability of the outer membrane," *Microbiology and Molecular Biology Reviews*, vol. 56, no. 3, pp. 395–411, 1992.

[58] A. Sathish and R. C. Sims, "Biodiesel from mixed culture algae via a wet lipid extraction procedure," *Bioresource Technology*, vol. 118, pp. 643–647, 2012.

[59] M. Demuez, A. Mahdy, E. Tomás-Pejó, C. González-Fernández, and M. Ballesteros, "Enzymatic cell disruption of microalgae biomass in biorefinery processes," *Biotechnology and Bioengineering*, vol. 112, no. 10, pp. 1955–1966, 2015.

[60] A. Zuorro, G. Maffei, and R. Lavecchia, "Optimization of enzyme-assisted lipid extraction from Nannochloropsis microalgae," *Journal of the Taiwan Institute of Chemical Engineers*, vol. 67, pp. 106–114, 2016.

[61] K. Kita, S. Okada, H. Sekino, K. Imou, S. Yokoyama, and T. Amano, "Thermal pre-treatment of wet microalgae harvest for efficient hydrocarbon recovery," *Applied Energy*, vol. 87, no. 7, pp. 2420–2423, 2010.

[62] Y.-S. Cheng, Y. Zheng, and J. S. VanderGheynst, "Rapid quantitative analysis of lipids using a colorimetric method in a microplate format," *Lipids*, vol. 46, no. 1, pp. 95–103, 2011.

[63] W. Chen, C. Zhang, L. Song, M. Sommerfeld, and Q. Hu, "A high throughput Nile red method for quantitative measurement of neutral lipids in microalgae," *Journal of Microbiological Methods*, vol. 77, no. 1, pp. 41–47, 2009.

[64] I. R. Sitepu, L. Ignatia, A. K. Franz et al., "An improved high-throughput Nile red fluorescence assay for estimating intracellular lipids in a variety of yeast species," *Journal of Microbiological Methods*, vol. 91, no. 2, pp. 321–328, 2012.

[65] Y. Tang, Y. Zhang, J. N. Rosenberg, N. Sharif, M. J. Betenbaugh, and F. Wang, "Efficient lipid extraction and quantification of fatty acids from algal biomass using accelerated solvent extraction (ASE)," *RSC Advances*, vol. 6, no. 35, pp. 29127–29134, 2016.

[66] L. Lardon, A. Helias, B. Sialve, J. P. Steyer, and O. Bernard, "Life-cycle assessment of biodiesel production from microalgae," *Environmental Science & Technology*, vol. 43, no. 17, pp. 6475–6481, 2009.

[67] P. Mercer and R. E. Armenta, "Developments in oil extraction from microalgae," *European Journal of Lipid Science and Technology*, vol. 113, no. 5, pp. 539–547, 2011.

[68] R. L. Mendes, A. D. Reis, and A. F. Palavra, "Supercritical CO_2 extraction of γ-linolenic acid and other lipids from *Arthrospira* (*Spirulina*)*maxima*: comparison with organic solvent extraction," *Food Chemistry*, vol. 99, no. 1, pp. 57–63, 2006.

[69] G. Andrich, U. Nesti, F. Venturi, A. Zinnai, and R. Fiorentini, "Supercritical fluid extraction of bioactive lipids from the microalga *Nannochloropsis* sp.," *European Journal of Lipid Science and Technology*, vol. 107, no. 6, pp. 381–386, 2005.

[70] C. Crampon, A. Mouahid, S.-A. A. Toudji, O. Lépine, and E. Badens, "Influence of pretreatment on supercritical CO2 extraction from Nannochloropsis oculata," *The Journal of Supercritical Fluids*, vol. 79, pp. 337–344, 2013.

[71] A. Mouahid, C. Crampon, S.-A. A. Toudji, and E. Badens, "Supercritical CO2 extraction of neutral lipids from microalgae: Experiments and modelling," *The Journal of Supercritical Fluids*, vol. 77, pp. 7–16, 2013.

[72] R. Halim, B. Gladman, M. K. Danquah, and P. A. Webley, "Oil extraction from microalgae for biodiesel production," *Bioresource Technology*, vol. 102, no. 1, pp. 178–185, 2011.

[73] L. Soh and J. Zimmerman, "Biodiesel production: The potential of algal lipids extracted with supercritical carbon dioxide," *Green Chemistry*, vol. 13, no. 6, pp. 1422–1429, 2011.

[74] B.-C. Liau, C.-T. Shen, F.-P. Liang et al., "Supercritical fluids extraction and anti-solvent purification of carotenoids from microalgae and associated bioactivity," *The Journal of Supercritical Fluids*, vol. 55, no. 1, pp. 169–175, 2010.

[75] A. Paudel, M. J. Jessop, S. H. Stubbins, P. Champagne, and P. G. Jessop, "Extraction of lipids from microalgae using CO2-expanded methanol and liquid CO2," *Bioresource Technology*, vol. 184, pp. 286–290, 2015.

[76] B. Subramaniam, R. V. Chaudhari, A. S. Chaudhari, G. R. Akien, and Z. Xie, "Supercritical fluids and gas-expanded liquids as tunable media for multiphase catalytic reactions," *Chemical Engineering Science*, vol. 115, pp. 3–18, 2014.

[77] P. G. Jessop and B. Subramaniam, "Gas-expanded liquids," *Chemical Reviews*, vol. 107, no. 6, pp. 2666–2694, 2007.

[78] H.-C. Wang, W. Klinthong, Y.-H. Yang, and C.-S. Tan, "Continuous extraction of lipids from Schizochytrium sp. by CO2-expanded ethanol," *Bioresource Technology*, vol. 189, pp. 162–168, 2015.

[79] B. Subramaniam and G. R. Akien, "Sustainable catalytic reaction engineering with gas-expanded liquids," *Current Opinion in Chemical Engineering*, vol. 1, no. 3, pp. 336–341, 2012.

[80] Y.-H. Yang, W. Klinthong, and C.-S. Tan, "Optimization of continuous lipid extraction from Chlorella vulgaris by CO2-expanded methanol for biodiesel production," *Bioresource Technology*, vol. 198, pp. 550–556, 2015.

[81] S. Wahidin, A. Idris, and S. R. M. Shaleh, "Ionic liquid as a promising biobased green solvent in combination with microwave irradiation for direct biodiesel production," *Bioresource Technology*, vol. 206, pp. 150–154, 2016.

[82] Y. Chisti, "Biodiesel from microalgae beats bioethanol," *Trends in Biotechnology*, vol. 26, no. 3, pp. 126–131, 2008.

[83] R. E. Teixeira, "Energy-efficient extraction of fuel and chemical feedstocks from algae," *Green Chemistry*, vol. 14, no. 2, pp. 419–427, 2012.

[84] K. Gao, V. Orr, and L. Rehmann, "Butanol fermentation from microalgae-derived carbohydrates after ionic liquid extraction," *Bioresource Technology*, vol. 206, pp. 77–85, 2016.

[85] P. G. Jessop, D. J. Heldebrant, X. Li, C. A. Eckertt, and C. L. Liotta, "Green chemistry: Reversible nonpolar-to-polar solvent," *Nature*, vol. 436, no. 7054, p. 1102, 2005.

[86] P. G. Jessop, "Switchable solvents as media for synthesis and separations: An update from the co-creator of GreenCentre Canada," *Aldrichimica Acta*, vol. 48, no. 1, pp. 18–21, 2015.

[87] V. C. A. Orr and L. Rehmann, "Ionic liquids for the fractionation of microalgae biomass," *Current Opinion in Green and Sustainable Chemistry*, vol. 2, pp. 22–27, 2016.

[88] P. G. Jessop, L. Phan, A. Carrier, S. Robinson, C. J. Dürr, and J. R. Harjani, "A solvent having switchable hydrophilicity," *Green Chemistry*, vol. 12, no. 5, pp. 809–814, 2010.

[89] P. G. Jessop, L. Kozycz, Z. G. Rahami et al., "Tertiary amine solvents having switchable hydrophilicity," *Green Chemistry*, vol. 13, no. 3, pp. 619–623, 2011.

[90] G. H. Huang, G. Chen, and F. Chen, "Rapid screening method for lipid production in alga based on Nile red fluorescence," *Biomass & Bioenergy*, vol. 33, no. 10, pp. 1386–1392, 2009.

[91] L. S. Inouye and G. R. Lotufo, "Comparison of macro-gravimetric and micro-colorimetric lipid determination methods," *Talanta*, vol. 70, no. 3, pp. 584–587, 2006.

[92] B. Fuchs, R. Süß, K. Teuber, M. Eibisch, and J. Schiller, "Lipid analysis by thin-layer chromatography—a review of the current state," *Journal of Chromatography A*, vol. 1218, no. 19, pp. 2754–2774, 2011.

[93] P. Pesaresi, J. S. Amthor, G. Mandolino, and etal., *Improvement of Crop Plants for Industrial End Uses*, Springer, Netherlands, 2007.

[94] H. Liu and W. Liu, "Concentration and distributions of fatty acids in algae, submerged plants and terrestrial plants from the northeastern Tibetan Plateau," *Organic Geochemistry*, vol. 113, pp. 17–26, 2017.

[95] V. Kumar, M. Muthuraj, B. Palabhanvi, A. K. Ghoshal, and D. Das, "Evaluation and optimization of two stage sequential in situ transesterification process for fatty acid methyl ester quantification from microalgae," *Journal of Renewable Energy*, vol. 68, pp. 560–569, 2014.

[96] S. Van Wychen, K. Ramirez, and L. M. Laurens, *Determination of Total Lipids as Fatty Acid Methyl Esters (FAME) by In Situ Transesterification*, Laboratory Analytical Procedure (LAP), National Renewable Energy Laboratory (NREL), Golden, Colo, USA, 2013.

[97] G. Knothe, "Improving biodiesel fuel properties by modifying fatty ester composition," *Energy & Environmental Science*, vol. 2, no. 7, pp. 759–766, 2009.

Hindawi
BioMed Research International
Volume 2018, Article ID 9192607, 10 pages
https://doi.org/10.1155/2018/9192607

Research Article

Effect of Free Nitrous Acid on Nitrous Oxide Production and Denitrifying Phosphorus Removal by Polyphosphorus-Accumulating Organisms in Wastewater Treatment

Zhijia Miao,[1,2,3,4] **Duo Li**,[1,2,3,4] **Shan Guo**,[1,2,3,4] **Zhirui Zhao**,[1,2,3,4] **Xiaofeng Fang**,[1,2,3,4] **Xueyou Wen**,[1,2,3,4] **Jingmin Wan**,[1,2,3,4] **and Aiguo Li**[1,2,3,4]

[1]*School of Water Resources and Environment, Hebei GEO University, Shijiazhuang 050031, China*
[2]*Hebei Province Key Laboratory of Sustained Utilization and Development of Water Resources, Shijiazhuang 050031, China*
[3]*Hebei Province Collaborative Innovation Center for Sustainable Utilization of Water Resources and Optimization of Industrial Structure, Shijiazhuang 050031, China*
[4]*Research Center of Natural Resources Assets, Hebei GEO University, Shijiazhuang 050031, China*

Correspondence should be addressed to Zhijia Miao; zhijia_miao@163.com

Received 28 December 2017; Accepted 18 March 2018; Published 26 April 2018

Academic Editor: Joseph Usack

The inhibition of free nitrous acid (FNA) on denitrifying phosphorus removal has been widely reported for enhanced biological phosphorus removal; however, few studies focus on the nitrous oxide (N_2O) production involved in this process. In this study, the effects of FNA on N_2O production and anoxic phosphorus metabolism were investigated using phosphorus-accumulating organisms (PAOs) culture highly enriched (91 ± 4%) in *Candidatus Accumulibacter phosphatis*. Results show that the FNA concentration notably inhibited anoxic phosphorus metabolism and phosphorus uptake. Poly-β-hydroxyalkanoate (PHA) degradation was completely inhibited when the FNA concentration was approximately 0.0923 mgHNO_2-N/L. Higher initial FNA concentrations (0.00035 to 0.0103 mgHNO_2-N/L) led to more PHA consumption/TN (0.444 to 0.916 mmol-C/(mmol-N·gVSS)). Moreover, it was found that FNA, rather than nitrite and pH, was likely the true inhibitor of N_2O production. The highest proportion of N_2O to TN was 78.42% at 0.0031 mgHNO_2-N/L (equivalent to 42.44 mgNO_2-N/L at pH 7.5), due to the simultaneous effects of FNA on the subsequent conversion of NO_2 into N_2O and then into N_2. The traditional nitrite knee point can only indicate the exhaustion of nitrite, instead of the complete removal of TN.

1. Introduction

Enhanced biological phosphorus removal (EBPR), operated with sequential anaerobic and aerobic periods, is considered as an efficient method for phosphorus removal. A group of bacteria known as polyphosphate-accumulating organisms (PAOs) are able to take up volatile fatty acids (VFAs) and store them as poly-β-hydroxyalkanoates (PHAs), which has been attributed to phosphorus release during the anaerobic phase. In the subsequent aerobic phase, PAOs use the stored PHA as an energy source for biomass growth and take up orthophosphate into polyphosphate (poly-p). Finally, phosphorus is removed from the system through the wastage of excess sludge. Phosphorus uptake also occurs under anoxic conditions. Previous studies have identified a subset of PAOs, known as denitrifying phosphorus-accumulating organisms (DPAOs), which can also denitrify and are able to oxidize intracellular PHA for energy and nitrite or nitrate as electronic acceptors, instead of oxygen, to remove phosphorus [1–3]. Compared to conventional biological nitrogen and phosphorus removal, DPAOs can take up a carbon source during the anaerobic phase, which could be used for both denitrification and phosphorus removal. Thus, the DPAO pathway is advantageous for the treatment of wastewater containing a relatively low level of organic carbon, while requiring less oxygen and resulting in lower sludge production.

N_2O, which is a significant greenhouse gas, has 300 times greater warming potential than CO_2 (IPCC, 2001). Most research on the pathway of nitrification, denitrification, and phosphorus removal has been conducted that N_2O was produced in wastewater treatment systems. The production of N_2O may be affected by many parameters, such as low dissolved oxygen concentrations, accumulation of nitrite, types of organic carbon sources, pH, and temperature [4, 5]. It has been frequently reported that the accumulation of nitrite leads to increased N_2O emission, rather than N_2, as the major end-product in the denitrifying phosphorus removal processes [6, 7]. Zhou et al. showed that free nitrous acid (FNA), rather than nitrite or pH, is likely the true inhibitor of N_2O reduction by DPAOs [8]. Wang et al. also observed the inhibitory effect of FNA on the N_2O reduction activity in a denitrifying phosphorus removal system [9]. These results indicate that FNA is associated with denitrifying phosphorus removal and N_2O production.

The level of the FNA can also affect the anoxic or aerobic phosphorus metabolism of PAOs. Zhou et al. reported that the concentration of FNA influenced the efficiency of anoxic phosphorus uptake. Specifically, the PAO uptake process was inhibited at lower FNA levels (<0.002 mg HNO_2-N/L) and ceased at an FNA concentration of 0.02 mg HNO_2-N/L [10]. It was found that FNA inhibited all key aerobic metabolic processes performed by a culture highly enriched (90 ± 5%) in *Candidatus Accumulibacter phosphatis* [11]. In contrast, some studies revealed that PAOs could acclimate to nitrite as the sole electron acceptor without experiencing inhibition [12, 13].

Most studies in this field have taken great efforts to understand the key roles of FNA in the metabolic processes of PAOs. Previous research has shown that N_2O production accompanies denitrifying phosphorus removal; however, little attention has been given to the effect of nitrite/FNA on N_2O production by highly enriched PAOs. The PAOs, named *Candidatus Accumulibacter phosphatis*, are dominant in both lab-scale EBPR reactors and full-scale wastewater treatment plants (WWTPs) [14–17]. If PAOs contribute to N_2O emission, we cannot ignore their role in WWTP operations. Therefore, the impact of nitrite/FNA on N_2O production in anoxic denitrifying phosphorus removal by PAOs should be further investigated.

In this study, a series of batch tests were carried out using a highly enriched culture of *Candidatus Accumulibacter phosphatis* under different pH values and nitrite concentrations. The objective was to determine the effects of FNA on PHA oxidation, nitrite reduction, phosphorus uptake, and N_2O accumulation during denitrifying phosphorus removal and to determine whether these effects are associated with N_2O metabolism.

2. Methods

2.1. Reactor and Operation. A laboratory-scale sequence batch reactor (SBR) with a working volume of 8 L was operated for 241 days under anaerobic-aerobic conditions. The SBR was fed with acetate or propionate switching at a frequency of one to two sludge ages. The cycle time was 6 h and consisted of a 150 min anaerobic period, a 180 min aerobic period, 25 min settle/decant period, and a 5 min idle period. In each cycle, 2 L of synthetic wastewater was fed to the reactor in the first 6 min of the anaerobic period, resulting in a hydraulic retention time (HRT) of 24 h. At the end of the cycle, 200 ml sludge was removed to achieve a solids retention time (SRT) of approximately 10 days and a mixed liquor suspended solid (MLSS) level of 2.5–3.5 g/L. The dissolved oxygen (DO) concentration was maintained at 2.0 ± 0.2 mg/L in aerobic period, using an online on/off controller. The pH was controlled during both the anaerobic and aerobic phases at the range of 7.2–8.0 through dosed 0.5 MHCL and 0.5 MNaOH. The temperature was maintained at 20°C.

2.2. Synthetic Wastewater. The 2 L synthetic wastewater described by Miao et al. was composed of 0.3 L of solution A and 1.7 L of solution B [18]. The mixed feed of solutions A and B contained 800 COD/L and 40 mgP·L^{-1}. Solution A contains (per liter) 3.41 g acetate or 1.76 ml propionic acid. In addition, solution A also contains (per liter) 1.02 g NH_4Cl, 0.01 g peptone, 0.01 g yeast extraction, 1.20 g$MgSO_4 \cdot 7H_2O$, 0.19 g $CaCl_2 \cdot 2H_2O$, 7.94 mgallyl-N thiourea (ATU, a nitrification inhibitor), and 4.00 mL trace elements liquid. Solution B contained (per liter) 173 mg $K_2HPO_4 \cdot 3H_2O$ and 104 mg KH_2PO_4. For the propionic acid feed, 10.47 ml of 5 M NaOH was used to adjust the pH to 7.5.

2.3. Batch Experiments

2.3.1. Batch Experiment 1. The tested sludge was taken from a SBR that was fed with acetate during the normal cycle. At the end of the anaerobic stage, the mixed liquor (6 L) was divided into six parts and put into a 1.25 L batch reactor. $NaNO_2$ (0.1971 g) was added to the batch reactors under different pH conditions, resulting in the initial nitrite concentrations varying between 39.98 and 48.63 mg NO_2-N/L. FNA concentration, pH, temperature, and anoxic operating time are shown in Table 1. The concentration of FNA (HNO_2-N) was calculated according to the following formula:

$$\text{FNA} = \frac{S_{(NO_2^- - N)}}{K_a \times 10^{\text{pH}}}, \quad K_a = e^{-2300/(273+T)} \tag{1}$$

(see [19]). In each set, the pH was kept approximately constant (±0.1) at a set-point, by manually adding 0.2 M HCl or 0.2 M NaOH.

2.3.2. Batch Experiment 2. The tested sludge was taken from a SBR at the end of the anaerobic stage. Six sets of batch tests were performed similar to that described above. The details are shown in Table 1.

2.4. Analytical Methods. The liquid samples were immediately filtered through Millipore filter units (0.45 μm pore size) for analysis of COD, VFA, NO_2-N, NO_3-N, and PO_4-P. During the experiment, COD, NO_2-N, and PO_4-P were measured according to standard methods (APHA, 1998).

PHA analysis was performed using the method of Miao et al. to determine poly-β-hydroxybutyrate (PHB),

Table 1: Batch experiment conditions applied in batch tests.

	Batch experiment 1						Batch experiment 2					
	Test 1	Test 2	Test 3	Test 4	Test 5	Test 6	Test 1	Test 2	Test 3	Test 4	Test 5	Test 6
NO_2-N (mg/L)	39.98	43.33	44.65	42.44	41.75	48.63	70.3	94.33	112.36	70	74.9	110.6
pH	6.0	6.5	7.0	7.5	8.0	8.5	7.5	7.5	7.5	7.0	7.0	7.0
T (°C)	24	24	24	24	24	24	19	19	19	20	20	20
FNA ($mgHNO_2$-N/L)	92.3×10^{-3}	31.6×10^{-3}	10.3×10^{-3}	3.10×10^{-3}	0.96×10^{-3}	0.35×10^{-3}	5.87×10^{-3}	7.88×10^{-3}	9.38×10^{-3}	17.81×10^{-3}	19.06×10^{-3}	28.14×10^{-3}
Anoxic phase (min)	360	360	360	220	220	220	150	150	150	150	150	150
MLVSS (g/L)	2.478	2.752	2.506	2.746	2.744	2.456	2.206	2.44	2.156	2.348	2.194	1.77

poly-β-hydroxyvalerate (PHV), and poly-β-hydroxy-2-methylvalerate (PH2MV) [18]. Weighed freeze-dried biomass, 2 ml chloroform, and 2 ml methanol acidified with 3% H_2SO_4 were added to glass tubes, respectively, and then the tubes were heated in 100°C for 20 h after being mixed. One millilitre of Milli-Q water was put into the tubes and mixed after cooling. After centrifugation, 1400 ml of the bottom organic phases was added to GC vial for analysis. The temperatures of injector and FID detector were maintained at 200°C and 250°C. The temperature program was set as follows: it was held at 80°C for 2 min; increased to 140°C at the rate of 10°C/min, and then maintained for 1 min. Glycogen was measured according to the method described by Lopez-Vazquez. Five millilitres of 0.6 M HCl was added to weighed freeze-dried biomass in crew-toped glass tubes and then heated at 105°C for 6 h [20]. After cooling and centrifugation, 1 ml of the supernatant was transferred to a high performance liquid chromatography vial for glucose analysis. N_2O analysed was using the N_2O sensor by microsensor multimeter.

Fluorescence in situ hybridization (FISH) was performed with cy5-labelled EUBMIX probes (for most bacteria), cy3-labelled GAOMIX probes (for competibacter, comprising equal amounts of probes GAO431 and GAO 989), and cy3-labelled PAOMIX (for *Candidatus Accumulibacter phosphatis* or *Accumulibacter*, comprising equal amounts of probes PAO462, PAO651, and PAO846) [21, 22].

3. Results and Discussion

3.1. Reactor Performance and Microbial Community. The SBR was operated for 241 days under anaerobic/aerobic conditions. The reactor was fed with acetate or propionate, which was switched at a frequency of one to two sludge ages. The phosphorus removal performance is shown in Figure 1(a). During the first 45 days, the phosphorus removal efficiency was not stable, with the P concentration higher in the effluent than in the influent for some days. The pump supplying the carbon source malfunctioned from days 83 to 85, leading to a shortage of carbon sources during the anaerobic metabolic process; thus, the P removal efficiency declined in the effluent. After the 95th day, the P concentration in the effluent was stably maintained at less than 0.8 mg/L for the remainder of the operation. The P concentration at the end of the anaerobic stage averaged 130 mg/L when fed with acetate, which was higher than when fed with propionate as the carbon source (approximately 80 mg/L). The composition of the microbial population was characterised using FISH (Figures 1(b) and 1(c)). FISH results showed that the abundance of *Accumulibacter* was initially 3% of the total bacteria on day 1 and then rose to 91% (±4%) on day 241. The glycogen accumulating organisms (GAOs) were hardly detected on the 241st day. After 241 days of sludge domestication, the fraction of PAOs could utilize nitrite instead of oxygen as electron acceptor was to be found. In addition, high N_2O accumulation occurred during the denitrifying phosphorus removal process. One possible explanation was that FNA affected this phase. Thus, batch experiments 1 and 2 were designed to investigate the influence of FNA on anoxic phosphorus metabolism by PAOs.

3.2. Effect of FNA on Denitrifying Phosphorus Removal and N_2O Production in Batch Experiment 1

3.2.1. Comparison of Nitrite Reduction in Batch Experiment 1. The variations in nitrite concentrations during the anaerobic denitrifying phosphorus process were monitored throughout batch experiment 1 (Figure 2(a)). Following addition of 40 mgN/L nitrite, the nitrite concentration decreased rapidly at the ranges of 0.0031, 0.00096, and 0.00035 mgHNO_2-N/L (corresponding to pH 7.5, 8.0, and 8.5 conditions, resp.) (Figure 2(a)), thereby resulting in nitrite reduction rates of 8.15, 8.25, and 11.7 mgNO_2-N/(h·gVSS), respectively. With the decrease of FNA, the nitrite reduction rate slowed and reached 1.16, 2.14, and 4.82 mgNO_2-N/(h·gVSS), corresponding to 0.0923, 0.0316, and 0.0103 mgHNO_2-N/L. In several studies the denitrifying phosphorus removal process was restrained at lower nitrite concentrations from approximately 5 to 10 mgN/L [3, 23]. In this study, nitrite addition of approximately 40 mg NO_2-N/L was not inhibitory to the anoxic metabolism of the PAOs at the FNA concentrations of 0.0103, 0.0031, 0.00096, and 0.00035 mgHNO_2-N·L^{-1}. However, the nitrite reduction rate was inhibited at FNA concentrations of 0.0923 and 0.0316 mgHNO_2-N/L. This result suggests that nitrite is not a main inhibitor of the denitrifying phosphorus removal process when 39.98–48.63 mg NO_2-N/L was added at the beginning of the experiment. Our findings are consistent with the research conducted by Zhou et al., who reported that FNA, rather than nitrite, was likely the true inhibitor of anoxic phosphorus uptake [10]. In that study, the concentration ranged from 0.002 to 0.02 mg HNO_2-N/L and anoxic phosphorus uptake ceased at 0.02 mg HNO_2-N/L. In this study, nitrite reduction occurred at an FNA concentration of 0.0923 mgHNO_2-N·L^{-1}. A possible explanation is that the higher proportion of PAOs (91% (±4%) of the total bacteria) would be tolerant of higher FNA concentrations.

3.2.2. Comparison of Phosphorus Uptake in Batch Experiment 1. Figure 2(b) shows the phosphorus concentration profiles measured in batch experiment 1. Similar to the nitrite reduction rate, phosphorus uptake occurred rapidly at the ranges of 0.0031, 0.00096, and 0.00035 mgHNO_2-N/L, and the average rates were determined as 6.13, 8.10, and 8.63 mgP/(h·gVSS), respectively. The phosphorus concentration decreased rapidly during the initial stage under these three conditions, with the turning point occurring when the terminal nitrite concentration was less than 0.5 mgN/L. However, the rate decreased sharply after the turning point (2.418, 3.686, and 3.715 mgP/(h·gVSS)), when N_2O replaced nitrite as the sole electronic acceptor. The concentration of phosphorus slightly decreased when FNA declined to 0.0316 mgHNO_2-N/L. Moreover, denitrifying phosphorus removal was completely inhibited at 0.0923 mgHNO_2-N/L, suggesting that phosphorus release occurs instead of phosphorus uptake under this condition. This observation confirms that PAO metabolism during the anoxic phosphorus removal process may be inhibited by FNA and that poly-P would be released

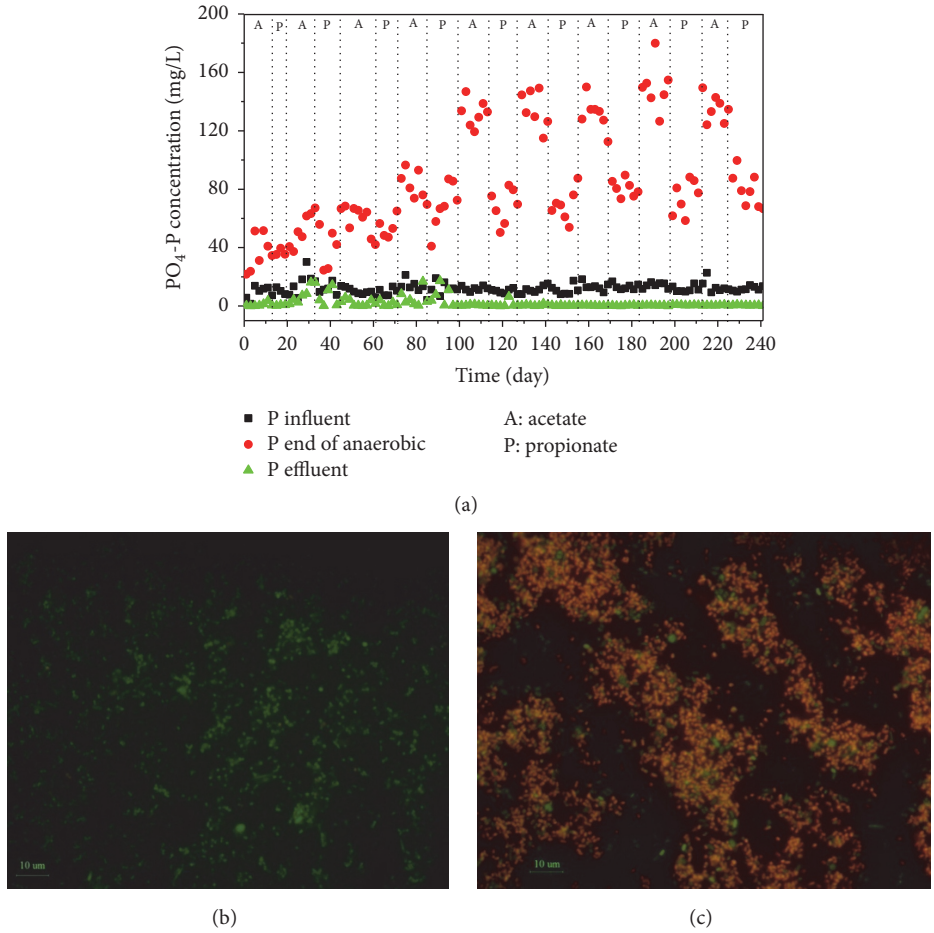

Figure 1: Performance of the reactor and FISH results: (a) Phosphorus removal performance; (b) FISH image of day 1; (c) FISH image of day 241.

from intracellular or dead biomass under these circumstances.

Figure 3 shows that the average P uptake rate significantly correlated with the FNA concentration, indicating the importance of FNA in the denitrifying phosphorus process. The rates were between −2.08 and 8.63 mgP/(h·gVSS), which is higher than some previously published research [10]. However, these rates were still lower than using oxygen as the electron acceptor when operated at normal cycle (data not shown). Therefore, it could be deduced that the nitrite is denitrified by PAOs when the concentration of FNA is below inhibitory levels.

3.2.3. Comparison of N_2O Production in Batch Experiment 1. High concentrations of N_2O accumulated during the denitrifying phosphorus removal process by PAOs, with the fact that the concentration of N_2O peaked when nitrite was exhausted (Figure 2(c)). This result suggests that it has different reduction rates between the different steps during the anoxic phosphorus removal process, namely, NO_2^- to N_2O and N_2O to N_2, thereby leading to N_2O accumulation. Some studies have shown that nitrite reductase and N_2O reductase play important roles in these two steps of denitrifying metabolism [24, 25]. Recently, Zhou et al. demonstrated that the N_2O reduction rate seemed to be independent of pH, whereas the inhibitory effect was much more moderate in comparison to that of FNA, when using denitrifying enhanced biological phosphorus removal sludge [8].

In batch experiment 1, at a similar nitrite concentration in the initial anoxic phase, the N_2O reduction rate was different before and after the exhaustion of nitrite (Figure 4). After nitrite was exhausted, the N_2O reduction rates were similar (6.65, 6.33, and 6.33 mgN/(h·gVSS)) despite different pH conditions when the N_2O was not detected in the reactor at 107 min, 90 min, and 80 min, respectively. However, before the exhaustion of nitrite, the rise in FNA concentrations resulted in the decrease of N_2O reduction rates (1.72, 3.15, and 6.52 mgN/(L·g VSS)), at the corresponding times of 113 min, 110 min, and 100 min. This may indicate that the N_2O reduction rate was mainly affected by FNA in the denitrifying phosphorus removal process. In contrast, as shown in Table 2 and Figure 2(a), FNA also inhibited the NO_2^- to N_2O step (nitrite reduction rate), which resulted in the highest N_2O accumulation occurring at 0.0031 mg HNO_2-N/L (corresponding to pH 7.5). The proportion of highest N_2O accumulation to TN was from 18.8 to 78.42%.

Table 2: Various rates of denitrifying phosphorus removal by PAOs.

	FNA concentration ($mgHNO_2$-N/L)	Phosphorus uptake rate ($mgPO_4$-P/h·gVSS)		Nitrite reduction rate ($mgNO_2$-N/h·gVSS)	The highest N_2O to TN proportion (%)	PHA degradation rate (mmol-C/h·gVSS)	PHA consumption to TN proportion (mmol-C/mmol-N·gVSS)
		Nitrite exit conditions	Average rate of anoxic phase			Nitrite exit conditions	Average rate of anoxic phase
pH 6.0	92.3×10^{-3}	−2.08	−2.08	1.16	18.80	−0.091	-
pH 6.5	31.6×10^{-3}	0.53	0.53	2.14	26.81	0.067	-
pH 7.0	10.3×10^{-3}	6.12	5.38	4.82	40.63	0.278	0.916
pH 7.5	3.10×10^{-3}	9.66	6.13	8.15	78.42	0.589	0.546
pH 8.0	0.96×10^{-3}	11.10	8.10	8.25	61.55	0.581	0.532
pH 8.5	0.35×10^{-3}	15.82	8.62	11.7	44.04	0.603	0.444

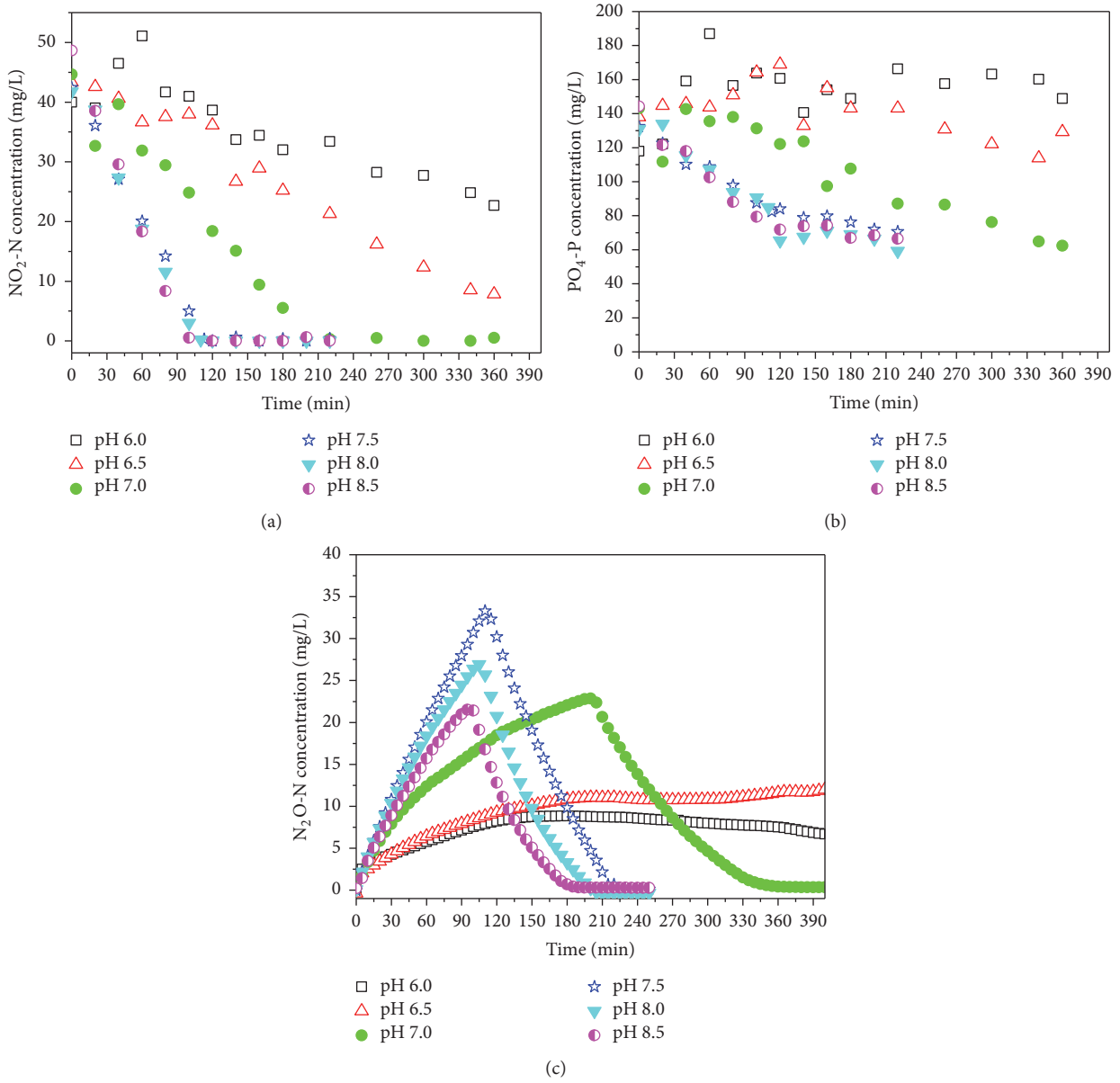

FIGURE 2: Profiles of nitrite, phosphorus, and nitrous oxide: (a) nitrite reduction; (b) phosphorus uptake; (c) N_2O production. (pH of 6.0, 6.5, 7.0, 7.5, 8.0, and 8.5 corresponds to 0.0923, 0.0316, 0.0103, 0.0031, 0.00096, and 0.00035 mgHNO_2-N/L, resp.).

3.2.4. Comparison of PHA Consumption Performance in Batch Experiment 1. The type of carbon source is important in influencing N_2O production under anoxic conditions. In the current study, PHA played a key role in N_2O production during denitrifying phosphorus removal [9]. In this study, the carbon source for denitrification was PHB and PHV. The surplus levels of PHB and PHV at the end of the anoxic phase were above 58%. This suggests that a shortage of carbon source was not a main inhibitory factor for the metabolic process. The PHA degradation rates for concentrations of 0.0316, 0.0103, 0.0031, 0.00096, and 0.00035 mgHNO_2-N/L were 0.067, 0.278, 0.589, 0.581, and 0.603 mmol-C/(h·g VSS), respectively, before exhaustion of nitrite in the reactor (Table 2). However, PHA was synthesized instead of being degraded at 0.0923 mgHNO_2-N/L. The PHA degradation rate sharply decreased from 0.0106 mgHNO_2-N/L to 0.0316 mgHNO_2-N/L. Some studies suggest that FNA has a stronger inhibitory effect on energy-consuming, rather than energy-generating, processes by DPAOs [26, 27]. In this study, the process related to energy generation, namely, PHA degradation, was seriously inhibited at high FNA levels and completely collapsed at 0.0923 mgHNO_2-N/L.

The quantity of PHA consumption per nitrite in the denitrifying phosphorus removal process by PAOs is shown in Table 2. Only the data that operated within the range of 0.00035 to 0.0103 mgHNO_2-N/L are listed, due to the complete consumption of TN during the processes above. The levels of PHA/TN per biomass were 0.444, 0.532, 0.546, and 0.916 mmol-C/(mmol-N·gVSS), respectively. Therefore, we could infer that a higher FNA concentration would lead

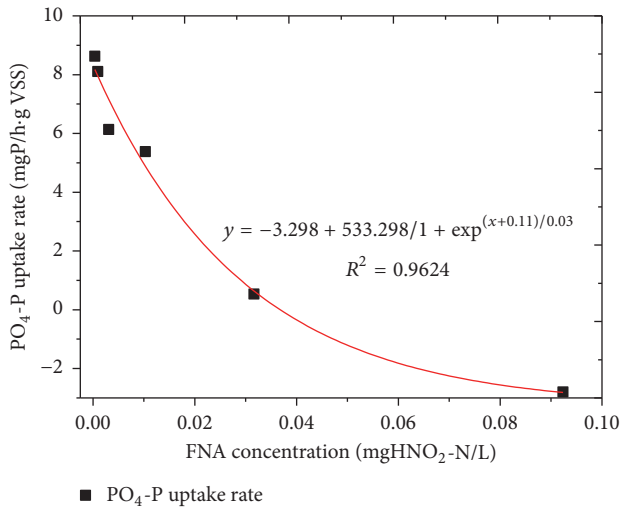

Figure 3: The inhibitory effect of FNA on PAO activity and P uptake rates.

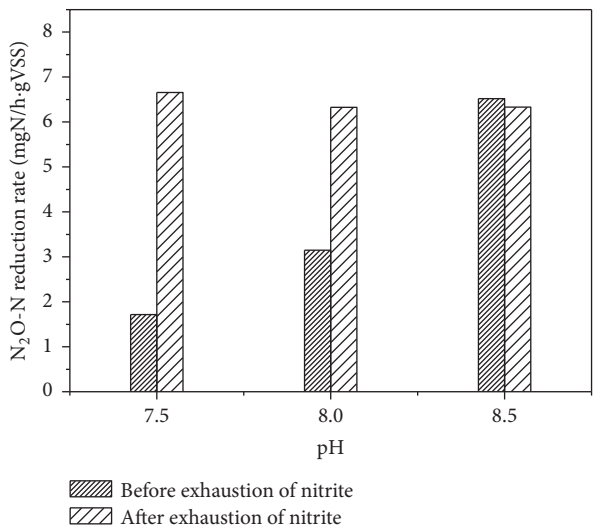

Figure 4: Various N_2O reduction rates in the presence or absence of nitrite (pH of 7.5, 8.0, and 8.5 corresponds to 0.0031, 0.00096, and 0.00035 mgHNO_2-N/L).

to more PHA consumption during the initial anoxic phase. A possible explanation is that FNA could passively diffuse across the cell membrane and shuttle protons between the two sides without generating energy, which may induce the collapse of the proton motive force (PMF); therefore, the cell should pump out more protons in order to resist this trend [8, 28]. In other words, more PHA was consumed to provide energy and protons to maintain the PMF balance or to recover from the inhibition that resulted from the absence of nitrite, when anoxic phosphorus removal occurred at the higher initial FNA concentration.

3.3. Batch Experiment 2. In batch experiment 1, the increase in FNA concentrations resulted in a decrease of the nitrite reduction rate, phosphorous uptake and N_2O reduction. N_2O accumulated due to the inhibition of the N_2O reduction rate. However, further evidence was needed to demonstrate whether FNA was more crucial than pH. In batch experiment 2, various quantities of nitrite were added to the PAO sludge at two pH levels to test effects of FNA on N_2O reduction rates and phosphorus uptake rates (Table 1).

At pH 7.5, the N_2O reduction rates were 3.465, 2.695, and 1.92 mgN/(h·gVSS), while the PO_4-P uptake rates were 12.24, 6.80, and 5.34 mgP/(h·gVSS) (Figures 5(a) and 5(b)). Both rates decreased under the same pH conditions. The average value of the maximum N_2O reduction rates and PO_4-P uptake rates decreased by 44.6% and 56.4%, respectively, at which time the FNA concentration increased from 0.01781 to 0.02814 mgHNO_2-N/L. Meanwhile, similar trends were observed for pH 7.0. The results provide evidence that higher initial FNA concentrations, not pH, cause a lower N_2O reduction rate and phosphorus uptake rate in denitrifying phosphorus removal by PAOs. Therefore, FNA has an important effect on anoxic phosphorus removal and on N_2O production. This finding is consistent with results from Wang et al., who reported that nitrite addition to DPAO sludge stimulated the net N_2O production rate due to FNA inhibition [9]. Zhou et al. reported a 50% inhibition at FNA concentrations between 0.0007 and 0.001 mgHNO_2-N/L, while the procedure was carried out to an FNA concentration of 0.004 mgHNO_2-N/L [8]. In our study, FNA concentrations ranged from 0.00587 to 0.02815 mgHNO_2-N/L (Table 1), and the total inhibitory concentration was 0.02815 mgHNO_2-N/L, providing strong evidence that FNA has a main inhibitory effect on the N_2O reduction rate, resulting in accumulation of N_2O.

3.4. The Performance of ORP in Batch Experiment 1. Many studies have reported that Oxidation-Reduction Potential (ORP) is the main parameter for determining the nitrate or nitrite depletion point during anoxic nitrogen removal [29, 30]. The nitrate or nitrite knees were a flex with a negative slope in the ORP curve and were more clearly shown in the sharply decreasing value of d_{ORP}/d_t. The ORP curve at pH 8.0 during denitrifying phosphorus removal is shown in Figure 6; similar results were observed at pH 7.0, 7.5, and 8.5. The nitrite knee appeared at 99 min while the concentration of nitrite was 3 mg/L (Figure 6). It is feasible to consider that this value was a nitrite knee point according to the traditional explanation; however, TN still existed in the form of N_2O at a concentration of 26.05 mg/L. Hence, using this nitrite knee to indicate the end of the denitrifying phosphorus removal process is not appropriate, and part of dissolved N_2O could be diffused into the air if the denitrifying phosphorus removal immediately stopped at this time. Meanwhile, it is also difficult to use an N_2O probe to indicate the end of denitrifying phosphorus removal due to its fragility. Further studies should focus on other efficiency parameters that can be used in denitrifying phosphorus removal.

4. Conclusions

The FNA concentration significantly influenced the denitrifying phosphorus removal process by PAOs when nitrite

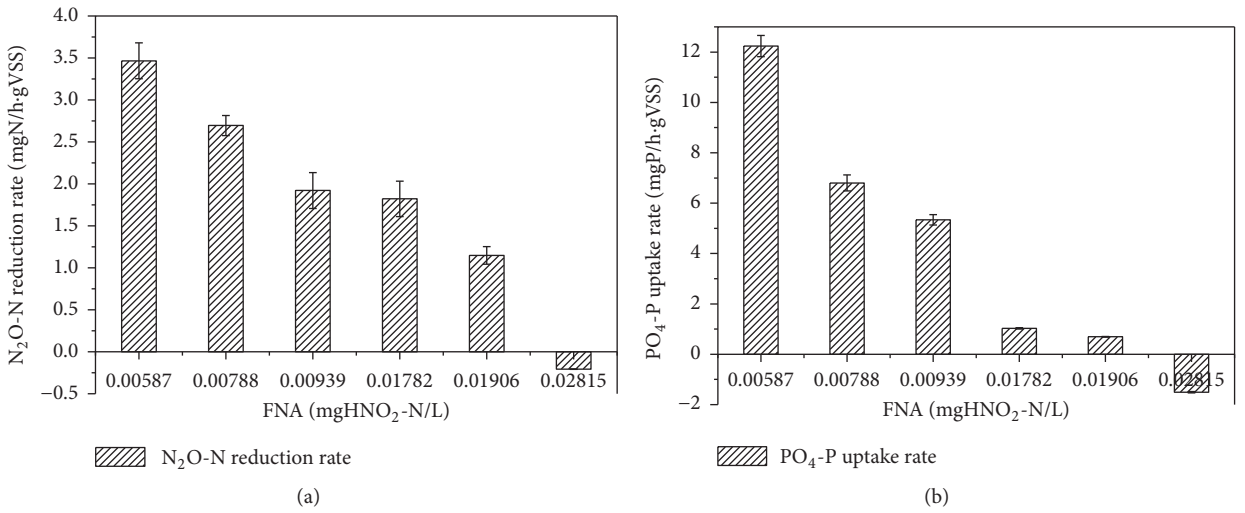

Figure 5: Effects of FNA on N_2O reduction rates and phosphorus uptake rates in batch experiment 2: (a) N_2O reduction rate; (b) phosphorus uptake rate.

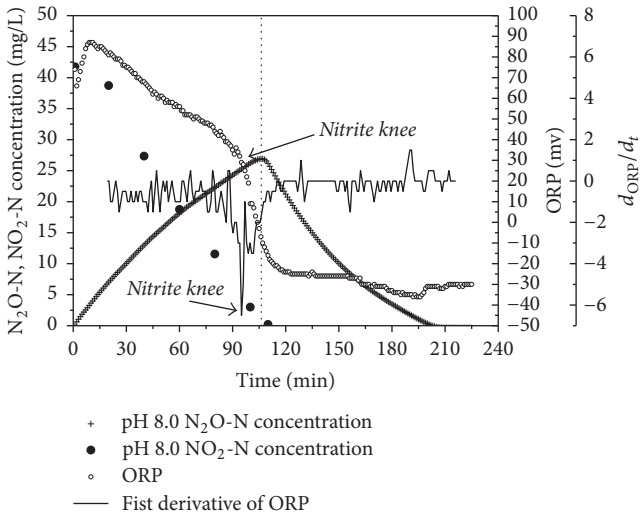

Figure 6: Various ORP in denitrifying phosphorus removal.

was added as the electron acceptor. The nitrite reduction rate, phosphorus uptake rate, N_2O reduction rate, and PHA degradation rate also decreased as the concentration of FNA increased. FNA prevented the step from NO_2 and N_2O to N_2O and N_2. In addition, when the FNA concentration was approximately 0.0031 mgHNO_2-N/L (equivalent to 42.44 mgNO_2-N/L at pH 7.5), the accumulation of N_2O approaches 33.28 mgN_2O-N/L during the anoxic denitrification process, accounting for 78.42% of the total nitrogen. The traditional nitrite knee point can only indicate the exhaustion of nitrite, instead of the complete removal of TN.

Conflicts of Interest

The authors declare that they have no conflicts of interest.

Acknowledgments

This research was financially supported by Natural Science Fund of Hebei Province (E2016403035); Colleges and Universities in Hebei Province Science and Technology Research Projects (QN2014037, ZD2016154); Science and Technology Project of Hebei Province (15274015D).

References

[1] J. Ahn, T. Daidou, S. Tsuneda, and A. Hirata, "Metabolic behavior of denitrifying phosphate-accumulating organisms under nitrate and nitrite electron acceptor conditions," *Journal of Bioscience and Bioengineering*, vol. 92, no. 5, pp. 442–446, 2001.

[2] S. Ge and P. Champagne, "Nutrient removal, microalgal biomass growth, harvesting and lipid yield in response to centrate wastewater loadings," *Water Research*, vol. 88, pp. 604–612, 2016.

[3] J. Meinhold, E. Arnold, and S. Isaacs, "Effect of nitrite on anoxic phosphate uptake in biological phosphorus removal activated sludge," *Water Research*, vol. 33, no. 8, pp. 1871–1883, 1999.

[4] M. J. Kampschreur, H. Temmink, R. Kleerebezem, M. S. M. Jetten, and M. C. M. van Loosdrecht, "Nitrous oxide emission during wastewater treatment," *Water Research*, vol. 43, no. 17, pp. 4093–4103, 2009.

[5] N. Yoshida, "15N-depleted N2O as a product of nitrification," *Nature*, vol. 335, no. 6190, pp. 528-529, 1988.

[6] S. Ge, Y. Peng, S. Wang, C. Lu, X. Cao, and Y. Zhu, "Nitrite accumulation under constant temperature in anoxic denitrification process: The effects of carbon sources and COD/NO_3-N," *Bioresource Technology*, vol. 114, pp. 137–143, 2012.

[7] Z. Wang, Y. Meng, T. Fan, Y. Du, J. Tang, and S. Fan, "Phosphorus removal and N2O production in anaerobic/anoxic denitrifying phosphorus removal process: Long-term impact of influent phosphorus concentration," *Bioresource Technology*, vol. 179, pp. 585–594, 2015.

[8] Y. Zhou, M. Pijuan, R. J. Zeng, and Z. Yuan, "Free nitrous acid inhibition on nitrous oxide reduction by a denitrifying-enhanced biological phosphorus removal sludge," *Environmental Science & Technology*, vol. 42, no. 22, pp. 8260–8265, 2008.

[9] Y. Wang, J. Geng, Z. Ren et al., "Effect of anaerobic reaction time on denitrifying phosphorus removal and N_2O production," *Bioresource Technology*, vol. 102, no. 10, pp. 5674–5684, 2011.

[10] Y. Zhou, M. Pijuan, and Z. Yuan, "Free nitrous acid inhibition on anoxic phosphorus uptake and denitrification by poly-phosphate accumulating organisms," *Biotechnology and Bioengineering*, vol. 98, no. 4, pp. 903–912, 2007.

[11] M. Pijuan, L. Ye, and Z. Yuan, "Free nitrous acid inhibition on the aerobic metabolism of poly-phosphate accumulating organisms," *Water Research*, vol. 44, no. 20, pp. 6063–6072, 2010.

[12] A. Guisasola, M. Qurie, M. D. M. Vargas, C. Casas, and J. A. Baeza, "Failure of an enriched nitrite-DPAO population to use nitrate as an electron acceptor," *Process Biochemistry*, vol. 44, no. 7, pp. 689–695, 2009.

[13] M. Vargas, A. Guisasola, A. Artigues, C. Casas, and J. A. Baeza, "Comparison of a nitrite-based anaerobic-anoxic EBPR system with propionate or acetate as electron donors," *Process Biochemistry*, vol. 46, no. 3, pp. 714–720, 2011.

[14] G. R. Crocetti, P. Hugenholtz, P. L. Bond et al., "Identification of polyphosphate-accumulating organisms and design of 16S rRNA-directed probes for their detection and quantitation," *Applied and Environmental Microbiology*, vol. 66, no. 3, pp. 1175–1182, 2000.

[15] R. P. X. Hesselmann, C. Werlen, D. Hahn, J. R. Van Der Meer, and A. J. B. Zehnder, "Enrichment, phylogenetic analysis and detection of a bacterium that performs enhanced biological phosphate removal in activated sludge," *Systematic and Applied Microbiology*, vol. 22, no. 3, pp. 454–465, 1999.

[16] Y. Chen, A. A. Randall, and T. McCue, "The efficiency of enhanced biological phosphorus removal from real wastewater affected by different ratios of acetic to propionic acid," *Water Research*, vol. 38, no. 1, pp. 27–36, 2004.

[17] M.-T. Wong, T. Mino, R. J. Seviour, M. Onuki, and W.-T. Liu, "In situ identification and characterization of the microbial community structure of full-scale enhanced biological phosphorous removal plants in Japan," *Water Research*, vol. 39, no. 13, pp. 2901–2914, 2005.

[18] Z. Miao, W. Zeng, S. Wang et al., "Effect of temperature on anoxic metabolism of nitrites to nitrous oxide by polyphosphate accumulating organisms," *Journal of Environmental Sciences*, vol. 26, no. 2, pp. 264–273, 2014.

[19] A. C. Anthonisen, R. C. Loehr, T. B. S. Prakasam, and E. G. Srinath, "Inhibition of nitrification by ammonia and nitrous acid," *Journal of the Water Pollution Control Federation*, vol. 48, no. 5, pp. 835–852, 1976.

[20] C. M. Lopez-Vazquez, Y.-I. Song, C. M. Hooijmans et al., "Short-term temperature effects on the anaerobic metabolism of glycogen accumulating organisms," *Biotechnology and Bioengineering*, vol. 97, no. 3, pp. 483–495, 2007.

[21] H. Daims, A. Brühl, R. Amann, K.-H. Schleifer, and M. Wagner, "The domain-specific probe EUB338 is insufficient for the detection of all bacteria: development and evaluation of a more comprehensive probe set," *Systematic and Applied Microbiology*, vol. 22, no. 3, pp. 434–444, 1999.

[22] G. Crocetti R., J. Banfield F., J. Keller, P. L. Bond, and L. L. Blackall, "Glycogen-accumulating organisms in laboratory-scale and full-scale wastewater treatment processes," *Microbiology*, vol. 148, no. 11, pp. 3353–3364, 2002.

[23] T. Kuba, G. Smolders, M. C. M. van Loosdrecht, and J. J. Heijnen, "Biological phosphorus removal from wastewater by anaerobic-anoxic sequencing batch reactor," *Water Science and Technology*, vol. 27, no. 5-6, pp. 241–252, 1993.

[24] T. Rasmussen, B. C. Berks, J. Sanders-Loehr, D. M. Dooley, W. G. Zumft, and A. J. Thomson, "The catalytic center in nitrous oxide reductase, Cu-z, is a copper-sulfide cluster," *Biochemistry*, vol. 39, no. 42, pp. 12753–12756, 2000.

[25] M. Poth and D. D. Focht, "15N kinetic analysis of N2O production by Nitrosomonas europaea: An examination of nitrifier denitrification," *Applied and Environmental Microbiology*, vol. 49, no. 5, pp. 1134–1141, 1985.

[26] Y. Zhou, L. Ganda, M. Lim, Z. Yuan, S. Kjelleberg, and W. J. Ng, "Free nitrous acid (FNA) inhibition on denitrifying poly-phosphate accumulating organisms (DPAOs)," *Applied Microbiology and Biotechnology*, vol. 88, no. 1, pp. 359–369, 2010.

[27] V. M. Vadivelu, J. Keller, and Z. Yuan, "Effect of free ammonia and free nitrous acid concentration on the anabolic and catabolic processes of an enriched Nitrosomonas culture," *Biotechnology and Bioengineering*, vol. 95, no. 5, pp. 830–839, 2006.

[28] J. S. Almeida, S. M. Júlio, M. A. M. Reis, and M. J. T. Carrondo, "Nitrite inhibition of denitrification by Pseudomonas fluorescens," *Biotechnology and Bioengineering*, vol. 46, no. 3, pp. 194–201, 1995.

[29] D. G. Wareham, K. J. Hall, and D. S. Mavinic, "Real-time control of aerobic-anoxic sludge digestion using ORP," *Journal of Environmental Engineering (United States)*, vol. 119, no. 1, pp. 120–136, 1993.

[30] Y. Z. Peng, J. F. Gao, S. Y. Wang, and M. H. Sui, "Use pH and ORP as fuzzy control parameters of denitrification in SBR process," *Water Science and Technology*, vol. 46, no. 4-5, pp. 131–137, 2002.

Hindawi
BioMed Research International
Volume 2018, Article ID 9536761, 9 pages
https://doi.org/10.1155/2018/9536761

Research Article

Keeping a Completely Autotrophic Nitrogen Removal over Nitrite System Effective in Treating Low Ammonium Wastewater by Adopting an Alternative Low and High Ammonium Influent Regime

Qinglong Chang, Weigang Wang, Jie Chen, and Yayi Wang

State Key Laboratory of Pollution Control and Resources Reuse, College of Environmental Science and Engineering, Tongji University, Siping Road, Shanghai 200092, China

Correspondence should be addressed to Yayi Wang; yayi.wang@tongji.edu.cn

Received 19 January 2018; Accepted 6 March 2018; Published 17 April 2018

Academic Editor: Shijian Ge

An alternative low and high ammonium influent regime was proposed and adopted to keep a completely autotrophic nitrogen removal over nitrite (CANON) effective when treating low ammonium wastewater. Results show that, by cyclic operating at an alternative low and high ammonium concentration for 10 days and 28 days, the CANON system could effectively treat low ammonium wastewater. Excessive proliferation of nitrite oxidizing bacteria (NOB) under low ammonium environment was still the challenge for the stable CANON operation; but with 28 days of a high ammonium treatment combined with a sludge retention time control, the NOB overproliferated in the low ammonium operational period could be under control. Specifically, when the nitrite oxidation rate reached 8 g $N/m^3/h$, the CANON system should enter the high ammonium influent operating mode. 16S rDNA high-throughput sequencing results show that the appropriate sludge discharging provided an environment favoring *Candidatus* Jettenia.

1. Introduction

Anaerobic ammonium oxidation (anammox) is a new pathway of autotrophic biological nitrogen removal for wastewater treatment with the advantages of less aeration consumption, low biomass production, and carbon savings [1, 2]. Complete autotrophic nitrogen removal over nitrite (CANON) system, which combines anammox with partial nitrification in a single reactor, is one of the most promising methods to achieve energy neutral or even positive in wastewater treatment plants (WWTPs) [3, 4]. In this process, ammonium is first partially oxidized to nitrite by aerobic ammonium oxidizing bacteria (AOB) through controlling dissolved oxygen (DO) at a low concentration. The residual ammonium is oxidized to nitrogen gas with the generated nitrite by anammox bacteria subsequently [5, 6]. Compared with the traditional nitrification and denitrification systems, CANON process can be a more promising and economic technology for wastewater treatment because of 63% less oxygen consumption, no requirement of biodegradable organic carbon addition, and less N_2O emissions [5, 6].

So far, CANON systems have been mostly applied to treat high ammonium wastewaters, such as landfill leachate, swine wastewater, and reject water in WWTPs (known as sidestream anammox) [7–12]. This is because high ammonia (as well as high free ammonia (FA)), high temperature, and a low DO control favor selecting both AOB and anammox bacteria as the dominant functional microorganisms, thus maintaining the stable partial nitrification and anammox processes. Specifically, the physiological differences between AOB and nitrite oxidizing bacteria (NOB) should be considered; that is, environmental factors such as pH, temperature, FA, free nitrous acid (FNA), and DO must be controlled favoring AOB proliferation in the partial nitritation step to produce an anammox-suited substrate [13].

When treating mainstream wastewater that is characterized with low ammonium and ambient temperature, stressing NOB and maintaining the activity of anammox bacteria are the two key factors determining the CANON performance [14]. Indeed, substantial efforts have been made to optimize the treatment process for a steady performance in CANON systems when treating mainstream wastewater. Han et al. [15] used screens to separate flocs and granules in mainstream deammonification to wash out NOB, and they found that over 80% of NOB was washed out and up to 70% of nitrogen removal efficiencies was achieved. Similarly, Malovanyy et al. [14] tried integrated fixed film activated sludge reactor for nitrogen removals from municipal wastewater using a deammonification process; by intermittent aeration with a high DO set-point (1.5 mg/L) and decreasing nonaerated time (30 min), NOB was successfully out-selected. However, other effective and operative approaches to ensure the effective nitrogen removal performance of CANON systems are still urgently required especially when treating low ammonium wastewater.

In this study, a novel operational pattern for CANON system treating low ammonium wastewater was developed by alternatively inflowing low ammonium concentration (mimic mainstream wastewater) and high ammonium concentration (mimic sidestream wastewater). The influent exchange frequency and the key controlling factors for effective CANON operation were examined. To elucidate the microbial structure of functional bacteria and their influence to the nitrogen removal performance, the composition of the bacterial communities in the CANON system during operational period was analyzed by 16S rDNA high-throughput sequencing technology. The proposed operational strategy hopes to help CANON processes to be effectively applied in municipal wastewater treatment.

2. Materials and Methods

2.1. Reactor Configuration. A lab-scale sequencing batch reactor (SBR) with a working volume of 2.5 L was used in this study. The SBR was set in a thermostatic water bath to keep temperature at 30°C. The experimental biomass in the reactor was mixed by a propeller stirrer at 100 rpm. An aeration device linked with an air pump was fixed at the bottom of the SBR to provide oxygen for partial nitrification. Air was regularly supplied to the SBR by an air pump.

2.2. Operational Strategies. An alternative low and high ammonium influent regime was adopted in the experiment. As shown in Figure 1, the whole experimental period was divided into four operational phases according to the influent ammonium concentration: Phase high I (0–60 d), Phase low I (61–148 d), Phase high II (149–256 d), and Phase low II (257–285 d). Phases high I and II were operated at a high ammonium concentration (approximately 240 mg NH_4^+-N/L) while Phases low I and II (approximately 61 mg NH_4^+-N/L) were operated at low ammonium concentration. A typical SBR cycle lasts for 4 h or 8 h, respectively, at low or high influent ammonium concentrations (Table 1). By operating in an alternative low and high ammonium influent regime, the NOB inhibition and the dominance of AOB and anammox bacteria in the CANON system can be ensured.

2.3. Seed Sludge and Feeding Medium. The seeding granular sludge (2.5 L) for the experimental CANON system was from another CANON system treating high ammonium saline wastewater in our laboratory (Figure S1(A)) [3].

Synthetic wastewater was continuously introduced into the reactor using a peristaltic pump in the inflow period and the pump was controlled by a liquid level controller to control the water volume of 2.5 L. The composition of the synthetic wastewater was KH_2PO_4 0.05 g/L, $CaCl_2$ 0.3 g/L, $MgSO_4{\cdot}7H_2O$ 0.3 g/L, $NaHCO_3$ 1.25 g/L, $FeSO_4{\cdot}7H_2O$ 0.00625 g/L, Na_2EDTA 0.00625 g/L, and 1.25 mL/L of trace elements solution. The composition of the trace elements solution was prepared according to Lotti et al. [16]. NH_4Cl was added to the feeding medium to reach a desired ammonium concentration in the influent. The pH was maintained at 8.0 at the beginning of each cycle by adding hydrochloric acid solution (0.2 M) or sodium hydroxide solution (0.2 M).

2.4. Analytical Methods. Water samples were collected and stored in a 4°C refrigerator until analysis. The concentrations of NH_4^+-N, NO_2^--N, and NO_3^--N were measured regularly according to the standard methods [17]. The DO concentration and pH were detected using online probes (WTW Multi350i, Germany).

2.5. Sample Collection, DNA Extraction, and PCR Amplification. Sludge samples were collected from the CANON system on days 60, 79, 124, 125, 148, 257, and 285 (the days before the change in the operating condition) and stored at −20°C after centrifugation. Total genomic DNA was extracted in triplicate from each sample using the Power Soil DNA Isolation Kit (Sangon, China) according to the manufacturer's instructions. The quality of the obtained genomic DNA was examined by 1% (w/v) agarose gel electrophoresis and concentration measured with NanoDrop spectrophotometer 2000 (Thermo Scientific, USA).

Polymerase chain reaction amplification of the V3-V4 region of the 16S rDNA gene was then conducted using primers 341F (5′-CCTACACGACGCTCTTCCGATCTN-3′) and 805R (5′-GACTACHVGGGTATCTAATCC-3′) with the reverse primer containing 6-bp barcodes to tag each sample (Majorbio Bio-Pharm Technology Co., Ltd., Shanghai China). PCR amplification and 16S rDNA high-throughput sequencing were performed according to our previous study [3].

3. Results and Discussion

3.1. The Stabilization of the CANON System at High Influent Ammonium Concentration. The CANON system operated for 285 days, and the long-term nitrogen removal performance was shown in Figure 1. The biomass was initially cultivated with high ammonium concentration (196 ± 18 mg/L) to set up the CANON system (Figure 1, Phase high I). After acclimation for 32 days, the TN removal rate

Table 1: Operating parameters of the CANON system.

Phase	High I	Low I	High II	Low II
Periods (d)	0–60	61–148	149–256	257–285
Cycle time (h)	8	4	8	4
Influent FA (mg N/L)	5–7	<3	7–10	<3
Influent NH_4^+-N (mg/L)	196 ± 18	77 ± 4.5	240 ± 21	61 ± 5.6
Volumetric exchange ratio	0.5			
DO (mg O_2/L)	0.2–0.4	0.2–0.4	0.2–0.4	0.4–0.6
Temperature (°C)	30	30	30	30
Aeration mode	3 aeration and anoxic stages in one SBR cycle (35 min/105 min, respectively)	50-min aeration stage in one SBR cycle	3 aeration and anoxic stages in one SBR cycle (60 min/60 min, respectively)	50-min aeration stage in one SBR cycle

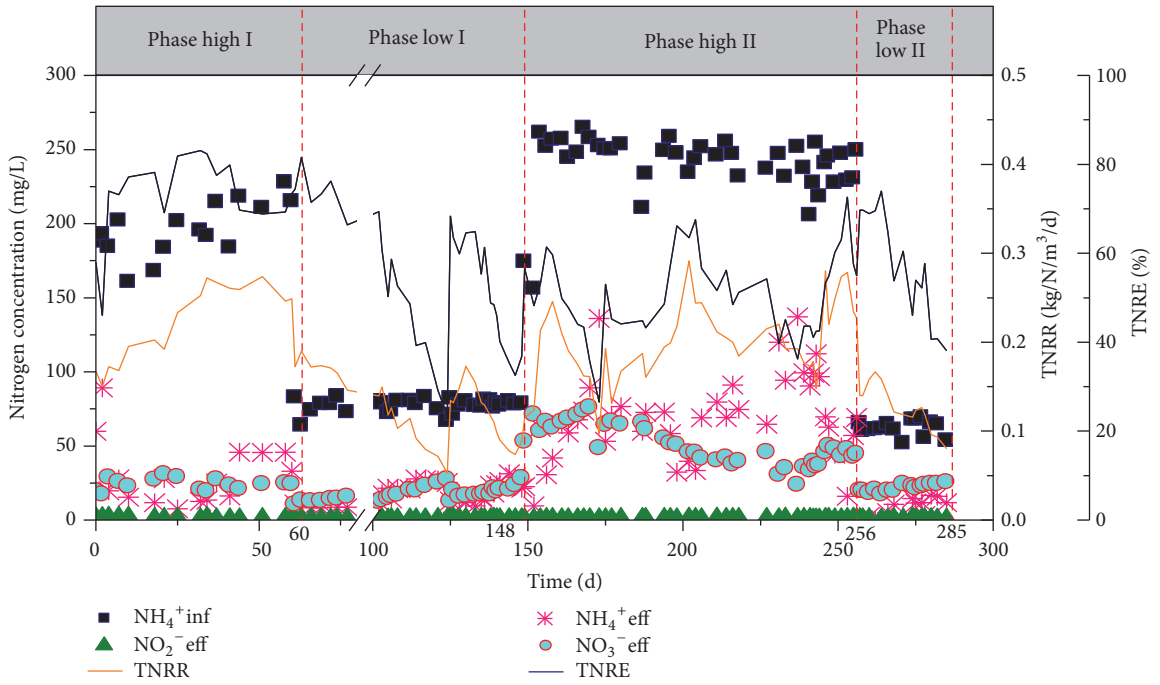

Figure 1: Profiles of nitrogen compounds (expressed as influent ammonium concentration, effluent ammonium concentration, effluent nitrite concentration, and effluent nitrate concentration), total nitrogen removal rate (TNRR), and total nitrogen removal efficiency (TNRE) of the CANON system over 285 days of operation.

(TNRR) and efficiency (TNRE) reached 15.1 g N/m^3/h and 80%, respectively.

Thereafter (days 32–60), the TNRE decreased to 70% as the influent NH_4^+-N concentration increased, but the TNRR remained stable at approximately 0.26 kg N/m^3/d, indicating that the studied CANON system had achieved steady-state nitrogen removal performance (Figure 1). Also, the ammonium oxidation rate (AOR) and the TN removal rate during the aeration stage (NRR) reached 21.2 g N/m^3/h and 0.26 kg N/m^3/day, respectively, and nitrite oxidation rate (NOR) was below 3 g N/m^3/h, suggesting that the NOB proliferation had been controlled.

3.2. The CANON Performance Operated at Alternative Low and High Ammonium Concentrations. After a stable nitrogen removal performance was achieved in Phase high I, the CANON system adopted an alternative low and high ammonium concentration inflowing mode, that is, Phase low I and Phase high II (Figure 1).

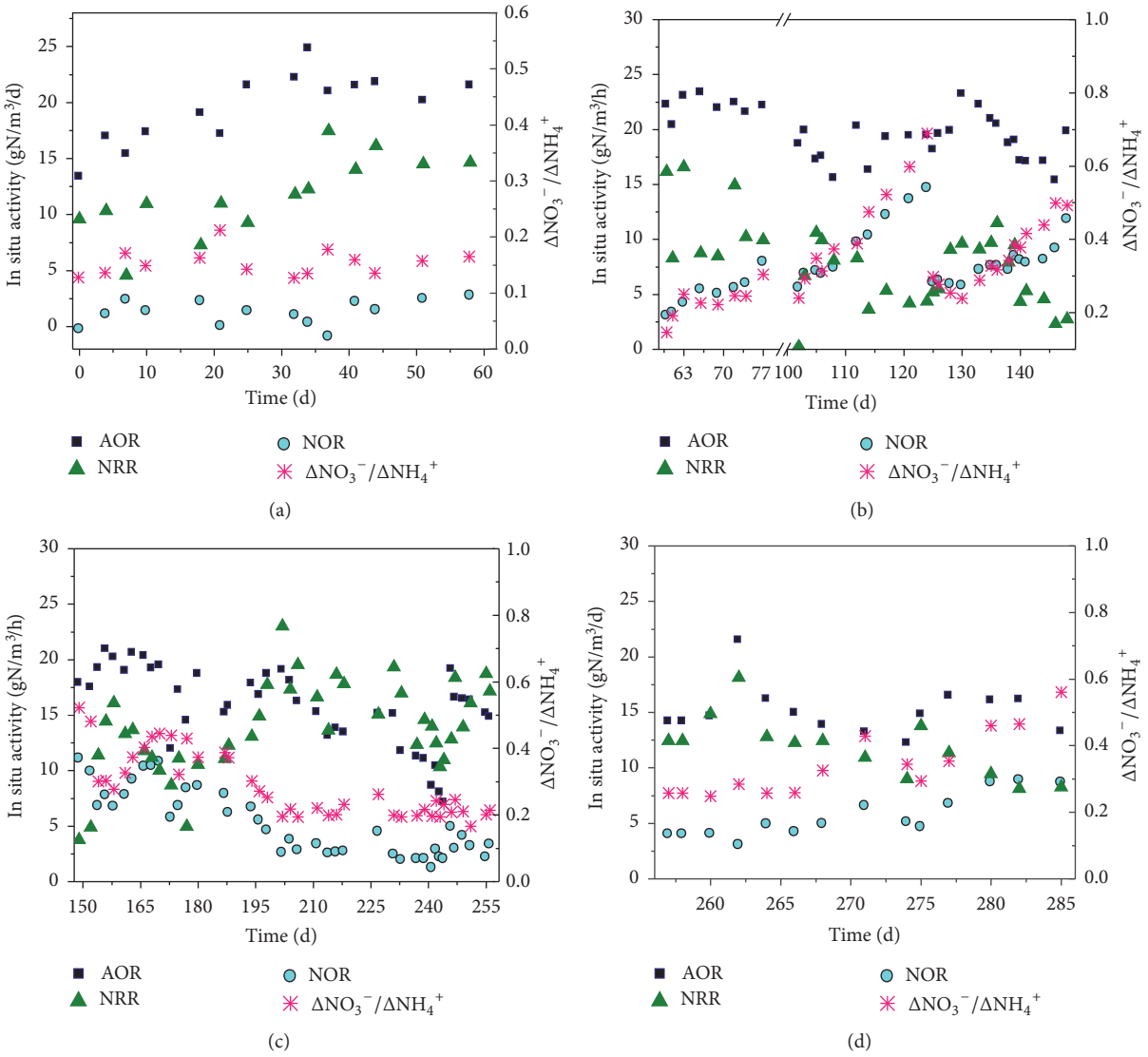

Figure 2: Changes in AOR, NOR, NRR, and $\Delta NO_3^-/\Delta NH_4^+$ ratio of the CANON system over the whole operational duration ((a) Phase high I; (b) Phase low I; (c) Phase high II; (d) Phase low II).

3.2.1. Operating at a Low Ammonium Concentration in Phase Low I

(1) Variations in Nitrogen Removal Performance. After the influent ammonium decreased, the nitrogen removal performance of the CANON system was stable firstly (days 61–74) and decreased thereafter (days 77–148) (Figure 1). Specifically, when the influent NH_4^+-N was decreased to 77 ± 4.5 mg/L on day 61, the TNRR immediately decreased from 0.26 kg N/m^3/d (day 60) to 0.17 kg N/m^3/d (day 61) with a decrease percentage of 32%. Luckily, the AOR was still stable at 22 g N/m^3/h for about 10 days at low influent ammonium concentration, even being slightly higher than 21.2 g N/m^3/h in Phase high I (Figures 2(a) and 2(b)). In contrast, NRR dropped to 11 g N/m^3/h, being lower than 15.1 g N/m^3/h of Phase high I, indicating that the low influent NH_4^+-N concentration had a greater impact on anammox reaction than on ammonia oxidation reaction.

Notably, NOR increased gradually to approximately 4.9 g N/m^3/h during days 61–74 at a low ammonium influent (Figure 2(b)), suggesting that anammox bacteria could not compete with NOB for nitrite under the low influent NH_4^+-N concentration operation [6]. As the inhibitory threshold of FA for AOB and NOB is 8–120 mg N/L and 0.08–0.82, respectively [18], NOB are generally more sensitive to FA than AOB and can be outcompeted by AOB under a high ammonium environment (generally high FA as well). However, as shown in Table 1, at low NH_4^+-N concentrations, the competitive capacity of AOB for oxygen was not much greater than that of NOB due to the low FA (below 3 mg N/L) in Phase low I in this study. Nevertheless, during days 61–74 in Phase low I, the TNRE of the CANON was stable at 75% as a whole. Also, when compared with Phase high I, $\Delta NO_3^-/\Delta NH_4^+$ increased

but was stable at approximately 0.23 (Figure 2(b)), indicating that the NOB abundance or activities were stable during these 14 days.

During days 74–124 (Phase low I), the nitrogen removal performance of the CANON continuously decreased (Figure 1). For instance, the TNRR and TNRE decreased to 0.05 kg N/m^3/d and 23%, respectively. Although the AOR was still stable at 18 g N/m^3/h, the NOR increased sharply to 14.6 g N/m^3/h with the $\Delta NO_3^-/\Delta NH_4^+$ being high at 0.69 (Figure 2(b)). Also, the nitrate concentration in the effluent increased to 27.4 mg/L (Figure 1). This is possibly because anammox bacteria was not able to compete with NOB for nitrite at a low influent NH_4^+-N concentration, which untimely exposed anammox bacteria to a famine scenario.

It should be noted that the CANON reactor was shut down from days 78 to 101 because of the time controlling breakdown. Then the NOR increased sharply from 5.57 g N/m^3/h on 102 d to 14.6 g N/m^3/h on 124 d (Figure 2(b)). Considering that NOB and AOB are prone to colony in flocs, and anammox bacteria tends to be aggregated as granules, we meshed the activated sludge of the CANON system, to quickly recover the CANON performance. Specifically, 1 L mixed liquid was drawn from the CANON reactor, and the flocs were removed using a screen with 80 mesh. The left granules were poured into the CANON reactor again with 1 L shortcut nitrifying sludge (mainly containing AOB) from a shortcut nitration reactor in our laboratory.

After 7 days' recovery (day 130), the TNRR and TNRE increased to 0.17 kg N/m^3/d and 64.5%, respectively (Figure 1). The AOR remained constant because of the low DO (0.2–0.4 mg/L) but NOR decreased by 60% from 14.6 g N/m^3/h (day 124 in Phase low I) to 6 g N/m^3/h (day 130). The NRR increased to 9.6 g N/m^3/h and $\Delta NO_3^-/\Delta NH_4^+$ decreased to 0.24 with decreasing NOR (Figure 2(b)). This result suggests that it was suitable to washout NOB and recover the nitrogen removal performance in a short time through removing the flocs, as AOB and NOB are mainly colonized in flocs [15].

After day 130 in Phase low I, the CANON reactor deteriorated again (Figure 1). Notably, the NOR increased to 8 g N/m^3/h on day 140 and to 11.8 g N/m^3/h on day 148 (Figure 2(b)). Meanwhile, TNRE decreased to 36.8% and $\Delta NO_3^-/\Delta NH_4^+$ increased to 0.5 (Figure 2(b)), indicating that NOB had proliferated again and competed nitrite with anammox bacteria. It seems that controlling only DO at a low level could not sustain a steady shortcut nitrification [19].

(2) The NOR Variation Characteristics. Remarkably, there was a linear relationship between NOR and operational days that NOR increased linearly with the operational days (Figure 3). When NOR was below 8 g N/m^3/h, the NOR was gradually increased along with the operational days with a slope of 0.39. However, after NOR was beyond 8 g N/m^3/h, the NOR sharply increased with a slope of 0.98 until the CANON SBR completely collapsed. It seems that the NOR should be controlled under 8 g N/m^3/h to ensure the stable nitrogen removal performance of the studied CANON system. Thus, NOR was selected as an indicting parameter for CANON operated at a low ammonium concentration.

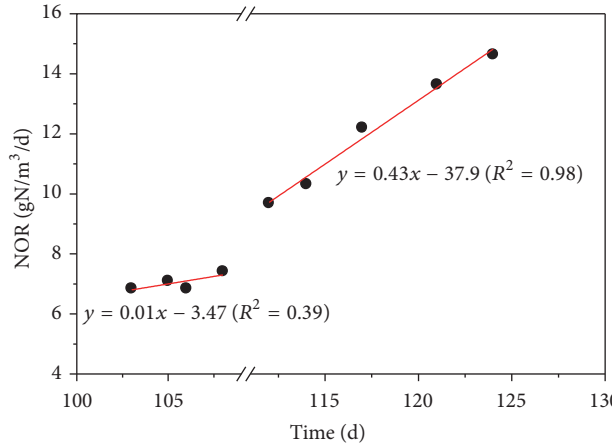

Figure 3: Linear fittings of NOR and time of the CANON reactor during the operation of days 103–108 and days 112–124 of Phase low I.

3.2.2. Operating at a High Ammonium Concentration in Phase High II. On day 149, the influent ammonium concentration was increased to 240 ± 21 mg/L again to recover the CANON performance (Figure 1, Phase high II). The pH in the inflow was still controlled at 8.0, and the influent FA concentration was about 7–10 mg N/L. By improving the FA concentration, we expected to stress the NOB proliferation and recover the functional bacteria such as AOB and anammox bacteria in the studied CANON. Corresponding to the increased influent ammonium, the aeration time increased by 80% from 300 min to 540 min for one day with the unchanged DO concentration at 0.2–0.4 mg/L. Then, both the FA and DO concentrations set in Phase high II were favorable to inhibition of NOB [18, 20, 21].

(1) The Stable Nitrogen Removal Performance at High Ammonium Concentration. During day 149 to day 158 when operating at a high ammonium concentration of approximately 240 mg/L, the nitrogen removal performance of the CANON system continued to increase with the TNRR and NRR up to 0.25 kg N/m^3/d and 16.1 g N/m^3/h, respectively, on day 158 (Figures 1 and 2(c)). Correspondingly, the NOR and $\Delta NO_3^-/\Delta NH_4^+$ decreased to 6.7 g N/m^3/h (below 8 g N/m^3/h) and 0.28, respectively (Figure 2(c)), indicating that NOB had been effectively inhibited at the high ammonium concentration, and then anammox bacteria could compete with NOB for nitrite.

However, the nitrogen removal performance of the CANON system decreased from day 159 (Figure 1). Specifically, the NRR decreased to 10 g N/m^3/h on day 170, and the NOR and $\Delta NO_3^-/\Delta NH_4^+$ increased to 10.7 g N/m^3/h and 0.45, respectively (Figure 2(c)). These results illustrate that NOB might have been adapted to the high FA and proliferated again even at the high ammonia environment [22]. Our results are somewhat in contrast to those of Wang and Gao

[23], who recovered the CANON system in 56 days from the excessive multiplication of NOB using simultaneous high ammonium and nitrite concentration in the inflow. The different results observed in this study with other studies are possible due to the fact that it was difficult to keep the high nitrite in the studied CANON system, as nitrite produced by AOB could be simultaneously or promptly be assumed by anammox bacteria in the CANON operational mode.

(2) SRT Adjustment to Washout NOB. Once the over proliferated NOB occurred in the CANON system, it is difficult to inhibit NOB due to the low decay rate of NOB [24]. This problem can be resolved by discharging the NOB sludge [8]. For example, in Strass WWTP (Austria), separation of AOB, NOB and anammox bacteria was handled by a hydrocyclone, and washing out NOB was effectively achieved by controlling of the selected SRT of AOB and anammox bacteria [25, 26]. Mimicking this case, from day 175, sludge discharging was adopted to the CANON system to control the SRT of approximately 60 d. Then, during days 175–202, the TNRR and TNRE increased to 0.29 kg N/m^3/d and 63.5% (day 202) (Figure 1), respectively; the NOR decreased to 2.6 g N/m^3/h with the effluent nitrate concentration decreased from 64.2 mg/L (day 175) to 45.6 mg/L (day 202) (Figures 1 and 2(c)). Also, the $\Delta NO_3^-/\Delta NH_4^+$ decreased to 0.2 on day 202, and NRR increased to 23 g N/m^3/h (Figure 2(c)).

Although a part of NOB was washed out by the sludge discharging, the AOR also decreased due to the loss of the activated sludge. Consequently, the TNRR decreased gradually with further discharge of sludge. Specifically, the AOR and NRR decreased to 13.4 g N/m^3/h and 17.8 g N/m^3/h, respectively, on day 218 (Figure 2(c)). As shown in Figure S2, the MLVSS of the studied reactor decreased gradually due to over discharge of the sludge. As a result, the amount and activity of AOB and anammox bacteria decreased. However, because NOB was less abundant in the biomass than AOB and anammox bacteria, sludge discharging would lead to a lower percentage of NOB in the residual CANON system. Therefore, the NOR was still stable at 2.6 g N/m^3/h (far below 8 g N/m^3/h) and $\Delta NO_3^-/\Delta NH_4^+$ was also stable at 0.2 during days 202–218 (Figure 2(c)). To prevent the continued decrease in the TNRR, the sludge discharging was stopped on day 219 (Figure 1). With increasing MLVSS during days 219–256, the TNRR and TNRE were increased to 0.23 kg N/m^3/d and 55% on day 256 (Figure 1), and the NOR and $\Delta NO_3^-/\Delta NH_4^+$ could be stable at 3.3 g N/m^3/h and 0.2 (Figure 2(c)), respectively.

Taken together, our results show that high ammonium concentration (240 mg/L) and controlled SRT (60 day) could improve the performance of CANON system through decreasing NOB to a low abundance in 28 days (days 175–202).

3.2.3. Stability of the CANON System in a Low Ammonium Concentration in Phase Low II. After day 257 (in Phase low II), the ammonium concentration was decreased to 61 ± 5.6 mg/L again (Figure 1) to examine the stability of CANON system at low ammonium concentrations. During day 257 to day 266 (approximately 10 days), the performance of the CANON system was stable. TNRR and TNRE were stable at 0.15 kg N/m^3/d and 70% (Figure 1), respectively. However, after day 267, the CANON system deteriorated again; that is, the TNRR was lower than 0.1 kg N/m^3/d and NOR increased to 8 g N/m^3/h after day 279 (Figures 1 and 2(d)). The operational results during Phase low II confirmed that the system would deteriorate once NOR reached 8 g N/m^3/h.

In summary, in Phase low I (day 61–74) and Phase low II (day 257–266) the CANON system could be stably operated for approximately 10 days at low ammonium concentrations (60 mg/L) with a relatively high TNRE (70%) and low effluent N concentrations (5 mg NH_4^+-N/L and 20 mg TN/L) (Figure 1).

3.2.4. Microbial Composition and Structure Variations with Cyclic Low and High Influent Ammonium

(1) Bacterial Community Composition. The composition of the bacterial communities in the CANON system was analyzed by 16S rDNA high-throughput sequencing. At phylum level, the CANON system was dominated by Chloroflexi, Proteobacteria, Planctomycetes, and Chlorobi (Figure 4(a)). Anammox bacteria and AOB, the functional bacteria in the CANON system, were affiliated to Planctomycetes and Proteobacteria, respectively. Chloroflexi and Chlorobi were also extensively detected in other anammox systems [27], and Chloroflexi could provide structure support for sludge granulation using the decayed anammox biomass [28, 29].

The N-related bacteria were *Nitrosomonas*-affiliated AOB, *Nitrospira*-affiliated NOB, and "*Candidatus* Jettenia" anammox bacteria (Figure 4(b)). Chu et al. [30] also found that "*Candidatus* Jettenia" and *Nitrosomonas* were the dominant functional bacteria in their CANON system treating high ammonium wastewater (500 mg N L^{-1}), with the relative abundances 16.8% and 20.1%, respectively. It should be noted that there also existed *Denitratisoma*-affiliated denitrifying bacteria in the CANON system. *Denitratisoma* was reported to be able to use 17b-oestradiol as the sole carbon source and energy and electron donor to reduce nitrite to nitrous oxide [31].

(2) The Variations of N-Transformation Microorganisms. In order to elucidate the variations in the abundances of the N-related bacterium, *Candidatus* Jettenia, *Candidatus* Kuenenia, *Nitrosomonas,* and *Nitrospira* were plotted in Figure 4(c). When the CANON system was stable in Phase high I (day 60), *Candidatus* Jettenia and *Candidatus* Kuenenia were the dominant anammox bacteria with the relative abundances of 3.56% and 6.9%, respectively. However, when the ammonium concentration decreased in Phase low I, *Candidatus* Jettenia outcompeted *Candidatus* Kuenenia and became the main anammox genera (day 79). Specifically, from day 124 to day 148 in Phase low I, the relative abundance of *Candidatus* Jettenia increased from 5.91% to 14.4%. This is primarily because the increased AOB amount and decreased NOB amount after sludge changing caused the increased nitrite concentration.

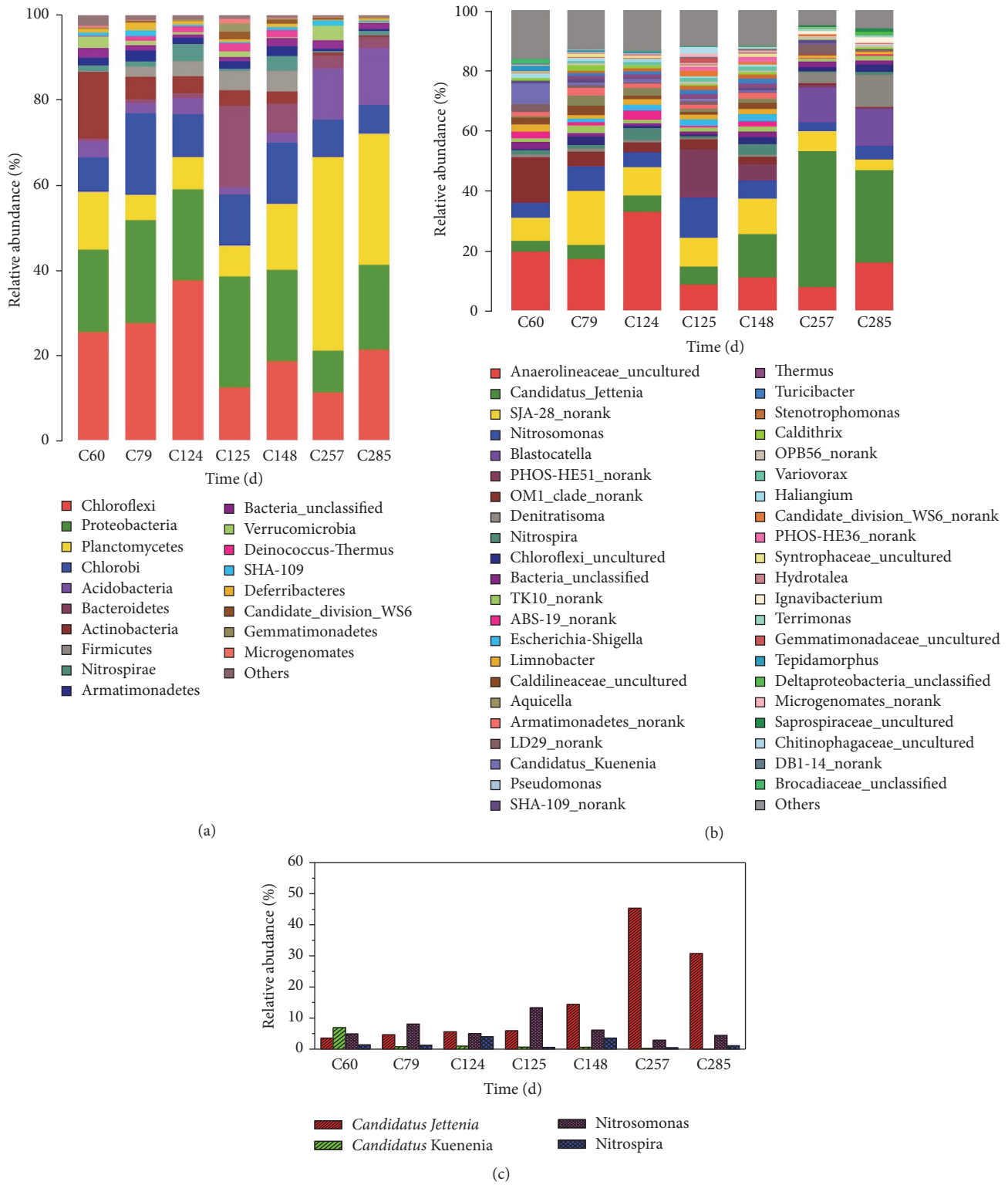

Figure 4: The microbial community taxonomic compositions in the studied CANON system: (a) at the phylum level; (b) at the genus level; (c) changes in the relative abundance of *Candidatus* Jettenia, *Candidatus* Kuenenia, *Nitrosomonas,* and *Nitrospira*.

After being cultivated during Phase high II, *Candidatus* Jettenia was still the dominant anammox bacteria (days 257–285), while the relative abundance of *Candidatus* Kuenenia was at an extremely low level (0.25% and 0.02% on days 257 and 285, respectively). For example, the relative abundance of *Candidatus* Jettenia increased from 14.4% (day 148, Phase low I) to 45.32% (day 257, Phase high II). Obviously, a high ammonium concentration had favored to enrich anammox bacteria. As each genus of anammox bacteria has its own special ecological niche [32], the higher relative abundance of *Candidatus* Jettenia than that of *Candidatus* Kuenenia indicates that the present experimental condition was more suitable for *Candidatus* Jettenia.

As shown in Figure 4(c), on days 124 (Phase low I), 148 (Phase low I), and 285 (Phase low II), the relative abundance of *Nitrospira* (NOB) increased slightly because of the low ammonium concentration. However, after the sludge changing on day 124, the relative abundance of *Nitrospira* decreased from 4.01% (day 124) to 0.57% (day 125), and *Nitrosomonas* increased from 5.03% to 13.32%. The relative abundance of *Nitrospira* also decreased from 3.55% (day 148) to 0.43% (day 257) after being cultivated at a high ammonium concentration in Phase high II, suggesting that it was suitable to enrich AOB and inhibit NOB using sludge changing and a high ammonium concentration.

Compared with Phases high I and low I, Phases high II and low II seem to be more robust in the nitrogen removal performance (Figure 1), possibly because the relative abundance of anammox bacteria was high in Phases high II and low II (Figures 4(b) and 4(c)). Our results suggest that replenishing anammox bacteria biomass into the CANON system could be an alternative strategy for stabilization of anammox treatment performance.

3.3. The Recommended Operation Strategy for Practical Operation of CANON Systems. According to our experimental results, the alternative low and high ammonium influent regime was feasible for CANON system to treat a part of low ammonium wastewater. It is recommended alternatively to operate CANON system at low ammonium concentration for 10 days and at high ammonium concentration for 28 days. Also, the NOR and sludge age (SRT), as two important parameters, were recommended to be below 8 g $N/m^3/h$ and approximately 60 d in the present CANON systems.

The proposed strategy can be realized if WWTPs have sludge digestion unit, from which the higher ammonium influent can be supplied. Also, several parallel CANON SBR units are required so that when a series CANON SBRs treat mainstream wastewater, other series can treat sidestream wastewater (i.e., sludge digestion supernatant) for enhancement of AOB and anammox bacteria, and inhibition of NOB. By this way, CANON system can treat nitrogen containing wastewater continuously. But to use this operational regime successfully in mainstream CANON system, the difference between actual ammonium concentration in real WWTPs and our experiment must be considered. Further research should be focused on improving the proportion of the low ammonium concentration treatment duration, and overcoming low temperature in real municipal wastewater. Our strategy hopes to help opening a new possibility for CANON processes used in municipal wastewater (mainstream wastewater) treatment.

4. Conclusions

An alternative low and high ammonium influent regime was proposed and investigated to keep CANON stable when treating low ammonium wastewater. Alternatively operating at a low ammonium concentration for 10 days and at a high ammonium concentration for 28 days was feasible for CANON to treat low ammonium wastewater. NOR and sludge age, as two important parameters, should be controlled to maintain a stable operation. NOR should be kept under 8 g $N/m^3/h$ to prevent CANON deterioration. To use CANON in mainstream successfully, further studies are needed to shorten the duration of operating at high ammonium concentrations and overcome low temperature.

Conflicts of Interest

The authors declare that they have no conflicts of interest.

Acknowledgments

This work was supported by the National Natural Science Foundation of China (NSFC) (51522809 and 51378370).

Supplementary Materials

Figure S1: the anammox granule of seeding CANON sludge (A); seeding CANON sludge (B); anammox granule after sieving on day 124 (C); flocs after sieving on day 124 (D). Figure S2: changes in the MLSS, MLVSS and $\Delta NO_3^-/\Delta NH_4^+$ ratio over the operation of Phase high II. Figure S3: rarefaction curve. Table S1: microbial community richness and diversity index of sludge samples. *(Supplementary Materials)*

References

[1] B. Kartal, N. M. De Almeida, W. J. Maalcke, H. J. M. Op den Camp, M. S. M. Jetten, and J. T. Keltjens, "How to make a living from anaerobic ammonium oxidation," *FEMS Microbiology Reviews*, vol. 37, no. 3, pp. 428–461, 2013.

[2] M. Strous, J. A. Fuerst, E. H. M. Kramer et al., "Missing lithotroph identified as new planctomycete," *Nature*, vol. 400, no. 6743, pp. 446–449, 1999.

[3] Y. Wang, J. Chen, S. Zhou et al., "16S rRNA gene high-throughput sequencing reveals shift in nitrogen conversion related microorganisms in a CANON system in response to salt stress," *Chemical Engineering Journal*, vol. 317, pp. 512–521, 2017.

[4] X. Zhang, D. Li, Y. Liang, Y. He, Y. Zhang, and J. Zhang, "Autotrophic nitrogen removal from domestic sewage in MBR-CANON system and the biodiversity of functional microbes," *Bioresource Technology*, vol. 150, pp. 113–120, 2013.

[5] A. O. Sliekers, N. Derwort, J. L. Campos Gomez, M. Strous, J. G. Kuenen, and M. S. M. Jetten, "Completely autotrophic nitrogen removal over nitrite in one single reactor," *Water Research*, vol. 36, no. 10, pp. 2475–2482, 2002.

[6] K. A. Third, A. O. Sliekers, J. G. Kuenen, and M. S. M. Jetten, "The CANON system (completely autotrophic nitrogen-removal over nitrite) under ammonium limitation: interaction and competition between three groups of bacteria," *Systematic and Applied Microbiology*, vol. 24, no. 4, pp. 588–596, 2001.

[7] M. Azari, U. Walter, V. Rekers, J.-D. Gu, and M. Denecke, "More than a decade of experience of landfill leachate treatment with a full-scale anammox plant combining activated sludge and activated carbon biofilm," *Chemosphere*, vol. 174, pp. 117–126, 2017.

[8] A. Joss, D. Salzgeber, J. Eugster et al., "Full-scale nitrogen removal from digester liquid with partial nitritation and anammox in one SBR," *Environmental Science & Technology*, vol. 43, no. 14, pp. 5301–5306, 2009.

[9] S. Lackner, E. M. Gilbert, S. E. Vlaeminck, A. Joss, H. Horn, and M. C. M. van Loosdrecht, "Full-scale partial nitritation/anammox experiences—an application survey," *Water Research*, vol. 55, pp. 292–303, 2014.

[10] W. R. L. van der Star, W. R. Abma, D. Blommers et al., "Startup of reactors for anoxic ammonium oxidation: Experiences from the first full-scale anammox reactor in Rotterdam," *Water Research*, vol. 41, no. 18, pp. 4149–4163, 2007.

[11] T. Yamamoto, K. Takaki, T. Koyama, and K. Furukawa, "Long-term stability of partial nitritation of swine wastewater digester liquor and its subsequent treatment by Anammox," *Bioresource Technology*, vol. 99, no. 14, pp. 6419–6425, 2008.

[12] F. Zhang, Y. Peng, L. Miao, Z. Wang, S. Wang, and B. Li, "A novel simultaneous partial nitrification Anammox and denitrification (SNAD) with intermittent aeration for cost-effective nitrogen removal from mature landfill leachate," *Chemical Engineering Journal*, vol. 313, pp. 619–628, 2017.

[13] S. W. H. Van Hulle, H. J. P. Vandeweyer, B. D. Meesschaert, P. A. Vanrolleghem, P. Dejans, and A. Dumoulin, "Engineering aspects and practical application of autotrophic nitrogen removal from nitrogen rich streams," *Chemical Engineering Journal*, vol. 162, no. 1, pp. 1–20, 2010.

[14] A. Malovanyy, J. Trela, and E. Plaza, "Mainstream wastewater treatment in integrated fixed film activated sludge (IFAS) reactor by partial nitritation/anammox process," *Bioresource Technology*, vol. 198, pp. 478–487, 2015.

[15] M. Han, S. E. Vlaeminck, A. Al-Omari et al., "Uncoupling the solids retention times of flocs and granules in mainstream deammonification: A screen as effective out-selection tool for nitrite oxidizing bacteria," *Bioresource Technology*, vol. 221, pp. 195–204, 2016.

[16] T. Lotti, R. Kleerebezem, Z. Hu, B. Kartal, M. S. M. Jetten, and M. C. M. van Loosdrecht, "Simultaneous partial nitritation and anammox at low temperature with granular sludge," *Water Research*, vol. 66, pp. 111–121, 2014.

[17] APHA, *Standard Methods for the Examination of Water and Wastewater*, American Public Health Association, Washington, DC, USA, 21st edition, 2005.

[18] A. C. Anthonisen, R. C. Loehr, T. B. S. Prakasam, and E. G. Srinath, "Inhibition of nitrification by ammonia and nitrous acid," *Journal of the Water Pollution Control Federation*, vol. 48, no. 5, pp. 835–852, 1976.

[19] N. Morales, Á. Val del Río, J. R. Vázquez-Padín, R. Méndez, J. L. Campos, and A. Mosquera-Corral, "The granular biomass properties and the acclimation period affect the partial nitritation/anammox process stability at a low temperature and ammonium concentration," *Process Biochemistry*, vol. 51, no. 12, pp. 2134–2142, 2016.

[20] R. Blackburne, Z. Yuan, and J. Keller, "Partial nitrification to nitrite using low dissolved oxygen concentration as the main selection factor," *Biodegradation*, vol. 19, no. 2, pp. 303–312, 2008.

[21] Y. Ma, Y. Peng, S. Wang, Z. Yuan, and X. Wang, "Achieving nitrogen removal via nitrite in a pilot-scale continuous pre-denitrification plant," *Water Research*, vol. 43, no. 3, pp. 563–572, 2009.

[22] O. Turk and D. S. Mavinic, "Maintaining nitrite build-up in a system acclimated to free ammonia," *Water Research*, vol. 23, no. 11, pp. 1383–1388, 1989.

[23] X. Wang and D. Gao, "In-situ restoration of one-stage partial nitritation-anammox process deteriorated by nitrate build-up via elevated substrate levels," *Scientific Reports*, vol. 6, Article ID 37500, 2016.

[24] I. Jubany, J. Lafuente, J. A. Baeza, and J. Carrera, "Total and stable washout of nitrite oxidizing bacteria from a nitrifying continuous activated sludge system using automatic control based on Oxygen Uptake Rate measurements," *Water Research*, vol. 43, no. 11, pp. 2761–2772, 2009.

[25] B. Wett, A. Omari, S. M. Podmirseg et al., "Going for mainstream deammonification from bench to full scale for maximized resource efficiency," *Water Science and Technology*, vol. 68, no. 2, pp. 283–289, 2013.

[26] B. Wett, M. Hell, G. Nyhuis, T. Puempel, I. Takacs, and S. Murthy, "Syntrophy of aerobic and anaerobic ammonia oxidisers," *Water Science and Technology*, vol. 61, no. 8, pp. 1915–1922, 2010.

[27] X. Li, S. Sun, H. Yuan, B. D. Badgley, and Z. He, "Mainstream upflow nitritation-anammox system with hybrid anaerobic pretreatment: Long-term performance and microbial community dynamics," *Water Research*, vol. 125, pp. 298–308, 2017.

[28] T. Kindaichi, S. Yuri, N. Ozaki, and A. Ohashi, "Ecophysiological role and function of uncultured Chloroflexi in an anammox reactor," *Water Science and Technology*, vol. 66, no. 12, pp. 2556–2561, 2012.

[29] P. Larsen, J. L. Nielsen, D. Otzen, and P. H. Nielsen, "Amyloid-like adhesins produced by floc-forming and filamentous bacteria in activated sludge," *Applied and Environmental Microbiology*, vol. 74, no. 5, pp. 1517–1526, 2008.

[30] Z.-R. Chu, K. Wang, X.-K. Li, M.-T. Zhu, L. Yang, and J. Zhang, "Microbial characterization of aggregates within a one-stage nitritation-anammox system using high-throughput amplicon sequencing," *Chemical Engineering Journal*, vol. 262, pp. 41–48, 2015.

[31] M. Fahrbach, J. Kuever, R. Meinke, P. Kämpfer, and J. Hollender, "Denitratisoma oestradiolicum gen. nov., sp. nov., a 17 β-oestradiol-degrading, denitrifying betaproteobacterium," *International Journal of Systematic and Evolutionary Microbiology*, vol. 56, no. 7, pp. 1547–1552, 2006.

[32] B. Kartal, J. Rattray, L. A. van Niftrik et al., "Candidatus "Anammoxoglobus propionicus" a new propionate oxidizing species of anaerobic ammonium oxidizing bacteria," *Systematic and Applied Microbiology*, vol. 30, no. 1, pp. 39–49, 2007.

Hindawi
BioMed Research International
Volume 2018, Article ID 6878741, 10 pages
https://doi.org/10.1155/2018/6878741

Research Article

The Productivity Dynamics of China's Environmentally Friendly Production Technologies in terms of Wastewater Treatment Techniques

Fuxia Yang,[1] Mian Yang ,[2,3] and Jiangchuan Xu[1]

[1]*College of Economics & Management, Huazhong Agricultural University, Wuhan 430070, China*
[2]*Economics and Management School, Wuhan University, Wuhan 430072, China*
[3]*Center of Population, Resource & Environmental Economics Research, Wuhan University, Wuhan 430072, China*

Correspondence should be addressed to Mian Yang; yangmian909@163.com

Received 22 December 2017; Revised 9 February 2018; Accepted 20 February 2018; Published 29 March 2018

Academic Editor: Shijian Ge

Low economic profit usually reduces the incentive of producers to operate their wastewater treatment technologies effectively. It is necessary to investigate the performance of environmentally friendly production technologies that reduce wastewater discharges and generate economic outputs simultaneously (EPTWs) in China over the past decade. In this paper, we apply the Malmquist-Luenberger productivity index widely used in the field of economics to evaluate the productivity change of EPTWs for 30 administrative provinces in China during 2003–2015. The pathways of the productivity change are further identified by decomposing the productivity index into two components: technological change and technical efficiency change. The results show that China's environmental productivity index associated with wastewater reduction had undergone a downward trend, and evident spatial disparities are observed among the 30 provincial regions. Moreover, the changes of China's environmental productivity over the whole studied period can mainly be attributed to technological progress, while the technical efficiency component has contributed little, although its annual contributing rate is in an increasing trend.

1. Introduction

Over the past three decades, China has witnessed a dramatic economic growth with the annual average growth rate at nearly 10%. At the same time, serious pollution issues emerged in large numbers resulting in obvious environmental degradations. As one of the most important pollutants, wastewater discharge is a very serious environmental problem resulting from the rapid urbanization, the numerous usages of fertilizer, and industrial activities and residents' living consumption [1, 2]. In order to improve the worsening water environment quality, the Chinese government has enforced a series of ambitious plans to decrease pollutant discharges and promote wastewater purification since 2000. For instance, the total chemical oxygen demand (COD) in China was required to be reduced by 10% during 2006 to 2010 (the 11th five-year plan, FYP) by the central government.

In this context, various wastewater treatment technologies (WTTs) and cleaner production techniques have been developed and adopted widely [3, 4]. It is reported that the number of municipal wastewater treatment plants have increased from 708 to 1944 over the period 2004–2015 (Figure 1), and the designed treatment capacity per day has been also improved by nearly two times. Nevertheless, with the continuous decline of total COD, the water environmental quality in this developing country has not been fundamentally improved. The total wastewater discharge has even observed a continuing increase with the average annual growth rate at about 4%, from 48.2 billion tons in 2004 to 73.5 billion tons in 2015 (Figure 1), and the total economic losses from water pollution in China are estimated to be around 240 billion yuan per year [5].

Numerous studies focus on the underlying reasons why the total effluent discharge kept increasing in the context

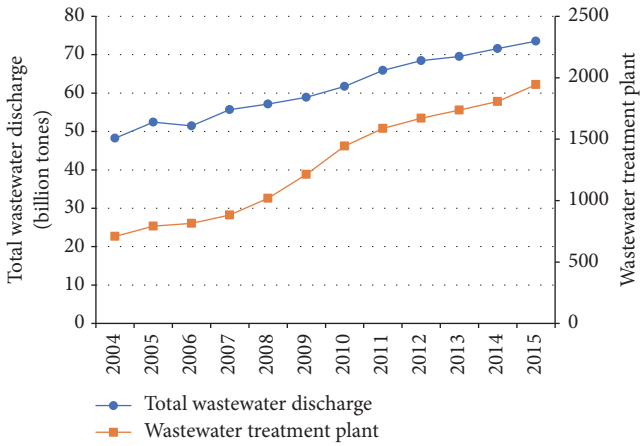

FIGURE 1: Total wastewater discharge and municipal wastewater treatment plants in China. *Data Source*: *China Environmental Statistical Yearbooks*, 2005–2016.

of stringent wastewater management regulation. A popular point of view is that WTTs in China have not been operated efficiently [6, 7]. First, the installations of wastewater treatment facilities and pipeline networks require huge upfront capital investment [8, 9], which reduces the incentives of producers to invest in wastewater reclaim and reuse programs [4]. Second, due to the very high operating expenditure including labor input and electricity consumption during the treatment processes (accounting for more than 50% of the total economic costs) [10], the sewage treatment facilities that have been put into operation are usually running with low efficiency; some of them are even left unused. Besides, the lack of integrated water resources management framework, incoherent water quality requirements, and weak public awareness also impede the adoption of WTTs [4]. By contrast, the economic returns of these technology adoptions are limited. In recent years, various advanced wastewater treatment techniques have been developed, by which the capital and operating costs have been remarkably reduced [3, 4, 11]. Since the benefits related to the adoption of WTTs accrue the unequal distribution among the stakeholders [12], the revenue gained from the implementation of WTTs is far from their total costs [13]. It can be inferred from previous studies that low economic profit is the crucial factor of inefficient use of current advanced WTTs. In practice, producers aiming to maximize their profits prefer environmentally friendly production technologies that generate economic revenues and reduce sewage discharges simultaneously (EPTW) in the face of stringent environmental regulation. Therefore, it is of great importance to evaluate the performance of EPTWs.

In this paper, we attempt to evaluate the level of EPTWs among 30 administrative provinces in China by constructing an environmentally sensitive productivity index. This productivity index captures the intertemporal change of productivity for EPTWs by examining the actual effect of economic returns and sewage reduction. The rest of this paper is organized as follows: Section 2 presents a literature review on environmental productivity analysis; Section 3 elaborates the methodology used in this study; Section 4 examines the intertemporal changes, spatial differences, and the main drivers of EPTWs' productivity for 30 administrative provinces in China; Section 5 concludes the paper and puts forward some useful policy recommendations.

2. Literature Reviews

The main purpose of productivity analysis is to evaluate the performance of one production technology in terms of economic gains. Traditional total factor productivity index (namely, Solow residual) is defined as outputs change not explained by input variations, which has gained popularity in the field of economics. However, the initial analysis framework ignores undesirable outputs in the production process, which fails to provide a full picture of sustainable economic development. With the continued deterioration in global environmental condition, more attention has been paid to green economic growth. To this end, Chung et al. [14] propose a Malmquist-Luenberger productivity index (ML index) based on a directional distance function. The ML index measures environmentally sensitive productivity change through incorporating undesirable byproducts of economic outputs.

Ever since this seminal work, the ML index has been widely used to analyze the change of productivity for a wide range of decision-making units (DMUs) with bad outputs. Färe et al. [15] compute the ML index of US state manufacturing sectors from 1974 to 1986 considering both marketed output and air pollution emissions. Hailu and Veeman [16] investigate the environmentally sensitive productivity change of the pulp and paper industry in Canada by employing a parametric input distance function. Yörük and Zaim [17] evaluate ML productivity indicator taking carbon dioxide, nitrogen oxide, and organic water into account. Mahlberg et al. [18] estimate environmental productivity change including greenhouse gas emissions as an undesirable output. Ananda and Hampf [19] measure environmentally sensitive productivity growth of the urban water sector.

With the increase of environmental degradation, the evaluation on China's environmental productivity has also attracted more and more attention from the scholars. The majority of available literature investigates environmentally friendly production technologies related to sulfur dioxide (SO_2), chemical oxygen demand (COD) and carbon dioxide (CO_2). For instance, some researches model CO_2 emissions as the undesirable output to analyze environmental productivity change of Chinese manufacturing industries [20–22], industrial sectors [23, 24], transportation industry [10, 25], and iron and steel industry [26]. Yang et al. [27] and F. Yang and M. Yang [28] incorporate SO_2 emissions as the bad output when computing environmental productivity index of 30 provincial regions in China. Being aware of the severity of water pollution issue, several studies try to take sewage discharge or the main pollutants in wastewater into account in their environmental productivity assessments. He et al. [29] measure the bad output of waste gas, wastewater (including biochemical oxygen demand and total suspended solids) and solid wastes to compute the ML productivity index of iron and steel industry. Tao et al. [30] and Xie et al. [31] assess green productivity growth by employing global ML productivity

index, where wastewater discharge, SO_2 emissions and soot serve as undesirable outputs.

Furthermore, deteriorating water quality turns some scholars' attention to assess water use efficiency considering undesirable outputs. For example, Wang et al. [32] investigate water use efficiency of China's regional industrial systems, taking two main pollutants in wastewater (i.e., COD and ammonia nitrogen) into account. Deng et al. [33] estimate water use efficiency of 31 provinces in China during 2004–2013 using slack based measure-data envelopment analysis (SBM-DEA) model, which takes consideration of sewage. Zhao et al. [34] incorporate COD in industrial wastewater and ammonia nitrogen output of urban sewage when water resource utilization efficiency for 31 provincial administrative regions in China is measured. These models make it possible to compare the environmental efficiency of water use for cross-sectional DMUs at a certain time. However, they do not describe the intertemporal change of water efficiency scores for one producer over time. Second, these models can say very little about the sources of changes in the efficiency scores.

This paper extends prior literature on the water utilization efficiency by attempting to address the above-mentioned two limitations. In the following analysis, we construct an environmental productivity index to evaluate the dynamic change of technical efficiency considering wastewater discharge reduction. Moreover, the productivity index allows us to identify the driver of the productivity change of EPTWs for one production unit by decomposing it into technical change (the shift of the water-friendly production frontier) and efficiency change (the move toward the water-friendly frontier).

3. Methodology

3.1. Environmental Directional Distance Function. To construct an environmentally sensitive productivity index in terms of wastewater reduction and economic gains (EPI_{WE}), it is necessary to define an environmental directional distance function first. Then consider an environmental production technology where one production unit uses a vector of input $\mathbf{x} = (x_1, x_2, \ldots, x_n) \in R_n^+$ to yield economic outputs $\mathbf{y} = (y_1, y_2, \ldots, y_m) \in R_m^+$ and discharge wastewater $\mathbf{u} \in R^+$. The production possibility set (PPS) for this production technology, $\mathbf{P}(\mathbf{x})$, can be expressed as $\mathbf{P}(\mathbf{x}) = \{(\mathbf{y}, \mathbf{u}) : \mathbf{x} \text{ can produce } (\mathbf{y}, \mathbf{u})\}$, which satisfies a set of axioms discussed in [35]. In addition, inputs and economic outputs are strongly disposable, and discharged wastewater is weak disposable.

To distinguish a specific production behavior such as input saving, economic growth, three kinds of the distance function including input-oriented, output-oriented, and directional one are developed to alternatively describe the PPS. The directional distance function has been widely used since the other two can be considered as its special case. Furthermore, the attractive merit is that it can expand desirable outputs and contract inputs/undesirable outputs simultaneously. Here, to recognize production activities that are friendly to wastewater reduction, the environmental directional distance function is defined as follows:

$$\begin{aligned}\overrightarrow{D}(x, y, u; \mathbf{g}) \\ = \sup\left\{\beta : \left(x, y + \beta \cdot g_y, u - \beta \cdot g_u\right) \in P\right\},\end{aligned} \tag{1}$$

where $\mathbf{g} = (g_y, -g_u)$ is the vector of directions which economic outputs and wastewater are scaled. To measure technical efficiency defined in the Farrell proportional distance function, we define $\mathbf{g} = (y, -u)$, by which wastewater and desirable outputs are proportionately adjusted. Obviously, this distance function determines the benchmark of EPTWs, where producers yield the maximum of economic outputs $y + \beta \cdot g_y$ but discharge the least of wastewater $u - \beta \cdot g_u$ with inputs held fixed. Accordingly, β is the proportions of maximum feasible increase in economic outputs and decrease in discharged wastewater towards the production frontier of EPTW. They take values larger than or equal to zero. The larger this value takes, the wider the gap between its current technology and the best practice is. Since the directional vector has been chosen at the observed outputs, the value of the distance function β is independent of measurement units for output variables [28, 36].

3.2. Environmental Productivity Index and Its Decomposition. According to Chung et al. [14], the above-defined directional distance function can be used to construct an environmentally sensitive productivity index (namely, EPI_{WE}). To avoid the impact of arbitrarily employing a reference technology on the final result, $EPI_{WE}^{t,t+1}$ is defined as follows:

$$\begin{aligned}\mathrm{EPI}_{\mathrm{WE}}^{t,t+1} = \Bigg(& \frac{1 + \overrightarrow{D}^{t}\left(\mathbf{x}^{t}, \mathbf{y}^{t}, \mathbf{u}^{t}\right)}{1 + \overrightarrow{D}^{t}\left(\mathbf{x}^{t+1}, \mathbf{y}^{t+1}, \mathbf{u}^{t+1}\right)} \\ & \cdot \frac{1 + \overrightarrow{D}^{t+1}\left(\mathbf{x}^{t}, \mathbf{y}^{t}, \mathbf{u}^{t}\right)}{1 + \overrightarrow{D}^{t+1}\left(\mathbf{x}^{t+1}, \mathbf{y}^{t+1}, \mathbf{u}^{t+1}\right)}\Bigg)^{1/2},\end{aligned} \tag{2}$$

where $\overrightarrow{D}^{t}(\mathbf{x}^{t}, \mathbf{y}^{t}, \mathbf{u}^{t})$ and $\overrightarrow{D}^{t+1}(\mathbf{x}^{t+1}, \mathbf{y}^{t+1}, \mathbf{u}^{t+1})$ are contemporaneous environmental directional distance functions capturing the distance of the observed input-output combination of one producer from the current best practice. $\overrightarrow{D}^{t}(\mathbf{x}^{t+1}, \mathbf{y}^{t+1}, \mathbf{u}^{t+1})$ and $\overrightarrow{D}^{t+1}(\mathbf{x}^{t}, \mathbf{y}^{t}, \mathbf{u}^{t})$ refer to cross-period distance functions, which compare the observed data at period $t + 1$ (or t) to the frontier at period t (or $t + 1$). Here $EPI_{WE}^{t,t+1}$ measures the intertemporal changes of the productivity level related to the EPTWs. $EPI_{WE}^{t,t+1} > 1$ shows the productivity improvement for one production unit in period $t + 1$ compared to period t. On the contrary, $EPI_{WE}^{t,t+1} < 1$ indicates productivity decline; that is, this producer uses some technologies not friendly to wastewater reduction and economic growth in period $t + 1$. It is worthwhile to note that there may exist productivity decline when the speed of one production unit undertaking wastewater reduction activities is slower than that of the frontier technology. $EPI_{WE}^{t,t+1} = 1$ indicates a relative stagnation in the EPTW's productivity level.

In general, one production unit can enhance its productivity of EPTWs by several measures, such as upgrading treatment technologies and optimizing the current technology process. To identify the drivers of the change in environmentally sensitive productivity, the $\mathrm{EPI}_{\mathrm{WE}}$ index can further be decomposed into two components: technological change ($\mathrm{EPITC}_{\mathrm{WE}}$) represented as the shift in the EPTWs' frontier and technical efficiency change ($\mathrm{EPIEC}_{\mathrm{WE}}$) as the move towards the best practice:

$$\mathrm{EPI}_{\mathrm{WE}}^{t,t+1} = \mathrm{EPITC}_{\mathrm{WE}}^{t,t+1} \cdot \mathrm{EPIEC}_{\mathrm{WE}}^{t,t+1}, \tag{3}$$

where

$$\mathrm{EPITC}_{\mathrm{WE}}^{t,t+1} = \left(\frac{1+\overrightarrow{D}^{t+1}\left(\mathbf{x}^t, \mathbf{y}^t, \mathbf{u}^t\right)}{1+\overrightarrow{D}^{t}\left(\mathbf{x}^t, \mathbf{y}^t, \mathbf{u}^t\right)} \cdot \frac{1+\overrightarrow{D}^{t+1}\left(\mathbf{x}^{t+1}, \mathbf{y}^{t+1}, \mathbf{u}^{t+1}\right)}{1+\overrightarrow{D}^{t}\left(\mathbf{x}^{t+1}, \mathbf{y}^{t+1}, \mathbf{u}^{t+1}\right)} \right)^{1/2},$$
$$\mathrm{EPIEC}_{\mathrm{WE}}^{t,t+1} = \frac{1+\overrightarrow{D}^{t}\left(\mathbf{x}^t, \mathbf{y}^t, \mathbf{u}^t\right)}{1+\overrightarrow{D}^{t+1}\left(\mathbf{x}^{t+1}, \mathbf{y}^{t+1}, \mathbf{u}^{t+1}\right)}. \tag{4}$$

Here $\mathrm{EPITC}_{\mathrm{WE}}^{t,t+1}$ measures the geometric mean of the shift in the frontier of the EPTW in each two-year period. $\mathrm{EPITC}_{\mathrm{WE}}^{t,t+1} > 1$ indicates the technological progress of EPTWs, resulting from the innovation activities that attain economic growth and wastewater reduction simultaneously. $\mathrm{EPITC}_{\mathrm{WE}}^{t,t+1} < 1$ and $\mathrm{EPITC}_{\mathrm{WE}}^{t,t+1} = 1$ reflect a regress and relative stagnation of the EPTW frontier, respectively. $\mathrm{EPIEC}_{\mathrm{WE}}^{t,t+1}$ is the change of distances between the used technologies and the current EPTW frontier throughout two periods, which captures the speed by which producer moves towards the current best practice, namely, catch-up or fall-behind effect. $\mathrm{EPIEC}_{\mathrm{WE}}^{t,t+1} > 1$ implies technical efficiency improvement of EPTWs, as a result of the enhancements of labors' operation skills and managerial and institutional environment with respect to the EPTW; $\mathrm{EPIEC}_{\mathrm{WE}}^{t,t+1} < 1$ shows that technical efficiency declines due to deteriorated operating environment.

3.3. Calculation of EPI_{WE} and Its Two Components. To avoid the misspecification of the functional form often confounded by econometrics methods, this paper employs nonparametric data envelopment analysis (DEA) technique to compute the values of $\mathrm{EPI}_{\mathrm{WE}}^{t,t+1}$, $\mathrm{EPITC}_{\mathrm{WE}}^{t,t+1}$, and $\mathrm{EPIEC}_{\mathrm{WE}}^{t,t+1}$. Given that the technologies developed in previous periods are still feasible in the following years, sequential DEA technique is used to construct the best practice with its main merit of eliminating the possibility of registering any technical regress by definition [28, 37]. Then the benchmark at period t should be $\overline{T}^t = T^1 \cup T^2 \cup \cdots \cup T^t$, where T^t derived from the observed data of a set of N entities at time t can be written as follows:

$$\begin{aligned} T^t\left(\mathbf{x}^t, \mathbf{y}^t, \mathbf{u}^t\right) &= \left\{\left(\mathbf{x}^t, \mathbf{y}^t, \mathbf{u}^t\right) : \mathbf{x}^t \text{ can produce } \left(\mathbf{y}^t, \mathbf{u}^t\right)\right\} \\ &= \left\{\left(\mathbf{x}^t, \mathbf{y}^t, \mathbf{u}^t\right) : \sum_{i=1}^{N} z_i^t x_{ki}^t \le x_{ki}^t,\ \sum_{i=1}^{N} z_i^t y_{mi}^t \right. \\ &\quad \left. \ge y_{mi}^t,\ \sum_{i=1}^{N} z_i^t u_i^t = u_i^t,\ z_i^t \ge 0,\ i = 1, \ldots, N\right\}, \end{aligned} \tag{5}$$

where z_i^t is the weight assigned to corresponding observation. The inequality constraints on the inputs and economic outputs as well as the equality constraint on discharged wastewater reflect their strong and weak disposability, respectively.

For the ith producer at time t, the contemporaneous distance function $\overrightarrow{D}^t(x^t, y^t, u^t; g^t)$ can be calculated by solving the following linear programming:

$$\begin{aligned} \overrightarrow{D}^t\left(x^t, y^t, u^t; g^t\right) = \max \quad & \beta_i^{t,t} \\ \text{s.t.} \quad & \sum_{s=1}^{t}\sum_{i=1}^{N} z_i^s x_{hi}^s \le x_{ki}^t, \\ & k = 1, \ldots, K \\ & \sum_{s=1}^{t}\sum_{i=1}^{N} z_i^s y_i^s \ge y_{mi}^t + \beta_i^{t,t} y_{mi}^t, \\ & m = 1, \ldots, M \\ & \sum_{s=1}^{t}\sum_{i=1}^{N} z_i^s u_i^s = u_i^t - \beta_i^{t,t} u_i^t, \\ & z_i^s, \beta_i^{t,t} \ge 0, \\ & \forall i, k, m;\ i = 1, \ldots, N. \end{aligned} \tag{6}$$

The intertemporal distance function $\overrightarrow{D}^t(x^{t+1}, y^{t+1}, u^{t+1}; g^{t+1})$ for the ith entity can be computed from the following linear programming:

$$\begin{aligned} \overrightarrow{D}^t\left(x^{t+1}, y^{t+1}, u^{t+1}; g^{t+1}\right) = \max \quad & \beta_i^{t,t+1} \\ \text{s.t.} \quad & \sum_{s=1}^{t}\sum_{i=1}^{N} z_i^s x_{hi}^s \le x_{ki}^{t+1}, \\ & k = 1, \ldots, K \\ & \sum_{s=1}^{t}\sum_{i=1}^{N} z_i^s y_i^s \\ & \ge y_{mi}^{t+1} \\ & + \beta_i^{t,t+1} y_{mi}^{t+1}, \end{aligned}$$

Table 1: Descriptive statistics of the variables, 2002–2015.

Variables	Units	Mean	Std.D.	Min	Max	Median	Obs.
K	Billion Yuan	2755	2518	129	13882	1977	420
L	Thousand Person	24667	16325	2470	66360	20605	420
W	Billion Cubic meters	20	14	2	59	18	420
Real GDP	Billion Yuan	900	849	32	4795	643	420
WD	Million tce	1962	1580	111	9115	1491	420

$$
\begin{aligned}
& m = 1, \ldots, M \\
& \sum_{s=1}^{t} \sum_{i=1}^{N} z_i^s u_i^s \\
& = u_i^{t+1} \\
& \quad - \beta_i^{t,t+1} u_i^{t+1}, \\
& z_i^s, \beta_i^{t,t+1} \geq 0, \\
& \forall i, k, m; \; i = 1, \ldots, N.
\end{aligned} \tag{7}
$$

Likewise, $\overrightarrow{D}^t(x^{t+1}, y^{t+1}, u^{t+1}; g^{t+1})$ and $\overrightarrow{D}^{t+1}(x^t, y^t, u^t; g^t)$ can also be calculated by solving a similar linear programming.

4. Results and Discussions

4.1. Data Descriptions. The study sample of this paper contains 30 inland administrative provinces (provinces, autonomous regions, and municipalities) in China during 2002–2015. Due to the absence of basic data on wastewater discharge, the Tibet autonomous region is not included in current study.

As shown in (6) and (7), there are three kinds of factor inputs (including capital, labor, and water) and two kinds of outputs (one desirable output and one undesirable output). Here the amounts of capital input (K) and labor input (L) are represented by capital stock and employed persons, respectively, while the water resource input (W) is measured by regional total water consumption. Besides, real GDP and total wastewater discharges (WD) serve as the proxies of desirable output and undesirable output, respectively.

First of all, the amount of province-level capital stock has not been reported in any China's official statistics. Following previous studied [38], we calculate it using perpetual inventory method. The data on employed persons is collected from annual *China Statistical Yearbooks* and *China Regional Economics Statistical Yearbook* (CRESY, 2007). The basic data on provincial total water consumption during 2002-2003 and 2004–2015 can, respectively, be obtained from *China Environmental Statistical Yearbooks* (CESYs, 2003-2004) and *China Statistical Yearbooks* (CSYs, 2005–2016). The real GDP is acquired from *China Statistical Yearbooks* (CSYs, 2003–2016) by deflating its nominal value with the GDP deflator, and the wastewater discharges are also collected from *China Statistical Yearbooks* (CSYs, 2003–2016). Furthermore, both real GDP and capital stock are measured with 1995 price levels.

Table 1 reports the descriptive statistics of the five variables over the whole study period. In general, the mean values for all the variables are much larger than the median values, indicating that most regions are observed near the left tail of the distribution. Moreover, the standard deviation is less than the mean value, showing that there are no outliers for all series.

4.2. Spatial-Temporal Variations of China's EPI_{WE}. The results of environmental productivity index concerning both economic growth and wastewater reduction for each administrative province as well as the national average during 2003–2015 are reported in the Appendix.

4.2.1. Intertemporal Change of China's Environmental Productivity Index. According to the results shown in Table 2, the dynamic feature of China's EPI_{WE} can be investigated (Figure 2). Generally speaking, the environmental productivity index of national average has experienced frequent fluctuations over the past decade, which declined gradually from 1.017 in 2003 to 1.010 in 2005 and then increased in 2006 due to the implementation of China's energy saving and emissions reduction policy. After that, the productivity index dropped sharply from 1.017 in 2007 to 1.001 in 2008 and then went up again from 1.002 in 2009 to 1.009 in 2010. With the overfulfillment of the target of ten percent COD reduction in the 11th five-year plan (FYP), the stress for emissions reduction from the central government temporarily relieved. In this context, the environmental productivity index declined greatly from 1.009 in 2010 to 1.002 in 2011 and even to 0.997 in 2012. In order to accomplish the target of COD reduction in the 12th FYP (2011–2015), the State Council issued *the Most Stringent Water Management System* in 2012, in which the strict system of limiting pollution discharges in water function area has been established. With the execution of a series of pollution control polices including administrative interventions, technical progress, and economic instruments, the water desirable productivity index went up consequently in the last three years of the 12th FYP.

Although frequent fluctuations for China's environmental productivity index over the whole study period have been identified, EPI_{WE} has been generally performing in a decline trend from a more long-term perspective (Figure 2). In particular, it was at a relatively high level (with the mean value

Table 2: Province-level productivity index of EPTW during 2003–2015.

Regions	2003	2004	2005	2006	2007	2008	2009	2010	2011	2012	2013	2014	2015
Beijing	1.043	1.134	1.028	1.038	1.184	1.006	1.110	0.959	1.026	0.848	0.977	0.981	1.000
Tianjin	1.000	1.023	1.000	1.000	1.000	1.002	1.000	1.000	1.000	1.000	1.000	1.000	1.000
Hebei	1.028	0.995	1.046	1.041	1.031	1.006	1.003	1.008	1.001	0.985	0.999	0.997	1.003
Shanxi	1.043	1.030	0.996	0.954	1.011	0.969	0.984	0.988	1.013	0.974	0.993	0.975	0.990
Inner Mongolia	1.007	1.052	1.066	1.070	1.012	1.012	1.043	0.956	1.010	1.026	1.017	1.012	1.036
Liaoning	1.011	1.000	1.000	1.000	1.012	0.962	1.013	1.024	0.999	0.995	1.005	0.963	1.002
Jilin	1.021	1.033	0.987	0.944	1.007	0.998	1.011	1.006	1.024	1.014	1.011	0.999	1.000
Heilongjiang	1.015	1.016	1.011	1.000	1.000	1.000	1.000	1.001	0.986	0.986	1.022	1.009	1.004
Shanghai	1.029	1.031	1.017	0.999	1.037	1.000	1.000	1.013	1.000	1.008	1.000	1.005	1.000
Jiangsu	1.020	1.022	1.018	0.989	1.040	1.016	1.005	1.004	0.996	0.999	1.022	1.024	1.016
Zhejiang	1.038	1.032	1.017	1.047	1.017	1.015	1.005	1.090	0.940	1.014	1.016	1.016	1.008
Anhui	1.026	1.006	1.012	0.989	1.032	0.982	0.990	1.012	1.002	1.017	0.922	0.996	0.993
Fujian	1.013	1.030	1.026	1.038	1.018	1.000	0.989	1.013	0.983	1.007	1.016	1.015	1.019
Jiangxi	0.997	0.972	0.986	0.999	0.984	1.019	0.996	1.014	0.981	1.014	1.001	1.022	1.099
Shandong	1.010	1.009	1.001	1.000	1.004	1.000	1.000	0.999	1.000	1.000	1.000	1.001	1.001
Henan	1.027	1.023	1.002	0.964	0.976	0.950	0.981	0.996	0.998	0.986	0.991	0.996	0.998
Hubei	1.020	1.038	1.027	1.017	1.031	1.014	0.998	1.007	1.009	0.966	0.991	1.001	0.996
Hunan	1.000	1.003	1.000	0.999	1.009	0.991	0.982	0.982	0.974	0.967	0.975	1.001	1.002
Guangdong	1.033	1.000	1.016	1.000	1.012	1.000	0.981	1.011	0.983	0.998	0.918	0.965	0.980
Guangxi	1.029	0.982	1.040	0.883	1.104	0.909	0.823	0.914	1.052	0.988	1.039	1.019	1.010
Hainan	1.007	0.956	1.010	1.042	1.045	1.021	1.021	1.051	1.039	1.015	1.040	0.999	1.027
Chongqing	0.993	0.937	0.977	0.975	0.998	0.985	1.014	1.032	1.045	1.036	0.981	1.016	1.020
Sichuan	1.032	1.019	1.011	1.078	1.018	1.013	1.034	1.058	1.035	1.037	1.009	1.003	1.010
Guizhou	1.000	1.033	1.039	1.071	1.025	1.028	1.012	1.026	0.973	0.986	1.012	0.967	1.003
Yunnan	1.022	0.992	1.038	1.035	1.009	1.035	1.022	1.013	0.913	1.005	1.166	0.859	0.843
Shannxi	1.018	1.019	1.012	1.055	0.987	1.026	1.011	1.013	1.007	1.002	1.001	0.987	0.974
Gansu	0.980	1.000	1.022	1.035	1.019	1.001	1.015	1.019	0.987	1.013	1.012	1.009	1.006
Qinghai	1.040	0.957	0.943	1.112	0.967	1.036	0.993	1.026	1.040	1.012	1.031	1.013	1.016
Ningxia	1.026	1.022	0.935	1.109	0.944	1.014	0.998	1.017	1.020	1.015	1.020	1.021	1.057
Xinjiang	0.982	1.012	1.018	1.077	0.980	1.006	1.011	1.003	1.029	0.991	0.994	1.200	1.014
National average	1.017	1.013	1.010	1.019	1.017	1.001	1.002	1.009	1.002	0.997	1.006	1.002	1.004

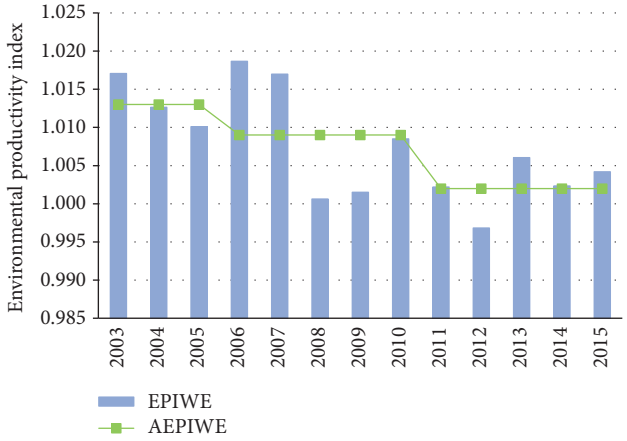

Figure 2: Intertemporal change of China's EPI_{WE}. *Note.* $AEPI_{WE}$ means the average EPI_{WE} in each period.

at 1.013) in the last three years of the 10th FYP; after that the EPI_{WE} decreased in the 11th FYP (2006–2010) with the mean value at 1.009, and then it continued to decline in the 12th FYP (2011–2015) with its mean value at merely 1.002. According to the definition of EPI_{WE} in the Section 3, the descending EPI_{WE} greater than one (with the sole exception in 2012) during different periods means that although the improvement of environmental productivity in China is observed through the whole studied period, its rate slowed down over time.

4.2.2. Regional Difference of China's EPI_{WE}. The spatial variations of China's environmental productivity index related to wastewater reduction during 2003–2015 are also examined (Figure 3). As we observe from Figure 3 that nearly three-fourths of the studied administrative provinces have achieved environmentally preferable productivity improvements over the whole study period. In particular, the productivity index in six provinces such as Sichuan, Beijing, Inner Mongolia, Xinjiang, Hainan, and Zhejiang has achieved significant increases with their annual mean values surpassing 1.02; seven provinces including Ningxia, Qinghai, Jiangsu, Fujian,

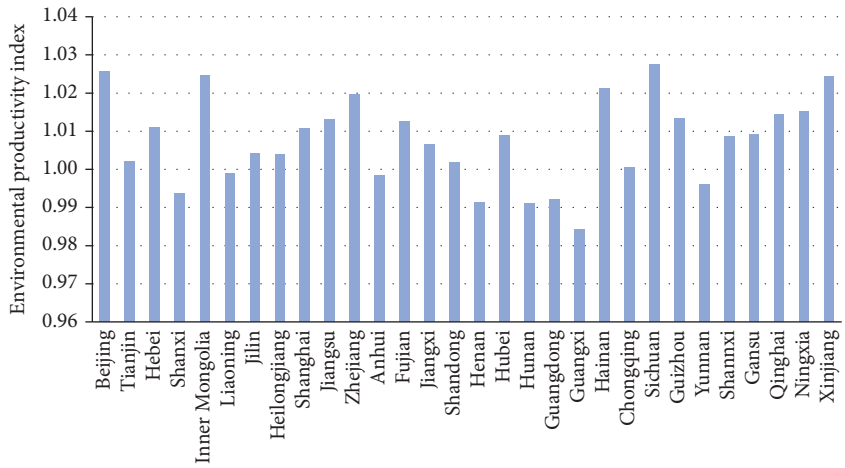

Figure 3: Spatial variations of China's EPI_{WE}.

Guizhou, Shanghai, and Hebei have also gotten moderate environmental productivity improvements with their annual mean values within 1.01–1.02; nine administrative provinces such as Hubei, Shannxi, Gansu, Jiangxi, Jilin, Heilongjiang, Tianjin, Shandong, and Chongqing saw little water desirable productivity improvement with their annual mean values within 1.00–1.01. In contrast, EPI_{WE} in the rest eight provinces (including Guangxi, Henan, Hunan, Guangdong, Shanxi, Yunnan, Anhui, and Liaoning) has undergone decrease by different extents. It can be concluded from the definition of environmental productivity index analyzed above that the actual performance of EPTWs in most of the administrative provinces had been meliorated.

4.3. Decompositions on China's EPI_{WE} Variations. Based on (4), the intertemporal changes of China's water preferable productivity index are decomposed and the main drivers of productivity change for all the studied regions are further identified. As shown in Figure 4, the mean values for $EPITC_{WE}^{t,t+1}$ component are higher than that of $EPI_{WE}^{t,t+1}$ in most of the years (excluding 2006, 2010, 2013, and 2015), which implies the improvements of environmental productivity with respect to wastewater reduction over the whole studied period can mainly be attributed to the shift of water desirable production technology frontier, as a result of innovation activities associated with water-saving and wastewater purification. By contrast, the mean values of the $EPIEC_{WE}^{t,t+1}$ component are persistently lower than that of $EPI_{WE}^{t,t+1}$ (with the sole exception in 2013), demonstrating that the technical efficiency change has overall impeded the improvements of China's water desirable productivity. Besides, another obvious evolution trend can be observed: the gap between the two components, that is, $EPITC_{WE}^{t,t+1}$ and $EPIEC_{WE}^{t,t+1}$, was very large before 2009; then it began to narrow since 2010, and the mean values of the technical efficiency change component were even higher than that of the technical change component in 2013 and 2015. It can be inferred from this evolution trend that the technical efficiency improvement will play a more and more important role in the enhancement of water preferable productivity in the future.

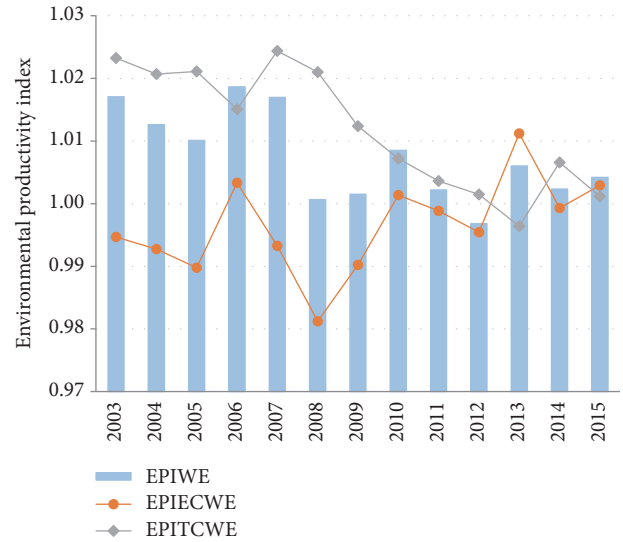

Figure 4: Decomposition on China's EPI_{WE}.

The decompositions on the intertemporal changes of cross-region environmental productivity index are also conducted. For the sake of saving space, we divide the whole study period into three substages, that is, 2003–2005 (the last 3 years in the 10th FYP), 2006–2010 (the 11th FYP), and 2011–2015 (the 12th FYP). The variation processes of the cross-region environmental productivity index decompositions are shown in Table 3.

In the first stage (2003–2005), the $EPITC_{WE}$ index is significantly higher than the $EPIEC_{WE}$ index for most of the regions with the sole exception of Guangxi Zhuang Autonomous Region. In the second stage, the gap between the two components began to narrow, which is highly consistent with the variation trend of the whole country. In the third stage, the gap between $EPITC_{WE}$ and $EPIEC_{WE}$ further

Table 3: Decomposition on cross-region EPI_{WE} in China.

Regions	2003–2005			2006–2010			2011–2015		
	EPI_{WE}	$EPITC_{WE}$	$EPIEC_{WE}$	EPI_{WE}	$EPITC_{WE}$	$EPIEC_{WE}$	EPI_{WE}	$EPITC_{WE}$	$EPIEC_{WE}$
Beijing	1.068	1.068	1.013	1.059	1.051	1.022	0.966	0.989	0.979
Tianjin	1.008	1.008	1.000	1.000	1.000	1.000	1.000	1.000	1.000
Hebei	1.023	1.030	0.994	1.018	1.018	0.999	0.997	1.002	0.995
Shanxi	1.023	1.032	0.991	0.981	1.007	0.974	0.989	1.001	0.988
Inner Mongolia	1.042	1.027	1.014	1.018	1.037	0.982	1.020	1.018	1.002
Liaoning	1.004	1.004	1.000	1.002	1.011	0.991	0.993	1.006	0.987
Jilin	1.014	1.021	0.993	0.993	1.021	0.973	1.010	1.005	1.004
Heilongjiang	1.014	1.014	1.000	1.000	1.000	1.000	1.002	1.002	1.000
Shanghai	1.026	1.026	1.000	1.010	1.010	1.000	1.003	1.003	1.000
Jiangsu	1.020	1.020	1.000	1.011	1.015	0.996	1.011	1.014	0.997
Zhejiang	1.029	1.045	0.985	1.035	1.035	1.000	0.999	0.997	1.002
Anhui	1.015	1.017	0.998	1.001	1.006	0.995	0.986	0.995	0.992
Fujian	1.023	1.035	0.989	1.012	1.014	0.998	1.008	1.009	0.999
Jiangxi	0.985	1.028	0.958	1.002	1.007	0.996	1.023	1.001	1.022
Shandong	1.007	1.007	1.000	1.001	1.001	1.000	1.000	1.000	1.000
Henan	1.018	1.013	1.004	0.973	1.005	0.968	0.994	1.002	0.992
Hubei	1.028	1.021	1.007	1.013	1.007	1.007	0.993	1.004	0.989
Hunan	1.001	1.001	1.000	0.993	1.002	0.991	0.984	1.002	0.982
Guangdong	1.016	1.016	1.000	1.001	1.001	1.000	0.969	1.001	0.968
Guangxi	1.017	0.977	1.045	0.927	0.995	0.932	1.022	1.001	1.020
Hainan	0.991	1.027	0.966	1.036	1.032	1.004	1.024	1.017	1.008
Chongqing	0.969	1.010	0.960	1.001	1.003	0.998	1.020	1.002	1.018
Sichuan	1.021	1.022	0.999	1.040	1.024	1.016	1.019	1.004	1.015
Guizhou	1.024	1.022	1.001	1.032	1.025	1.007	0.988	1.002	0.986
Yunnan	1.017	1.026	0.991	1.023	1.026	0.996	0.957	0.978	0.996
Shannxi	1.016	1.027	0.990	1.018	1.021	0.998	0.994	1.001	0.993
Gansu	1.001	1.034	0.968	1.018	1.029	0.989	1.005	1.002	1.003
Qinghai	0.980	1.027	0.954	1.027	1.027	1.000	1.023	1.013	1.010
Ningxia	0.994	1.017	0.978	1.016	1.016	1.001	1.026	1.008	1.018
Xinjiang	1.004	1.031	0.975	1.015	1.033	0.983	1.045	0.977	1.082

Note. Theoretically speaking, EPI_{WE} equals the product of $EPITC_{WE}$ and $EPIEC_{WE}$. However, given that all the figures in the table are multiyear mean values, EPI_{WE} does not equal to the product of $EPITC_{WE}$ and $EPIEC_{WE}$ sometimes. Fortunately, this situation is rare.

shrinks; and the $EPITC_{WE}$ in some of the studied regions is even lower than the $EPIEC_{WE}$, such as in Jiangxi, Chongqing, Sichuan, Ningxia, and Xinjiang. It can be well interpreted by the rising marginal abatement cost of wastewater treatment technologies. As the low-hanging fruits are picked, the potential of promoting wastewater reduction by means of adopting environmentally friendly technologies is getting less and less, and more attention should be paid to the approach of enhancing management skills and institutional renovations.

5. Conclusions and Policy Implications

In the face of China's deteriorated water environmental quality, the central government had formulated and carried out a series of environmental regulation policies for effluent discharge reduction during the past one and a half decades. Although the total emissions for some key indicators such as COD and ammonia nitrogen are in a decline trend, the overall water environmental quality in this developing country has not been fundamentally improved, and the total wastewater discharge has even increased by nearly 50% during the last decade. Low economic profit is considered the main barrier for firms to operate wastewater treatment technologies effectively.

In this study, we aim to evaluate the productivity change of EPTWs for 30 provincial regions in China during 2003–2015 using the ML index. To clearly identify the dominant drivers of the productivity change, this productivity index is further decomposed into two components including technological change and technical efficiency change. The results indicate that, first, the average environmental productivity index nationwide has experienced frequent fluctuations over the whole study period; when we further compare the mean values of EPI_{WE} among different substages, this key index has been generally performing in a decline trend (the

mean values were 1.013 in the last three years of the 10th FYP, 1.009 in the 11th FYP, and 1.002 in the 12th FYP, resp.). Second, there exist significant spatial variations of China's environmental productivity index. In particular, the EPI_{WE} in Sichuan, Beijing, and Inner Mongolia had achieved great increases, while it had undergone decrease by different extents in eight administrative provinces such as Guangxi, Henan, and Hunan. Last but not least, the improvements of China's water desirable productivity over the whole studied period can mainly be attributed to technological innovation activities, while the technical efficiency change has contributed relatively little. However, as the low-hanging fruits have been picked, the technical efficiency component is expected to play a more and more important role in the future.

According to the conclusions drawn above, we put forward the following policy recommendations: (1) given that the total discharges of some key indicators for wastewater pollutant, such as COD and ammonia nitrogen, have been well controlled, more attention should be paid to the total sewage discharge reduction. Otherwise, the water environment quality in China can hardly be improved fundamentally without a clear and powerful environmental regulation policy. (2) Since the marginal abatement cost for wastewater discharge through engineering technology approaches (the technological change component) becomes higher and higher, more importance should be given to industrial restructuring as well as management institutional innovation (the technical efficiency component) from a long run. In this way, the abatement cost for effluent discharge can be well controlled, and the performance for wastewater treatment technologies can be enhanced. (3) The stringent wastewater environmental regulations should be persistently implemented without any loosening. In this respect, some market-based policies such as the labeling instrument can be taken into account since they encourage voluntary actions by enterprises and consumers to undertake wastewater treatment activities [39–41].

Appendix

Results of EPI_{WE} for 30 administrative provinces from 2003 to 2015 are shown in Table 2.

Conflicts of Interest

The authors declare that there are no conflicts of interest regarding the publication of this paper. The mentioned received funding in Acknowledgments did not lead to any conflicts of interest regarding the publication of this manuscript.

Acknowledgments

Financial supports from the Natural Science Foundation of China (Grants nos. 71503094, 71774122, and 71303177), the Major Program of the National Social Science Foundation of China (Grants nos. 16ZDA006 and 16ZDA039), Key Project of Philosophy and Social Sciences Research, Ministry of Education in China (Grant no. 15JZD014), and the Fundamental Research Funds for the Central Universities (2017QN035) are greatly acknowledged.

References

[1] D. Han, M. J. Currell, and G. Cao, "Deep challenges for China's war on water pollution," *Environmental Pollution*, vol. 218, pp. 1222–1233, 2016.

[2] Q. Wang and Z. Yang, "Industrial water pollution, water environment treatment, and health risks in China," *Environmental Pollution*, vol. 218, pp. 358–365, 2016.

[3] X. Zheng, Z. Zhang, D. Yu et al., "Overview of membrane technology applications for industrial wastewater treatment in China to increase water supply," *Resources Conservation & Recycling*, vol. 105, pp. 1–10, 2015.

[4] S. Lyu, W. Chen, W. Zhang, Y. Fan, and W. Jiao, "Wastewater reclamation and reuse in China: opportunities and challenges," *Journal of Environmental Sciences*, vol. 39, no. 1, pp. 86–96, 2016.

[5] http://env.people.com.cn/n/2015/0304/c1010-26633791.html.

[6] G. Wu, Z. Miao, S. Shao et al., "Evaluating the construction efficiencies of urban wastewater transportation and treatment capacity: evidence from 70 megacities in China," *Resources Conservation & Recycling*, vol. 128, pp. 373–381, 2018.

[7] Q. H. Zhang, W. N. Yang, H. H. Ngo et al., "Current status of urban wastewater treatment plants in China," *Environment International*, vol. 92-93, pp. 11–22, 2016.

[8] D. Bixio, C. Thoeye, J. D. Koning et al., "Wastewater reuse in Europe," *Desalination*, vol. 187, no. 1–3, pp. 89–101, 2006.

[9] T. Asano, F. L. Burton, H. L. Leverenz et al., Eds., *Water Reuse: Issue, Technologies, and Applications*, McGraw-Hill, New York, NY, USA, 2007.

[10] Z. Li, N. Meng, and X. Yao, "Sustainability performance for China's transportation industry under the environmental regulation," *Journal of Cleaner Production*, vol. 142, pp. 688–696, 2017.

[11] W. Jiao, S. Luo, Z. He, and Y. Liu, "Applications of high gravity technologies for wastewater treatment: A review," *Chemical Engineering Journal*, vol. 313, pp. 912–927, 2017.

[12] F. Boons, C. Montalvo, J. Quist, and M. Wagner, "Sustainable innovation, business models and economic performance: an overview," *Journal of Cleaner Production*, vol. 45, no. 2, pp. 1–8, 2013.

[13] W. Chen, S. Lu, W. Jiao, M. Wang, and A. C. Chang, "Reclaimed water: A safe irrigation water source?" *Environmental Development*, vol. 8, no. 1, pp. 74–83, 2013.

[14] Y. H. Chung, R. Färe, and S. Grosskopf, "Productivity and undesirable outputs: A directional distance function approach," *Journal of Environmental Management*, vol. 51, no. 3, pp. 229–240, 1997.

[15] R. Färe, S. Grosskopf, and C. A. Pasurka Jr., "Accounting for air pollution emissions in measures of state manufacturing productivity growth," *Journal of Regional Science*, vol. 41, no. 3, pp. 381–409, 2001.

[16] A. Hailu and T. S. Veeman, "Environmentally sensitive productivity analysis of the Canadian pulp and paper industry, 1959–1994: an input distance function approach," *Journal of Environmental Economics & Management*, vol. 40, no. 3, pp. 251–274, 2000.

[17] B. K. Yörük and O. Zaim, "Productivity growth in OECD countries: A comparison with Malmquist indices," *Journal of Comparative Economics*, vol. 33, no. 2, pp. 401–420, 2005.

[18] B. Mahlberg, M. Luptacik, and B. K. Sahoo, "Examining the drivers of total factor productivity change with an illustrative example of 14 EU countries," *Ecological Economics*, vol. 72, no. 1725, pp. 60–69, 2011.

[19] J. Ananda and B. Hampf, "Measuring environmentally sensitive productivity growth: An application to the urban water sector," *Ecological Economics*, vol. 116, pp. 211–219, 2015.

[20] A. Emrouznejad and G.-L. Yang, "A framework for measuring global Malmquist–Luenberger productivity index with CO2 emissions on Chinese manufacturing industries," *Energy*, vol. 115, pp. 840–856, 2016.

[21] H. Fujii, J. Cao, and S. Managi, "Firm-level environmentally sensitive productivity and innovation in China," *Applied Energy*, vol. 184, pp. 915–925, 2016.

[22] K. Li and B. Lin, "Impact of energy conservation policies on the green productivity in China's manufacturing sector: Evidence from a three-stage DEA model," *Applied Energy*, vol. 168, pp. 351–363, 2016.

[23] S. Chen and J. Golley, "'Green' productivity growth in China's industrial economy," *Energy Economics*, vol. 44, pp. 89–98, 2014.

[24] K. Li and B. Lin, "Measuring green productivity growth of Chinese industrial sectors during 1998–2011," *China Economic Review*, vol. 36, pp. 279–295, 2015.

[25] N. Zhang, P. Zhou, and C.-C. Kung, "Total-factor carbon emission performance of the Chinese transportation industry: A bootstrapped non-radial Malmquist index analysis," *Renewable & Sustainable Energy Reviews*, vol. 41, pp. 584–593, 2015.

[26] H. Fujii, S. Kaneko, and S. Managi, "Changes in environmentally sensitive productivity and technological modernization in China's iron and steel industry in the 1990s," *Environment and Development Economics*, vol. 15, no. 4, pp. 485–504, 2010.

[27] F. Yang, M. Yang, and H. Nie, "Productivity trends of Chinese regions: A perspective from energy saving and environmental regulations," *Applied Energy*, vol. 110, pp. 82–89, 2013.

[28] F. Yang and M. Yang, "Analysis on China's eco-innovations: regulation context, intertemporal change and regional differences," *European Journal of Operational Research*, vol. 247, no. 3, pp. 1003–1012, 2015.

[29] F. He, Q. Zhang, J. Lei, W. Fu, and X. Xu, "Energy efficiency and productivity change of China's iron and steel industry: Accounting for undesirable outputs," *Energy Policy*, vol. 54, pp. 204–213, 2013.

[30] F. Tao, H. Zhang, J. Hu, and X. H. Xia, "Dynamics of green productivity growth for major Chinese urban agglomerations," *Applied Energy*, vol. 196, pp. 170–179, 2017.

[31] H. Xie, W. Wang, Z. Yang, and Y. Choi, "Measuring the sustainable performance of industrial land utilization in major industrial zones of China," *Technological Forecasting & Social Change*, vol. 112, pp. 207–219, 2016.

[32] Y. Wang, Y. Bian, and H. Xu, "Water use efficiency and related pollutants' abatement costs of regional industrial systems in China: a slacks-based measure approach," *Journal of Cleaner Production*, vol. 101, p. 310, 2015.

[33] G. Deng, L. Li, and Y. Song, "Provincial water use efficiency measurement and factor analysis in China: Based on SBM-DEA model," *Ecological Indicators*, vol. 69, pp. 12–18, 2016.

[34] L. Zhao, C. Sun, and F. Liu, "Interprovincial two-stage water resource utilization efficiency under environmental constraint and spatial spillover effects in China," *Journal of Cleaner Production*, vol. 164, pp. 715–725, 2017.

[35] R. Färe and D. Primont, Eds., *Multi-Output Production and Duality: Theory and Applications*, Springer, Dordrecht, The Netherlands, 1995.

[36] N. Adler and E. Yazhemsky, "Improving discrimination in data envelopment analysis: PCA–DEA or variable reduction," *European Journal of Operational Research*, vol. 202, no. 1, pp. 273–284, 2010.

[37] V. Shestalova, "Sequential Malmquist indices of productivity growth: an application to OECD industrial activities," *Journal of Productivity Analysis*, vol. 19, no. 2-3, pp. 211–226, 2003.

[38] M. Yang, F.-X. Yang, and X.-P. Chen, "Effects of substituting energy with capital on China's aggregated energy and environmental efficiency," *Energy Policy*, vol. 39, no. 10, pp. 6065–6072, 2011.

[39] R. Zhao, X. Zhou, J. Han, and C. Liu, "For the sustainable performance of the carbon reduction labeling policies under an evolutionary game simulation," *Technological Forecasting & Social Change*, vol. 112, pp. 262–274, 2016.

[40] R. Zhao, X. Zhou, Q. Jin, Y. Wang, and C. Liu, "Enterprises' compliance with government carbon reduction labelling policy using a system dynamics approach," *Journal of Cleaner Production*, vol. 163, pp. 303–319, 2017.

[41] R. Zhao, Y. Geng, Y. Liu, X. Tao, and B. Xue, "Consumers' perception, purchase intention, and willingness to pay for carbon-labeled products: A case study of Chengdu in China," *Journal of Cleaner Production*, vol. 171, pp. 1664–1671, 2018.

Hindawi
BioMed Research International
Volume 2018, Article ID 8278970, 8 pages
https://doi.org/10.1155/2018/8278970

Research Article

Analysis of Bacterial Community Structure of Activated Sludge from Wastewater Treatment Plants in Winter

Shuang Xu, Junqin Yao, Meihaguli Ainiwaer, Ying Hong, and Yanjiang Zhang

College of Resources and Environmental Science, Xinjiang University, Urumqi, China

Correspondence should be addressed to Junqin Yao; 779855923@qq.com

Received 21 December 2017; Accepted 5 February 2018; Published 7 March 2018

Academic Editor: Bin Ma

Activated sludge bulking is easily caused in winter, resulting in adverse effects on effluent treatment and management of wastewater treatment plants. In this study, activated sludge samples were collected from different wastewater treatment plants in the northern Xinjiang Uygur Autonomous Region of China in winter. The bacterial community compositions and diversities of activated sludge were analyzed to identify the bacteria that cause bulking of activated sludge. The sequencing generated 30087–55170 effective reads representing 36 phyla, 293 families, and 579 genera in all samples. The dominant phyla present in all activated sludge were Proteobacteria (26.7–48.9%), Bacteroidetes (19.3–37.3%), Chloroflexi (2.9–17.1%), and Acidobacteria (1.5–13.8%). Fifty-five genera including *unclassified_f_Comamonadaceae*, *norank_f_Saprospiraceae*, *Flavobacterium*, *norank_f_Hydrogenophilaceae*, *Dokdonella*, *Terrimonas*, *norank_f_Anaerolineaceae*, *Tetrasphaera*, *Simplicispira*, *norank_c_Ardenticatenia*, and *Nitrospira* existed in all samples, accounting for 60.6–82.7% of total effective sequences in each sample. The relative abundances of Saprospiraceae, *Flavobacterium*, and *Tetrasphaera* with the respective averages of 12.0%, 8.3%, and 5.2% in bulking sludge samples were higher than those in normal samples. Filamentous Saprospiraceae, *Flavobacterium*, and *Tetrasphaera* multiplied were the main cause for the sludge bulking. Redundancy analysis (RDA) indicated that influent BOD_5, DO, water temperature, and influent ammonia had a distinct effect on bacterial community structures.

1. Introduction

Activated sludge process has been extensively used in industrial and domestic wastewater treatment because of its high microbial diversity and activity, resulting in the removal of most organic pollutants and nutrients [1]. It is reported that the composition and diversity of the microbial community had the greatest impact on stability and performance of the wastewater treatment systems [2]. The biological community of activated sludge has a large biological diversity and contains a variety of viruses, bacteria, protozoa, fungi, algae, and metazoan. In this complex ecosystem, bacteria typically account for 95% of the total number of microbes and play a crucial part in wastewater treatment [3]. In the secondary clarifying pond, good compaction (thickening) and separation (settling) of the activated sludge has a positive effect on the effluent quality. However, bulking sludge due to overgrowth of filamentous bacteria and/or *Zoogloea* organisms has a significant influence on the performance of the activated sludge system as it can result in poor settling and poor compaction [4]. The overgrowth of filamentous bacteria of activated sludge has significantly affected the operation of wastewater treatment plants for many years [5]. Sludge bulking can easily occur at low temperature, resulting in adverse effects on effluent treatment [6]. Therefore, sludge bulking in winter caused by low temperature is the focus of the study.

The high-throughput sequencing technologies originated several years ago are easier and less expensive for high-throughput sequencing [7]. This method has been broadly used in the evaluation of microbial communities of many environmental samples types such as activated sludge [8, 9], marine water [10], soil [11], and human distal intestine [12]. Some studies have focused on the difference in microbial community composition of activated sludge due to temporal and spatial changes [13], wastewater characteristics [14], and environmental and operational conditions [15] in municipal wastewater systems. The microbial communities in activated

Table 1: Characteristics of samples and wastewater treatment plants.

Sample	Sampling date	Flow rate (10^3 m^3/d)	DO (mg/L)	pH	SRT (days)	Tem (°C)	SV/%	MLSS (mg/L)	SVI/(mL/g)	BOD_5 (mg/L)		NH_4^+-N (mg/L)	
										Influent	Effluent	Influent	Effluent
ALT1	2016.12.1	3	3.8	7.0	27	9.8	35	5980	59	119	8	33.1	1.6
ALT2	2017.1.7	3	3.9	7.1	27	8.5	33	4861	69	97	9	29.7	2.0
SHZ1	2016.3.2	10	4.0	7.50	23	12.8	17	4186	41	147	39	28	3.0
SHZ2	2017.1.7	10	3.7	7.4	23	12.9	19	4297	44	164	30	27	3.2
CJ1	2016.1.25	10	1.5	6.75	30	13.6	88	3355	262	539	27	58	21.9
CJ2	2016.3.2	10	1.4	7.01	30	13.5	91	4512	202	533	25	47	20.6
HX1	2016.1.25	10	3.6	7.20	25	10.8	88	4354	199	276	11	50	5.8
HX2	2016.3.2	10	3.5	7.30	25	10.9	62	3543	175	276	26	31	5.2

sludge samples collected from wastewater treatment plants have been studied in different geographical location [16–18]. However, only few studies investigated the bacterial community compositions and diversities in various wastewater treatment plants (WWTPs) at different geographic locations in Xinjiang Uygur Autonomous Region of China via Illumina high-throughput sequencing technology, especially in winter.

The purpose of this study was to analyze bacterial community structures and diversities of activated sludge samples of different wastewater treatment plants in the north of Xinjiang Uygur Autonomous Region of China in winter via Illumina high-throughput sequencing technology. This study facilitates the evaluation of the similarities and differences in bacterial community composition of samples from different geographic locations and understanding the microbial interaction of activated sludge in Xinjiang.

2. Materials and Methods

2.1. Description of WWTPs and Sample Collection. Activated sludge samples were collected from the aeration tanks of four WWTPs located in the north of Xinjiang Uygur Autonomous Region of China in winter. These four WWTPs applied oxidation ditch process. The following 8 samples were collected: ALT1 and ALT2 from ALT WWTP; SHZ1 and SHZ2 from SHZ WWTP; CJ1 and CJ2 from CJ WWTP; HX1 and HX2 from HX WWTP. Sampling date, flow rate, influents, effluents, and operational parameters of the WWTPs are presented in Table 1. All WWTPs treat domestic wastewater, except for the SHZ WWTP. The influent of SHZ WWTP is composed of domestic and industrial wastewater, of which industrial wastewater accounts for 24%. SVI greater than 150 $mL \cdot g^{-1}$ is considered as bulking sludge [19]. Since the SVI of the samples from CJ and HX WWTPs were greater than 150 $mL \cdot g^{-1}$, the samples were bulking sludge, while the samples from ALT and SHZ WWTPs were normal sludge since their SVI were less than 150 $mL \cdot g^{-1}$ (Table 1). Additionally, the microscopic investigation showed that the sludge samples were filamentous bulking sludge.

The samples for the microbial analysis were stored in the laboratory at −40°C and were sent to Majorbio Bio-Pharm Technology Co. Ltd. (Shanghai, China) for DNA extraction, PCR amplification, and Illumina high-throughput sequencing.

2.2. DNA Extraction, PCR Amplification, and Illumina Sequencing. Microbial DNA was extracted from sludge samples collected from four WWTPs using the E.Z.N.A.® soil DNA Kit (Omega Bio-tek, Norcross, GA, US). The final DNA concentration and purification were determined by NanoDrop 2000 UV-vis spectrophotometer (Thermo Scientific, Wilmington, USA), whereas DNA quality was checked by 1% agarose gel electrophoresis. The V4-V5 hypervariable regions of the bacteria 16S r RNA gene were amplified with primers 515 F (5′-GTGCCAGCMGCCGCGG-3′) and 907 R (5′-CCGTCAATTCMTTTRAGTTT-3′) by thermocycler PCR system (GeneAmp 9700, ABI, USA). The PCR reactions were conducted using the following program: 3 min of denaturation at 95°C, 27 cycles of 30 s at 95°C, 30 s for annealing at 55°C, 45 s for elongation at 72°C, and a final extension at 72°C for 10 min. PCR reactions were performed in triplicate of 20 μL mixture containing 4 μL of 5x FastPfu Buffer, 2 μL of 2.5 mM dNTPs, 0.8 μL of each primer (5 μM), 0.4 μL of FastPfu Polymerase, and 10 ng of template DNA. The PCR products were extracted from a 2% agarose gel and further purified using the AxyPrep DNA Gel Extraction Kit (Axygen Biosciences, Union City, CA, USA). Then, the products were quantified using QuantiFluor™-ST (Promega, USA).

Purified amplicons were pooled in equimolar and paired-end sequenced (2 × 300) on an Illumina MiSeq platform (Illumina, San Diego, USA) according to the standard protocols of Majorbio Bio-Pharm Technology Co. Ltd. (Shanghai, China). The raw reads were deposited into the NCBI Sequence Read Archive (SRA) database (Accession Numbers: SRP113278, SRP125654, and SRP126028).

2.3. Data Analysis. Data analysis was conducted using the i-Sanger platform (http://www.i-sanger.com/) provided by Majorbio Bio-Pharm Technology Co. Ltd. (Shanghai, China). The microbial phylotype richness levels were calculated using the Chao/Ace estimator and the Shannon diversity index. The similarity and difference of samples were compared using the shared and unique OTUs of Venn diagram. The species diversity of the ecosystem was compared using the rarefaction curves, which are the commonly used

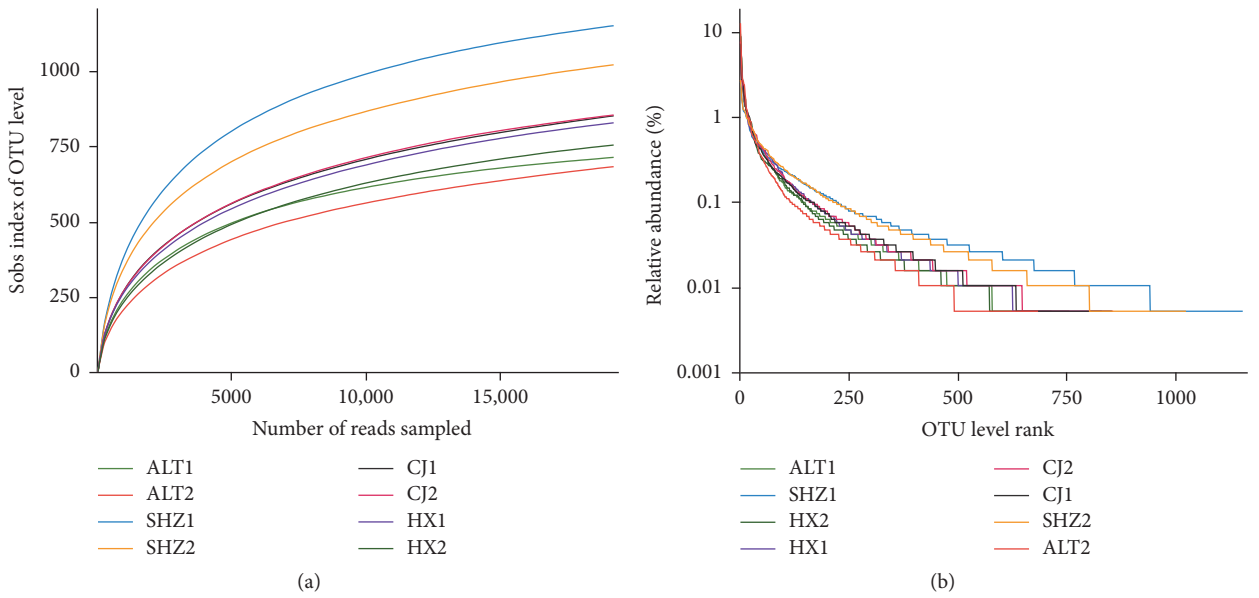

Figure 1: Diversity of bacterial communities in activated sludge samples. (a) Rarefaction curves and (b) rank abundance curves.

methods. Redundancy analysis (RDA) was used to analyze the relationship between the relative abundance of bacteria (genus level) and environmental variables, which is a type of constrained ordination. The Chao/Ace estimator, the Shannon diversity index, and the coverage percentage were also calculated by the Mothur program version v.1.30.1 (https://www.mothur.org/wiki/Schloss_SOP#Alpha_diversity). The similarity and differences between samples were compared using the shared and unique OTUs of the Venn diagram. The species diversity of the ecosystem was compared using the rarefaction curves, which are the commonly used methods. Redundancy analysis (RDA) was used to analyze the relationship between the relative abundance of bacteria (genus level) and environmental variables, which is a type of constrained ordination. These analyses were performed using the R Programming Language software.

3. Results and Discussion

3.1. Diversity Analysis for Bacterial Communities. As shown in Table 2, total effective reads of all activated sludge samples were 30087–55170. The microbial diversity index is listed in Table 2, comprising community richness (Ace, Chao) and community diversity (Shannon). Each sample was more than 99% of the coverage, indicating that the depth of the sequence was sufficient. According to the OTU number, the sample from SHZ WWTP had the richest diversity, followed closely by those from CJ and HX WWTP, whereas the sample from ALT WWTP displayed considerably less richness. According to Table 2, the values of Ace, Chao, and Shannon indices demonstrate that SHZ WWTP had the highest microbial diversity, while ALT WWTP had the lowest one.

As shown in Figure 1(a), the rarefaction curves of these samples are approaching plateaus, indicating that highly diverse microbial communities were present in each sample.

Table 2: Richness and diversity indices of microbial communities for sludge samples.

Sample	Reads	OTUs	Shannon	Ace	Chao	Coverage
ALT1	32390	714	4.88	811	802	0.992
ALT2	38394	683	4.52	863	908	0.989
SHZ1	53363	1152	5.93	1292	1281	0.988
SHZ2	30087	1022	5.78	1200	1192	0.988
CJ1	46680	852	5.09	1054	1047	0.988
CJ2	55170	855	5.16	1031	1024	0.989
HX1	48497	829	5.13	1003	994	0.989
HX2	52873	755	4.76	909	905	0.990

The distribution rarefaction curves and rank abundance curves also illustrated a much lower microbial diversity in ALT WWTP (Figure 1).

The ALT WWTP had the lowest microbial diversity, which can be because the temperature was lower than other WWTPs. Temperature has a decisive role in the metabolism of microorganisms, and lowering temperature has a significant effect on the reduction of the maximum specific growth [20]. In addition, wastewater types, industrial, domestic, and/or mixed, and their influent qualities have an important impact on microbial communities of activated sludge system [21]. The SHZ WWTP had the highest microbial diversity, which can be because the wastewater type was mixed.

3.2. Bacterial Community Composition and Similarity Analysis. The difference and similarity of bacterial community of activated sludge samples collected from different WWTPs were analyzed based on OTUs through the Venn diagram (Figure 2). The number of shared OTUs was 441 accounting for 26.6% of the total observed OTUs (1655). The shared OTUs indicated that some microorganisms always existed

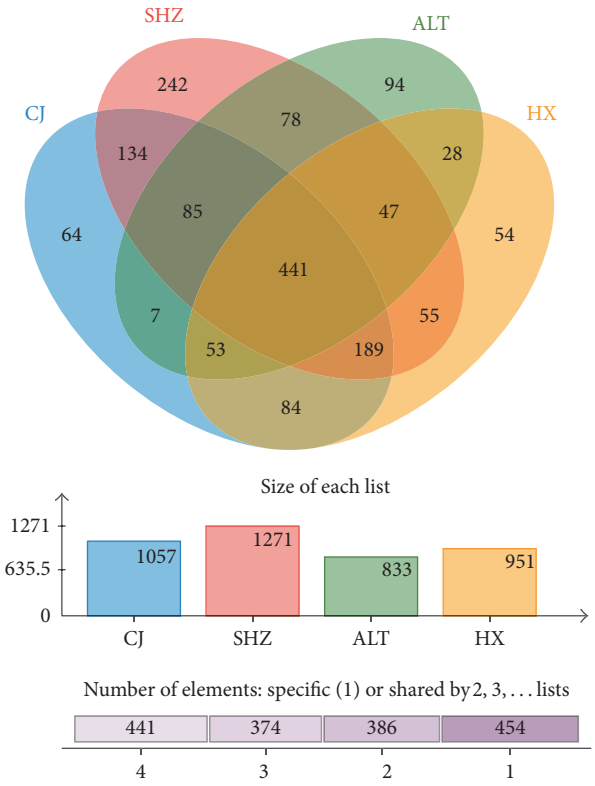

Figure 2: Overlap of the bacterial communities from four WWTPs based on OTU (3% distance).

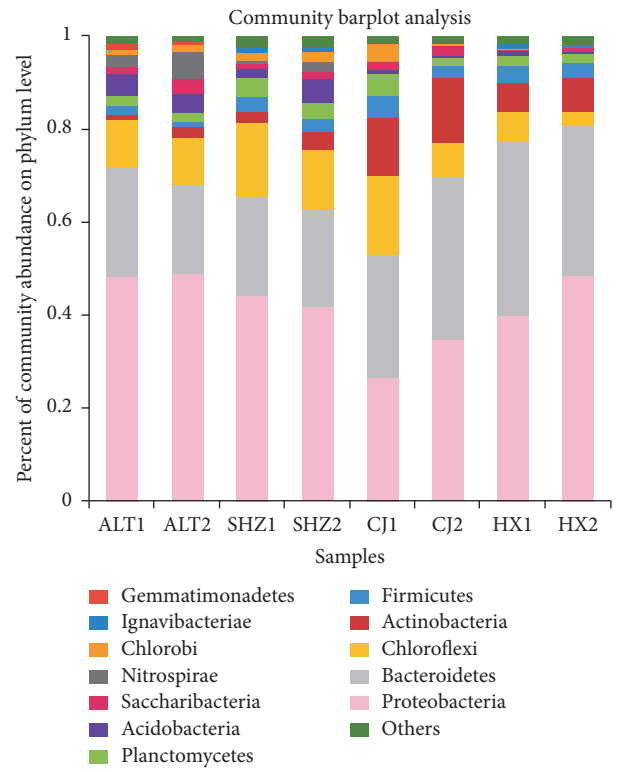

Figure 3: Percentages of the major phyla in all samples (the sequence percentage is above 1% in at least one sample).

in the activated sludge collected from different WWTPs. In addition, the unique OTU numbers in sludge samples from ALT WWTP, SHZ WWTP, CJ WWTP, and HX WWTP were 94, 242, 64, and 54, respectively. The unique OTU number accounted for 3.3–5.7% with an average of 4.3%; the small quantity of unique microorganism appeared in the activated sludge, except for the SHZ WWTP (14.6%). The SHZ WWTP had a higher quantity of unique microorganism than the others, which can be because of the mixed wastewater type.

A total of 36 phyla were observed in eight samples. As shown in Figure 3, Proteobacteria, which accounted for 26.7–48.9% of the classified sequences, was the most dominant phylum in all samples. Bacteroidetes, Chloroflexi, and Actinobacteria were the other important groups, comprising 19.3–37.3%, 2.9–17.1%, and 1.5–13.8% of the total sequences in each sample, respectively. These four groups accounted for 79.6–91.2% with the average of 85.3% of the total effective sequences of the eight samples. Proteobacteria was the most leading community, which is consistent with the results of the bacterial communities in soil [11, 22, 23] and activated sludge [18, 24]. Bacteroidetes, Acidobacteria, and Chloroflexi were also often found in activated sludge [25, 26]. In addition, several phyla accounted for more than 1% at least in one sample, for example, Firmicutes (1.4–4.8%), Planctomycetes (1.7–4.5%), Chlorobi (0.2–3.8%), Acidobacteria (0.5–5.1%), Saccharibacteria (0.4–3.2%), and Ignavibacteriae (0.03–1.3%).

Among Proteobacteria, Betaproteobacteria was the most abundant class (34.4–65.8%). Gammaproteobacteria was the second dominant class, accounting for 16.2 to 39.8%. Alphaproteobacteria and Deltaproteobacteria were the other important classes, comprising 11.0–38.6% and 2.2–9.1%, respectively. Epsilonproteobacteria had at the lowest abundance in the range from 0.02 to 4.3%. This result was consistent with other studies concluding that Betaproteobacteria was the largest class [18]. Within Betaproteobacteria, eleven orders were identified. Burkholderiales was the predominant main order within Betaproteobacteria between 44.1 and 82.5% of all samples. Rhodocyclales was the subdominant main order in all samples, except for ALT, in which Hydrogenophilales was the subdominant abundant order. Besides, the other eight classes with lower abundances were detected, including Methylophilales, Neisseriales, Nitrosomonadales, and Procabacteriales.

Among the 293 families identified, 44 families including Saprospiraceae, Comamonadaceae, Anaerolineaceae, Xanthomonadaceae, Rhodocyclaceae, Flavobacteriaceae, Rhodobacteraceae, Intrasporangiaceae, Caldilineaceae, *norank_c_Ardenticatenia*, *norank_c_Nitrospira*, and *Xanthomonadales_Incertae_Sedis* were generally shared by all samples (>1% relative abundance at least in one sample), accounting for 71.9–87.5% of total effective sequences in each sample (Figure 4). ALT WWTP had higher abundances of Xanthomonadaceae (11.4–15.9%), Chitinophagaceae (6.9–7.5%), Hydrogenophilaceae (5.1–5.2%), and norank_c_*Nitrospira* (2.7–5.6%) compared to other samples in ranges of 1.7–3.4%, 1.5–3.0%, 0.01–3.3%, and 0.0–2.1%, respectively. Flavobacteriaceae accounted for 12.7–15.1% in HX and Intrasporangiaceae

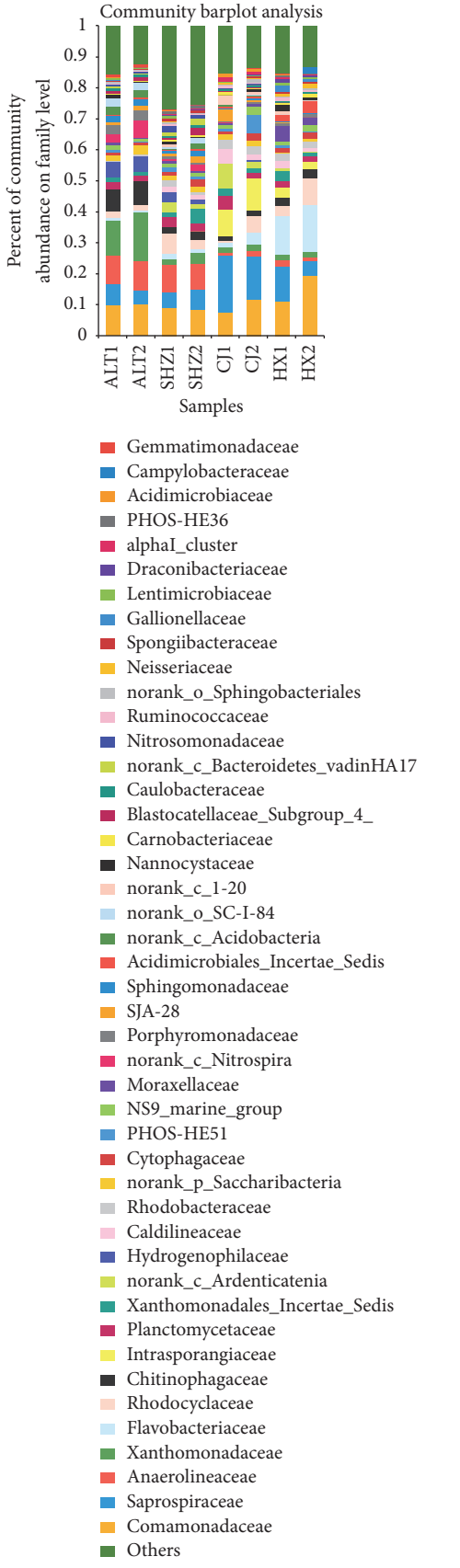

Figure 4: Percentages of the major families in all samples (the sequence percentage is above 1% in at least one sample).

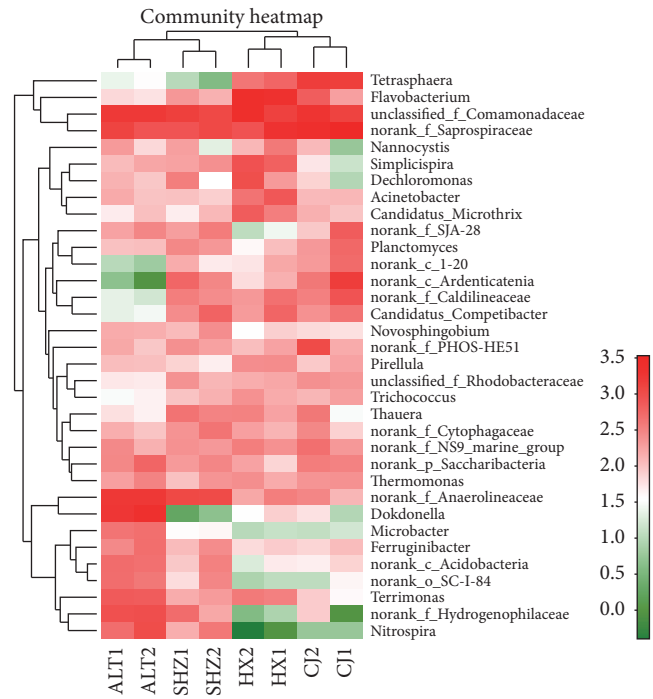

Figure 5: Heatmap of the first ten dominant genera in each sample.

and *norank_c_Ardenticatenia* accounted for 8.6–10.5% and 2.2–8.0% in CJ, whereas their abundances were higher than other samples, in the range of 0.6–4.0% and 0.05–3.3%, 0.01–3.1%, respectively. The relative abundances of family Saprospiraceae (4.9–18.2%) were higher in bulking samples (CJ and HX WWTPs) than those in normal samples. The relative abundances of family Anaerolineaceae (8.4–9.3%) were higher in normal samples (ALT and SHZ WWTPs) than those in bulking sludge samples.

Comamonadaceae were in charge of aromatic degrading and denitrifying processes and were the chief families in numerous wastewater treatment plants [27]. The family Rhodocyclaceae contains primarily denitrifying rod-shaped or aerobic bacteria [28], which display highly multipurpose metabolic capabilities. Members of the Anaerolineae class are largely distributed in different types of natural and artificial anaerobic ecosystems, which are obligate anaerobes [29]. Filamentous Saprospiraceae and Flavobacteriaceae can cause sludge bulking [30].

579 genera were shared in all samples, in total. Fifty-five genera, which accounted for 60.6–82.7% of the classified sequences and included the *unclassified_f_Comamonadaceae*, *norank_f_Saprospiraceae*, *Flavobacterium*, *norank_f_Hydrogenophilaceae*, *Dokdonella*, *Terrimonas*, *norank_f_Anaerolineaceae*, *Tetrasphaera*, *Simplicispira*, *norank_c_Ardenticatenia*, and *Nitrospira* genera were generally shared by all samples. Most of them were discovered to be chief genera and were shared by activated samples from WWTPs [25]. From all samples, the first ten dominant genera in each sample were chosen (a total of 34 genera) and the comparison of their abundance was analyzed using the heatmap (Figure 5). The relative abundances of genera

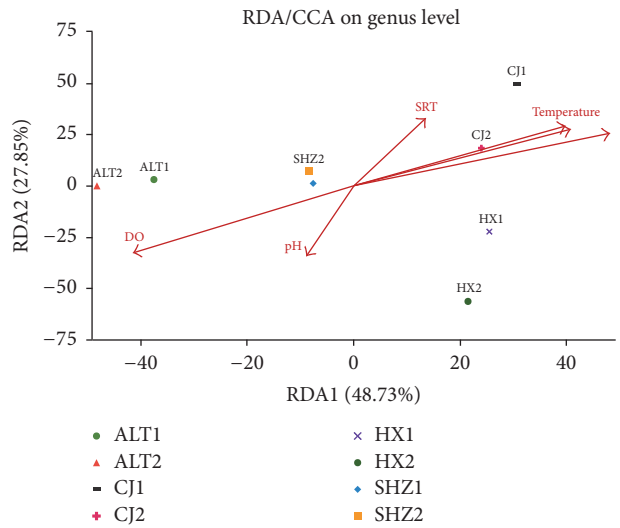

Figure 6: RDA analysis to investigate the relationship between microbial communities and environmental variables.

Dokdonella (11.0%), *norank_f_Hydrogenophilaceae* (5.1%), *Terrimonas* (3.8%), and *Nitrospira* (4.1%) were much higher in ALT WWTP than those in others. *norank_f_Anaerolineaceae* (averaging at 7.08%) was higher in SHZ and ALT WWTPs than those in other sludge samples (averaging at 1.43%). The samples in CJ WWTP had high levels of genus *norank_f_Saprospiraceae* (averaging at 15.5%), whereas the other samples contained relatively less (averaging at 6.3%). HX WWTP had higher abundances of *Simplicispira* (4.1%) and *Flavobacterium* (12.7%) compared to other samples with ranges of 0.1–1.3% and 0.3–3.7%, respectively. CJ and HX WWTP had higher abundances of *Tetrasphaera*, in the range of 7.7–7.9% and 3.2–2.2%, respectively, while the proportion of other samples was in ranges of 0.02–0.2%. Genus *Tetrasphaera* from family Intrasporangiaceae has a certain contribution to sludge bulking [31, 32].

Filamentous Saprospiraceae and *Tetrasphaera* multiplied had a positive impact on the sludge bulking in CJ WWTP, while filamentous *Flavobacterium* and Saprospiraceae multiplied had a positive impact on the sludge bulking in HX WWTP.

3.3. Relationships between Environmental Factors and Community Structure. The possible relationship between microbial communities and environmental variables was analyzed using a constrained ordination of redundancy analysis (RDA). Six variables including influent BOD_5, influent ammonia, pH, water temperature, dissolved oxygen (DO), and solid retention time (SRT) were selected, and the ordination biplot was shown in Figure 6. As evident in Figure 6, the canonical axes of first and second showed 48.73% and 27.85% of data variance, respectively. RDA indicated that influent BOD_5, DO, water temperature, and influent ammonia had a distinct effect on bacterial community structures, though pH exhibited the least effect.

Influent BOD_5 is the most crucial environmental factor influencing the community compositions. Previous studies have found that the types of feeding substrate have an impact on bacterial diversity [33]. Similarly, the biodegradability of influent wastewater was affected by the compositions of bacteria in the wastewater treatment [21]. The organic components are normally represented by the proxies of COD and/or biochemical oxygen demand (BOD) in wastewater. The significance of influent BOD in the process of the bacterial community formation was found in activated sludge systems, which is consistent with the result of this study [34, 35]. In this study, different WWTPs had different wastewater quality, resulting in difference in the wastewater constituents. Therefore, influent BOD_5 can possibly interpret the difference of bacterial communities.

DO had a significant influence on the bacterial communities. In the context of its influence on microbial activity and the high operating costs of aeration, DO is a key operational parameter in wastewater treatment systems. However, the explicit selection by DO concentration is not completely understood for diverse bacterial lineages. The results showed that DO had an important influence for shaping the compositions of the microbial community of wastewater treatment processes. Several studies have found that DO concentration was a significant structuring factor for bacterial community compositions running at high and low DO concentrations in bioreactors of two laboratory scales [36].

The water temperature was correlated with variance of the bacterial community, which is in agreement with other studies [24, 37]. Some studies have shown that bacterial community structures were influenced significantly by the influent ammonia, which disagrees with the result of this study [38].

In this study, pH was found to have the least impact on bacterial community structures, which is in disagreement with the other studies [18]. Several studies have illustrated that the whole diversity and structures of microbial communities were affected by the pH in a series of aquatic and terrestrial environments [39, 40]. In the present study, it might not be generated on the whole microbial communities, because pH did not change significantly among these WWTPs (Table 1). Thus, further investigation is needed to understand this aspect.

4. Conclusions

In conclusion, 36 phyla, 293 families, and 579 genera were found in activated sludge samples from WWTPs of Xinjiang in winter. The number of shared OTUs accounted for 26.6% of the total observed OTUs; it can be concluded that some microorganisms always existed in the activated sludge collected from different WWTPs. The WWTP with low temperature and single wastewater type was found to have the lowest microbial diversity. The WWTP with mixed wastewater type was found to have the highest microbial diversity. Proteobacteria, Bacteroidetes, Chloroflexi, and Acidobacteria, accounting for 79.6–91.2% of the classified sequences, were the most abundant phyla in all samples. Fifty-five genera, which accounted for 60.6–82.7% of the classified sequences and included *unclassified_f_Comamonadaceae*,

norank_f_Saprospiraceae, *Flavobacterium*, *norank_f_Hydrogenophilaceae*, *Dokdonella*, *Terrimonas*, *norank_f_Anaerolineaceae*, *Tetrasphaera*, *Simplicispira*, *norank_c_Ardenticatenia*, and *Nitrospira* genera, were generally shared by all samples. The relative abundances of Saprospiraceae, *Flavobacterium*, and *Tetrasphaera* in bulking sludge samples were much higher than that in normal samples. Filamentous Saprospiraceae, *Flavobacterium*, and *Tetrasphaera* multiplied were the main cause for the sludge bulking. Redundancy analysis (RDA) indicated that influent BOD_5, DO, water temperature, and influent ammonia had a significant impact on bacterial community compositions, whereas pH exhibited the least influence.

Conflicts of Interest

The authors declare that they have no conflicts of interest.

Acknowledgments

This work was supported by the National Natural Science Foundation of China (51568061).

References

[1] M. Wagner and A. Loy, "Bacterial community composition and function in sewage treatment systems," *Current Opinion in Biotechnology*, vol. 13, no. 3, pp. 218–227, 2002.

[2] Y. Miura, M. N. Hiraiwa, T. Ito, T. Itonaga, Y. Watanabe, and S. Okabe, "Bacterial community structures in MBRs treating municipal wastewater: Relationship between community stability and reactor performance," *Water Research*, vol. 41, no. 3, pp. 627–637, 2007.

[3] D. Jenkins, *Manual on the Causes and Control of Activated Sludge Bulking and Foaming*, Lewis, 2nd edition, 1993.

[4] A. M. P. Martins, K. Pagilla, J. J. Heijnen, and M. C. M. Van Loosdrecht, "Filamentous bulking sludge—a critical review," *Water Research*, vol. 38, no. 4, pp. 793–817, 2004.

[5] C. Kragelund, C. Levantesi, A. Borger et al., "Identity, abundance and ecophysiology of filamentous bacteria belonging to the Bacteroidetes present in activated sludge plants," *Microbiology*, vol. 154, no. 3, pp. 886–894, 2008.

[6] Z. C. Liu, F. Li, and Q. Li, "Effect of ozone on filamentous bulking under low temperature," *China Water & Wastewater*, vol. 31, no. 15, pp. 35–39, 2015 (Chinese).

[7] T. C. Glenn, "Field guide to next-generation DNA sequencers," *Molecular Ecology Resources*, vol. 11, no. 5, pp. 759–769, 2011.

[8] M. Albertsen, L. B. S. Hansen, A. M. Saunders, P. H. Nielsen, and K. L. Nielsen, "A metagenome of a full-scale microbial community carrying out enhanced biological phosphorus removal," *Isme Journal Multidisciplinary Journal of Microbial Ecology*, vol. 6, no. 6, pp. 1094–1106, 2012.

[9] F. Ju, F. Guo, L. Ye, Y. Xia, and T. Zhang, "Metagenomic analysis on seasonal microbial variations of activated sludge from a full-scale wastewater treatment plant over 4 years," *Environmental Microbiology Reports*, vol. 6, no. 1, pp. 80–89, 2014.

[10] P.-Y. Qian, Y. Wang, O. O. Lee et al., "Vertical stratification of microbial communities in the Red Sea revealed by 16S rDNA pyrosequencing," *The ISME Journal*, vol. 5, no. 3, pp. 507–518, 2011.

[11] L. F. W. Roesch, R. R. Fulthorpe, A. Riva et al., "Pyrosequencing enumerates and contrasts soil microbial diversity," *The ISME Journal*, vol. 1, no. 4, pp. 283–290, 2007.

[12] M. J. Claesson and P. W. O'Toole, "Evaluating the latest high-throughput molecular techniques for the exploration of microbial gut communities," *Gut Microbes*, vol. 1, no. 4, pp. 277-278, 2014.

[13] S. Xia, L. Duan, Y. Song et al., "Bacterial community structure in geographically distributed biological wastewater treatment reactors," *Environmental Science & Technology*, vol. 44, no. 19, pp. 7391–7396, 2010.

[14] Q.-Y. Hu, M. Li, C. Wang, and M. Ji, "Influence of powdered activated carbon addition on water quality, sludge properties, and microbial characteristics in the biological treatment of commingled industrial wastewater," *Journal of Hazardous Materials*, vol. 295, pp. 1–8, 2015.

[15] Y. M. Kim, H. U. Cho, D. S. Lee, D. Park, and J. M. Park, "Influence of operational parameters on nitrogen removal efficiency and microbial communities in a full-scale activated sludge process," *Water Research*, vol. 45, no. 17, pp. 5785–5795, 2011.

[16] D. Shu, Y. He, H. Yue, and Q. Wang, "Microbial structures and community functions of anaerobic sludge in six full-scale wastewater treatment plants as revealed by 454 high-throughput pyrosequencing," *Bioresource Technology*, vol. 186, pp. 163–172, 2015.

[17] M. Wagner, A. Loy, R. Nogueira, U. Purkhold, N. Lee, and H. Daims, "Microbial community composition and function in wastewater treatment plants," *Antonie van Leeuwenhoek*, vol. 81, no. 1–4, pp. 665–680, 2002.

[18] P. Gao, W. Xu, P. Sontag et al., "Correlating microbial community compositions with environmental factors in activated sludge from four full-scale municipal wastewater treatment plants in Shanghai, China," *Applied Microbiology and Biotechnology*, vol. 100, no. 10, pp. 4663–4673, 2016.

[19] Y. Z. Peng and J. H. Gao, "Mechanism, cause and control of activated sludge expansion," Beijing, China, 2012 (Chinese).

[20] G. Lettinga, S. Rebac, and G. Zeeman, "Challenge of psychrophilic anaerobic wastewater treatment," *Trends in Biotechnology*, vol. 19, no. 9, pp. 363–370, 2001.

[21] F. M. Ibarbalz, E. L. M. Figuerola, and L. Erijman, "Industrial activated sludge exhibit unique bacterial community composition at high taxonomic ranks," *Water Research*, vol. 47, no. 11, pp. 3854–3864, 2013.

[22] A. M. Spain, L. R. Krumholz, and M. S. Elshahed, "Abundance, composition, diversity and novelty of soil *Proteobacteria*," *The ISME Journal*, vol. 3, no. 8, pp. 992–1000, 2009.

[23] M. Sun, T. Xiao, Z. Ning, E. Xiao, and W. Sun, "Microbial community analysis in rice paddy soils irrigated by acid mine drainage contaminated water," *Applied Microbiology and Biotechnology*, vol. 99, no. 6, pp. 2911–2922, 2015.

[24] X. Wang, M. Hu, Y. Xia, X. Wen, and K. Ding, "Pyrosequencing analysis of bacterial diversity in 14 wastewater treatment systems in China," *Applied and Environmental Microbiology*, vol. 78, no. 19, pp. 7042–7047, 2012.

[25] D. Zhao, R. Huang, J. Zeng et al., "Pyrosequencing analysis of bacterial community and assembly in activated sludge samples from different geographic regions in China," *Applied Microbiology and Biotechnology*, vol. 98, no. 21, pp. 9119–9128, 2014.

[26] T. Zhang, M.-F. Shao, and L. Ye, "454 Pyrosequencing reveals bacterial diversity of activated sludge from 14 sewage treatment plants," *The ISME Journal*, vol. 6, no. 6, pp. 1137–1147, 2012.

[27] A. Loy, C. Schulz, S. Lücker et al., "16S rRNA gene-based oligonucleotide microarray for environmental monitoring of the betaproteobacterial order 'Rhodocyclales'," *Applied and Environmental Microbiology*, vol. 71, no. 3, pp. 1373–1386, 2005.

[28] J. F. A. R. Kuever and F. Widdel, *Bergey's Manual of Systematic Bacteriology, the Proteobacteria. Part C, the Alpha-, Beta-, Delta-, and Epsilonproteobacteria*, Springer, 2005.

[29] F. Rosenkranz, L. Cabrol, M. Carballa et al., "Relationship between phenol degradation efficiency and microbial community structure in an anaerobic SBR," *Water Research*, vol. 47, no. 17, pp. 6739–6749, 2013.

[30] Z. H. Duan, P. L. M. Pan, C. X. O. Chen, X. D. Wang, L. J. Zhao, and L. Q. Tian, "Changes of microbial community structure in activated sludge bulking at low temperature," *Environmental Science*, vol. 37, no. 3, pp. 1070–1074, 2016 (Chinese).

[31] C. M. McKenzie, E. M. Seviour, P. Schumann et al., "Isolates of "Candidatus Nostocoida limicola" Blackall et al. 2000 should be described as three novel species of the genus Tetrasphaera, as Tetrasphaera jenkinsii sp. nov., Tetrasphaera vanveenii sp. nov. and Tetrasphaera veronensis sp. nov," *International Journal of Systematic and Evolutionary Microbiology*, vol. 56, no. 10, pp. 2279–2290, 2006.

[32] P. Wang, Z. Yu, R. Qi, and H. Zhang, "Detailed comparison of bacterial communities during seasonal sludge bulking in a municipal wastewater treatment plant," *Water Research*, vol. 105, pp. 157–166, 2016.

[33] M. K. Pholchan, J. D. C. Baptista, R. J. Davenport, and T. P. Curtis, "Systematic study of the effect of operating variables on reactor performance and microbial diversity in laboratory-scale activated sludge reactors," *Water Research*, vol. 44, no. 5, pp. 1341–1352, 2010.

[34] B.-C. Kim, S. Kim, T. Shin, H. Kim, and B.-I. Sang, "Comparison of the bacterial communities in anaerobic, anoxic, and oxic chambers of a pilot A_2O process using pyrosequencing analysis," *Current Microbiology*, vol. 66, no. 6, pp. 555–565, 2013.

[35] C. J. Van Der Gast, D. Ager, and A. K. Lilley, "Temporal scaling of bacterial taxa is influenced by both stochastic and deterministic ecological factors," *Environmental Microbiology*, vol. 10, no. 6, pp. 1411–1418, 2008.

[36] H.-D. Park and D. R. Noguera, "Evaluating the effect of dissolved oxygen on ammonia-oxidizing bacterial communities in activated sludge," *Water Research*, vol. 38, no. 14-15, pp. 3275–3286, 2004.

[37] G. F. Wells, H.-D. Park, C.-H. Yeung, B. Eggleston, C. A. Francis, and C. S. Criddle, "Ammonia-oxidizing communities in a highly aerated full-scale activated sludge bioreactor: Betaproteobacterial dynamics and low relative abundance of Crenarchaea," *Environmental Microbiology*, vol. 11, no. 9, pp. 2310–2328, 2009.

[38] Q. Ma, Y. Qu, W. Shen et al., "Bacterial community compositions of coking wastewater treatment plants in steel industry revealed by Illumina high-throughput sequencing," *Bioresource Technology*, vol. 179, pp. 436–443, 2015.

[39] E. Hörnström, "Phytoplankton in 63 limed lakes in comparison with the distribution in 500 untreated lakes with varying pH," *Hydrobiologia*, vol. 470, no. 1–3, pp. 115–126, 2002.

[40] N. Fierer and R. B. Jackson, "The diversity and biogeography of soil bacterial communities," *Proceedings of the National Acadamy of Sciences of the United States of America*, vol. 103, no. 3, pp. 626–631, 2006.

Hindawi
BioMed Research International
Volume 2017, Article ID 2057035, 6 pages
https://doi.org/10.1155/2017/2057035

Research Article

Efficient Utilization of Waste Carbon Source for Advanced Nitrogen Removal of Landfill Leachate

Kai Wang, Wenjun Yin, Fengxun Tan, and Daoji Wu

School of Municipal and Environmental Engineering, Shandong Jianzhu University, Jinan 250101, China

Correspondence should be addressed to Kai Wang; wangkai@sdjzu.edu.cn and Daoji Wu; wdj@sdjzu.edu.cn

Received 8 November 2017; Accepted 27 November 2017; Published 24 December 2017

Academic Editor: Shijian Ge

A modified single sequencing batch reactor (SBR) was developed to remove the nitrogen of the real landfill leachate in this study. To take the full advantage of the SBR, stir phase was added before and after aeration, respectively. The new mechanism in this experiment could improve the removal of nitrogen efficiently by the utilization of carbon source in the raw leachate. This experiment adopts the SBR process to dispose of the real leachate, in which the COD and ammonia nitrogen concentrations were about 3800 mg/L and 1000 mg/L, respectively. Results showed that the removal rates of COD and total nitrogen were above 85% and 95%, respectively, and the effluent COD and total nitrogen were less than 500 mg/L and 40 mg/L under the condition of not adding any carbon source. Also, the specific nitrogen removal rate was 1.48 mgN/(h·gvss). In this process, polyhydroxyalkanoate (PHA) as a critical factor for the highly efficient nitrogen removal (>95%) was approved to be the primary carbon source in the sludge. Because most of the organic matter in raw water was used for denitrification, in the duration of this 160-day experiment, zero discharge of sludge was realized when the effluent suspended solids were 30–50 mg/L.

1. Introduction

Landfill leachate is produced from municipal waste deposited in the landfill. The leachate contains high concentrations of organics and ammonia nitrogen that are severe pollutants of the subsurface environment [1]. The efficient and cost-effective treatment of the leachate, aiming to meet discharge requirements, has become a worldwide interest. There is two kinds of technologies used for leachate treatments: physical/chemical treatment and biological treatment. The physical/chemical methods, such as ammonia stripping or advanced oxidation methods, are usually used for pretreatment or posttreatment because of their secondary pollution and high cost [2–4]. Biological treatments have been widely applied to treat landfill leachate because the reagents are reusable and cost-effective, and these procedures generate less secondary pollution [5–8].

The biological treatment of landfill leachate focuses on the removal of organics and ammonia nitrogen [9–14]. The organics are removed through conventional biological treatments, and the ammonia nitrogen is oxidized into NO_2^--N or NO_3^--N under aeration. Since the NO_2^--N or NO_3^--N is more poisonous than ammonia nitrogen, many countries (e.g., China) require that landfills meet total nitrogen (TN) emission standards on the landfill leachate. TN removal via denitrification requires a carbon source. However, most organics in the leachate have been oxidized into CO_2 during aeration, resulting in a low concentration of carbon. The conventional biological treatments realize only 30%–70% nitrogen removal efficiency. For example, Laitinen et al. used sequencing batch reactor (SBR) activated sludge process combined with membrane bioreactor (MBR) to dispose of landfill leachate that contained 2200 mg/L chemical oxygen demand (COD) and 240 mg/L TN. The TN removal efficiency was below 60%. Yanjie et al. used granule sequencing batch reactors to dispose of landfill leachate, and the removal efficiency of TN was about 35.0%, with the ammonium of the leachate being 1105 mg/L. Mehdi used MBR to dispose of landfill leachate, and the removal efficiency of TN was about 28.0%. Some studies have reported high nitrogen removal in the leachate by adding an external carbon source, but this approach increased the cost and wasted the organics naturally present in the leachate [15].

Table 1: The characteristics of the leachate.

Item	pH	NH_4^+-N (mg/L)	TN (mg/L)	NO_x-N (mg/L)	COD (mg/L)	BOD_5 (mg/L)
Range	7.8~8.2	860~1012	910~1106	0.11~0.8	3360~4210	1082~1380
Mean value	8.0	1010	1021	<1	3820	1215

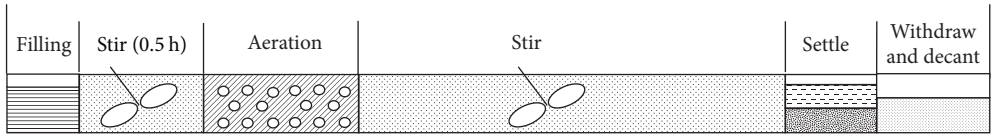

Figure 1: Operational mode of modified SBR.

Compared to other bioprocessing technologies, SBR has many advantages, such as simple structure and flexible operation. SBR has become a widely used method to dispose of landfill leachate [16]. Studies of SBR had focused on the removal of organics and ammonia, but little of them focused on the removal of total nitrogen.

Vock et al. discovered that activated sludge could store a carbon source, by transforming organic carbon from wastewater to the form of PHA stored in bacteria cells [17]. If the carbon-storage capability of the activated sludge could be strengthened, then TN removal would be able to use the stored indigenous carbon source, which would also improve the nitrogen removal efficiency and eliminate the addition of external sources of carbon [18].

To realize high nitrogen removal without the additional external sources of carbon, a modified SBR to treat real landfill leachate was used. The modified SBR differs from conventional SBR by adding a stirring phase before and after aeration phase, which allows for the full use of the carbon source in the leachate. Some parameters of SBR in one cycle which included COD, NH_4^+-N, NO_2^--N, NO_3^--N, TN, pH, and oxidation-reduction potential (ORP) were investigated. Also, the effect of variation of PHA of the sludge in one cycle of SBR was studied.

2. Materials and Methods

2.1. Landfill Leachate and Seed Sludge. Raw landfill leachate for this study was taken from the third MSW Sanitation Landfill Site, Jinan, Shandong province, China. The COD of the leachate was 3360 mg/L–4210 mg/L. The ammonia of the leachate was 860 mg/L–1012 mg/L, and NO_2^--N and NO_3^--N could be ignored. The characteristics of leachate were shown in Table 1. Inoculum was obtained from two sources: 80% of the inoculum is from the excess sludge of a pilot-scale SBR used to treat domestic wastewater, with MLSS and sludge volume index (SVI) being 10,000 mg/L and 350 mg/L, respectively; the rest of the inoculum (20%) came from an experimental SBR that had already produced nitridation with mature leachate, with MLSS and SVI being 3,500 mg/L and 56 mg/L, respectively. The MLSS, MLVSS, and SVI of the mixture were 8,523 mg/L, 6,375 mg/L, and 290 mg/L, respectively.

2.2. Experimental Setup and Operational Procedure. An SBR with working volume of 10 L was used in this study. The temperature was controlled at 25°C ± 1°C through the temperature control device, and the aeration was controlled through an air pump and gas flow meter.

The operation mode of the modified SBR is shown in Figure 1, including the filling phase, the anaerobic stir phase (synthesis of PHA in activated sludge), the aeration phase (nitration and simultaneous nitrification and denitrification), the anoxic phase (endogenesis denitrification), the settling phase, and the decanting phase, respectively. The dissolved oxygen (DO) concentration of nitritation was maintained in the range of 1.5–2.0 mg/L.

The sludge of the testing which investigated the content variation of PHA in one cycle was taken from the 120th experiment. In the testing, liquid samples and sludge samples were collected every 30 minutes before nitrification and every 60 minutes after nitrification. The liquid samples were analyzed for NH_4^+-N, NO_2^--N, NO_3^--N, TN, and COD. The sludge samples were analyzed for PHA.

During the experiment, COD, NH_4^+-N, NO_2^--N NO_3^--N, MLSS, and MLVSS were measured according to standard methods (APHA, 1998). The TN concentration was measured with Multi N/C3000 TOC (Analytik Jena AG, Germany). BOD_5 was measured with an OxiTop Control WTW. DO, pH, and ORP were monitored using a pH/Oxi 340i analyzer (WTW Company, Germany). PHB was determined using the method of Zeng et al. [19].

3. Results and Discussion

3.1. Performance of the Modified SBR

3.1.1. Quick Launch Strategy of Modified SBR to Realize Leachate Advanced Nitrogen Removal. The start-up phase lasted 35 d so that the inoculum had time to adapt to the characteristics of the leachate. The volumetric exchange rate (EVR) of SBR during this period was 10%.

In order to enrich the quantity of the denitrifying bacteria, the operation time of anoxic stir stage was 10 hours. If TN was not removed in one cycle, external carbon sources (such as sodium acetate) were added to ensure the denitration finished. Since the initial SVI was high (290 mg/L), the

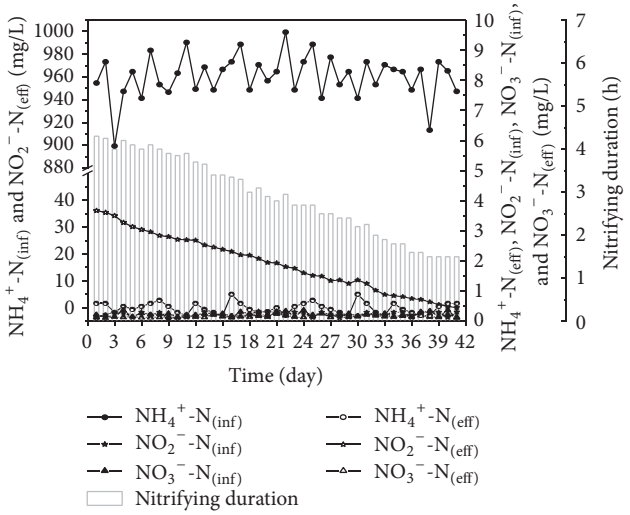

Figure 2: Fast start-up performance of modified SBR treating landfill leachate.

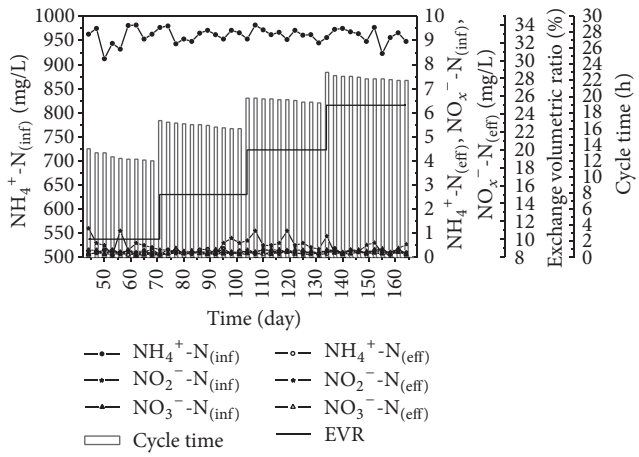

Figure 3: Performance of modified SBR treating landfill leachate with nitrogen load increasing.

settling time was set to 2 h to ensure the sludge would not flow away. Figure 2 shows the performance of SBR during the start-up phase. The effluent NO_2^--N concentration was measured at the completion of the anoxic stir stage without the addition of an external carbon source. The activity of the nitrite oxidizing bacteria (NOB) was inhibited because the free ammonia (FA) concentration in the leachate was 1.2918 mg/L (higher than domestic wastewater [0.775 mg/L]) and the DO concentration was low (i.e., 1.5–2.0 mg/L) during nitrification. Therefore, the system successfully achieved nitritation with a low production of NO_3^--N (≤3 mg/L). During the previous 3 d of the experiment, the sludge did not adapt to the leachate, resulting in a system-specific ammonia oxidation rate (SAOR) of 3.55 mg NH_4^+-N/gvss·h and a nitritation stage that lasted 4 h. Moreover, there was about 35 mg/L NO_2^--N remaining at the conclusion of the first cycle because of the small amount of denitrifying bacteria. Therefore, an external carbon source was added to remove more of the nitrogen.

After the ammonia oxidizing bacteria (AOB) adapted to the leachate, the nitritation stage decreased from 4.4 h (1st d) to 1.5 h on 38th d, while the SAOR increased to 9.64 mg NH_4^+-N/gvss·h and remained at about 10 mg NH_4^+-N/gvss·h for the rest of the experiment. The number of denitrifying bacteria grew rapidly in response to the addition of an external carbon source. On 41st d, the system achieved complete denitration without the addition of an external carbon source in one 14 h cycle, completing the start-up phase of the modified SBR.

3.1.2. Ascension and Stability of Leachate Nitrogen Removal Performance of Modified SBR. After the completion of the start-up phase, the modified SBR system was able to efficiently remove nitrogen without adding external sources of carbon during any part of the cycle. As shown in Figure 3, the system operated for 30 d with the 10% EVR. The cycle completion time decreased from 13.4 h on 42nd d to 12 h on 70th d. Accordingly, the specific nitrogen removal rate (SNRR) increased from 0.99 mgN/h·gvss on 42nd d to 1.12 mgN/h·gvss on 70th d. After the cycle time was stable, the EVR was increased to enhance the denitrification capability of the sludge. On 71st d the EVR was increased to 15% and the influent TN of the system increased by 50%. However, the cycle time only increased to 17 h, suggesting an improvement in the denitrification efficiency.

Between 71st d and 101st d, the cycle time decreased from 17 h to 16 h and the SNRR increased to 1.29 mgN/h·gvss. Then we raised the EVR to 20% and the cycle time increased to 19.8 h. The cycle time did not improve proportionally with TN (the 20% EVR was only 65% longer than the 10% EVR and 23.7% longer than the 15% EVR). On 164th d we increased the EVR to 25% and the cycle time remained at 22 h with an SNRR of 1.48 mgN/h·gvss. The nitrogen removal efficiency of the 25% EVR increased by 30%, compared to the 10% EVR.

3.2. Detecting Reaction Progress with Parameter Variations. During the SBR reaction process, we could easily discern the conclusion of nitrification and denitrification stages by detecting changes in the system parameters, such as pH and ORP [20]. Variations of the parameters during one cycle of the modified SBR were shown in Figure 4. When the mixture contained an NH_4^+-N concentration of 225 mg/L after filling (EVR was 25%), the nitritation stage lasted 4.5 h. During the 4th h, a decrease in ammonia (Figure 4 point A) was easily discerned in the pH profile and signaled the end of nitritation. At this time, the aeration was stopped quickly in order to increase the denitration potentiality of SBR. During the last 3 h of nitritation, COD levels were greatly reduced, and after 3.5 h, COD remained at about 490 mg/L, indicating that the degradable organics had almost been entirely removed. During aeration, the levels of ammonia nitrogen decreased along with COD, which suggests high AOB activity. AOB acted as the dominant bacteria because there was no added nitrate. Furthermore, TN was also removed during aeration, as expected simultaneous nitrification and denitrification (SND). By the end of nitritation, TN concentration was

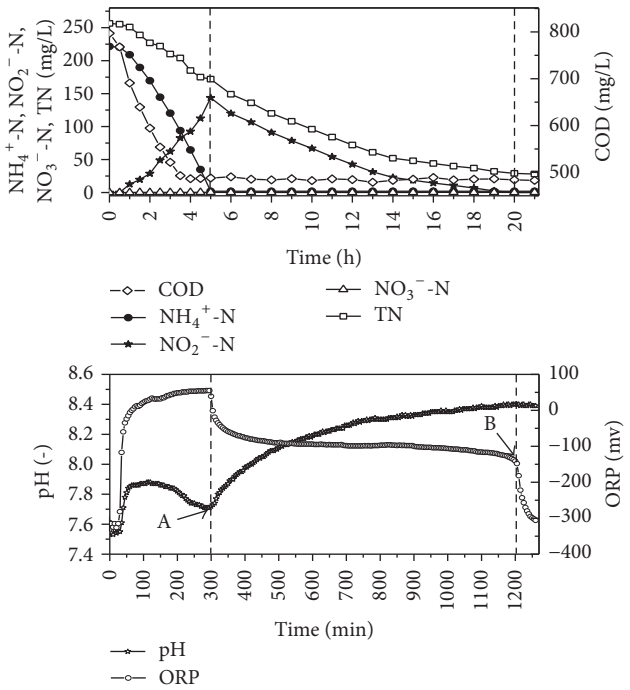

Figure 4: Key parameters variations of modified SBR in one cycle.

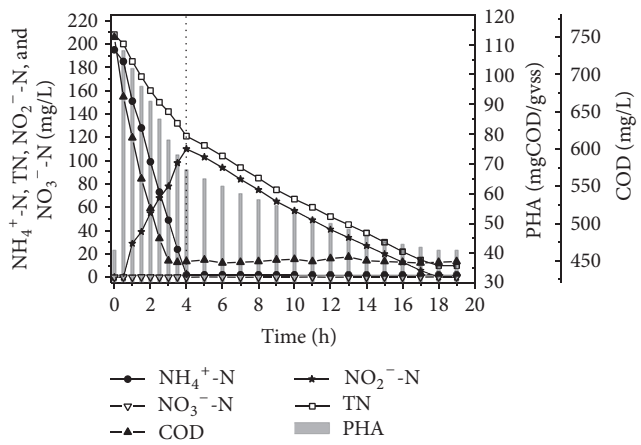

Figure 5: PHA variations of modified SBR in one cycle.

reduced from 256 mg/L to172 mg/L, and the removal rate was 32.8%.

After the nitritation phase, the SBR system began to use the stored carbon source (such as PHA) to denitrify the leachate during a 15 h anoxic stage. During the 19th and 21st h of the whole reaction, a nitrate plateau (point B) was recorded in the ORP profile and suggested the end of denitration. At this time, NH_4^+-N and TN concentrations decreased below 5 mg/L and 30 mg/L, respectively. The nitrogen removal rate was above 95%. It is worth noting that there was no significant change in pH point during the anoxic stir stage, so the ORP was the only parameter which could be used to judge the terminal point of denitration.

During one cycle, about 2280 mg of nitrogen and 8540 mg of COD were removed. The total amount of COD used during denitration was above 4000 mg. At least 46.8% of the COD was consumed during denitrification. The modified SBR improved the utilization ratio of carbon and also reduced the aeration level in the leachate.

3.3. The PHA Variation of the Sludge in One Cycle. The system realized advanced nitrogen removal without adding any carbon source after aeration. It suggested that the activated sludge used its carbon source for denitrification. To understand the change of carbon sources during the denitrification process, on the 120th d of the test, the variation of PHA, NH_4^+-N, TN, NO_2^--N, NO_3^--N, and COD in one cycle was investigated. The test results are shown in Figure 5. According to the results of Figure 5, during the first half hour of the test, as the anaerobic mixing stage, the COD showed noticeable decline, while the PHA of sludge showed visible growth. This suggested that the organic matter of the wastewater was adsorbed by activated sludge and then was transformed to PHA. The PHA was the foundation of realizing advanced nitrogen removal. After half an hour, the system started to aerate, and the concentration of ammonia nitrogen and COD decline rapidly. At the same time, the PHA of the sludge was also reduced. Four hours later, the ammonia of the system was less than 5 mg/L which suggested the end of nitrification. At this point, the COD of the system was about 450 mg/L, and the removal rate of COD was about 85%. Because of the low DO concentration during the aeration, after the nitrification, the total nitrogen removal rate was about 40% by the simultaneous nitrification and denitrification (SND). The rest of the entire nitrogen mainly exists in the form of the nitrite. After aeration, the concentration of PHA decreased by about 40% in comparison with the very beginning of aeration, but compared to the beginging of the filling, the concentration of PHA increased significantly.

After the nitration, the system continues to stir. Due to the low dissolved oxygen of the system after stopping the aeration, the sludge began endogenous denitrification. During the process of endogenous denitrification, the concentration of TN and nitrate nitrogen steadily decreased and the PHA decreased synchronously. It is important to note that during the process of denitrification, the level of ammonia was not increased obviously, so we could deduce that the sludge used PHA for denitrification, rather than the carbon source from cell lyses. After 19 hours, the concentration of the nitrate nitrogen was nearly zero, and TN was about 20 mg/L which showed that advanced nitrogen removal had been completed. At this time, the concentration of PHA in sludge was about 40 mgCOD/GVSS which is equal to the concentration before filling.

According to this test, we knew that the concentration of PHA in sludge was the key point to realize advanced nitrogen removal. The anaerobic stir after filling provided the sludge opportunity to generate PHA which was the foundation of advanced nitrogen removal. The continue stir after nitration was the approach to realize advanced nitrogen removal. Under the joint action of efficient SND and reinforced

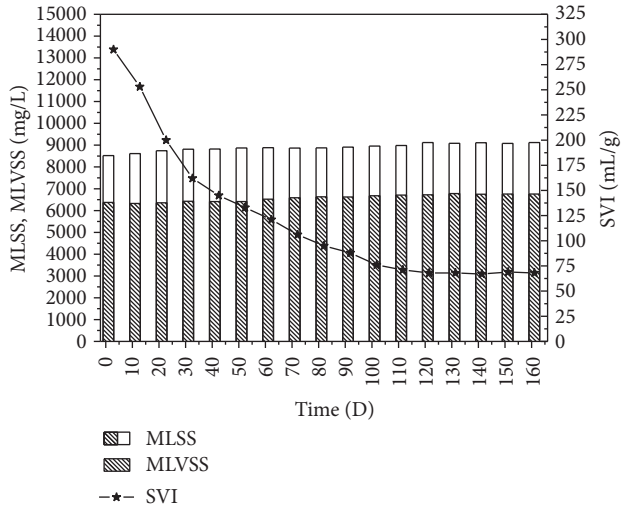

Figure 6: Variation of sludge during the experiment.

endogenous denitrification, the system achieved advanced nitrogen removal without any external carbon source.

3.4. Sludge Variation during the Experiment. The activated sludge of modified SBR was fully adapted to the water quality of landfill leachate by more than one hundred days of cultivation and domestication. Variations of the MLSS, MLVSS, and SVI during the experiment were shown in Figure 6. At the beginning, the SVI value was 300 mL/g. The main reason was that the sludge contained a large number of filamentous bacteria. Since this experiment used alternative anaerobic/anoxic-aerobic modes, the growth of filamentous bacteria was inhibited. After 40 d, the SVI value of the sludge dropped to approximately 150 mL/g and then continued to reduce gradually, until eventual stabilization at about 65 ml/g. Since the sludge SVI value was high at the beginning of the test, we adopted tactics to prolong the precipitation time of the activated sludge. Denitrifying bacteria absorbed the vast majority of leachate organic matter, and there was limited growth of aerobic heterotrophic bacteria. In addition, the toxicity of leachate also inhibited the growth of sludge. After more than 160 experiment days, the growth speed of sludge in the system was slow, and there was zero discharge of sludge when the effluent SS was 30–50 mg/L.

4. Conclusions

This study modified the SBR operation mode by adding a stirring phase before and after the aeration stage. When the influent mixture had a COD of 3820 mg/L and a TN of 1000 mg/L, the modified SBR could achieve high COD removal (>85%) and extremely high total nitrogen removal (>95%) from real leachate without adding any external carbon source, and the maximum specific nitrogen removal rate reached 1.48 mgN/h·gvss.

In this study, the addition of stir before and after aeration was key element to achieve advanced nitrogen removal. The stir before aeration could cause the denitrifying bacterium to absorb carbon source and transfer it into an internal carbon source (e.g., PHA). The stir after nitrification could enable the denitrifying bacterium to realize endogenous denitrification through the utilization of internal carbon. Under the anaerobic/anoxic-aerobic operation mechanism, the utilization rate of organic matter (about 50%) for denitrification in wastewater was increased significantly. Because of that, during the 160 d experiment, the sludge concentration was maintained in the range of about 8000–9000 mg/L, and the system achieved sludge reduction dramatically.

Conflicts of Interest

The authors declare that they have no conflicts of interest.

Acknowledgments

Funding for this project was provided by Shandong Provincial Natural Science Foundation, China (ZR2017BEE067); Science and Technology Planning of Ministry of Housing and Urban-Rural Development, China (UDC2017031712); National Key Research and Development Program of China (2017YFF0209903).

References

[1] S. Renou, J. G. Givaudan, S. Poulain, F. Dirassouyan, and P. Moulin, "Landfill leachate treatment: review and opportunity," *Journal of Hazardous Materials*, vol. 150, no. 3, pp. 468–493, 2008.

[2] K. C. Cheung, L. M. Chu, and M. H. Wong, "Ammonia stripping as a pretreatment for landfill leachate," *Water, Air, & Soil Pollution*, vol. 94, no. 1-2, pp. 209–221, 1997.

[3] F. Wang, D. W. Smith, and M. G. El.-Din, "Application of advanced oxidation methods for landfill leachate treatment," *Journal of Environmental Engineering Science*, vol. 2, pp. 413–427, 2003.

[4] Y. W. Kang and K. Hwang, "Effects of reaction conditions on the oxidation efficiency in the Fenton process," *Water Research*, vol. 34, no. 10, pp. 2786–2790, 2000.

[5] F. N. Ahmed and C. Q. Lan, "Treatment of landfill leachate using membrane bioreactors: A review," *Desalination*, vol. 287, pp. 41–54, 2012.

[6] T. Ismail, D. Tarek, S. Mejdi et al., "Cascade bioreactor with submerged biofilm for aerobic treatment of Tunisian landfill leachate," *Bioresource Technology*, vol. 102, no. 17, pp. 7700–7706, 2011.

[7] E. Klimiuk and D. Kulikowska, "Organics removal from landfill leachate and activated sludge production in SBR reactors," *Waste Management*, vol. 26, no. 10, pp. 1140–1147, 2006.

[8] C.-Y. Lin, F.-Y. Chang, and C.-H. Chang, "Co-digestion of leachate with septage using a UASB reactor," *Bioresource Technology*, vol. 73, no. 2, pp. 175–178, 2000.

[9] J. Bohdziewicz, E. Neczaj, and A. Kwarciak, "Landfill leachate treatment by means of anaerobic membrane bioreactor," *Desalination*, vol. 221, no. 1-3, pp. 559–565, 2008.

[10] Y. Peng, S. Zhang, W. Zeng, S. Zheng, T. Mino, and H. Satoh, "Organic removal by denitritation and methanogenesis and nitrogen removal by nitritation from landfill leachate," *Water Research*, vol. 42, no. 4-5, pp. 883–892, 2008.

[11] T. H. Hoilijoki, R. H. Kettunen, and J. A. Rintala, "Nitrification of anaerobically pretreated municipal landfill leachate at low temperature," *Water Research*, vol. 34, no. 5, pp. 1435–1446, 2000.

[12] E. Neczaj, E. Okoniewska, and M. Kacprzak, "Treatment of landfill leachate by sequencing batch reactor," *Desalination*, vol. 185, no. 1-3, pp. 357–362, 2005.

[13] N. Yusof, M. A. Hassan, L. Y. Phang et al., "Nitrification of ammonium-rich sanitary landfill leachate," *Waste Management*, vol. 30, no. 1, pp. 100–109, 2010.

[14] C. Visvanathan, M. K. Choudhary, M. T. Montalbo, and V. Jegatheesan, "Landfill leachate treatment using thermophilic membrane bioreactor," *Desalination*, vol. 204, no. 1-3, pp. 8–16, 2007.

[15] L. Wu, C. Peng, S. Zhang, and Y. Peng, "Nitrogen removal via nitrite from municipal landfill leachate," *Journal of Environmental Sciences*, vol. 21, no. 11, pp. 1480–1485, 2009.

[16] Y. Wei, M. Ji, R. Li, and F. Qin, "Organic and nitrogen removal from landfill leachate in aerobic granular sludge sequencing batch reactors," *Waste Management*, vol. 32, no. 3, pp. 448–455, 2012.

[17] M. Vocks, C. Adam, B. Lesjean, R. Gnirss, and M. Kraume, "Enhanced post-denitrification without addition of an external carbon source in membrane bioreactors," *Water Research*, vol. 39, no. 14, pp. 3360–3368, 2005.

[18] K. Wang, S. Wang, R. Zhu, L. Miao, and Y. Peng, "Advanced nitrogen removal from landfill leachate without addition of external carbon using a novel system coupling ASBR and modified SBR," *Bioresource Technology*, vol. 134, pp. 212–218, 2013.

[19] R. J. Zeng, R. Lemaire, Z. Yuan, and J. Keller, "Simultaneous nitrification, denitrification, and phosphorus removal in a lab-scale sequencing batch reactor," *Biotechnology and Bioengineering*, vol. 84, no. 2, pp. 170–178, 2003.

[20] C. Wu, Z. Chen, X. Liu, and Y. Peng, "Nitrification-denitrification via nitrite in SBR using real-time control strategy when treating domestic wastewater," *Biochemical Engineering Journal*, vol. 36, no. 2, pp. 87–92, 2007.

Hindawi
BioMed Research International
Volume 2017, Article ID 3691819, 5 pages
https://doi.org/10.1155/2017/3691819

Research Article

Study of Nitrogen Removal Performance When Treating Low Carbon Sewage Using External Solid Carbon Sources in SBBR Systems

Li-qiu Zhang,[1,2] Pei-fen He,[1] Dan Wu,[1] Shu-geng Li,[2,3] Yi-liang Huang,[1] You-wen Huang,[1] and Deng-min Wang[1]

[1]*School of Civil Engineering, Guangzhou University, Guangzhou 510006, China*
[2]*Key Laboratory for Water Quality and Conservation of the Pearl River Delta, Ministry of Education, Guangzhou University, Guangzhou 510006, China*
[3]*School of Environmental Science and Engineering, Guangzhou University, Guangzhou 510006, China*

Correspondence should be addressed to Shu-geng Li; lishugeng@163.com

Received 27 October 2017; Accepted 22 November 2017; Published 14 December 2017

Academic Editor: Bin Ma

Based on low carbon wastewater as the research object and using corncob as an external solid carbon source, the performance of corncob organic matter was assessed for its release potential, quantity of release, and safety of use. The effects of varying quantities of the solid carbon source on simultaneous nitrification and denitrification were investigated in a sequencing biofilm batch reactor (SBBR). Results show that the regularity of corncob as solid carbon source material was linear, with released concentrations of heavy metals being below the Chinese national standard limit values for heavy metals according to the surface water environment quality standards (I and II) (GB3838-2002). When temperatures were within 28~31°C, the dissolved oxygen level was 4.0 ± 0.2 mg/L and the pH conditions were within 7.5~8.0. The optimal quantity for corncob dosing was 5 g per 1.5 L of low carbon wastewater. Following treatment, the average effluent concentrations of NH_4^+-N and TN were 2.85 mg/L and 4.51 mg/L, respectively. The effluent concentration of NH_4^+-N, TN had reached the A level national standard of sewage treatment plant pollutant discharge standard (GB18918-2002).

1. Introduction

Recently, with the constant development of social economies and urbanization, significant pressures have been placed on our environment resources. An example of this is the discharge of wastewater and water pollutants into the aquatic environment, from both domestic, agricultural and industrial sources, posing a major threat to water resources and aquatic environment. In particular, the level of discharge of nitrogen containing sewage has increased rapidly, while the phenomenon of low carbon source wastewater is becoming an increasingly common issue, causing major problems in sewage treatment plants and causing the need for upgrading and retrofitting [1–3].

At present, sewage treatment plants generally use a liquid carbon source for denitrification, such as carbinol, acetic acid, or amylaceum, although some shortcomings exist with this method. It can be difficult to accurately control the quantities of carbon sources, with complicated operation procedures, and there is a risk of causing secondary organic pollution of effluent, which will greatly increase the cost of pretreatment systems [4–7]. Therefore, there is much current research focus on the optimization of denitrification technologies and understanding the role of solid carbon sources [8–12].

This study assesses synthetic low carbon sewage treatment, using corncob as an agricultural solid waste material providing an external solid carbon source. The release of carbon and heavy metals were quantified, allowing the safety and performance of corncob organic matter to be assessed. The effectiveness of varying quantities of solid carbon source in the removal of NH_4^+-N and TN was assessed during simultaneous nitrification and denitrification in a sequencing biofilm

batch reactor (SBBR). And optimal quantity on simultaneous nitrification and denitrification in sequencing biofilm batch reactor (SBBR) were confirmed.

2. Materials and Methods

2.1. Reagents and Materials. The corncob utilized as an external carbon source was purchased from Guangzhou farmers market. Once returned to the laboratory, the corncob was washed with running water, cut into 1 cm^3 segments, and dried in the oven at 80°C. Once cooled, corncob segments were placed on a drying container for preservation. To reduce variation, we utilized the same batch of corncob material for the duration of the experiment.

The reactor consisted of an organic glass column, with an internal column diameter of 14 cm, column height of 115 cm, containing eight biomembrane diaphragm filters, with an effective volume of 12 L. The synthetic sanitary low carbon wastewater was adopted in this experiment, containing starch, NH_4Cl, KH_2PO_4, $CaCl_2$, $MgSO_4{\cdot}7H_2O$, $FeSO_4{\cdot}7H_2O$. To obtain varying influent qualities, adjustments were made to the concentration of the main ingredients, starch and NH_4Cl. During the film-forming period of the experiment, sufficient sources of organic substances and carbon were supplied to ensure enough nutrition and energy was available for the promotion of biomembrane formation, reproduction, and growth. The influent concentration of COD_{Cr} remained consistently within 250~300 mg/L, while the concentration of NH_4^+-N varied within 19.8~27.5 mg/L. Biomembranes were cultured 25 d until they remained attached, at which point the concentration of COD_{Cr} was reduced 90~120 mg/L and systems were allowed to continue acclimatizing 15 d.

2.2. Experiment Design

2.2.1. Static Experiment to Assess Carbon and Heavy Metal Release from Solid Carbon Source Material. The corncob material utilized as a solid carbon source was weighted into 5 g, 10 g, 15 g, and 20 g portions, which were then divided into eight 2 L beakers, submerged in 1 L of deionized water, and sealed using a preservative film. Beakers were divided into separate groups for TOC and COD_{Cr} analysis. Samples were collected using an injector at 12 h, 24 h, 36 h, 48 h, 64 h, and 72 h, for the analysis of concentrations of TOC, TC, and COD_{Cr} in the water surrounding the immersed corncob. Analysis of the concentration of heavy metals in water surrounding the immersed corncob was performed at the end of the static experiment.

2.2.2. Assessment of Optimum Dose of Solid Carbon Source Material. Parallel experiments were performed, with control levels for every factor simultaneously applied to ensure uniformity of conditions. Every period is 12 h; 12 L of wastewater was treated using the SBBR system containing eight biomembranes, resulting in 1.5 L of wastewater treated per biomembrane. Each cultured biomembrane was transferred to a 2 L beaker and submerged in 1.5 L of synthetic influent along with the corncob material at varying doses of 1.25 g, 3.75 g, 5 g, 7.5 g, and 10 g and the corncobs are replaced every 6 periods, when the characteristics of effluent are stable, showing the ending of sludge acclimatizing.

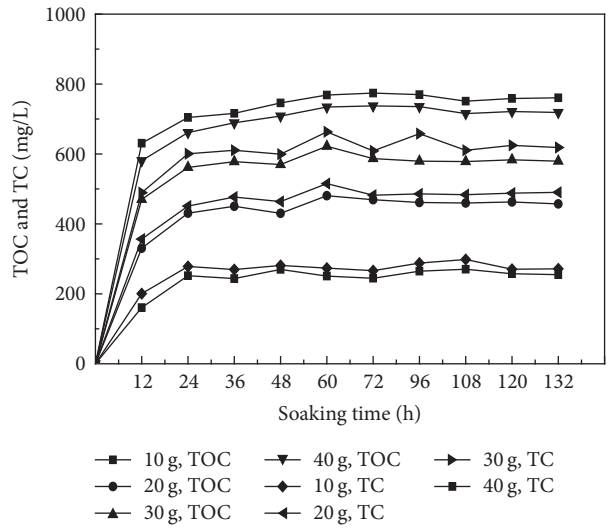

Figure 1: Level of release of TOC and TC from corncob at varying doses into surrounding deionized water.

2.3. Analytical Measurements. The parameters measured during wastewater treatment were the concentration of COD_{Cr}, NH_4^+-N, NO_2^--N, NO_3^--N, TN, pH, TOC/TC, and heavy metals and were measured according to the national standard methods [13]. The pH and DO were measured using pH probes (WTW-pH/Oxi340i, Germany).

3. Results and Discussion

3.1. Effectiveness of Corncob Material as a Carbon Source. The corncob solid carbon material was assessed for its level of carbon release at doses of 5 g, 10 g, 15 g, and 20 g, with concentrations assessed every 12 h, up to 132 h. Concentrations of TOC, TC, and COD_{Cr} were assessed in the water surrounding the immersed corncob, with results provided in Figures 1 and 2.

Figures 1 and 2 show that the concentrations of TOC and TC increased according to immersion time, to varying degrees depending on the dose of corncob material immersed in 1 L deionized water. After 24 h of immersion, TOC and TC concentrations were rapidly increased due to release from the corncob material, while, from 24 h to 96 h, concentrations fluctuated and then stabilized after 96 h. The concentrations of TOC and TC released from corncob material increased according to the quantity of corncob material applied, following the same immersion time. After the rate of release of carbon stabilized, a distinct linear relationship with time was observed. In water samples exposed to different quantities of corncob material, the ratio of TOC to TC was consistently over 90%, showing that corncob effectively releases high concentrations of organic carbon. In addition, corncob has the ability to provide an immediate carbon source, with a relatively stable rate of carbon release, suggesting that corncob may be a suitable material to apply as a solid carbon source in wastewater treatment.

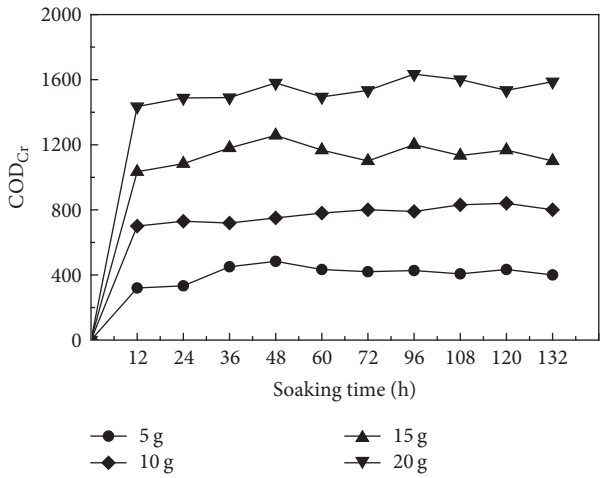

Figure 2: Level of release of COD_{Cr} from corncob at varying doses into surrounding deionized water.

During the initial 12 h, corncob was found to have a rapid release of high concentrations of COD_{Cr} and TOC under all scenarios assessed, although the rate of release was not consistent. The concentrations of COD_{Cr} increased according to immersion time, until 48 h when a steady state was maintained. The average concentration of COD_{Cr} released from corncob material was 406.9 mg/L released from 5 g corncob, 746.9 mg/L released from 10 g corncob, 1137.4 mg/L released from 15 g corncob, and 1503.4 mg/L released from 20 g corncob. In the initial 12 h, the rapid increase in concentrations of COD_{Cr} is due to water-soluble material on the surface of the corncob being degraded, with inner smaller molecules quickly dissolving into the surrounding media, increasing the effluent concentrations of COD_{Cr}. After 48 h a steady state was observed as most available COD_{Cr} has been released via hydrolysis and the remaining corncob inner fiber is formed of material that is difficult to decompose, such as lignin. It is of note that after immersion for 48 h corncob material showed signs of ageing, with white regions appearing and a foul odor, potentially because the decomposition of corncob material was restrained.

By calculating the average level of release of COD_{Cr} during the linear period, from varying quantities of corncob, the average concentration of carbon released by 1 g corncob was 76.8 mg/L deionized water.

3.2. The Safety of Corncob Material as a Solid Carbon Source. It has been established that there are some elements released into surrounding water from corncob material, such as Ca, K, Mg, Na, Si, and P, among others, which are indispensable nutritional materials and essential constituents for microbes. Additionally, metal microelements are also released, which have an important role in microbial growth and reproduction. The enzyme active gene consists of inorganic mineral elements for adjusting the osmotic pressure in cells. It has been reported that metal ions released from carbon source materials into surrounding water during the process of denitrification can increase the fermentation activity of microbes and therefore increase the rate of denitrification [14]. Standard limit values (Table 1) exist for concentrations of metal ions in surface water (environment quality standard [15] (GB 3838-2002)), with any excess of these limits presenting a hazard to biofilm microbes and the natural environment. Therefore, when selecting a solid carbon source material, the safety and potential release of harmful substances must be considered. To assess the safety of corncob material as a solid carbon source, 6 kinds of typically regulated heavy metals were studied, including As, Cu, Cd, Cr, Pb, and Zn.

Table 1: Standard limit values for heavy metals according to the surface water environment quality standards (I and II), with the concentration of heavy metals released from corncob material into surrounding water.

Metal species	The level of I (mg/L)	the level of II (mg/L)	corncob (mg/L)
Cu	0.01	1.0	0.023
Zn	0.05	1.0	0.134
As	0.05	0.05	0.006
(+6) Cd	0.001	0.005	n.d.
Cr	0.01	0.05	0.02
Pb	0.01	0.01	0.006

n.d. means undetected.

The results show that no Cd was detected in the corncob immersion water, while the concentrations of Cu, Cr, and Zn were lower than the II class limit value and the concentration of Pb was below the I class limit value. It is of note that the water flow and velocity applied were significantly far less than in actual water-treatment situations, in addition the large volume of reactors used in wastewater treatment mean that the concentration of metal ion would be diluted greatly. Therefore, based on these findings, we may assume that the use of corncob as an external solid carbon source does not result in harmful levels of release of heavy metals and is not likely to pose a risk to environmental safety.

3.3. Effects of Varying Quantities of Solid Carbon Source in an SBBR System Treating Low Carbon Sewage. The synthetic low carbon urban sewage was used in influent of these experiments. The influent concentration of COD_{Cr} remained consistently within 250~300 mg/L, while the concentration of NH_4^+-N varied within 19.8~27.5 mg/L. The concentration of TN was 21.5~29.6 mg/L, the temperature was 28~31°C, the DO was 4.0 ± 0.2 mg/L, and the pH value was at 7.5~8.0, The synthetic low carbon urban sewage was treated with varying quantities of corncob material (1.25 g, 3.75 g, 5 g, 7.5 g, and 10 g), while all other conditions remained unchanged. The water quality of synthetic effluent was assessed following steady operation for a period and the results of the continuous 12 periods are shown in Figures 3–5.

When the dose of corncob applied was within 1.25~5 g, the average removal ratio of NH_4^+-N increased according to increased quantity. When the applied dose of corncob was increased to 5 or 7.5 g, a stable level of removal NH_4^+-N was achieved, with an average removal ratio of 89% and 90%, respectively. Therefore, increased quantities of corncob

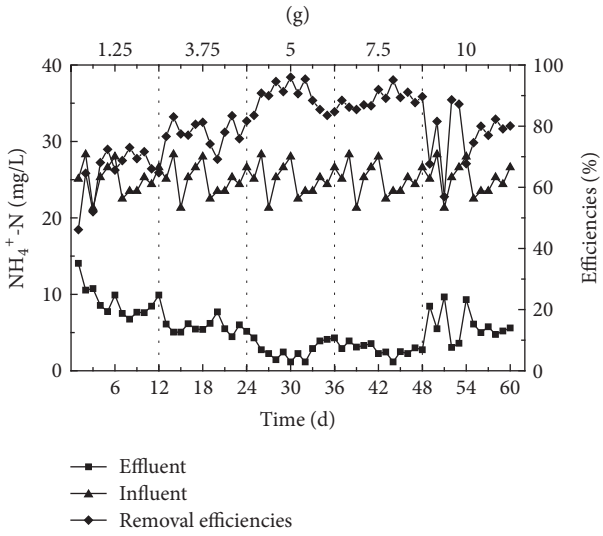

Figure 3: The degree of NH_4^+-N removal from synthetic wastewater following exposure to varying quantities of corncob.

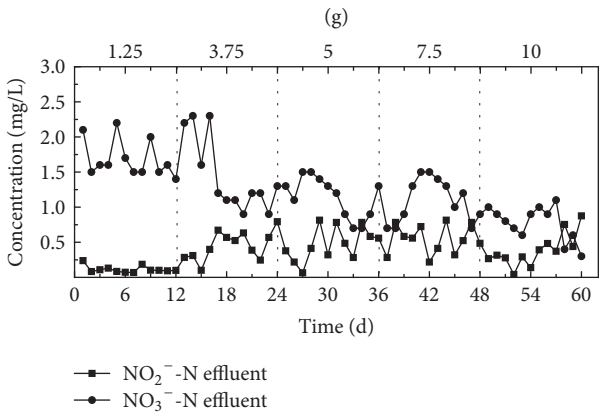

Figure 4: The degree of NO_2^--N and NO_3^--N removal from synthetic wastewater following exposure to varying quantities of corncob.

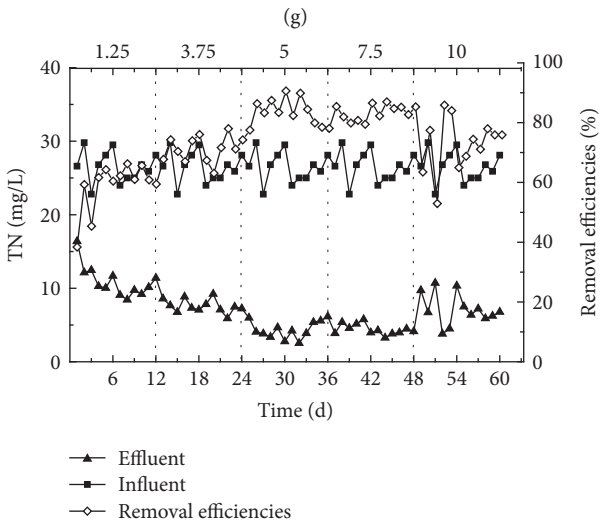

Figure 5: The degree of TN removal from synthetic wastewater following exposure to varying quantities of corncob.

material result in increasing the available carbon source and, consequently, an improved average removal rate of NH_4^+-N was observed. Conversely, when the dose of corncob applied was increased to 10 g, the average effluent concentration of NH_4^+-N increased, showing that the average removal ratio of NH_4^+-N was reduced. This phenomenon is likely due to the high concentration of COD_{Cr} causing a reduction in competition in nitrifying species following an extended period of operation, which is not effective in the removal of NH_4^+-N.

Figures 4 and 5 show the effectiveness of removing NO_2^--N, NO_3^--N, and TN from synthetic wastewater, under different corncob dose quantities. Figure 4 shows that average effluent concentrations of NO_2^--N and NO_3^--N remained consistently low under all tested quantities of corncob and that the denitrification rate increased according to increased corncob quantity. The denitrifying bacteria is key heterotrophic and facultative anaerobes during the denitrification processes, which, under anaerobic conditions, utilize the carbon source, and NO_2^--N and NO_3^--N as electron donors to support denitrification processes [16–18]. Therefore, a close interaction exists between the concentration of the organic carbon source and the rate of denitrification in sewage, with the corncob material providing all organic carbon in this study, allowing the dosed quantity of corncob to be the determining factor for promoting the rate of denitrification. Due to average effluent concentration of NO_2^--N and NO_3^--N being consistently low, the overall removal rate of TN was dominated by changes in the removal rate of NH_4^+-N, when the dosed quantity of corncob was within 1.25~5 g, the average removal rate of TN increased according to carbon source quantity. However, when the dosed quantity of corncob was 5 g or 7.5 g, the effect of TN removal was more stable, with average removal rates of 83% and 84%, respectively. When the dosed quantity of corncob was increased to 10 g, the average removal rate of TN decreased slightly; this effect is likely due to excessive organic matter being released by corncob, causing the increase of denitrification rate but decrease of nitrification rate.

As shown in Figure 6, when the dosed quantity of corncob ranged from 1.25 to 10 g, the effluent concentration of COD_{Cr} remained largely stable below 30 mg/L, showing that no effect was observed on the removal rate of COD_{Cr} when the dosed quantity of corncob varied within 1.25~10 g.

Overall, corncob was found to be effective as an external solid carbon source for the treatment of low carbon wastewater in SBBR systems, with optimal effects being observed when the dosed quantity of corncob was within 5 g~7.5 g per 1.5 L of wastewater. The use of 5 g corncob resulted in an average effluent NH_4^+-N concentrations of 2.85 mg/L, an average NH_4^+-N removal rate of 89%, with average effluent TN concentrations of 4.51 mg/L, an average TN removal rate of 83%, and average effluent concentrations of NO_2^--N and NO_3^--N, of 1.16 and 0.48 mg/L, respectively. Following treatment, the quality of effluent reached the level of A standard in "urban sewage treatment plant pollutant discharge standard" (GB18918-2002).

4. Conclusions

Corncob was found to be an effective external solid carbon source, showing a consistent release of carbon source, with

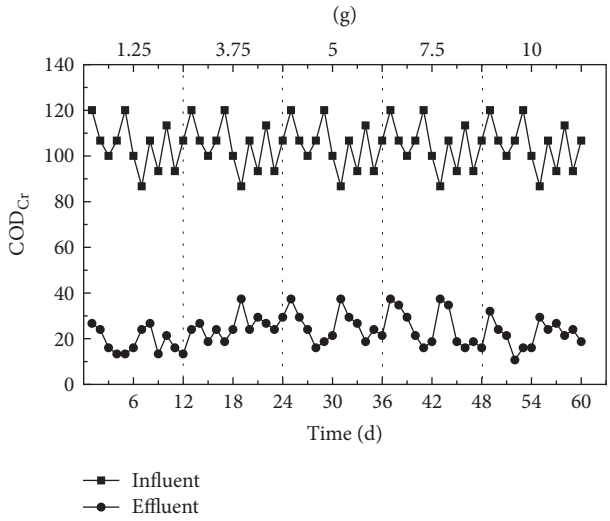

FIGURE 6: The change of COD_{Cr} concentrations in effluent following exposure to varying quantities of corncob solid carbon source material.

a rapid level of release in the first 12 h and a stable rate of carbon release after 24 h. This pattern of carbon release was observed at all tested dose quantities of corncob organic matter. In addition, no harmful levels of heavy metal ions were released from corncob, with surrounding water metal content being below the standard limit value.

When corncob was applied as an external solid carbon source to treat low carbon wastewater in an SBBR system, the best dosed quantity of corncob was 5 g per 1.5 L wastewater. The average effluent concentrations of NH_4^+-N and TN were reduced from over 19.8 mg/L and 21.5 mg/L to 2.85 mg/L and 4.51 mg/L, respectively. The average effluent concentrations of NO_2^--N and NO_3^--N were reduced to 1.16 mg/L and 0.48 mg/L, respectively. Therefore, the effluent water quality was treated to level A of the standard in urban standard of wastewater treatment plant pollutant discharge standard (GB18918-2002).

Conflicts of Interest

The authors declare that there are no conflicts of interest regarding the publication of this article.

Acknowledgments

This work was supported by the National Natural Science Foundation of China (NSFC) (Projects nos. 51478127 and 51708140) and the Science and Technology Bureau Foundation of Guangzhou (Project no. 201510010051).

References

[1] B. N. Lv, Z. Q. Chen, X. B. Jia et al., *New Technology of Biological Wastewater Treatment*, Harbin Institute of Technology Press, 2013.

[2] Z. Chen and X. J. Tan, *Problems about upgrading and retrofitting of wastewater treatment plants*, China Water & Wastewater, 2008.

[3] X. C. Zheng and Y. X. Li, *Phosphorus and Nitrogen Removal Technology*, China Architecture & Building Press, Beijing, China, 1998.

[4] M. I. M. Soares and A. Abeliovich, "Wheat straw as substrate for water denitrification," *Water Research*, vol. 32, no. 12, pp. 3790–3794, 1998.

[5] M. Volokita, S. Belkin, A. Abeliovich, and M. I. M. Soares, "Biological denitrification of drinking water using newspaper," *Water Research*, vol. 30, no. 4, pp. 965–971, 1996.

[6] M. Volokita, A. Abeliovich, and M. I. M. Soares, "Denitrification of groundwater using cotton as energy source," *Water Science and Technology*, vol. 34, no. 1-2, pp. 379–385, 1996.

[7] B. Ovez, S. Ozgen, and M. Yuksel, "Biological denitrification in drinking water using Glycyrrhiza glabra and Arunda donax as the carbon source," *Process Biochemistry*, vol. 41, no. 7, pp. 1539–1544, 2006.

[8] L. Shao, Z. X. Xu, W. Jin, and H. L. Yin, "Rice husk as carbon source and biofilm carrier for water denitrification," *Polish Journal of Environmental Studies*, vol. 18, no. 4, pp. 693–699, 2009.

[9] H. X. Fu, M. Qian, J. M. Li et al., "Study on Removal of Nitrate from Water by Using Newspaper as Solid Carbon Source," *Acta Agriculturae Jiangxi*, vol. 26, no. 7, pp. 92–95, 2014.

[10] Z. H. Shen, Z. Q. Zhang, F. Shen, Y. Chen, and Y. Wang, "Effect of sawdust and ethanol as mixed carbon sources on nitrate removal from groundwater," *Acta Scientiae Circumstantiae*, vol. 33, no. 1, pp. 105–110, 2013.

[11] L. Shao, Z. X. Xu, J. W, and H. L. Yin, "Optimization of solid carbon source for denitrification of agriculture wastes," *Zhongguo Huanjing Kexue/China Environmental Science*, vol. 31, no. 5, pp. 748–754, 2011.

[12] J. F. Xiong, H. Xu, N. Yan, and Y. M. Zhang, "Leaves of Platanus orientalis as the carbon source for denitrification," *Huanjing Kexue*, vol. 33, no. 11, pp. 4057–4061, 2012.

[13] National Environmental Protection Agency, *Editor of water and wastewater monitoring and analysis methods. Water and Wastewater Monitoring and Analysis Methods*, China Environmental Science Press, Beiging, China, 1997.

[14] Y. Tan and Q. Luo, "Study on the denitrification of drinking water with upflow anaerobic sludge blanket reactor," *Journal of Hygiene Research*, vol. 31, no. 1, pp. 19–21, 2002.

[15] Ministry of Construction, CJ/T206-2005(Water quality standards for urban water supply, Beijing, China, 2005.

[16] C. N. Li, X. W. Lv, and I. Yuhei, "Study on Nitrogen Removal by Simultaneous Nitrification and Denitrification," *Water & Wastewater Engineering*, vol. 27, no. 1, pp. 22–24, 2001.

[17] A. Islam, D. Chen, and R. E. White, "Heterotrophic and autotrophic nitrification in two acid pasture soils," *Soil Biology & Biochemistry*, vol. 39, no. 4, pp. 972–975, 2007.

[18] J. Burton, C. Chen, Z. Xu, and H. Ghadiri, "Gross nitrogen transformations in adjacent native and plantation forests of subtropical Australia," *Soil Biology & Biochemistry*, vol. 39, no. 2, pp. 426–433, 2007.

Hindawi
BioMed Research International
Volume 2017, Article ID 2564363, 10 pages
https://doi.org/10.1155/2017/2564363

Research Article

Analysis of the Metabolites of Indole Degraded by an Isolated *Acinetobacter pittii* L1

Zuoyi Yang, Junhui Zhou, Yanbin Xu, Yaping Zhang, Haien Luo, KenLin Chang, and Yujie Wang

School of Environmental Science and Engineering, Guangdong University of Technology, Guangzhou 510006, China

Correspondence should be addressed to Junhui Zhou; cms5211110@mail2.gdut.edu.cn

Received 27 August 2017; Accepted 19 November 2017; Published 13 December 2017

Academic Editor: Shijian Ge

Indole and its derivatives are typical nitrogen heterocyclic compounds and have been of immense concern since they are known for the risk of their toxic, recalcitrant, and carcinogenic properties for human and ecological environment. In this study, a Gram-negative bacterial strain of eliminating indole was isolated from a coking wastewater. The strain was confirmed as *Acinetobacter pittii* L1 based on the physiological and biochemical characterization and 16S ribosomal DNA (rDNA) gene sequence homology. 400 mg/L indole could be completely removed within 48 h by the strain on the optimum condition of 37°C, pH 7.4, and 150 rpm. The organic nitrogen was converted to NH_3-N and then to NO_3^- and the organic carbon was partially transferred to CO_2 during the indole biodegradation. The metabolic pathways were proposed to explain the indole degradation based on the liquid chromatography tandem mass spectrometry (LC-MS/MS) analysis of indigo, 4-(3-Hydroxy-1H-pyrrol-2-yl)-2-oxo-but-3-enoic acid, and isatin. The toxicity of the biodegradation products was evaluated using the Microtox test, which revealed that the metabolites were more toxic than indole. Our research holds promise for the potential application of *Acinetobacter pittii* L1 for NHCs degradation, production of indigoids, and soil remediation as well as treatment of indole containing wastewater.

1. Introduction

Indole and its derivatives, with highly toxic and carcinogenic properties, are mainly generated in large quantities as a result of industrial wastewater from pharmaceutical synthesis, fuel, cosmetics, pesticide, disinfectant, agrochemicals, and dyestuff and have recently gained wide attention [1–4]. These compounds also existed in large amounts of livestock manure emissions, which are serious pollution to the ecological environment with a sharp odor. Their heterocyclic structure makes them not only merely more soluble but also more difficult to degradation; therefore these cyclic compounds could be transformed through the soil and contaminated ground water.

Indole is a typical tryptophan metabolite in the natural environment, acting as plant hormone precursor and microbial signal molecule [5–7]. Furthermore, indole also acted as a gas pollutant because of its unfavorable odor, especially released from the pharmaceutical, coking, and livestock wastewater.

The technologies of contact glow discharge plasma degradation, photocatalytic degradation, and electro-Fenton oxidation were used to degrade indole, and the chemical oxidants such as chlorine and chlorine dioxide were used to control indole release [8, 9]. The photocatalytic degradation and chemical oxidation can efficiently break up indole, but the high investment and energy consumption confined the engineering applications, and the chemical oxidants could induce new toxic and carcinogenic compounds [8, 10, 11].

Some bacteria demonstrated their abilities of decomposing N-heterocyclic compounds. For example, a novel endophytic fungus *Phomopsis liquidambari* could catalyze indole into 2-aminobenzoic acid and 2-dioxindole and an isolated strain *Bacillus* sp. from petroleum-contaminated soil was able to decompose quinoline under aerobic conditions [12, 13]. Bacteria from genera *Alicycliphilus*, *Alcaligenes*, and *Thauera* were thought to be responsible for indole degradation [4]. Moreover, Qu et al. indicated that a rich set of oxidoreductases was expressed from a newly isolated *Cupriavidus*

sp. SHE, which might be the most important factor for the efficient indole degrading [14].

It was reported that the C-N position of pyridine ring in indole and quinoline can be broken down by the microbe [12, 13]. One of the indole metabolic pathways was known as the isatin pathway, in which indole was degraded via the formation of indoxyl, 2,3-dihydroxyindole, isatin, N-formylanthranilic acid, anthranilic acid, salicylic acid, and catechol [15]. The other metabolic pathway was reported as the gentisate pathway, in which indole was degraded via indoxyl, isatin, anthranilic acid, and gentisate [16]. In this study, the metabolites were analyzed and the indole metabolic pathways of *Acinetobacter pittii* were illuminated.

The Microtox test was widely employed for evaluating the toxicity of the compounds and their products by using the prokaryote *Vibrio fischeri*. According to the Microtox test, Chen et al. indicated that the toxicity of the photoproducts of mefenamic acid were more toxic than their parent compounds [3]. Wang et al. analyzed the toxicity and mineralization of IDM under the conditions of AOPs; the results indicated that the inhibition rates of IDM declined dramatically in the presence of 1.0 g/L NCDs/g-C_3N_4 [17]. According to compounds, the types of degradation, and the toxicity assay methods, we can find out that the toxicity of different contaminants might increase or decrease in different occasion.

Acinetobacter spp. has been applied in a wide range of fields such as pharmaceutical industry and soil remediation. Researchers demonstrated that *Acinetobacter* spp. could utilize phenol or 4-nitroaniline as the sole carbon source and remove PAHs [18–21]. *Acinetobacter* spp. was also reported to be able to degrade N-heterocyclic compounds [20, 22]. The effective biotechnology has been reported to optimize the indole removal rate [15, 22, 23]. The initial indole concentrations were usually controlled to be lower than 200 mg/L to prevent them from inhibiting the bacterial growth [14, 15].

In this study, we isolate a bacterial from a coking wastewater and investigate the degradation of indole; meanwhile, the metabolites were analyzed and the indole metabolic pathways of *Acinetobacter pittii* were illuminated and the toxicity changes about NHCs have also been detected.

2. Materials and Methods

2.1. Chemicals and Mediums. Indole (98.5%), quinoline (99.5%), and phenol (98%) were purchased from Aladdin Industrial Co., Ltd. Pyridine (99%) was purchased from Chengdu Kelong Chemical Reagent Co., Ltd. (Sichuan, China). High-performance liquid chromatography (HPLC) grade reagent methanol was obtained from Shanghai ANPEL Scientific Instrument Co., Ltd. (Shanghai, China). Ultrapure water from a Milli-Q apparatus (Smart2 Pure ultrapure water/water system integration, TKA, Germany) was applied in the HPLC and LC-MS/MS. All the other reagents were of analytic grade or above.

The mineral salt medium (MSM medium) was used for the isolation and biodegradation, which contained ($g \cdot L^{-1}$): K_2HPO_4, 0.8; KH_2PO_4, 0.2; $CaCl_2$, 0.05; $MgCl_2 \cdot H_2O$, 1.07; $FeCl_2 \cdot H_2O$, 0.016; $(NH_4)_2SO_4$, 1.0; NaCl, 5.0; pH 7.0. The Luria-Bertani medium (LB medium) contained ($g \cdot L^{-1}$): yeast extract, 5.0; peptone, 10; NaCl, 5.0; pH 7.0. All the media appending different indole concentration were autoclaved at 121°C for 30 min, and 2.0% *(w/v)* agar was added in the corresponding solid medium.

2.2. Bacterial Isolation and Identification. The target microorganism came from the sludge in a coke quenching effluent treatment system. The initial sludge was inoculated into 100 mL sterilized MSM containing 50 mg/L indole and then cultivated at 37°C with 150 rpm for 48 h. To get the indole-acclimating bacteria, 10% *(v/v)* of the above culture was transferred into the MSM with the addition of indole ranging from 50 to 400 mg/L every other five days for a month. Finally, the isolated strain L1 was characterized by morphological, physiological, and biochemical identification.

With the help of the BLAST software, 16S rDNA gene sequence was used to explore the homological relationship of the isolated strain L1. 16S rDNA gene of the strain L1 was amplified by PCR with universal primer pair 8F (5′-AGA GTT TGA TCC TGG CTC AG-3′) and 1492R (5′-GGT TAC CTT GTT ACG ACT T-3′). The phylogenetic tree of the isolated strain was inferred by MEGA 5.1 software using neighbor-joining method with a bootstrap value of 1000 replicates.

2.3. Evaluation of Indole Biodegradation. The strain L1 was cultivated in LB medium (37°C, 150 rpm, 24 h); the cells in logarithmic growth phase were collected and then centrifuged at 6000 ×g for 10 min (TDL-60B, Anting Scientific Instrument, Shanghai, China). Remove the medium and wash the pellet with PBS, and then resuspend the cell pellet to make $OD_{600} = 1$. The suspension was used immediately in the biodegradation experiments. To further investigate its capability of degrading indole, the removal rate at the different initial indole concentrations, temperatures, and pH values were analyzed by HPLC. The removal rates of pyridine, quinoline, and phenol, which are the typical compounds in the coking wastewater, were also tested when they acted as the sole carbon source in MSM medium inoculated *Acinetobacter pittii* L1. All samples were measured in triplicate. Moreover, the removal efficiency (RE) of indole was calculated with the equation $RE\ (\%) = (C_0 - C_t)/C_0 \times 100\%$, in which C_0 and C_t are the initial and residual concentration.

2.4. Analytical Methods. The concentration of indole was detected by HPLC that contains a Shimadzu SPD-M20A photodiode array detector and two Shimadzu LC-20AD pumps (Shimadzu, Japan). The HPLC was equipped with a Zorbax Eclipse XDB-C18 column (2.1 mm × 150 mm, 3.5 μm) and the mobile phase was composed of methanol : water (70 : 30 *v/v*) at 40°C, with the flow rate of 0.2 $mL \cdot min^{-1}$. Total organic carbon (TOC) was measured by Shimadzu (TOC-VCPH). UV spectrophotometer (UV-2100, Beijing Rayleigh) was utilized to determine the concentration of pyridine, quinoline, and phenol at 257 nm, 313 nm, and 280 nm, respectively. Ammonia nitrogen determination was detected by Nessler's reagent spectrophotometry.

In order to elucidate the possible indole degradation pathways, the metabolites of indole biodegradation were analyzed by LC-MS/MS, consisting of an Agilent 1100 series HPLC coupled to a 6410 triple quadrupole mass spectrometer (Agilent Technologies, USA). *Acinetobacter pittii* L1 was inoculated (5% v/v) into MSM including 200 mg/L indole and cultivated on the optimum conditions for 24 h. Then the culture was centrifuged at 6000 ×g for 10 min; the supernatant was filtered by 0.22 μm micropolyether sulfone (PES) membrane syringe filter (Jinteng Experimental Equipment Co., Ltd. Tianjin). The solution was then transferred to a sample vial for characterization by LC-MS/MS. Separation was accomplished using an Agilent SB-C18 column (4.6×150 mm, 5 μm). The eluent was made up of the ultrapure water (A) and methanol (B) at the flow rate of 1 mL·min^{-1}. An autosampling device was employed to inject the sample which was detected at 270 nm. The elution was analyzed by the UV-vis detector of a mass spectral equipped with electrospray ionization (ESI) under negative mode. A mass full scan was conducted over a range of 50–550 m/z to identify the intermediates in the indole biodegradation, and the operation parameters were as follows: capillary voltage 3.5 kV, fragmentor 125 V, temperature 350°C, nebulizer pressure 30 psi, and nitrogen as the desolvation gas.

The samples were collected after every 3 hours of biodegradation of 100 mg/L indole solution, which was degraded by *Acinetobacter pittii* L1 at 37°C with 150 rpm for 24 h. Then Microtox Model DXY-2 was employed to determine the toxicity of samples and initial indole solution, which evaluates the ability of the metabolites to inhibit the bioluminescence of the strain *V. fischeri*. According to the equation I (%) = $(I_0 - I_t)/I_0 \times 100\%$, the inhibition of *V. fischeri* can be calculated.

3. Results and Discussion

3.1. Microorganism Isolation and Identification. The strain L1 was isolated from the sludge in a facultative coke quenching tank. The growth curve of the strain and the indole remove rate in MSM were shown in Figure 1. 100 mg/L indole could be completely removed within 15 h, showing the better degradation efficiency compared with *Phomopsis liquidambari* (degrading efficiency 41.7%, 100 mg/L indole in 120 h) and *Pseudomonas aeruginosa* Gs (degrading 1.0 mM indole in 36 h) [13, 24]. As depicted in Figure 1, the bacteria were in logarithmic growth phase, OD_{600} increased with increasing biomass in 6–12 h. Therefore, the efficiency of indole degradation was improved dramatically.

The isolated strain L1 was a short rod-shaped, Gram-negative aerobe, and the physiological and biochemical properties were shown in Table 1. 16S rDNA gene sequence was applied to confirm the phylogeny relationships, and the strain was nominated as *Acinetobacter pittii* L1, which showed 99% gene sequence similarity with *Acinetobacter pittii* ATCC19004 (GenBank accession number: NR117621). Figure 2 showed the phylogenetic tree correlated to the other species from the NCBI GenBank database by the method of neighbor-joining on the program MEGA 5.1.

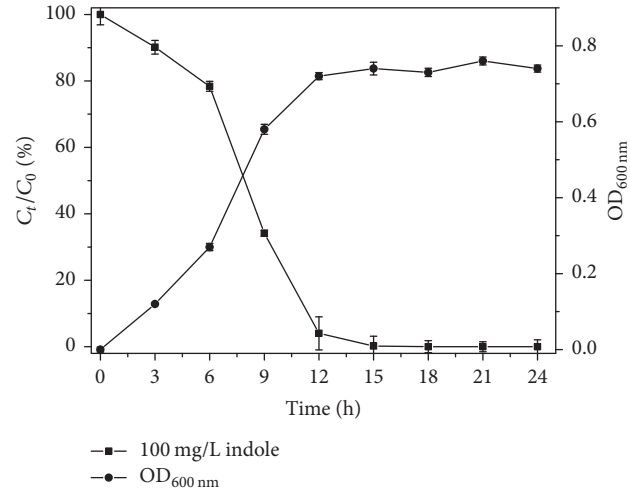

Figure 1: Growth curve of *Acinetobacter pittii* L1 and the change of indole concentration.

Table 1: Biochemical characteristics of *Acinetobacter pittii* L1.

Biochemical and culture conditions	Results
Gram-staining	−
Anaerobic growth	−
Glucose utilization	−
Catalase	+
Oxidase	−
Citrate utilization	+
V-P test	−
Gelatin liquefaction	−
Hydrogen sulfide test	−
Hydrolysis of starch	−
MR test	−

+: positive reaction; −: negative reaction.

3.2. Major Parameters Affecting the Biodegradation

3.2.1. Initial Concentration. When the initial indole concentration ranged from 100 to 400 mg/L, indole could be completely degraded within 48 h on the condition of 37°C, pH 7.0, and 150 rpm. As shown in Figure 3(a), the higher the initial indole concentration is, the smaller the removing rate of indole is. Qu et al. also reported the inhibited effect of indole to the stain SHE; for example, 50–100 mg/L indole could be completely degraded within 24 h, but 200 mg/L indole should be removed within 80 h [14].

3.2.2. Temperature. The temperature was essential and sensitive to the microbe growth and the enzyme catalysis [25]. As shown in Figure 3(b), 200 mg/L indole was degraded by the strain L1 at pH 7.0 and 150 rpm for 48 h. The indole removal rates were determined as 54.81%, 97.36%, 100%, 74.07%, and 14.87%, respectively, at 25°C, 30°C, 37°C, 45°C, and 50°C. Therefore, *Acinetobacter pittii* L1 showed the optimum temperature to degrade indole at 37°C in this study, compared with white rot fungus at 25°C, *Phomopsis liquidambari*

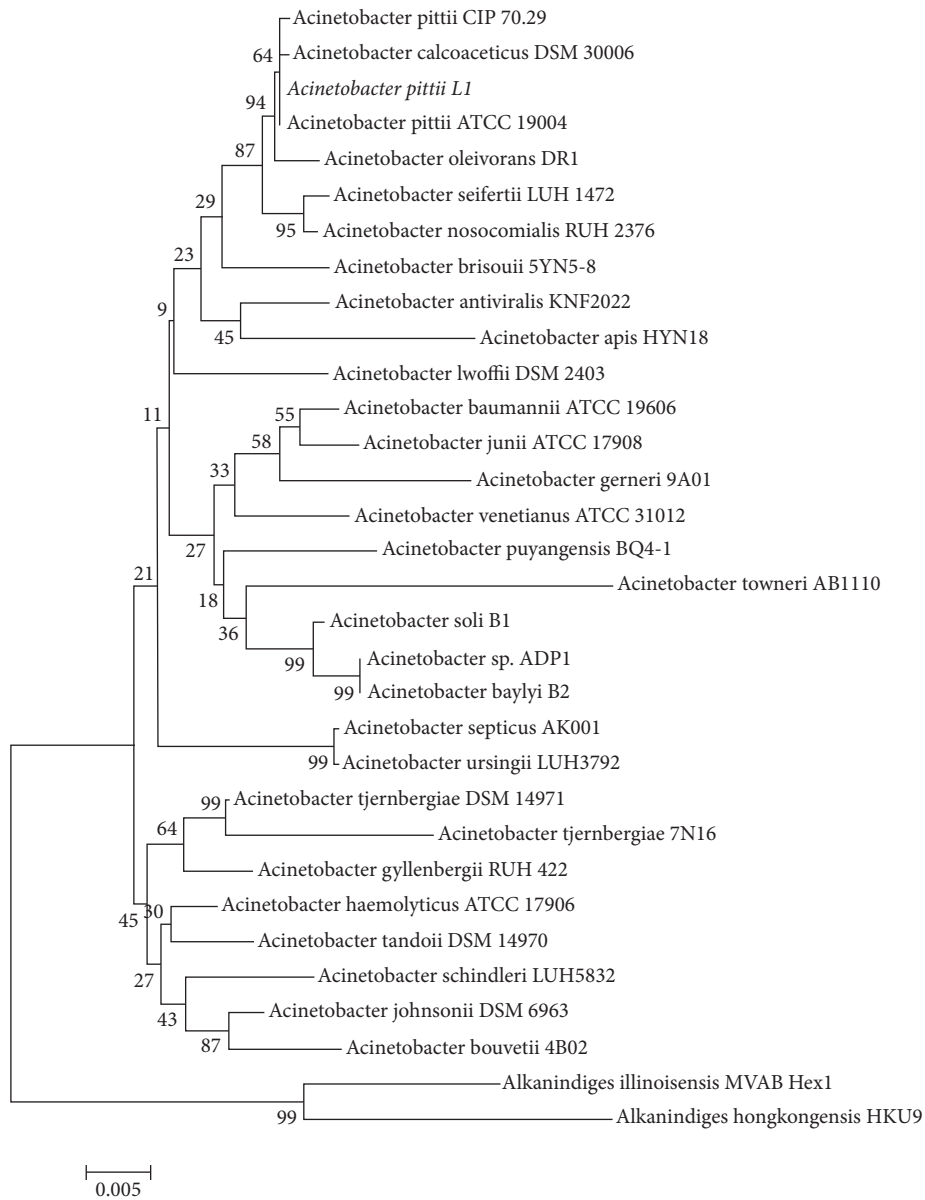

Figure 2: Phylogenetic tree of the strain L1 based on 16S rDNA analysis with the neighbor-joining method of the program MEGA 5.1. The numbers shown next to the nodes indicated the bootstrap values of 1000 for the confidence level.

at 28°C, *Ps aeruginosa* and *Bacillus* sp. at 30°C [12, 13, 24, 26], and the fungus *Sporotrichum thermophile* at 45°C [23].

3.2.3. pH Value. It was shown in Figure 3(c) that indole could be degraded by the strain L1 at pH 6.0, 7.0, and 8.0 at 36 h, and the indole removal rate was distinct at pH 7.0. Qu et al. [14] demonstrated indole could eliminate almost 90% by the strain SHE at pH 4.0–9.0. White rot fungus and *Ps aeruginosa* were reported to degrade indole at pH 5.0–9.0 [26, 27]. Besides, *Phomopsis liquidambari* showed the optimal efficiency to degrade indole at pH 4.5 [13].

3.3. Nitrogen Conversion. The changes of NH_3-N, NO_3^-, and NO_2^- were described in Figure 4(a) when 100 mg/L indole was absolutely removed within 24 h by the strain L1 in the MSM medium appended with 100 mg/L $(NH_4)_2SO_4$. At the same time, the initial NH_3-N decreased from 252.29 mg/L to 220.65 mg/L within 15 h, showing the microbial utilization of only about 31.64 mg/L. While the removal efficiency of indole was decreased, the concentration of NH_3-N was increased after 15 h. Theoretically, NO_3^- could be 90.13 mg/L (40.09 mg/L from ammonia nitrogen and 50.04 mg/L from indole), if all the nitrogen source was converted into NO_3^-. However, NO_3^- was measured about 77.70~86.31 mg/L after 15 h, and NO_2^- was not detected. According to Claus and Kutzner's reports, some nitrogen could be utilized to synthesize the intracellular substances [16]. Therefore, indole-N may be partially converted to NH_3-N and then to NO_3^- by *Acinetobacter pittii* L1.

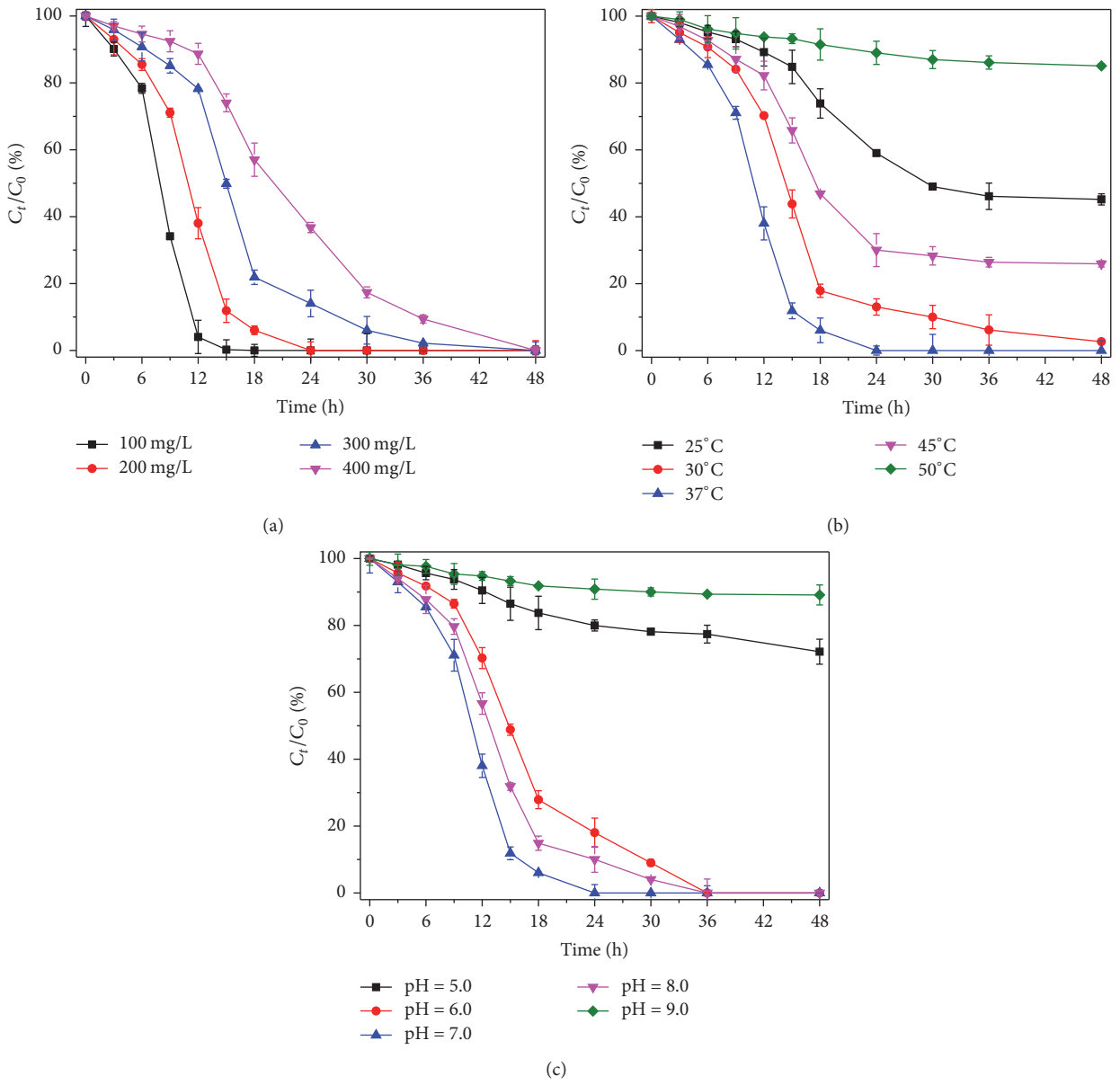

FIGURE 3: Different biodegrading efficiencies affected by the initial indole concentrations (a), temperatures (b), and pH values (c) in batch culture and the error bar value stand for the standard deviation of the triplicate.

3.4. Organic Carbon Changes. TC, TOC, and IC were investigated when 100 mg/L indole was biodegraded. As shown in Figure 4(b), the initial TOC 77.34 mg/L (similar to the theoretical value of 78.17 mg/L) was decreased to 15.37 mg/L at 24 h, but IC reached 8.94 mg/L at 12 h in the same way and decreased afterwards. It was demonstrated that some organic carbons were transferred to H_2CO_3 at first and then to CO_2 during the indole biodegradation. Figure 4(c) showed the removal efficiency of indole, pyridine, quinoline, and phenol by the strain L1. All the compounds could be degraded by *Acinetobacter pittii* L1 to some extent: indole and quinoline could be degraded completely within 48 h, 55.81% of phenol could be removed, and only 20% of pyridine was wiped over. Both indole and quinoline are structurally benzene-condensed heterocyclic compounds, but pyridine is a monocyclic compound. It was shown that the strain L1 was good at degrading condensed heterocyclic compounds, presumably because of the crucial metabolizing enzymes in the microbe.

3.5. Analysis of the Metabolic Pathways. The metabolites of blue, pink, and virescent hues were visible during the indole biodegradation by *Acinetobacter pittii* L1. LC-MS/MS was performed to detect the metabolites, the prominent molecular ion $[M\text{-}H]^-$ peak at m/z 260.7, 180.0, and 145.9 of the intermediates was, respectively, shown at the retention time of 2.2 min, 4.5 min, and 2.1 min, and their formulas and major mass fragmentation values were listed in Table 2.

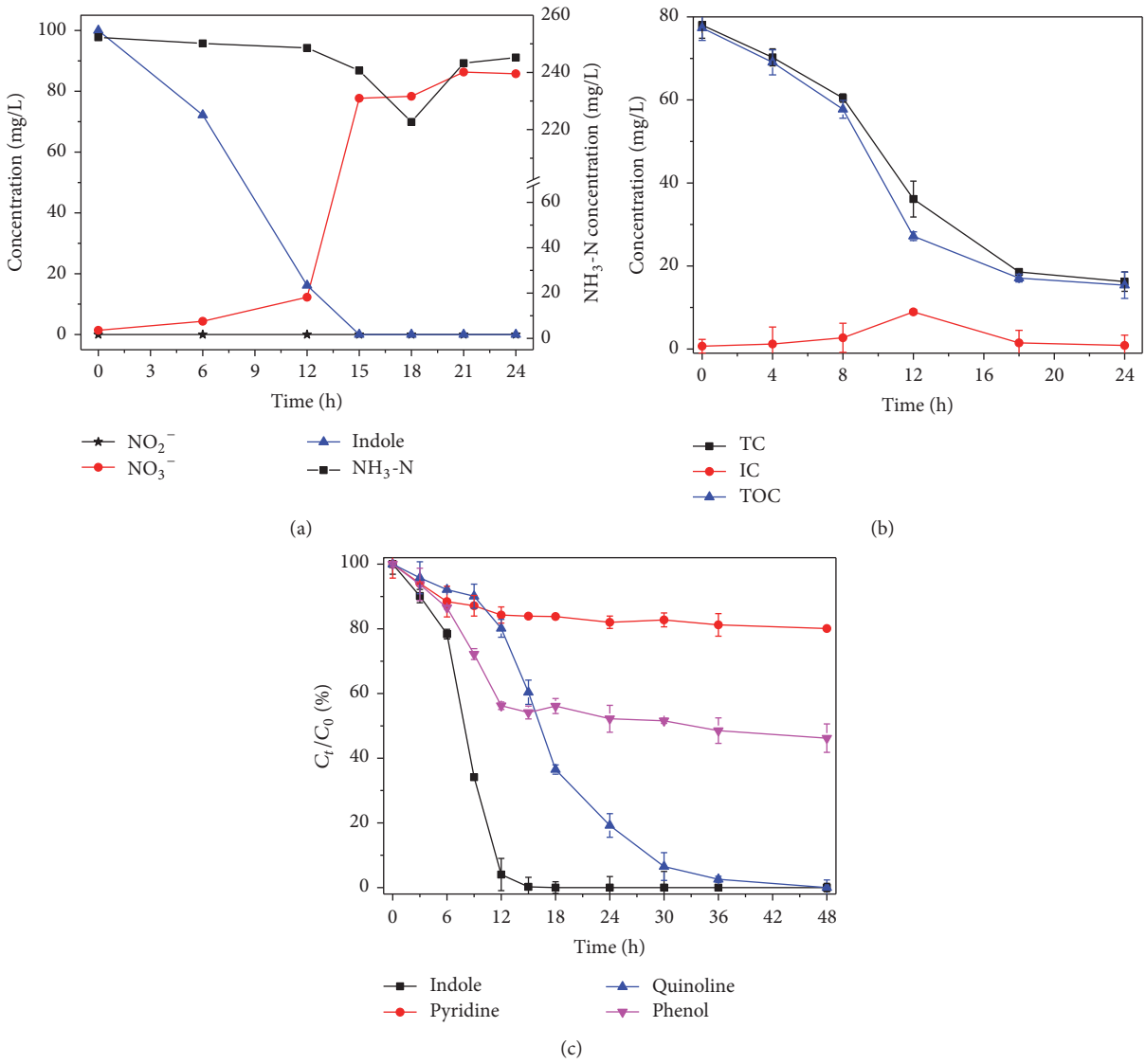

FIGURE 4: Organic carbon and nitrogen transformations during the indole degradation by *Acinetobacter pittii* L1, analyzed by the nitrogen source conversions (a), TC, IC, and TOC changes (b), and the different substrate degrading rates (c).

TABLE 2: LC-MS/MS data of the retention time, formula, and major mass fragmentation values to identify the indole biodegrading metabolites.

Parent ion $[M\text{-}H]^-$	t_r (min)	Formula	Major mass fragmentation value *(m/z)*	Compounds
260.7	2.2	$C_{16}H_{10}N_2O_2$	ES-: 247.1/242.8/221.6/214.7/200.7/176.8/146.7/118.7	Indigo
180.0	2.1	$C_8H_7NO_4$	ES-: 152.0/135.9/124.1/107.3	4-(3-Hydroxy-1H-pyrrol-2-yl)-2-oxo-but-3-enoic acid
145.9	4.5	$C_8H_5NO_2$	ES-: 128.3/118.2	Isatin

Figure 5(a) showed the deprotonated molecule at m/z 260.7 by the full scan analysis of the samples; the ions scan revealed the major mass spectra fragments at m/z 242.8 (−18), 221.6 (−39), 214.7 (−46), 200.7 (−60) 176.8 (−84), 146.7 (−114), and 118.7 (−142). The analysis revealed that the fragmentation ions at m/z 242.8, 176.8, 146.7, and 118.7 corresponded to the losses of 18, 44, 30, and 28 Da, showing the losses of H_2O, $CONH_2$, NO, and CO, respectively, from the parent deprotonated molecule. Considering the molar mass of 262 Da, the losses of CO, $CONH_2$, NO, and H_2O from the parent deprotonated molecule, the metabolite of indigo ($C_{16}H_{10}N_2O_2$) was confirmed.

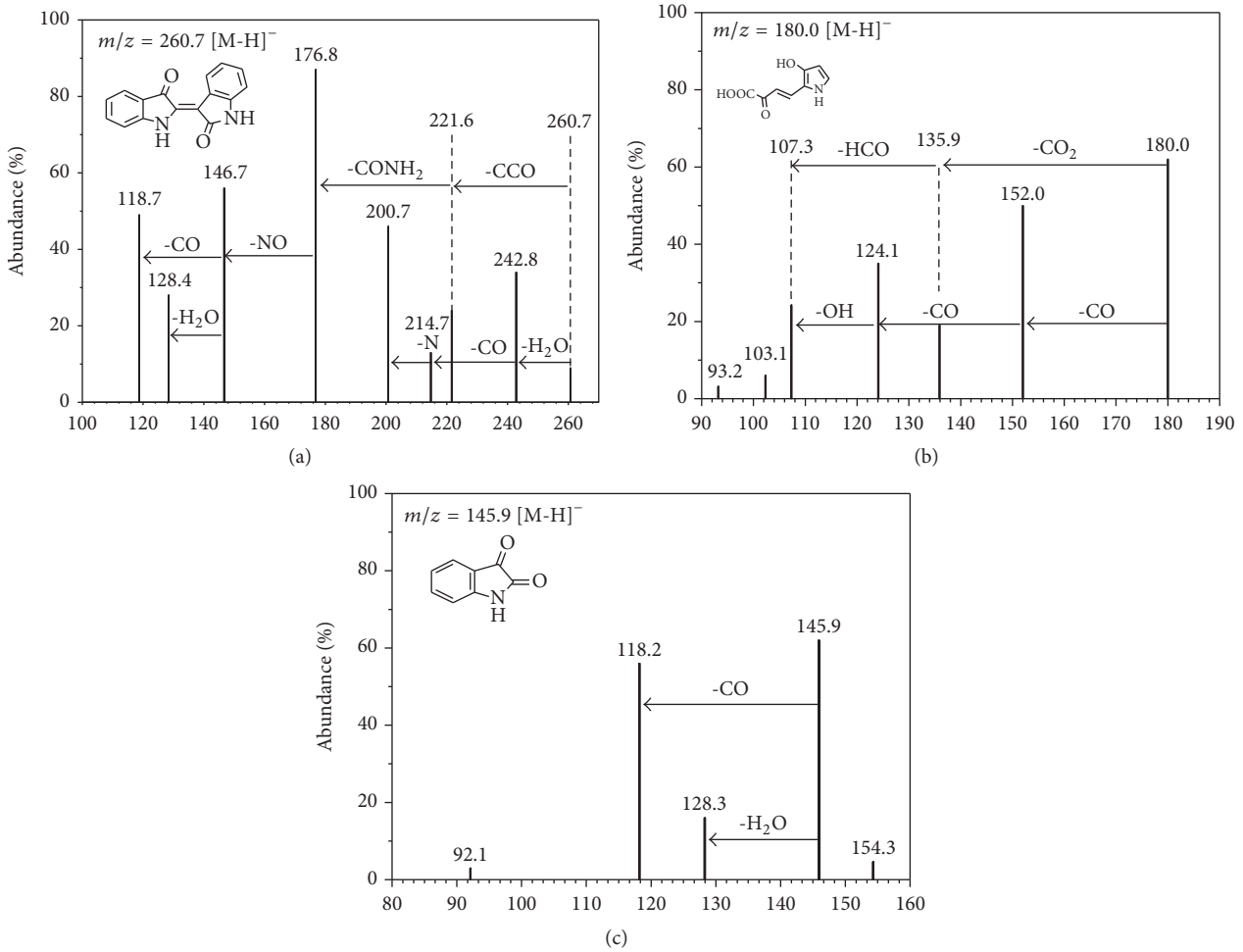

Figure 5: Fragment analysis of the secondary ion mass spectrometry of all the metabolite.

Figure 5(b) showed the deprotonated molecule at m/z 180.0 by the MS^2 fragmentation spectrum. Four major fragment ions of carboxide (CO), carboxylation (CO_2), aldehyde (CHO), and hydroxide (OH) could be speculated, according to the mass losses of 28 Da at m/z 152.0 and 124.1, 44 Da at m/z 135.9, and 29 Da and 17 Da at m/z 107.3. Fukuoka et al. reported that a pyrrole ring could be contained in such compound as the MS^2 fragmentation spectrum of ions at m/z 180.0 [28]. Therefore, the intermediate was proposed to be the 4-(3-hydroxy-1H-pyrrol-2-yl)-2-oxo-but-3-enoic acid according to the analytical data and the molecular formula of $C_8H_7NO_4$.

During the indole biodegradation, a pink compound briefly appeared less than 4 h, which was detected in the MS^2 fragmentation spectrum of ions at m/z 145.9 (Figure 5(c)). Additional ion fragments at m/z 118.2 (−28) and 128.3 (−18) indicated the isatin mass losses of 28 Da as CO and 18 Da as H_2O, respectively. Qu et al. indicated that indoleoxide, hydroxyindole, or 2,3-dihydroxyindole was the metabolites from the aerobic biodegradation of indole and then was oxidized to isatin immediately [14]. Because of the mass losses of (−28) and (−18) detected in the MS^2 fragmentation spectrum of ions at m/z 145.9, this metabolite might be derived from the carboxide and hydroxyl additions. Similarly, Zou and Koh observed the same mass losses with the determination of indigotin by LC/ESI-MS/MS at m/z 242.8, but the mass loss means the derivation of carboxide addition and phenolic hydroxyl [29].

Nevertheless, other familiar metabolites reported such as indoxyl, oxindole, anthranilate, salicylate and gentisic acid, and hydroxyindole in similar researches were not observed [14]. Therefore, the metabolic pathways of indole degradation by *Acinetobacter pittii* L1 were speculated (Figure 6), based on the analysis of the identified metabolites in this study.

3.6. Analysis of the Toxicity. To elucidate the ecological risk of the biodegradation products of indole, it is necessary to determine the toxicity evolution of indole contaminated, and the luminescent bacteria *Vibrio fischeri* were used to assess the changes of the acute toxicity of the compound. Figure 7 represents the inhibition rate, biodegradation rate, and TOC value of 100 mg/L indole solution fewer than 24 h of biodegradation. As depicted in Figure 7, the initial inhibition rate of indole was 36.97% based on the above equation.

As 14.51% indole was degraded, the *Vibrio fischeri* inhibition rate decreased dramatically to 16.34%. Subsequently,

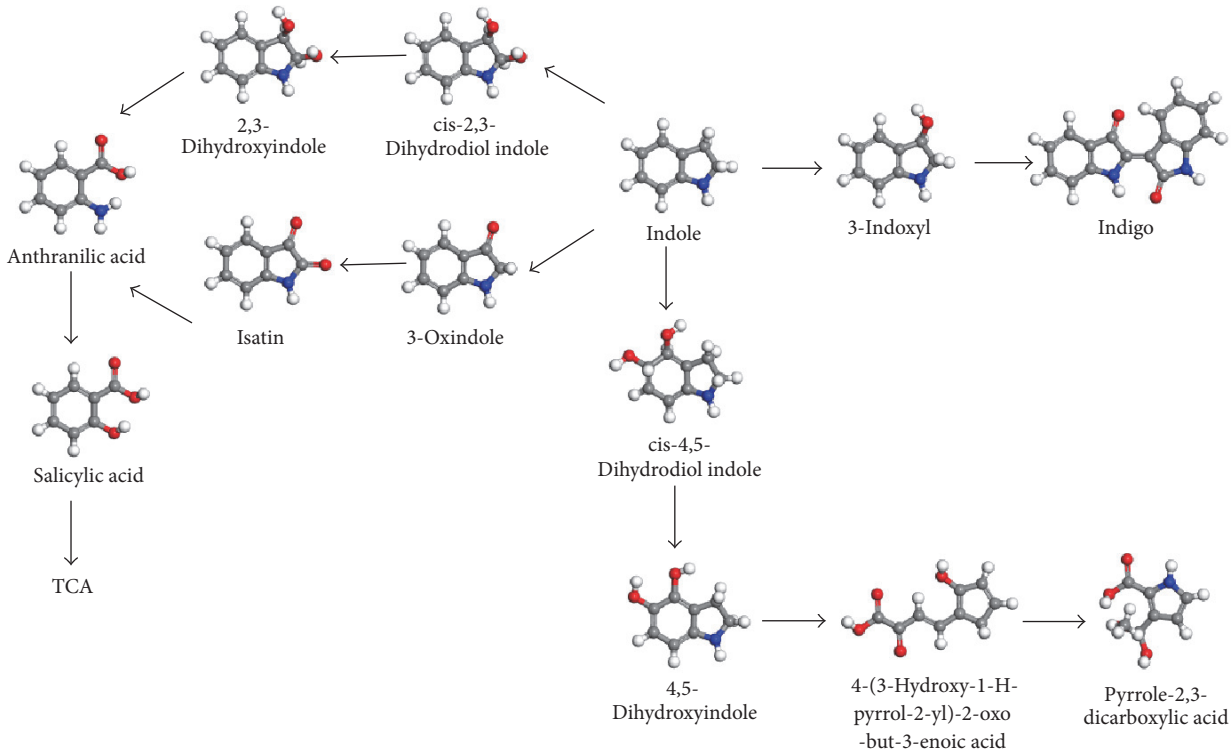

Figure 6: Speculated indole metabolic pathway degraded by *Acinetobacter pittii* L1. The gray, white, blue, and red balls are carbon, hydrogen, nitrogen, and oxygen atoms, respectively.

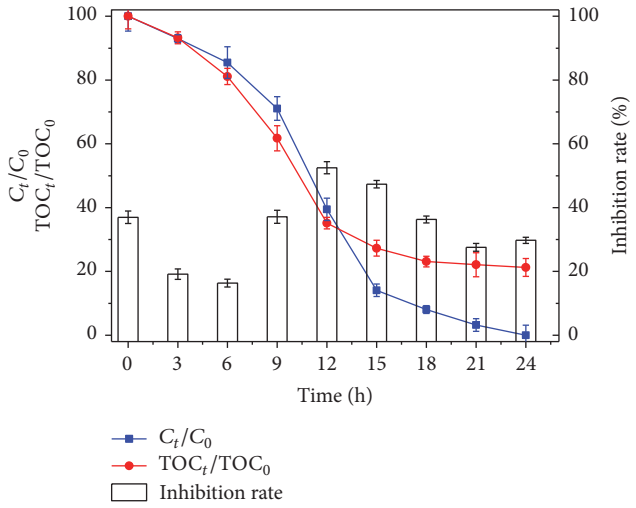

Figure 7: Variation of toxicity by Microtox test, inhibition rate, indole concentration, and TOC during degradation process.

the inhibition rate was quickly increased to 52.49% when a ~60.53% degradation rate of indole was obtained. It demonstrated the generation of more toxic products during the degradation of indole. Then the inhibition rate declined dramatically in the second 12 h. The inhibition rate reached an increasing tendency, which means that a new metabolite may be produced in the last. But the final inhibition (28.93%) was less than the initial inhibition (36.97%), which means that the metabolites products of indole were ultimately less toxic than the parent compound indole.

In general, the majority of indole was metabolized into intermediate products without the complete mineralization of CO_2 and H_2O. Therefore, the ecological risk of indole in engineered systems and ambient aquatic environments must be more closely scrutinized.

4. Conclusions

Indole and its derivatives are the representative compounds of NHCs, which are difficult degradable organic pollutants with lethal effect on ecological environment and characteristic odor. An efficient indole degrading *Acinetobacter pittii* L1 was isolated from a coking wastewater, 400 mg/L indole in 48 h, which could be thoroughly degraded in the optimum conditions. The removal efficiency of indole decreased after 15 h, but the concentration of NH_3-N and NO_3^- increased, showing the change of indole-N, and some organic carbon of indole was likely transferred into CO_2 eventually, and the metabolites products of indole were ultimately less toxic than the parent indole. It is shown that the isolated *Acinetobacter pittii* L1 could eliminate indole effectively and the metabolic pathways were speculated by the analysis of metabolites. Our results elucidated that the high efficiency of degradation ability to degrade indole makes *Acinetobacter pittii* L1 as an excellent candidate for producing indigo and eliminating NHCs and for printing and dyeing industrials with indole contaminated area.

Conflicts of Interest

The authors declare that there are no conflicts of interest regarding the publication of this paper.

Acknowledgments

This research was funded by the Science and Technology Project of Guangdong Province, China (nos. 2014A020216038 and 2016B020240003), Guangdong Natural Science Foundation (no. 2016A030313695), and the Youth Fund of Guangdong University of Technology (no. 14QNZD006).

References

[1] S. Mudliar, B. Giri, K. Padoley et al., "Bioreactors for treatment of VOCs and odours - A review," *Journal of Environmental Management*, vol. 91, no. 5, pp. 1039–1054, 2010.

[2] S.-Y. He, Y.-H. Lin, K.-Y. Hou, and S.-C. J. Hwang, "Degradation of dimethyl-sulfoxide-containing wastewater using airlift bioreactor by polyvinyl-alcohol-immobilized cell beads," *Bioresource Technology*, vol. 102, no. 10, pp. 5609–5616, 2011.

[3] P. Chen, W. Lv, and Z. Chen, "Phototransformation of mefenamic acid induced by nitrite ions in water: mechanism, toxicity, and degradation pathways," *Environmental Science & Pollution Research International*, vol. 22, pp. 1–12, 2015.

[4] X. Hong, X. Zhang, B. Liu, Y. Mao, Y. Liu, and L. Zhao, "Structural differentiation of bacterial communities in indole-degrading bioreactors under denitrifying and sulfate-reducing conditions," *Research in Microbiology*, vol. 161, no. 8, pp. 687–693, 2010.

[5] F. Bak and F. Widdel, "Anaerobic degradation of indolic compounds by sulfate-reducing enrichment cultures, and description of *Desulfobacterium indolicum* gen. nov., sp. nov.," *Archives of Microbiology*, vol. 146, no. 2, pp. 170–176, 1986.

[6] M. Frey, C. Stettner, P. W. Paré, E. A. Schmelz, J. H. Tumlinson, and A. Gierl, "An herbivore elicitor activates the gene for indole emission in maize," *Proceedings of the National Acadamy of Sciences of the United States of America*, vol. 97, no. 26, pp. 14801–14806, 2000.

[7] D. Blom, C. Fabbri, E. C. Connor et al., "Production of plant growth modulating volatiles is widespread among rhizosphere bacteria and strongly depends on culture conditions," *Environmental Microbiology*, vol. 13, no. 11, pp. 3047–3058, 2011.

[8] K. Gai, H. Qi, Y. Zhang, and D. Ma, "Degradation of indole in aqueous solution using contact glow discharge plasma," *Journal of Applied Electrochemistry*, vol. 40, no. 3, pp. 615–619, 2010.

[9] S. Lin and R. M. Carlson, "Susceptibility of environmentally important heterocycles to chemical disinfection: Reactions with aqueous chlorine, chlorine dioxide, and chloramine," *Environmental Science & Technology*, vol. 18, no. 10, pp. 743–748, 1984.

[10] S. Merabet, D. Robert, J.-V. Weber, M. Bouhelassa, and S. Benkhanouche, "Photocatalytic degradation of indole in UV/TiO2: Optimization and modelling using the response surface methodology (RSM)," *Environmental Chemistry Letters*, vol. 7, no. 1, pp. 45–49, 2009.

[11] S. Merabet, A. Bouzaza, and D. Wolbert, "Photocatalytic degradation of indole in a circulating upflow reactor by UV/TiO_2 process-Influence of some operating parameters," *Journal of Hazardous Materials*, vol. 166, no. 2-3, pp. 1244–1249, 2009.

[12] B.-H. Tuo, J.-B. Yan, B.-A. Fan, Z.-H. Yang, and J.-Z. Liu, "Biodegradation characteristics and bioaugmentation potential of a novel quinoline-degrading strain of Bacillus sp. isolated from petroleum-contaminated soil," *Bioresource Technology*, vol. 107, pp. 55–60, 2012.

[13] Y. Chen, X.-G. Xie, C.-G. Ren, and C.-C. Dai, "Degradation of N-heterocyclic indole by a novel endophytic fungus *Phomopsis liquidambari*," *Bioresource Technology*, vol. 129, pp. 568–574, 2013.

[14] Y. Qu, E. Shen, Q. Ma et al., "Biodegradation of indole by a newly isolated Cupriavidus sp. SHE," *Journal of Environmental Sciences*, vol. 34, pp. 126–132, 2015.

[15] Y. Qu, B. Xu, X. Zhang et al., "Biotransformation of indole by whole cells of recombinant biphenyl dioxygenase and biphenyl-2,3-dihydrodiol-2,3-dehydrogenase," *Biochemical Engineering Journal*, vol. 72, pp. 54–60, 2013.

[16] G. Claus and H. J. Kutzner, "Degradation of indole by *Alcaligenes* spec," *Systematic and Applied Microbiology*, vol. 4, no. 2, pp. 169–180, 1983.

[17] F. Wang, P. Chen, Y. Feng et al., "Facile synthesis of N-doped carbon dots/g-C3N4 photocatalyst with enhanced visible-light photocatalytic activity for the degradation of indomethacin," *Applied Catalysis B: Environmental*, vol. 207, pp. 103–113, 2017.

[18] Z. H. M. Yadzir, M. Y. Shukor, A. Ahmad, M. S. Nazir, S. M. U. Shah, and M. A. Abdullah, "Phenol removal by newly isolated Acinetobacter baumannii strain Serdang 1 in a packed-bed column reactor," *Desalination and Water Treatment*, vol. 57, no. 28, pp. 13307–13317, 2016.

[19] S. K. Karn and X. Pan, "Role of Acinetobacter sp. in arsenite As(III) oxidation and reducing its mobility in soil," *Chemistry and Ecology*, vol. 32, no. 5, pp. 460–471, 2016.

[20] S. Silambarasan and A. S. Vangnai, "Biodegradation of 4-nitroaniline by plant-growth promoting Acinetobacter sp. AVLB2 and toxicological analysis of its biodegradation metabolites," *Journal of Hazardous Materials*, vol. 302, pp. 426–436, 2016.

[21] M. Song, L. Jiang, D. Zhang et al., "Bacteria capable of degrading anthracene, phenanthrene, and fluoranthene as revealed by DNA based stable-isotope probing in a forest soil," *Journal of Hazardous Materials*, vol. 308, pp. 50–57, 2016.

[22] J. Wang, X. Zhang, J. Fan, Z. Zhang, Q. Ma, and X. Peng, "Indigoids biosynthesis from indole by two phenol-degrading strains, pseudomonas sp. PI1 and Acinetobacter sp. PI2," *Applied Biochemistry and Biotechnology*, vol. 176, no. 5, pp. 1263–1276, 2015.

[23] P. Katapodis, M. Moukouli, and P. Christakopoulos, "Biodegradation of indole at high concentration by persolvent fermentation with the thermophilic fungus *Sporotrichum thermophile*," *International Biodeterioration & Biodegradation*, vol. 60, no. 4, pp. 267–272, 2007.

[24] B. Yin, J.-D. Gu, and N. Wan, "Degradation of indole by enrichment culture and *Pseudomonas aeruginosa* Gs isolated from mangrove sediment," *International Biodeterioration & Biodegradation*, vol. 56, no. 4, pp. 243–248, 2005.

[25] G. M. M. Moghanloo, E. Fatehifar, S. Saedy, Z. Aghaeifa, and H. Abbasnezhad, "Biological oxidation of hydrogen sulfide in mineral media using a biofilm airlift suspension reactor," *Bioresource Technology*, vol. 101, no. 21, pp. 8330–8335, 2010.

[26] D. Ren, X. Zhang, and K. Yan, "Studies on the degradation of indole using white rot fungus," *Fresen Environ Bull*, vol. 15, pp. 1238–1243, 2006.

[27] N. R. Krieg, J. T. Staley, D. R. Brown et al., *Bergey's Manual of Systematic Bacteriology*, Springer, 2011.

[28] K. Fukuoka, K. Tanaka, Y. Ozeki, and R. A. Kanaly, "Biotransformation of indole by Cupriavidus sp. strain KK10 proceeds through N-heterocyclic- and carbocyclic-aromatic ring cleavage and production of indigoids," *International Biodeterioration & Biodegradation*, vol. 97, pp. 13–24, 2015.

[29] P. Zou and H. L. Koh, "Determination of indican, isatin, indirubin and indigotin in Isatis indigotica by liquid chromatography/electrospray ionization tandem mass spectrometry," *Rapid Communications in Mass Spectrometry*, vol. 21, no. 7, pp. 1239–1246, 2007.

Hindawi
BioMed Research International
Volume 2017, Article ID 1089696, 8 pages
https://doi.org/10.1155/2017/1089696

Research Article

Start-Up and Aeration Strategies for a Completely Autotrophic Nitrogen Removal Process in an SBR

Xiaoling Zhang,[1,2] Fan Zhang,[1] Yanhong Zhao,[1] and Zhengqun Li[1]

[1] *School of Environmental Science and Engineering, Chang'an University, Xi'an 710064, China*
[2] *Key Laboratory of Subsurface Hydrology and Ecological Effect in Arid Regions, Ministry of Education, Xi'an 710064, China*

Correspondence should be addressed to Xiaoling Zhang; zhangxiaoling101@126.com

Received 7 October 2017; Accepted 23 November 2017; Published 13 December 2017

Academic Editor: Bin Ma

The start-up and performance of the completely autotrophic nitrogen removal via nitrite (CANON) process were examined in a sequencing batch reactor (SBR) with intermittent aeration. Initially, partial nitrification was established, and then the DO concentration was lowered further, surplus water in the SBR with high nitrite was replaced with tap water, and continuous aeration mode was turned into intermittent aeration mode, while the removal of total nitrogen was still weak. However, the total nitrogen (TN) removal efficiency and nitrogen removal loading reached 83.07% and 0.422 kgN/(m^3·d), respectively, 14 days after inoculating 0.15 g of CANON biofilm biomass into the SBR. The aggregates formed in SBR were the mixture of activated sludge and granular sludge; the volume ratio of floc and granular sludge was 7 : 3. DNA analysis showed that Planctomycetes-like anammox bacteria and *Nitrosomonas*-like aerobic ammonium oxidization bacteria were dominant bacteria in the reactor. The influence of aeration strategies on CANON process was investigated using batch tests. The result showed that the strategy of alternating aeration (1 h) and nonaeration (1 h) was optimum, which can obtain almost the same TN removal efficiency as continuous aeration while reducing the energy consumption, inhibiting the activity of NOB, and enhancing the activity of AAOB.

1. Introduction

Biological nitrogen removal processes are generally used for the elimination of nitrogen from wastewater. However, wastewater with low carbon to nitrogen ratios (C/N), such as supernatants of anaerobic sludge digesters, landfill leachate, and special industrial wastewater, makes the conventional nitrification and heterotrophic denitrification processes more difficult [1, 2]. The discovery of the anaerobic ammonium oxidation (anammox) process has revolutionized the removal of nitrogen from wastewater that contains high amounts of nitrogen and has low C/N [3]. The anammox process involves the oxidation of ammonia into nitrogen gas, with nitrite serving as an electron acceptor in the absence of oxygen and organic carbon compounds [4]. Anammox is a promising process in which the costs related to aeration and external carbon addition are lowered by 60% and 100%, respectively, and which results in 90% less sludge compared to conventional nitrification-denitrification processes [5–7]. Several autotrophic nitrogen removal processes have been developed based on anammox, such as the two-stage SHARON-ANAMMOX process [8] and the one-stage CANON (completely autotrophic nitrogen removal via nitrite) [9, 10] and OLAND (oxygen-limited autotrophic nitrification-denitrification) [11] processes. One-stage processes combine two reactions that are catalyzed by two different microbial groups, aerobic ammonium oxidizing bacteria (AerAOB) and anaerobic ammonium oxidizing bacteria (AnAOB). Initially, AerAOB oxidizes NH_4^+ to NO_2^- under aerobic conditions (i.e., partial nitrification), which is followed by AnAOB converting NH_4^+ and NO_2^- into N_2 [12]. CANON is one of the autotrophic nitrogen removal processes that maintain AerAOB and AnAOB in a single reactor by controlling low DO levels [13].

The long start-up period of the CANON process is the bottleneck for its application due to the very slow growth rate (doubling time is 11 d) and the low yield coefficient (0.13 g dry weight/g NH_4-N oxidized) of AnAOB [4, 14, 15]. There are two strategies used to initiate the CANON process [16]. The

first strategy is to inoculate an anammox reactor with nitrifying biomass and subsequently maintain the oxygen-limited conditions [13, 17]. The second is to operate a nitrifying reactor under oxygen-limited conditions in order to wash out NOB and later inoculate the AnAOB biomass [18, 19]. For the application of the CANON process, the strategy of initially inoculating universally nitrifying activated sludge, and then inoculating small amounts of AAOB in order to partially nitrify the reactor, was the most practical [20].

The CANON process can be developed in both biofilm and suspended systems. For suspended-growth systems, there are two challenges: biomass retention and the equilibration of different microbial group activities [21]. Granular sludge not only guarantees high biomass retention efficiency but also protects inner AAOB from dissolved oxygen [22]. Recent studies state that small and large aggregates play different functional roles in the nitrite-anammox process [21, 22]. It was reported that large type aggregates (>500 μm) accounted for 68% of the AnAOB, whereas 65% of the nitrification potential was observed in the smaller aggregates (<500 μm) in a granular reactor [21]. The aggregates formed in granular sludge reactors contain a mixture of flocs, small granules, and large granules [23–26]. Granular sludge can be defined as compact and dense aggregates with an approximately spherical external appearance that did not coagulate under decreased hydrodynamic shear conditions and that settle significantly faster than floc [27]. In comparison, floc is characterized by loose, permeable aggregates that are composed of microcolonies enmeshed in extracellular polymers [28]. In granular aggregates, AerAOB lies in the outer layer and AnAOB in the inner layer, while in floc, AerAOB were the dominant bacteria [22]. To achieve high nitrogen removal efficiency, a good balance of AerAOB and AnAOB activity is needed, which is related to the aggregate characteristics in the reactor.

In the CANON process, the continuous aeration mode was applied more often than the intermittent aeration mode. Lackner stated that continuous aeration is preferred under normal operating conditions, while intermittent aeration is primarily used during start-up or periods of low sludge activities [1]. It was also reported that the intermittent aeration strategy can obtain similar total nitrogen removal efficiency as the continuous aeration strategy, thereby saving energy consumption due to shorter aeration times [29], but the proper ratio of aeration to nonaeration time should be well considered.

In this study, partial nitrification was established in a sequencing batch reactor by carefully controlling the aeration, initially using activated sludge as seed sludge and then inoculating CANON biofilm in the SBR. This method achieved both partial nitrification and anammox in one single-stage reactor by reducing the aeration amount and altering the continuous and intermittent aeration amounts. This process was examined, the sludge characteristics were studied with SEM, and the polymerase chain reaction (PCR) technique was used to analyze the microbial community in the reactor. Additionally, the influence of aeration strategy on the CANON process was studied in batch tests.

2. Materials and Methods

2.1. Reactor Description. This study used a SBR with a working volume of 13 L. Dimensions of the SBR were the following: height of 545 mm, inner diameter of 174 mm, and height to diameter ratio of 3.13 : 1. Two or three cycles were performed each day during the whole experiment. One cycle consisted of a 20 min filling period, an aerating period (continuous or intermittent) of 11 h in 12 h cycle or 7 h in 8 h cycle, a 30 min settling period, a 5 min drawing period, and a 5 min idling period. The exchange volume was fixed at 50%, and a mass-flow controller was used to keep aeration constant. Two different aeration strategies were applied in this study, namely, continuous aeration and intermittent aeration, both characterized by the ratio (R) between the aerated and nonaerated duration times. The reactor was stirred at a rate of 700 rpm and maintained at a temperature of 30 ± 2°C.

2.2. Biomass and Synthetic Wastewater. In this study, the conventional nitrification sludge originated from the oxidation ditch of a municipal wastewater plant, was inoculated and developed to partial nitrification in the SBR, and was later inoculated with a small CANON biofilm biomass (0.15 g) to partial nitrification in the SBR.

The synthetic wastewater used in this study mainly contained NH_4^+ from NH_4HCO_3 (N source, C source, and buffer), $NaHCO_3$ (supplementary C source and buffer), and phosphate from KH_2PO_4. The influent concentrations were sampled from the filing tank. The influent ammonium concentration was in the range of 100~300 mg/L and the pH was between 7.4 and 8.2.

2.3. Chemical Analysis. The concentrations of NH_4^+-N, NO_2^--N, NO_3^--N, MLSS, and MLVSS were measured according to standard methods (APHA, 1995). Total nitrogen (TN) was defined as the sum of NH_4^+-N, NO_2^--N, and NO_3^--N. Dissolved oxygen (DO) concentrations and pH values in the reactor were determined using a portable analyzer (HQ30d, Hach, USA) and a pH meter (PHS-10, Fangzhou, China). Nitrite accumulation ratio (NAR) and free ammonia (FA) were calculated as follows [30]:

$$\mathrm{NAR}\% = \frac{[\mathrm{NO_2^-}\text{-}\mathrm{N}]_{\mathrm{Eff}}}{[\mathrm{NO_2^-}\text{-}\mathrm{N}]_{\mathrm{Eff}} + [\mathrm{NO_3^-}\text{-}\mathrm{N}]_{\mathrm{Eff}}} \times 100\% \quad (1)$$

$$\mathrm{FA}\left(\frac{\mathrm{mg}}{\mathrm{L}}\right) = \frac{17}{14} \times \frac{\left([\mathrm{NH_4^+}\text{-}\mathrm{N}] + [\mathrm{NH_3}\text{-}\mathrm{N}]\right)(\mathrm{mg/L}) \times 10^{\mathrm{pH}}}{e^{(6334/(273+T))+10^{\mathrm{pH}}}}. \quad (2)$$

2.4. Batch Tests. Tests to determine the effect of different aeration strategies (including continuous and intermittent aeration) on process efficiency were performed in batch reactors inoculated with the mixed liquor collected from the SBR prior to the end of the reaction period during the quasi-steady state. Tested sludge was washed to remove nitrogen compounds and was divided into four parts. Each part of the sludge was put into a 1.5 L batch reactor. Four batch reactors were supplied with synthetic wastewater. The initial

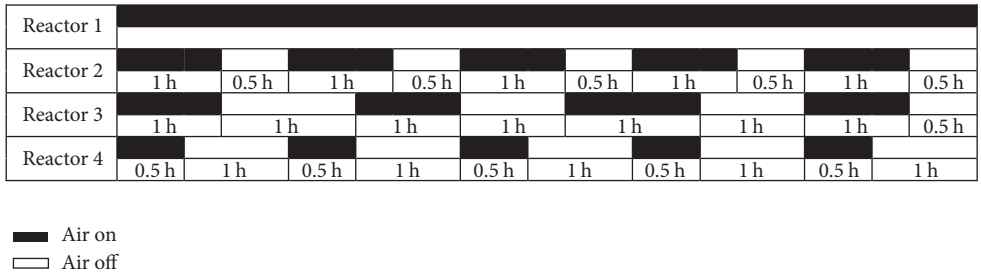

Figure 1: Aerated and nonaerated durations in batch reactors.

NH_4^+-N concentration in four batch reactors was controlled at 280 mg N/L by adding equal amounts of ammonium bicarbonate. The first batch reactor received continuous aeration, and the remaining three all received intermittent aeration with different ratios of aerated to nonaerated duration: 0.5 h (aerated duration) to 1.5 h (nonaerated duration) for the second batch reactor, 1.0 h (aerated duration) to 1.0 h (nonaerated duration) for the third batch reactor, and 1.0 h (aerated duration) to 0.5 h (nonaerated duration) for the fourth batch reactor. The test duration was 450 min for each batch reactor. The aeration and nonaeration durations are depicted in Figure 1. pH was not controlled during the tests, and temperature was controlled at 30 ± 1°C.

2.5. DNA Analysis. A sludge sample was taken from the reactor on day 100 used for analysis of the microbial community. Direct DNA extraction was implemented using a fast DNA spin kit (SK8233) for soil (Sangon, Shanghai) according to the manufacturer's instructions. Partial 16S rRNA genes were amplified by PCR with a eubacteria primer set, F357 (5′-CCTACGGGAGGCAGCAG-3′) and R518 (5′-ATTACCGCGGCTGCTGG-3′). A GC clamp (CGCCCGCCGCGCCCCGCGCCCGGCCCGCCGCCCCCGCCCC) was added to 5′ of the forward primer to improve the detection of sequence variations in amplified DNA fragments by DGGE. The PCR reaction mixture was 50 mL and contained 5 mL of 10 × PCR buffer (Mg^{2+} plus), 1 mL of dNTP (10 mm L^{-1}), 1 mL of each primer (10 mm L^{-1}), 0.25 mL of Taq enzyme (5 U mL^{-1}), and 0.5 mL of template DNA. The PCR reaction was carried out according to the following conditions: 4 min initial denaturation at 94°C, 30 cycles of 30 sec at 94°C, 60 sec at 56°C, 30 sec at 72°C, and 7 min final elongation at 72°C. The products were later resolved by denaturing gradient gel electrophoresis (DGGE) for 16 h at a constant voltage of 60 V at 60°C using the DCode system (Bio-Rad, Hercules, USA). An 8% polyacrylamide gel with a 30%–60% denaturing gradient was used to separate the PCR products (7 mol L^{-1} urea and 40% formamide comprised of 100% denaturant). Prominent DGGE bands were excited from the gel and dissolved in a 50 mL ITE buffer solution at 4°C, which was then reamplified as a template using the same methods previously described. The DNA fragments were later excited and reamplified using the primer sets F357 (without GC clamp) and R518, and the products were purified using the purification kit (Tiangen, China) and cloned using the pMD19-T plasmid vector system (TaKaRa, Japan). Sequencing was performed using an ABI 3730 DNA sequencer by a commercial service (Sangon, China). All sequences achieved were compared with similar sequences of the reference organisms using a BLAST search.

3. Results and Discussion

3.1. Performance of SBR. The reactor was operated in two phases over a time interval of 124 days. Each phase was characterized by the aeration mode and hydraulic retention time (HRT). Parameter settings of the different phases are summarized in Table 1. The concentrations of nitrogen compounds in the influent and effluent are depicted in Figure 2(a). The removal efficiency of ammonia nitrogen and total nitrogen (TN) and the nitrite accumulation ratio in effluent (i.e., the ratio of nitrite to the sum of nitrite nitrogen and nitrate nitrogen in effluent) are depicted in Figure 2(b). The ratios of nitrate production to ammonium consumption during start-up are shown in Figure 2(c). The solids retention time (SRT) was on average 120 days throughout the experiment. The biomass concentration was on average 2.14 g/L, and the ratio of VSS to TSS was 0.80 on average.

During phase A, three cycles were performed each day, and the continuous aeration mode was applied. In the first 10 days, the DO level in the bulk liquid was maintained between 1 and 2 mg/L, and the ammonia concentration in the influent was 150 mg/L. Figure 2(a) illustrates that the NH_4^+-N removal efficiency increased from 74.0% to 94.9% and that the nitrite concentration in the effluent was in the range of 0.24 to 1.16 mg/L. This finding indicates that ammonia oxidizers and nitrite oxidizers were cultivated in the SBR and converted the ammonia to nitrate via nitrite. To achieve partial nitrification in the system during days 11–50, DO concentrations were diminished, high free ammonia (FA) concentrations were maintained in the SBR, the mean DO concentration was fixed at 0.17 mg/L, and the mean FA concentration was increased to 7.36 mg/L. Under these conditions, nitrite concentration began to increase in the effluent due to DO limitation of the NOB and the inhibition of free ammonia, which when presented to NOB has characteristic lower oxygen affinities and higher sensitivities to free ammonia inhibition [31]. During this period, the removal efficiency of NH_4^+-N fluctuated in the range of 35.0% to 85.2%, while the nitrite accumulation ratio in effluent increased from 4.0% to 87.3%, as shown in Figure 2(b). This demonstrates that partial nitrification was achieved in the SBR at the end of phase A.

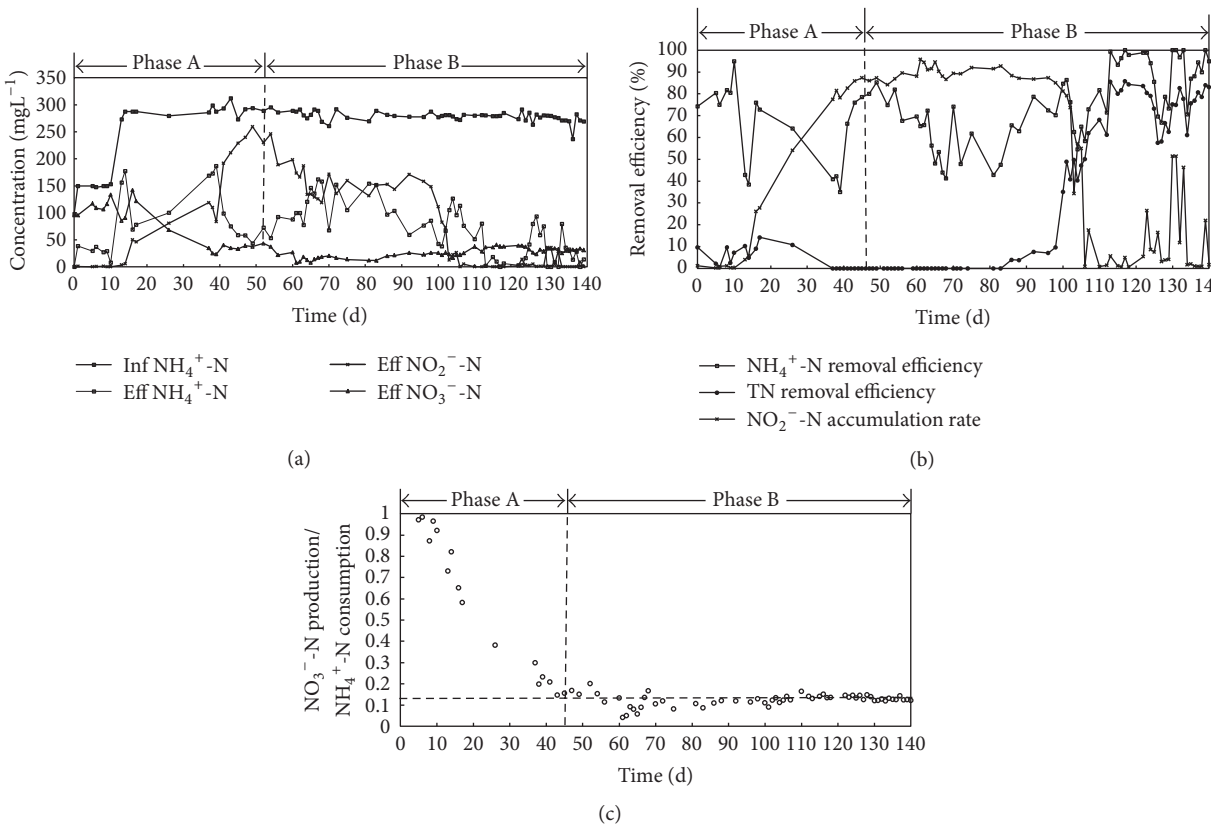

Figure 2: Performance of the CANON reactor: (a) influent and effluent concentrations of nitrogen species; (b) ammonium, TN removal efficiency, and nitrite accumulation rate (NAR); (c) ratio of nitrate production to ammonium consumption.

Table 1: Operating parameters of each phase in SBR.

Parameters	Phase A	Phase B
Time range (d)	0~50	51~140
Hydraulic retention time (h)	16	24 (51~123 days), 16 (124~140 days)
Aeration mode	Continuous	Intermittent (2 h aeration : 2 h no aeration : 2 h aeration : 1.5 h no aeration)
DO concentration during aeration phase	1~2 mg/L (1~11 days), 0.16~0.18 mg/L (12~51 days)	0.04~0.15 mg/L (aeration time), 0 mg/L (no aeration time)
Intermittent aeration (R)	—	1/1 (except the last nonaeration duration)

During phase B, two cycles were performed each day and intermittent aeration was applied from day 51 to day 123, after which three cycles were applied again to increase the nitrogen load of the SBR. The DO concentration in the aerated portion of the SBR cycle was maintained in the range of 0.04~ 0.15 mg/L. The removal of TN was minimal and was increased slowly between days 51 and 98. On the 99th day, 0.15 g of CANON biofilm biomass was taken into the SBR, after which the TN removal efficiency increased obviously, exceeding 80% on day 113 (14 days after CANON biofilm inoculation). The ratio of nitrate production to ammonium consumption was approximately 0.13, which one would expect for the CANON process [9] in the end of period B. This finding demonstrates the successful start-up of the CANON process in the SBR and indicates that the inoculation of AAOB biomass can significantly shorten the start-up time of the

CANON process. Low DO concentrations and intermittent DO modes also played important roles in the realization of autotrophic nitrogen removal via nitrite.

3.2. Aeration Strategies. Changes of nitrogen compounds under different aeration strategies are depicted in Figures 3(a), 3(b), 3(c), and 3(d). It is demonstrated in Figure 3(a) that ammonia concentrations decreased almost linearly under continuous aeration. Nitrite concentration increased in the first 60 min, later decreased, and subsequently remained steady between 1.5 and 2.0 mg/L. Nitrate concentration increased from 28.33 mg/L to 57.48 mg/L. The removal efficiency of ammonia was 73.72%, the total nitrogen removal efficiency was 65.56%, and the ratio of nitrate production to ammonium consumption was 0.154, which was much higher than what one would expect for the CANON system [9]. The second aeration strategy included 5 aeration times and 5 nonaeration times (Figure 1), where each aeration time lasted 60 min and each nonaeration time lasted 30 min. The nitrogen compounds of the second aeration strategy are shown in Figure 3(b). It can be seen that ammonia decreased in each aeration time, while the variation of ammonia in each nonaeration time differed. Ammonia concentration decreased in the first two nonaeration times but remained unchanged in the following three nonaeration times. Additionally, it was observed that nitrite concentrations were very low in the subsequent three nonaeration times, which limited the activity of AAOB and resulted in unchanged ammonia concentrations. The total nitrogen removal efficiency of the second aeration strategy was 67.02%, and the ratio of nitrate production to ammonia consumption was 0.137, which was still higher than what one would expect for the CANON system. There were 4 aeration times and 4 nonaeration times in the third aeration strategy. All aeration times were 1 h, and nonaeration times were 1 h, 1 h, 1 h, and 0.5 h. Variation of nitrogen compounds used in the third aeration strategy was similar to those used in the second aeration strategy. The ammonia and total nitrogen removal efficiencies of the third aeration strategy were 62.93% and 69.21%, respectively. The ratio of nitrate production to ammonium consumption was 0.128, which was closest to what one would expect for the CANON system in the four batch tests. The fourth aeration strategy also included 5 aeration times and 5 nonaeration times, and the ratio of aeration time to nonaeration time was 0.5 h : 1 h. The ammonia and total nitrogen removal efficiencies of the fourth strategy were only 49.83% and 54.22%, respectively, due to the aeration times being too short to convert enough ammonia to nitrite. The activity of AAOB was also limited by the lack of nitrite.

The total aeration times in the four aeration strategies were 450 min (continuous aeration), 300 min (aeration time : nonaeration time = 1 h : 0.5 h), 240 min (aeration time : nonaeration time = 1 h : 1 h), and 150 min (aeration time : nonaeration time = 0.5 h : 1 h). The total nitrogen removal efficiencies of the first, second, third, and fourth strategies were 65.56%, 62.93%, 65.33%, and 54.22%, respectively. The ratios of nitrate production to ammonia consumption for the first, second, third, and fourth strategies were 0.154, 0.142, 0.128, and 0.103, respectively. This finding suggests that the ammonia conversion rate and the nitrate production rate decreased with decreasing aeration times, which were also related to the activities of AOB, NOB, and AAOB. The CANON process relied on the incorporation of AOB and AAOB, while NOB was not expected in the reactor. The ratio of nitrate production to ammonia consumption was 0.13 when the NOB had washed out completely [9]. A ratio higher than 0.13 indicated that NOB was not washed out completely from the SBR. The activity of AAOB was inhibited by oxygen when oxygen penetrated into the inner of floc in the aeration duration, while the nonaeration duration can not only inhibit the activity of NOB but also help the AAOB to restore its activity, which was inhibited by oxygen in the aeration duration. The strategy of 0.5 h aeration and 1 h nonaeration is not recommended because the short aeration time limited the production of nitrite, resulting in ammonia and total nitrogen removal efficiencies being very low. The very low ratio of nitrate production to ammonia consumption further verified that the short aeration time limited the conversion of ammonia. The strategy of 1 h aeration and 1 h nonaeration was the optimal one, which resulted in similar total nitrogen removal and continuous aeration efficiency and shortened the duration of aeration. The ratio of nitrate production to ammonia consumption under this strategy was also close to the one expected for the CANON system [9].

3.3. Biomass Morphology. At the start of this experiment, 1 liter of activated sludge from a municipal WWTP was taken into the SBR, and a small CANON biofilm was inoculated in the SBR after the partial nitrification was set up. Over time, the granular sludge started to grow in the SBR. At the end of the experiment, the sludge in the SBR was a mixture of floc and granules, with the granules occupying 31% (w/w) and the flocs occupying 69% (w/w). Three scanning electron microscopy (SEM) images of the granules are shown in Figure 4: (a) the outside of a granule, (b) one slice of a granule (a rectangle), and (c) another slice of a granule (an ellipse). Arrows in Figure 4(b) indicated holes inside the granule. Granules had distinct boundary and had spherical or ellipsoidal appearance, while flocs were more loose and amorphous. The average diameter of the granules was 900 μm, while the size of floc was smaller than 300 μm.

3.4. DNA Analysis. PCR-DGGE was used to examine the microbial community in the SBR, and parts of the results are shown in Table 2. Results show that six groups had high identity to *Candidatus Brocadia* belonging to the order Planctomycetales. *Candidatus Brocadia* was identified as the dominant species of AnAOB in the CANON process. This finding indicates that only one genus of anammox bacteria is dominant under the applied growth conditions [32]. Three groups of AerAOB belonging to β-proteobacteria were found in this reactor, all of which were closely related to *Nitrosomonas*, which have been found as dominant populations in other CANON systems [33, 34]. NOB belonging to *Nitrospira* was also present in the reactor, which further supports the results of batch tests. The NOB was present in floc when the DO was sufficient, producing nitrate and resulting in unstable performance of the CANON system.

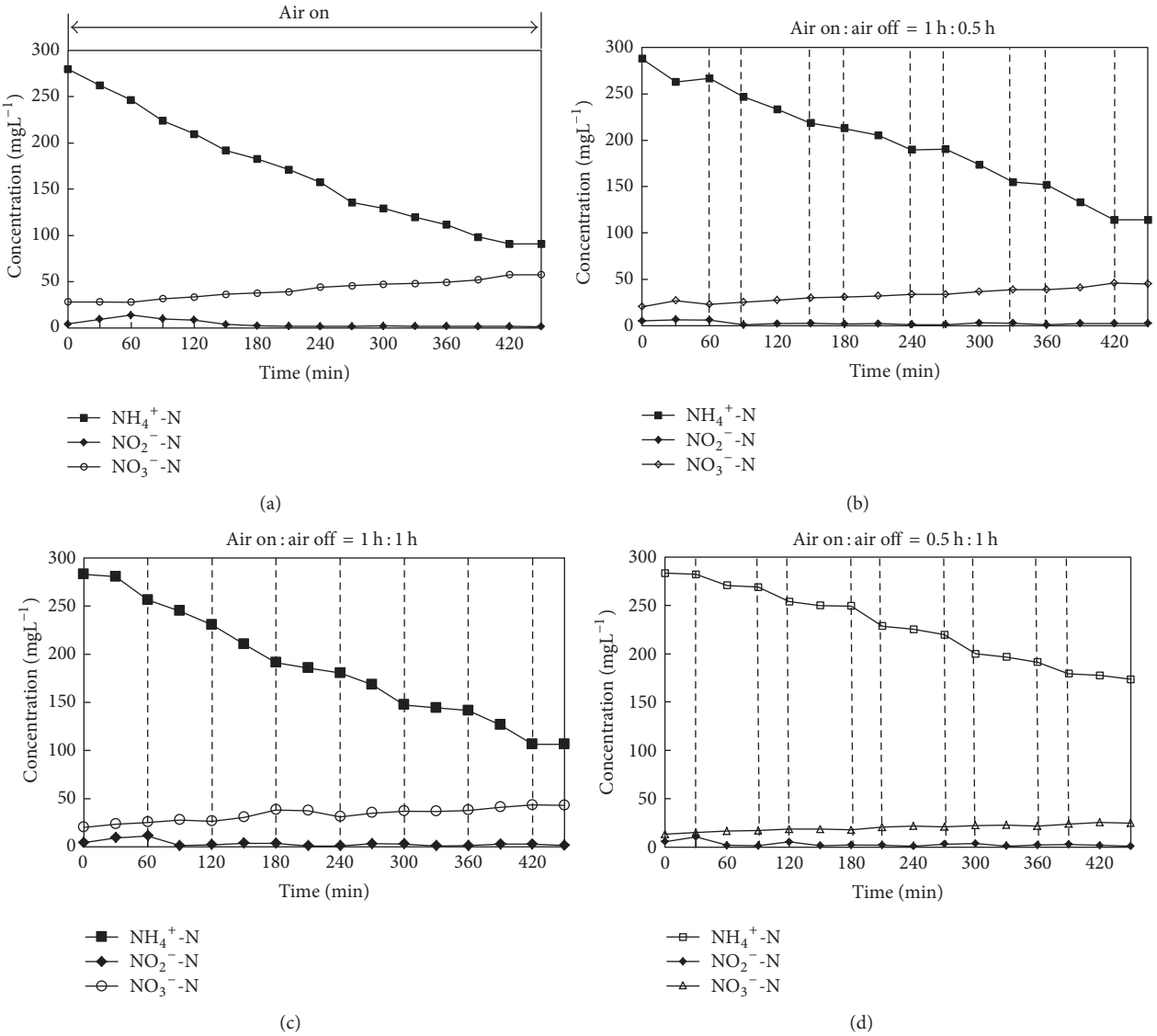

Figure 3: Profiles of nitrogen compounds in bulk solutions for a typical reaction time (450 min) of the SBR with four aeration strategies: (a) continuous aeration; (b) aeration time : nonaeration time = 1 h : 0.5 h; (c) aeration time : nonaeration time = 1 h : 1 h; (d) aeration time : nonaeration time = 0.5 h : 1 h.

Table 2: Phylogenetic sequence similarities to the closest relative from DGGE bands.

Band	Taxon	Identity	Accession	Phylum (classifier)
4	*Candidatus Brocadia* sp. RAS-Ina-1 16S rRNA gene	97%	HM769652	Planctomycetia
5	*Candidatus Brocadia* sp. S08-01 16S rRNA gene	99%	JN205347	Planctomycetia
7	*Candidatus Brocadia fulgida* isolate R1 16S rRNA gene	97%	JQ864321	Planctomycetia
15	*Candidatus Brocadia* sp.ODS-1 16S rRNA gene	98%	HM769653	Planctomycetia
19	Uncultured *Candidatus Brocadia* sp.16S rRNA gene	98%	KF606756	Planctomycetia
23	*Candidatus Brocadia caroliniensis* 16S rRNA gene	98%	KF810110	Planctomycetia
1	Uncultured *Nitrosomonas* sp. gene for 16S rRNA gene	100%	AB500059	β-proteobacteria
26	*Nitrosomonas* sp. HP8 partial 16S rRNA gene	99%	HF678378	β-proteobacteria
28	Uncultured *Nitrosomonas* sp.DGGE 16SRNA gene	100%	KF452288	β-proteobacteria
2	*Nitrospira*	98%	KF472236	β-proteobacteria

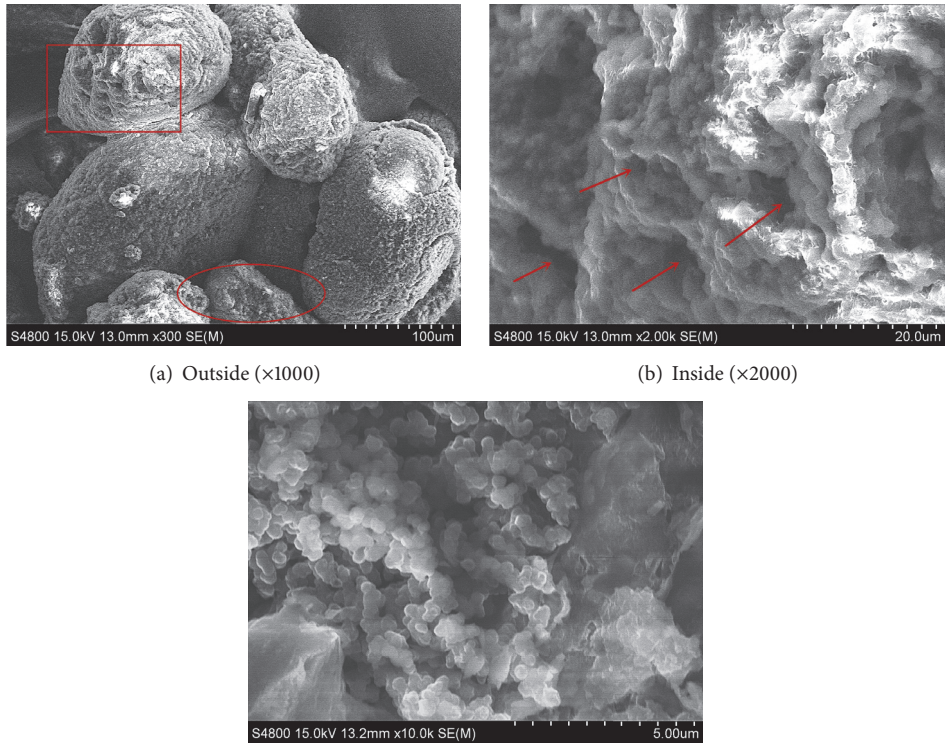

(a) Outside (×1000)

(b) Inside (×2000)

(c) Inside (×5000)

Figure 4: Scanning electron microscopy (SEM) images of granules.

4. Conclusions

Inoculating AAOB biomass in a partial nitrification system can start the CANON process rapidly, resulting in total nitrogen removal efficiencies of up to 80% after inoculation. The presence of complete granular sludge was not necessary. The mixture of granular sludge and floc present in the SBR and the NOB present in the floc and sludge influenced the total nitrogen removal efficiency. Granules had distinct boundary and were spherical or ellipsoidal, while floc was more loose and amorphous. The average diameter of the granules was 900 μm, while the size of floc was smaller than 300 μm. The intermittent aeration strategy was important not only for ammonia and total nitrogen efficiencies but also for the inhibition of NOB and the protection of AAOB from oxygen. The optimal ratio of aeration time to nonaeration time for the intermittent aeration strategy was 1 h : 1 h.

Conflicts of Interest

The authors declare that they have no conflicts of interest.

References

[1] S. Lackner, E. M. Gilbert, S. E. Vlaeminck, A. Joss, H. Horn, and M. C. M. van Loosdrecht, "Full-scale partial nitritation/anammox experiences—an application survey," *Water Research*, vol. 55, pp. 292–303, 2014.

[2] J. Vázquez-Padín, A. Mosquera-Corral, J. L. Campos, R. Méndez, and N. P. Revsbech, "Microbial community distribution and activity dynamics of granular biomass in a CANON reactor," *Water Research*, vol. 44, no. 15, pp. 4359–4370, 2010.

[3] A. Mulder, A. A. van de Graaf, L. A. Robertson, and J. G. Kuenen, "Anaerobic ammonium oxidation discovered in a denitrifying fluidized bed reactor," *FEMS Microbiology Ecology*, vol. 16, no. 3, pp. 177–183, 1995.

[4] M. Strous, J. J. Heijnen, J. G. Kuenen, and M. S. M. Jetten, "The sequencing batch reactor as a powerful tool for the study of slowly growing anaerobic ammonium-oxidizing microorganisms," *Applied Microbiology and Biotechnology*, vol. 50, no. 5, pp. 589–596, 1998.

[5] D. Güven, K. Van De Pas-Schoonen, M. C. Schmid et al., "Implementation of the anammox process for improved nitrogen removal," *Journal of Environmental Science and Health, Part A: Toxic/Hazardous Substances and Environmental Engineering*, vol. 39, no. 7, pp. 1729–1738, 2004.

[6] N. Chamchoi and S. Nitisoravut, "Anammox enrichment from different conventional sludges," *Chemosphere*, vol. 66, no. 11, pp. 2225–2232, 2007.

[7] B. Molinuevo, M. C. García, D. Karakashev, and I. Angelidaki, "Anammox for ammonia removal from pig manure effluents: Effect of organic matter content on process performance," *Bioresource Technology*, vol. 100, no. 7, pp. 2171–2175, 2009.

[8] B. Valverde-Pérez, M. Mauricio-Iglesias, and G. Sin, "Systematic design of an optimal control system for the SHARON-Anammox process," *Journal of Process Control*, vol. 39, pp. 1–10, 2016.

[9] K. A. Third, A. O. Sliekers, J. G. Kuenen, and M. S. M. Jetten, "The CANON system (completely autotrophic nitrogen-removal over nitrite) under ammonium limitation: interaction and competition between three groups of bacteria," *Systematic and Applied Microbiology*, vol. 24, no. 4, pp. 588–596, 2001.

[10] A. O. Sliekers, K. A. Third, W. Abma, J. G. Kuenen, and M. S. M. Jetten, "CANON and Anammox in a gas-lift reactor," *FEMS Microbiology Letters*, vol. 218, no. 2, pp. 339–344, 2003.

[11] K. Windey, I. De Bo, and W. Verstraete, "Oxygen-limited autotrophic nitrification-denitrification (OLAND) in a rotating biological contactor treating high-salinity wastewater," *Water Research*, vol. 39, no. 18, pp. 4512–4520, 2005.

[12] X. Hao, J. J. Heijnen, and M. C. M. Van Loosdrecht, "Model-based evaluation of temperature and inflow variations on a partial nitrification-ANAMMOX biofilm process," *Water Research*, vol. 36, no. 19, pp. 4839–4849, 2002.

[13] A. O. Sliekers, N. Derwort, J. L. Campos Gomez, M. Strous, J. G. Kuenen, and M. S. M. Jetten, "Completely autotrophic nitrogen removal over nitrite in one single reactor," *Water Research*, vol. 36, no. 10, pp. 2475–2482, 2002.

[14] M. Schmid, K. Walsh, R. Webb et al., "Candidatus "Scalindua brodae", sp. nov., Candidatus "Scalindua wagneri", sp. nov., Two New Species of Anaerobic Ammonium Oxidizing Bacteria," *Systematic and Applied Microbiology*, vol. 26, no. 4, pp. 529–538, 2003.

[15] C. Trigo, J. L. Campos, J. M. Garrido, and R. Méndez, "Start-up of the Anammox process in a membrane bioreactor," *Journal of Biotechnology*, vol. 126, no. 4, pp. 475–487, 2006.

[16] S. Cho, N. Fujii, T. Lee, and S. Okabe, "Development of a simultaneous partial nitrification and anaerobic ammonia oxidation process in a single reactor," *Bioresource Technology*, vol. 102, no. 2, pp. 652–659, 2011.

[17] S. Liu, F. Yang, Z. Gong, and Z. Su, "Assessment of the positive effect of salinity on the nitrogen removal performance and microbial composition during the start-up of CANON process," *Applied Microbiology and Biotechnology*, vol. 80, no. 2, pp. 339–348, 2008.

[18] K. Pynaert, B. F. Smets, D. Beheydt, and W. Verstraete, "Start-up of autotrophic nitrogen removal reactors via sequential biocatalyst addition," *Environmental Science & Technology*, vol. 38, no. 4, pp. 1228–1235, 2004.

[19] Z. Gong, F. Yang, S. Liu, H. Bao, S. Hu, and K. Furukawa, "Feasibility of a membrane-aerated biofilm reactor to achieve single-stage autotrophic nitrogen removal based on Anammox," *Chemosphere*, vol. 69, no. 5, pp. 776–784, 2007.

[20] Y. Lv, L. Wang, T. Sun, X. Wang, Y. Yang, and Z. Wang, "Autotrophic nitrogen removal discovered in suspended nitritation system," *Chemosphere*, vol. 79, no. 2, pp. 180–185, 2010.

[21] S. E. Vlaeminck, A. Terada, B. F. Smets et al., "Aggregate size and architecture determine microbial activity balance for one-stage partial nitritation and anammox," *Applied and Environmental Microbiology*, vol. 76, no. 3, pp. 900–909, 2010.

[22] M. Nielsen, A. Bollmann, O. Sliekers et al., "Kinetics, diffusional limitation and microscale distribution of chemistry and organisms in a CANON reactor," *FEMS Microbiology Ecology*, vol. 51, no. 2, pp. 247–256, 2005.

[23] B. Arrojo, A. Mosquera-Corral, J. L. Campos, and R. Méndez, "Effects of mechanical stress on Anammox granules in a sequencing batch reactor (SBR)," *Journal of Biotechnology*, vol. 123, no. 4, pp. 453–463, 2006.

[24] T. Schaubroeck, S. Bagchi, H. De Clippeleir, M. Carballa, W. Verstraete, and S. E. Vlaeminck, "Successful hydraulic strategies to start up OLAND sequencing batch reactors at lab scale," *Microbial Biotechnology*, vol. 5, no. 3, pp. 403–414, 2012.

[25] A. K. Vangsgaard, A. G. Mutlu, K. V. Gernaey, B. F. Smets, and G. Sin, "Calibration and validation of a model describing complete autotrophic nitrogen removal in a granular SBR system," *Journal of Chemical Technology and Biotechnology*, vol. 88, no. 11, pp. 2007–2015, 2013.

[26] S. E. Vlaeminck, L. F. F. Cloetens, H. De Clippeleir, M. Carballa, and W. Verstraete, "Granular biomass capable of partial nitritation and anammox (Water Science and Technology 58(5) 1113-1120)," *Water Science and Technology*, vol. 59, no. 3, pp. 609–617, 2009.

[27] R. Lemaire, R. I. Webb, and Z. Yuan, "Micro-scale observations of the structure of aerobic microbial granules used for the treatment of nutrient-rich industrial wastewater," *The ISME Journal*, vol. 2, no. 5, pp. 528–541, 2008.

[28] S. Scuras, G. T. Daigger, and C. P. L. Grady Jr., "Modeling the activated sludge floc microenvironment," *Water Science and Technology*, vol. 37, no. 4-5, pp. 243–250, 1998.

[29] J. Yang, J. Trela, M. Zubrowska-Sudol, and E. Plaza, "Intermittent aeration in one-stage partial nitritation/anammox process," *Ecological Engineering*, vol. 75, pp. 413–420, 2015.

[30] A. C. Anthonisen, R. C. Loehr, T. B. S. Prakasam, and E. G. Srinath, "Inhibition of nitrification by ammonia and nitrous acid," *Journal of the Water Pollution Control Federation*, vol. 48, no. 5, pp. 835–852, 1976.

[31] W. R. L. van der Star, A. I. Miclea, U. G. J. M. van Dongen, G. Muyzer, C. Picioreanu, and M. C. M. van Loosdrecht, "The membrane bioreactor: a novel tool to grow anammox bacteria as free cells," *Biotechnology and Bioengineering*, vol. 101, no. 2, pp. 286–294, 2008.

[32] B.-L. Hu, P. Zheng, C.-J. Tang et al., "Identification and quantification of anammox bacteria in eight nitrogen removal reactors," *Water Research*, vol. 44, no. 17, pp. 5014–5020, 2010.

[33] S. Liu, F. Yang, Y. Xue et al., "Evaluation of oxygen adaptation and identification of functional bacteria composition for anammox consortium in non-woven biological rotating contactor," *Bioresource Technology*, vol. 99, no. 17, pp. 8273–8279, 2008.

[34] T. Liu, D. Li, H. Zeng et al., "Biodiversity and quantification of functional bacteria in completely autotrophic nitrogen-removal over nitrite (CANON) process," *Bioresource Technology*, vol. 118, pp. 399–406, 2012.